Alma Mater Studiorum – Università di Bologna

DOTTORATO DI RICERCA IN

Ingegneria Civile, Chimica, Ambientale e dei Materiali

Ciclo XXXIII

Settore Concorsuale: 09/D3 - IMPIANTI E PROCESSI INDUSTRIALI CHIMICI

Settore Scientifico Disciplinare: ING-IND/25 - IMPIANTI CHIMICI

Ultra-Low Temperature Partial Oxidation: Detailed Kinetics, Safety, and Environmental Issues

Presentata da: Gianmaria PIO

Coordinatore Dottorato
Prof. Ing. Luca VITTUARI

Supervisore
Prof. Ernesto SALZANO

Co Supervisore
Prof. Ing. Valerio COZZANI

Esame finale anno 2021

“Be always yourself. Unless you can be Batman.
In that case, you should always be Batman.”

Homer J. Simpson

“I never said you're not good at what you do.
It's just that what you do isn't worth doing”

Sheldon Cooper referring to Howard Wolowitz (an engineer)

Table of Contents

Abstract

The innovation in several industrial sectors has been recently characterized by the need for reducing the operative temperature either for economic or environmental related aspects. Promising technological solutions require the acquisition of fundamental-based knowledge to produce safe and robust systems. In this sense, reactive systems often represent the bottleneck. For these reasons, this work was focused on the integration of chemical (i.e., detailed kinetic mechanism) and physical (i.e., computational fluid dynamics) models. A theoretical-based kinetic mechanism mimicking the behaviour of oxygenated fuels and their intermediates under oxidative conditions in a wide range of temperature and pressure was developed. Its validity was tested against experimental data collected in this work by using the heat flux burner, as well as measurements retrieved from the current literature. Besides, estimations deriving from existing models considered as the benchmark in the combustion field were compared with the newly generated mechanism. The latter was found to be the most accurate for the investigated conditions and fuels. Most influential species and reactions on the combustion of butyl acetate were identified. The corresponding thermodynamic parameter and rate coefficients were quantified through *ab initio* calculations. A reduced detailed kinetic mechanism was produced and implemented in an open-source computational fluid dynamics model to characterize pool fires caused by the accidental release of aviation fuel and liquefied natural gas, at first. Eventually, partial oxidation processes involving light alkenes were optimized following the quick, fair, and smoot (QFS) paradigm. The proposed procedure represents a comprehensive and multidisciplinary approach for the construction and validation of accurate models, allowing for the characterization of developing industrial sectors and techniques.

Research question

In the last decades, the increased attention on environmental issues and the fluctuations in fossil fuel prices and/or availability have pushed toward the development of alternative solutions in several industrial fields. A clear example of this tendency is the energy supply chain, where several molecules showing the potentiality to be alternative fuels have been produced and deeply investigated. The novelty in the chemical structure, leading to different physical properties, has required the adaption of the existing combustion conditions and combustor layout. Besides, the utilization of low-temperature conditions has been largely suggested because of the reduced production of pollutants in the combustion chamber. Similarly, several strategies aiming at the decrease in operative temperature have been largely adopted for chemical process optimization, as well, providing more effective and competitive alternatives. Among them, the development of integrated catalysts, plasma-assisted processes, and alternative separation systems are notable examples of growing solutions. Moreover, also the storage and transportation systems are facing an era of great changes. One of the main actors involved in this mutation is liquefied natural gas (LNG). Indeed, cryogenic transportation has favoured the diffusion of light and cleaner species as alternative fuels for mid- and long- term solutions. The knowledge and know-how required for the realization of infrastructures and processes suitable for LNG production, transportation, and utilization have positive spillovers toward the development of technological solutions promoting the hydrogen economy. Indeed, the liquid hydrogen (LH_2) has been considered as one of the most promising fuel, especially for the civil and industrial transportation fields, mainly because of its carbon-free nature and elevated energy density [1]. However, poor understandings of fundamentals and phenomenological aspects have limited the implementation of low-temperature solutions on an industrial scale, so far. On the other hand, the continuous increase in the available computational power has promoted the realization of detailed kinetic mechanisms by using automated approaches, and their implementation, in a reduced form, in computational fluid dynamic (CFD) models to reproduce the behaviour of real systems [2]. This innovative approach allows for an accurate evaluation of physical-chemical interactions in a wide range of operative conditions, thus may provide useful information for consequence analysis, as well. On the other hand, the main drawbacks are represented by the increase in complexity and the requirements of preliminary analyses to validate and reduce the kinetic mechanisms. In this view, the present work was focused on the development and application for low-temperature systems of a robust methodology guaranteeing the integration of validated kinetic mechanisms and appropriate physical models for the representation of simplified reactive systems relevant in several industrial fields. To this aim, either experimental or theoretical approaches have been adopted, indicating a self-contained approach for the evaluation of peculiar reactive systems.

Section 1 - State of the art

The implementation of technological solutions exploiting the advantages of low-temperature conditions involves several industrial fields and require a deep understanding of phenomenological and practical aspects. Several aspects have been clarified and fully understood through the application of experimental and theoretical approaches, as well as some fundamental knowledge need to be acquired to master the low-temperature processes. In this light, the present chapter has been devoted to the description and critical comparison of the current knowledge achieved and techniques developed for the optimization of technological systems applying low-temperature conditions.

Based on the application analyzed, the conditions where low-temperature behaviour is commonly considered can dramatically change. Some of the most glaring examples of these differences are combustion, storage and transportation, and chemical processes.

In the combustion field, three different regimes are commonly observed for most of the fuels, namely low-temperature, intermediate temperature, and high temperature [3]. The first is characterized by hydrogen abstraction by oxygenated radicals (e.g., OH, O, HO_2) acting as primary reaction producing fuel radicals and, thus, laying the foundations for ignition phenomena. The last can be characterized by unimolecular reactions involving the investigated fuel, such as cracking, due to the elevated energy density of the systems. The resulting intermediate species can be either radicals or more stable compounds. Typical conditions of high-temperature behaviour include the adiabatic flame temperatures. In the latter case, they can be activated by hydrogen abstraction by radicals more stable under these conditions (e.g., H). Eventually, the intermediate regime includes the conditions where both mechanisms compete and hydrogen abstraction by oxygenated and non-oxygenated radicals can be observed [4]. Typically, this regime includes temperature within 850 – 1300 K.

Similarly, storage and transportation systems can be classified based on the operative temperature utilized. In this case, room temperature is considered as “normal conditions” covering the large majority of the applications. However, different temperatures can be required for peculiar applications. Indeed, microbiological or material applications sometimes require a controlled temperature higher than room conditions to avoid degradation leading to loss of integrity or functionality [5]. Besides, light gas storage found economical convenience in low-temperature, because of the increased density. This aspect is of particular interest for alternative fuels such as methane and hydrogen, where a decrease in temperature up to cryogenic conditions can lead to liquefaction, with obvious advantages in energy density [6]. The elevated energy content per unit volume together with the limited impacts on the environment related to the combustion of these cryogenic fuels makes them convenient for transportation purposes [7], including aviation

applications [8]. If the development of effective liquefaction and storage processes for liquid hydrogen is still moving its first steps [9], the infrastructures using methane-based mixtures in liquefied form, i.e., liquefied natural gas (LNG), are robust and already spread worldwide [10].

Eventually, the range of temperature of interest for chemical processes spans from temperature close to room conditions up to thousands of Kelvin [11]. The last decades have been characterized by increasing interest in epoxidized products [12], playing a determining role as intermediate for plastics, additives, or coolants [13][14]. Quite obviously, a decrease in operative temperature is the preferred condition for these processes, because of the hindering effects on the complete oxidation reaction. However, this variation has a detrimental effect on the activity of the available catalysts, as well, requiring the achievement of a trade-off between selectivity toward the desired products and conversion of reactants.

Regardless of the considered application, the implementation of low-temperature conditions represents a novelty in terms of fundamental and practical characteristics, requiring studies tackling the phenomenological aspects involved to provide suitable guidelines for optimization and correct handling of reactive systems.

Kinetic aspects

Structure of typical detailed kinetic mechanisms

Considering the differences in the nature of the mixtures involved and the wide range of conditions of interests, the adoption of comprehensive and theoretical-based kinetic mechanisms should be promoted. Detailed kinetic mechanisms represent a combination of thermodynamic and kinetic databases composed of hundreds of species and thousands of reactions. They aim to the reproduction of the elemental steps and decomposition pathways characterizing the investigated species [15].

The number of reactions included in the models, I, has been roughly represented by a linear proportionality to the number of species, K, under the correlation $I = 5\,K$ [16]. However, the needs of representing wider conditions, together with the inclusion of additional functional groups (e.g., oxygenated species representative of biofuels [17] or hetero atom rings for chemical production [18]) have led to a steeper curve relating these two parameters. Indeed, the implementation of a hierarchical approach makes the detailed kinetic mechanism prone to an undesired increase in size. Kinetic mechanisms have been historically developed and adopted to characterize chemical phenomena occurring during combustion processes. However, no reasons exist to narrow their application to this field, as testified by recent studies addressing issues related to pharmaceutical [19] and bulk chemicals

[20] production by using detailed kinetic mechanisms. Besides, most of the analyses available in the current literature have been focused on the evaluation of high- or intermediate- temperatures behaviour, whereas only recently the relevance of low-temperature conditions has been pointed out [21]. The novelty together with the potentiality of this concept has attracted the researcher's attention to fill the gap and perform in-depth investigations. However, still, several aspects are unclear or poorly understood [3]. Hence, the utilization of detailed kinetic mechanisms for the characterization of low-temperature oxidation can be beneficial under several aspects.

Regardless of the investigated conditions and reactive systems, reactions can be distinguished between the following classes: 1) initiation; 2) chain branching, 3) chain propagation; 4) chain termination.

The initiation step is an activated reaction, e.g., by a spark or catalysts, producing more reactive species, e.g., radicals, starting from stable compounds. This reaction class can be expressed in the generic form:

$$AB + C \leftrightarrow A + BC \qquad \textit{(Eq. 1)}$$

where A, B, and C are generic molecules or groups. Typical examples of these reactions are dissociation reaction and hydrogen abstraction. The former is characterized by A = B and the absence of C, whereas in the latter case A usually stands for hydrocarbons chain and is substituted by the symbol R, B represents the hydrogen atom, and C is referred to as abstracting agent. C may represent several species, mostly radicals. Among the others, OH, H, O, O_2, and HO_2 are worth mentioning in combustion applications [15]. The relevance of radicals indicated by C and, thus the ruling decomposition path, is strongly affected by the temperature. Indeed, low-temperature regimes are assumed when hydrogen abstraction by HO_2 is dominant [22].

Chain branching reactions are characterized by the production of radical(s) starting from unstable intermediates as reactants, increasing the overall number of radicals available and reactivity of the systems. Hence, the so-called growth phase observable by monitoring the heat release rate of flames can be attributed to this reaction class [23]. Assuming this reaction class as a continuation of the initiation step, a generic representation can be expressed as follows in terms of the generic molecules or chemical groups D and E:

$$DE + A \leftrightarrow DA + E \qquad \textit{(Eq. 2)}$$

D = E representing a hydrogen atom or oxygen atom and, conversely, A standing for oxygen atom or hydrogen atom, are typical examples of chain branching reactions of interests for combustion being the major paths for the formation of OH radicals [24].

Chain propagation reactions are characterized by the same number of radicals on the reactants and product sides. However, a slight decrease in the overall reactivity is commonly attributed to the occurrence of this class of reactions, because it tends to consume OH radicals to form less reactive species [25]. Eventually, chain termination reactions considerably reduce the tendency to react to the system. Third bodies, such as reactor walls or inert species, can be involved in partially absorbing the energy of excited species and producing more stable species [26].

The ignition behaviour for the initial conditions can be determined under Zeldovich theory [27], by estimating the evolution of the free-radical density (ρ_e) with respect to time (t)

$$\frac{d\rho_e}{dt} = \omega_0 + (cb - ct) \cdot \rho_e \qquad \textit{(Eq. 3)}$$

where ω_0 account for the inverses of the characteristic time of the system; *cb* and *ct* stand for chain branching and chain termination, respectively. Indeed, depending on the sign of the brackets a decrease or an increase in free-radical density will be observed, determining the fate of the system.

Undoubtedly, migration from high to low temperatures has a terrific impact on the ruling reaction pathways and, thus to overall reaction rates. Further clarifications and insights corroborating this statement can be gained by analysis of a specific case. In this sense, the case of alkanes combustion may represent a convenient option, because of the large availability of information [28]. To this aim, simplified schemes of high- and low- temperatures primary reaction paths were reported in the following figures, in accordance with considerations collected in dedicated literature reviews [29][30].

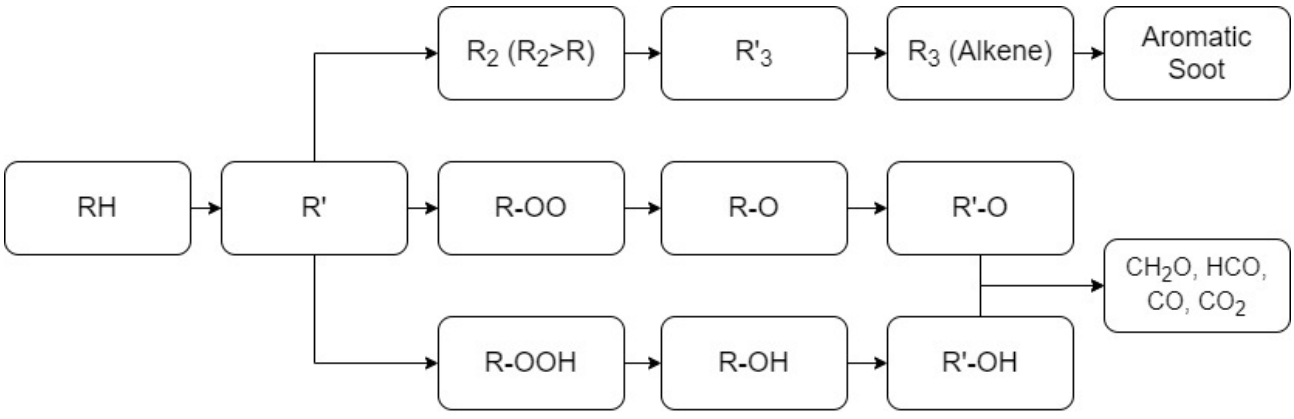

Figure 1. Simplified representation of the primary reactions constituting high-temperature combustion mechanisms.

The high-temperature mechanisms are characterized by the presence of pyrolysis path, leading to the formation of aromatics and soot precursors via an increase in the aliphatic chain and hydrogen addition reactions (as indicated in the path on the left of Figure 1). Besides, two distinct paths can be conducted to high-temperature oxidation. Both follow the $CH_2O \rightarrow HCO \rightarrow CO \rightarrow CO_2$ route as final steps. However, in one case CH_2O is produced via alcohol intermediate by hydrogen abstraction reaction followed by double bond formation, whereas in the other case the abstraction site is on the hydrocarbons side.

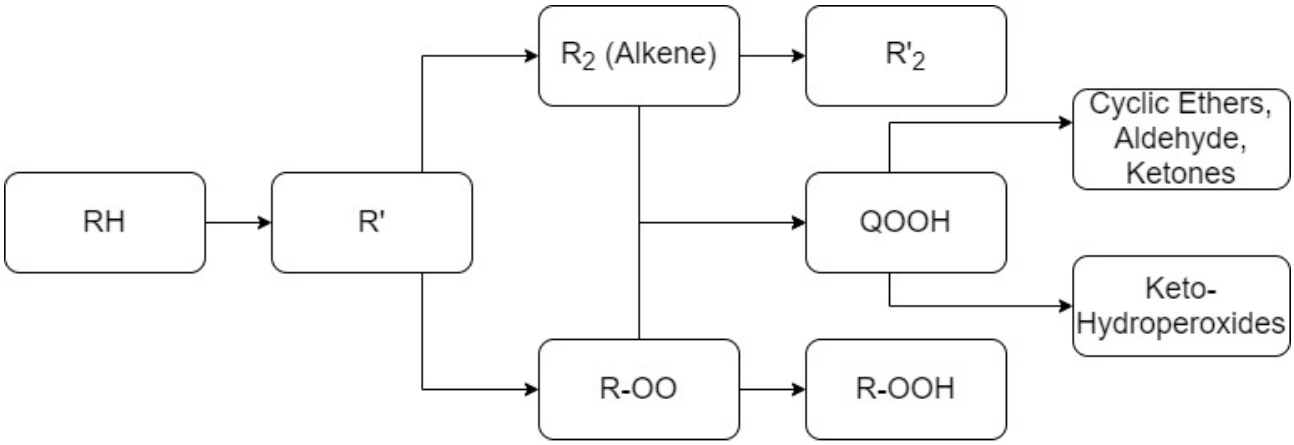

Figure 2. Simplified representation of the primary reactions constituting low-temperature combustion mechanisms.

It is well-established that hydrogen abstraction is the ruling primary reaction for alkanes combustion, provided that the initial temperature is below 1200 K [31]. Low-temperature combustion is characterized by having oxygen molecules as dominant abstracting agents, producing the alkyl group (indicated as R in Figure 2) and hydroperoxy radical (HO_2). This phenomenon can be attributed to the reduced availability of small radicals, deriving from dissociation reactions. Indeed, this reaction class is favoured by elevated internal energy and momentum, thus hindered by decreases in temperature. The produced alkyl radical may undergo further hydrogen abstraction by oxygen, to form an additional hydroperoxy radical and alkene, or attract an oxygen molecule and produce a peroxyalkyl radical (R-OO). The latter is considered being a barrierless reaction [32], justifying the fact that it is dominant at low temperatures. The production of HO_2 (as reported for the primary and secondary reactions with O_2) represents a peculiarity of low-temperature combustion and characterizes the whole ignition phenomena. Indeed, this radical can be easily involved in chain branching reactions breaking the O-O bond and generating hydrogen atom (H) and hydroxyl radical (OH). The formation of these radicals fastens the reactivity of the system, determining the ignition. On the other hand, more stable compounds, such as alkenes, are produced by the left side path reported in Figure 2, reducing the overall reactivity. Hence, the relative rates of these branches

determine the ignition behaviour at low temperatures, causing the negative temperature coefficient (NTC) behaviour in some cases, i.e., a decrease in the global reactivity determined by an increase in temperature [33]. Other than temperature, the branching ratio is affected by the number of carbon atoms forming the reactants. Indeed, concerted elimination of HO_2 forming alkene is neglected for alkyl radicals having more than 4 carbon atoms [34]. Hence, a full understanding of low-temperature combustion mechanisms assumes relevance, especially for light hydrocarbons. Since the scope of this review is to report the main understandings of the combustion mechanisms occurring at low-temperature, emphasis will be posed on the reaction paths starting from the R-OO. In this light, two major reactions should be highlighted: the disproportionation with other radical, forming a hydroperoxide (ROOH), and the internal migration of hydrogen atom, resulting in an hydroperoxyalkyl radical (QOOH). Based on the analysis reported by Curran et al. (1998) [34], the latter reaction is dominant when the temperature is above 600 K. Once formed, ROOH decomposes to RO and OH radicals via a degenerate branching step. On the other side, QOOH can be involved in three major paths: the addition of oxygen molecule, decomposition to cyclic ethers, or decomposition to acyclic species. The first option results in peroxyhydroperoxyalkyl radicals (OOQOOH), which reacts as QOOH. The major path leads to the formation of keto hydroperoxides [30].

Generation of detailed kinetic mechanisms - Principles of quantum chemistry

Typically, the knowledge-based and the automatized approaches are implemented for the selection of criteria for model enlargement. The former is centred on the experts' judgment, whereas the latter uses suitable algorithms, such as the rate-based algorithm. The enormous amount of data and calculations required for the development of these mechanisms has incentivized the adoption of automatized tools. Among the others, the reaction mechanism generator (RMG) is considered a robust feature for the generation of theoretical based kinetic models [35]. It is centred on a rate-based algorithm to automatically select reactions to be included to enlarge the generating mechanism. An isothermal reactor in the transient phase is simulated iteratively, starting from a set of reactants and conditions. User-defined termination criteria, such as threshold values for reaction time or reactant conversion, can be set to conclude the iterative process. A schematic representation of the procedure adopted by RMG for the construction of a detailed kinetic mechanism is given in the following figure, indicating A, B, C, D, E, F, G, and H as generic species.

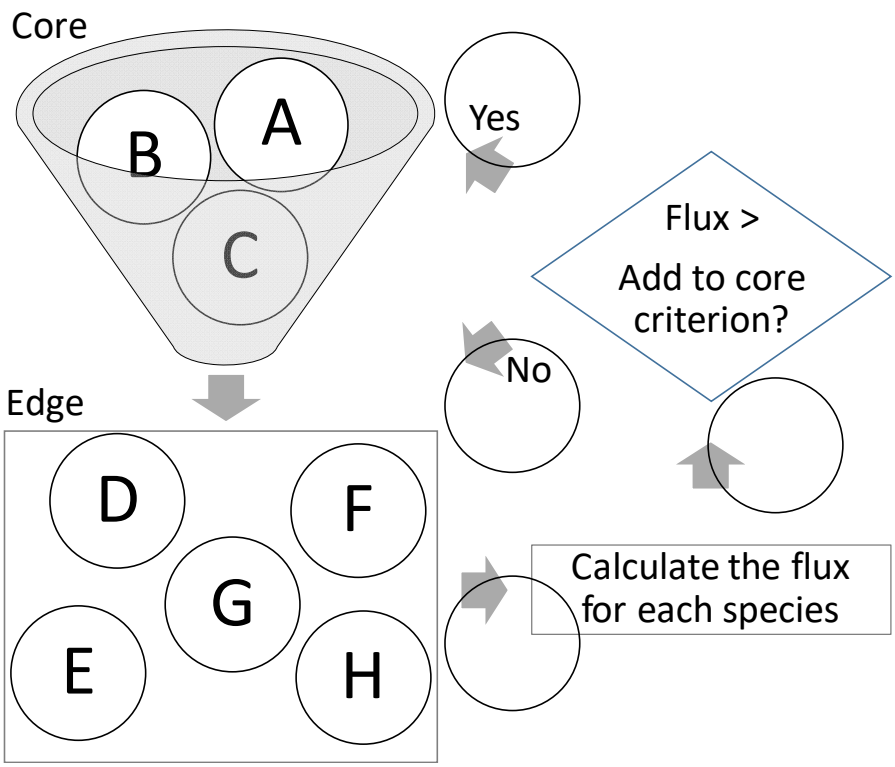

Figure 3. Schematic representation of the procedure adopted for the construction of the detailed kinetic mechanisms by RMG.

During each iteration, an edge model is generated based on the species incorporated in the core model obtained by the previous iteration. Starting from the conditions analysed, thermodynamic properties (e.g., free Gibbs's energy) of the species included in the edge and kinetic coefficients of the reactions producing them from the core species are estimated. Based on these data, the production rates of each species included in the edge are evaluated and compared with a given threshold value, the so-called "add to core value". Indeed, only if the production rate overcomes this value, the species and the related reactions are added to the core model for the following iterations. Thermodynamic and kinetic data required in this stage are taken from appropriate libraries, when available, or estimated via group contribution method and kinetic families, respectively. The former estimates the missing properties using linear combinations of the corresponding properties of sub-molecular fragments forming the analyzed molecule. Whereas rate coefficients are estimated starting from training datasets classified in reaction families based on functional group interactions. Additional information describing RMG software can be found elsewhere [35]. Undoubtedly, the model accuracy largely relies on the quality of the input data for thermodynamic and kinetic parameters. For these reasons, several approaches can be adopted, including experimental measurements, quantum mechanics calculations, and estimations based on the fuel structure chemistry [36]. The indirect estimations have the intrinsic drawbacks of a limited range of applicability, potentially elevated inaccuracy, and need for more

accurate data for similar reactions as input. On the other hand, experimental measurements and quantum mechanics calculations are usually expensive and time-demanding. Besides, the former cannot be applied for the evaluation of very fast reactions, where residence time is smaller than the sampling time. The latter is based on the individuation of the most stable conformer, usually followed by the estimation of the energy associated with the rotation of each routable bonds and frequencies calculations, under the rigid-rotor-harmonic-oscillator (RRHO) method [37]. Eventually, quantities related to the partition function (e.g., heat capacity, enthalpy variation, and entropy) can be calculated starting from the obtained data by solving the molecular Schrodinger equation. A level of theory and a basis set is required to expand the molecular orbitals as a linear combination of atomic orbitals [38]. Density functional theory (DFT) is usually utilized for geometry optimization and frequency calculation [39]. However, lower levels, such as the composite methods, are suggested for large systems [40]. G3, G4, CBS-QB3, and CBS-APNO belong to this class and are examples of the level of theory, i.e., the method, commonly adopted to address the numerical combustion chemistry topic [41]. A detailed overview of theoretical approaches, together with an in-depth comparison of assumptions, computational requirements, and accuracy of these methods is not the purpose of this review, but they have been covered by dedicated publications available in the current literature [42][43]. Nevertheless, it should be reported that the CBS-QB3 level of theory is considered as optimized in terms of accuracy for hydrocarbons generated species and computational required [42]. A large number of basis functions make solutions more accurate and, at the same time, the solution of the Schrodinger equation more demanding. Besides, structuring basis sets in the gaussian form make computations easier. Hence, several basis sets were developed with these premises. Among the others, Pople- and Dunning- types are worth mentioning [44]. A generic representation of Pople-type basis sets is A-BCG, where A represents the number of primitive Gaussians considered for each core atomic orbital basis function and it can assume values equal to 3, 4, and 6, B and C are the numbers of bases adopted for valence orbitals, commonly 1, 2, or 3, G indicate the use of Gaussian functions. It can be preceded by the symbol + in the case of diffusion functions and followed by polarization notations. Alternatively, the information reporting information related to the Dunning-type basis sets can be expressed in the compacted form cc-pV, where cc-p indicates correlation-consistent polarized, v valence-only basis sets. Sometimes, this notation can be preceded by aug, representing the augmented version of the indicated basis sets. Further information on the nomenclature and the theoretical principles founding the quantum mechanics can be found elsewhere [45][46] [38]. The elevated computational costs make these calculations unfeasible and impractical to provide all the properties listed in the mechanisms. For these reasons, sensitivity analyses are commonly performed to individuate the reactions and species having larger effects on the resulting model [47]. This

approach is based on the evaluation of normalized sensitivity coefficients (NSC) for the generic i-th species or reactions included in the model. NSC can be expressed in the generic form as reported in *Eq. 4*.

$$NSC_i = (\mathrm{x}_i/y) \cdot \frac{\partial y}{\partial x_i} \qquad \textit{(Eq. 4)}$$

where *x* represents the perturbed variable, namely rate coefficient or Gibbs energy, and *y* stands for a measurable property. The mole fraction of reactants, carbon monoxide (CO), hydroxyl radical (OH), formaldehyde (HCHO), formyl radical (HCO), methyl radical (CH_3) are examples of measurable that can be considered in this analysis. This parameter represents the fractional variation in the obtained output caused by a fractional variation in each input, thus indicates the input parameters having a larger impact on the generated models. Hence, by sorting the input data by decreasing the absolute values of the NSC, a priority list for the implementation of accurate methods is produced. Alternatively, the acceptance criteria for NSC can be set. More specifically, the implementation of accurate methods for the evaluation of the required properties is imposed if the input parameter is characterized by NSC values higher than the given threshold, whereas simplified estimators, such as group additivity [48] and rate rules, can be utilized if NSC assumes smaller values.

Validation of detailed kinetic mechanisms - Overview on experimental systems

Considering the nature of the kinetic mechanism, the comparison of numerical predictions against experimental data is essential to guarantee meaningful results and validate it. To disregard chemical phenomena from turbulence and physical aspects, premixed and laminar flames are preferred for these investigations. To this aim, either the characterization of the flame structure or the measurement of the overall reactivity can be implemented. The former is performed via jet stirred reactors, where gaseous streams are fed in a spherical reactor by opposed nozzles providing sufficient stir to the mixture, temperature distribution along the reactor is monitored by conveniently located thermocouples, and the composition of the mixture is measured through a movable probe connected to an online FTIR [49]. The overall reactivity can be expressed in terms of laminar burning velocity (S_u) or ignition delay time (IDT), depending on the selected conditions. Indeed, the S_u is representative of low-temperature initial temperature, being measurable at room temperature, as well [50], whereas IDT is suitable for the investigation of oxidative phenomena occurring at intermediate and high-temperature conditions [51]. This approach has the intrinsic advantage of keeping most of the most relevant chemical information in a stand-alone parameter for each initial condition, making the

validation for several conditions easier. Moreover, these parameters may allow for the estimation of safety parameters [52] and optimal residence time [53]. further information on this topic will be given in the following paragraphs.

Despite the apparent simplicity, several experimental systems have been developed to measure the S_u. Among them, the opposed jet method, the closed vessel method, and the flat burner method are commonly used, whereas the utilization of a Bunsen burner is strongly discouraged by the well-known limitations regarding the ambiguous definition of the flame surface [46]. The opposed jet method consists of two counter-flowing jets of fuel or oxidizer, creating stretched flames due to the flue gases flowing to the side of the flame. The strain rate is dependent on the distance from the nozzles, meaning that the unstretched burning velocity can be estimated by repeating the experiments at different strain rates and extrapolating data employing logarithmic correlation (*Eq. 5*), as introduced by Kelley and Law (2009) [54], or linear correlation (*Eq. 6*), as proposed by Dowdy et al. (1991) [55], to Markstein length (L_b) and stretch rate (K).

$$(S_b/S_b^0)^2 ln(S_b/S_b^0)^2 = -2(L_b \cdot k/S_b^0) \quad \textit{(Eq. 5)}$$

$$S_b = S_b^0 + L_b\, k \quad \textit{(Eq. 6)}$$

where S_b and S_b^0 are unstretched and stretched flame velocity, respectively.

The closed vessel method often referred to as a combustion bomb, generates a rotationally symmetric, transient, and stretched flame in a closed vessel, which is often spherical. The burning velocity is obtained by monitoring the pressure profile to time via the extrapolating methods reported for the counterflow flame method.

The flat burner consists of a cylindrical perforated burner plate where steady-state and unstretched flames can be generated, where the assumption of a mono-dimensional flame is commonly accepted since homogeneous inlet conditions are provided [56]. When the stabilization is performed using a heating/cooling fluid controlling the burner plate temperature, this method is referred to as the heat flux method (HFM). The technique, first introduced by de Goey et al. (1993) [57] is based on the balance between the heat loss required for flame stabilization and convective heat flux from the burner surface to the reacting front. In this case, S_u has assumed as the velocity at which the burner plate shows a constant temperature, and is determined by measuring the temperature profile of the plate burner at different gas flow rates and given fuel/oxidant ratio, temperature and pressure conditions.

Rapid compression machines and shock tubes are commonly adopted for the evaluation of the IDT at intermediate and high temperatures, respectively [16]. The first represents an essential rig for the

evaluation of fuel-specific effect occurring at intermediate temperature combustion [58] and consists of the chamber, almost adiabatic, where the fuel-oxidizer mixture is rapidly compressed by the movement of a piston, simulating a single compression stroke of an internal combustion engine. The latter consists of a cylindrical tube divided by a diaphragm and filled with high-pressure gas on one side and analyzing mixture on the other side. Once the diaphragm bursts a shock wave travels along the tube toward the closed end wall of the tube, heating the test gas instantaneously and creating a reflected shock wave. The gas behind this plane is at rest, thus it is analyzed for the sake of IDT measurements [18]. Considering the system peculiarities, zero-dimensional reactors with either a constant-volume or constant-pressure constraint can be adopted for the shock tube modelling, if a very thin boundary layer is excluded [59]. This parameter can be measured by detecting the time evolution of pressure, temperature, or the concentration of significant radicals for the combustion processes (i.e., OH and/or CH) [60].

The IDT functions to the inverse of temperature (T), pressure (P), and composition are commonly expressed as following [61]:

$$IDT = \mathrm{A}\, P^{\alpha} \varphi^{\beta} x_f^{\gamma} \mathrm{e}^{\left(\frac{E_a}{RT}\right)} \qquad \textit{(Eq. 7)}$$

where E_a is the apparent activation energy, R the universal gas constant and A, α, β, γ are constants, which depend on the fuel type, x_f is the fuel mole fraction and ϕ stands for the equivalence ratio. Similarly, several tools, approaches, and software have been developed for the generation of reaction networks [62], resulting in several detailed kinetic models and thermodynamics databases.

Environmental aspects

The implementation of low-temperature strategies has several spillovers on the environmental issue. Indeed, besides the fact that reduced operative temperature implies a reduction in pre-heating and less severe conditions for constructive materials where reactions occur, several chemical advantages can be identified. Some of the most relevant applications reporting significant impacts by low-temperature conditions on environmental-related aspects will be reported and discussed in this section. Particular attention will be given to the issues and main findings related to energy production systems, because of the well-known needs for alternative technologies reducing the emission of pollutants.

Low-temperature combustion

Clear examples of these positive effects involve the formation of nitrogen oxides (NOx) [63] and precursors of a particular matter [56]. Excluding the cases where a significant amount of nitrogen is bonded with primary fuels, the formation of NO is mainly attributable to the fixation of N2 from the air. Different mechanisms can be identified, including the thermal NO and prompt NO [64]. The former also referred to as the Zeldovich mechanism, is the ruling pathway for NO production at high-temperature [65] and consists of an initiating step where oxygen atom attacks the triple bond in N2, forming NO and N, followed by further oxidations involving the produced N atom. The first reaction represents the rate-determining step and it is strongly favoured at high-temperature only, thus the reduction in operative temperature considerably reduces the NO production via this route [66]. This phenomenon is one of the founding principles making moderate or intense low-oxygen dilution (MILD) combustion attractive for the limitation of the impact of combustion on the environment [67]. Similarly, the elevated energy density associated with the molecules at high temperatures facilitates the pyrolysis of the reactants, forming local pockets characterized by low-oxygen content, thus favouring the formation of soot precursors [68]. In this light, oxygenated species have been considered as alternative fuels, as well [69]. Numerous studies have been performed to unravel the chemistry of long-chain esters [70], [71], however, the relevance of small chain esters chemistry has been recently pointed out, incentivizing accurate analysis addressing this issue [72]. Indeed, several investigations have tackled the combustion of methyl formate, methyl acetate, methyl propanoate, and methyl butanoate, either experimentally or numerically [73]–[75]. However, the chemistry of the homologous alkyl acetate (i.e., ethyl acetate, propyl acetate, and butyl acetate) has been poorly studied, so far, although their promising properties for energy supply purposes [76]. In this regard, butyl acetate has been indicated as a species having great potential as a sustainable biofuel additive, because of its low freezing point, higher flash point, and limited impacts on the cetane number and heat of combustion of the resulting mixture [77]. Bearing in mind the significant differences in terms of reactivity, the isomeric structures (i.e., n-, i-, s-, and t- butyl acetate) should be distinguished to properly account for the chemistry of this species [78]. For the sake of clarity, Figure 4 shows the molecular structures and nomenclature considered in this work to distinguish the carbon atoms.

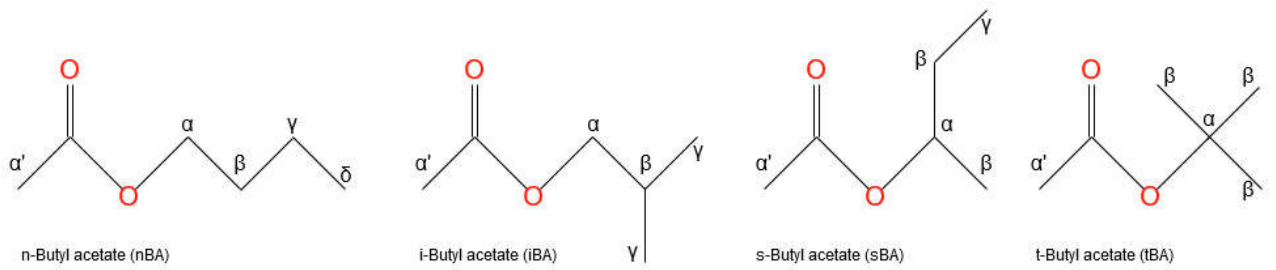

Figure 4. Schematic representation of the structures of the butyl acetate isomers and the labels adopted in this work.

For these reasons, the development and validation of detailed kinetic mechanisms suitable for the representation of the combustion behaviour of butyl acetate isomers in wide ranges of temperatures and pressures are desirable. Regardless of the investigated conditions, hydrogen atom abstraction by small radicals (e.g., H, OH, and HO_2) plays a significant role in combustion science [15]. More specifically, the hydrogen atom abstractions from the α and α' positions have been reported as dominant for several esters at low- and intermediate temperatures (i.e., lower than 1300 K) [79][80]. Besides, unimolecular decomposition, such as retro-ene reactions forming acetic acid and olefins, is the dominant primary route for the decomposition of oxygenated biofuels at high temperatures [71]. It consists of intra-molecular decomposition transferring hydrogen atom from β-position to the carbonyl oxygen to a six-membered ring transition state [81]. This step is followed by the bond scission connecting ester oxygen and the carbon atom in α position. Eventually, the aliphatic biradical is stabilized via double bond formation and the remaining structure rearranges to form acetic acid. Hence, robust sub-mechanisms including alkenes and acetic acid chemistry are essential for the construction of reliable models for oxygenated fuels. In this light, a brief overview of some of the existing models including light alkenes chemistry is provided in the following table. Considering that this review is devoted to the individuation of a proper core model for the development of a detailed kinetic mechanism for the estimation of the combustion behaviour of short-chain esters, particular attention was posed to light alkenes chemistry up to C_4, highlighting when butene isomers are distinguished.

Table 1. List of kinetic mechanisms available in the current literature.

Mechanism name (species focused on)	Year of release	Number of species	Distinguishing Butene isomers
USC Mech C1-C3 [82]	1999	71	No
GRI-mech 3.0 [83]	1999	53	No
Konnov 0.5 [84]	2000	127	No
Polimi (C1-C3 HT NOx) [85]	2003	115	No
CaltechMech [86]	2007	174	No
USC Mech II [87]	2007	111	Yes**
JetSurF 2.0 [88]	2010	348	Yes
NUIG (Butane) [89]	2010	230	Yes**
LLNL (n-Heptane) [90]	2011	654	Yes
LLNL (Butanol) [91]	2011	431	Yes
MIT (Butanol) [92]	2011	263	Yes
Bielefeld University (Butene) [93]	2013	163	Yes**
Polimi (C1-C3 LT HT) [94]	2014	107	No
UC San Diego [95]	2014	50	No
NUIG (Pentane Isomers) [96]	2015	293	Yes**
NUIG (n-Hexane) [97]	2015	1120	Yes**
CNRS-INSIS Orleans (Butene) [98]	2015	201	Yes*
NUIG (n-Heptane) [99]	2016	1268	Yes**
AramcoMech2.0 [100]	2013	493	Yes**
Lund University (Propanal) [101]	2018	119	No
AramcoMech3.0 [102]	2018	581	Yes
Polimi (C1-C16 HT+LT) [103]	2019	488	Yes
Princeton (Butane) [104]	2019	148	Yes

* Model validated for atmospheric pressure, only
** Included as the core model in an updated version
*** LT and HT stand for low temperature and high temperature, respectively

It should be specified that this list represents a comprehensive but not exhaustive list of kinetic mechanisms suitable for light alkenes, integrating the literature review recently published by Jach and co-workers (2019) [105]. Kinetic mechanisms commonly considered as a benchmark for the evaluation of newly generated mechanisms, such as GRI-mech 3.0 [83], USC Mech II [87], and AramcoMech3.0 [102], should be highlighted. Besides, the model developed by CNRS-INSIS Orleans groups focused on the evaluation of butene [98] has been validated for atmospheric pressure, only. Hence, the implementation of this mechanism to reproduce systems at higher pressure should be carefully considered and monitored. More specifically, the comparison of obtained data with estimations resulting from more comprehensive and widely validated models is strongly suggested.

Several approaches have been adopted for the construction of these mechanisms, leading to the formation of several alternatives for the core combustion model, as well. For these reasons, the adoption of a theoretical-based approach should be preferred for model generation.

Reactivity of biomass-derived mixtures

The increased interest in alternative solutions for energy production has promoted the adoption of fuel mixtures deriving from biological processes. As a way of example, the transformation of biomass and municipal wastes to flammable gaseous mixtures can be cited [106]. These processes usually produce a methane-rich stream having light hydrocarbons, carbon monoxide, carbon dioxide, hydrogen, hydrogen sulfide, and/or nitrogen, commonly referred to as bio-syngas [107]. The flexibility in raw material composition leads to significant alterations in the composition of the resulting stream, as well. This variability has incentivized the development of simplified methods for the estimation of the overall reactivity of the mixtures with respect to their composition, for the sake of process management. In this light, several empirical rules can be adopted for the evaluation of S_u of pure chemical species and fuel mixtures in the oxidative environment [108]. Different approaches have been historically adopted for this scope, namely correlations based on properties of the mixtures, purely empirical rules, and correlations evaluating the effect of initial conditions on S_u obtained at standard conditions. As a way of example, a list of correlations is given in the following table.

Table 2. Overview of empirical correlations for the estimation of laminar burning velocity of gaseous mixtures.

Correlation Name	Correlation
Le Chatelier's rule [108]	$S_{u,mix} = \frac{1}{\sum_i^n \frac{z_i}{S_{u,i}}}$
Weighted arithmetic mean by mole [109]	$S_{u,mix} = \sum_i^n x_i S_{u,i}$
Weighted arithmetic mean by energy [109]	$S_{u,mix} = \sum_i^n h_i S_{u,i} = \sum_i^n \left(\frac{\Delta H_{c,i} x_i}{\sum_i^n \Delta H_{c,i} x_i} \right) S_{u,i}$
Coppens' correlation [110] (modified Gulder's correlation [111])	$S_{u,mix} = W \cdot \phi^{\eta}\, exp^{-\xi(\phi-\sigma-\sum_i x_i \Omega_i)^2} \cdot \prod_i \left(1 + \gamma_i \cdot x_i^{\tau_i}\right)$
Semenov's rule [112]	$S_{u,mix}^2 = \frac{2K_f}{\rho_0 c_{p,0}^2 (T_f - T_0)^2} \left(\frac{T_o}{T_f}\right) \left(\frac{K}{\rho D}\right)_f \left(\frac{n_0}{n_f}\right) \left(\frac{R T_f^2}{E}\right)^2 A e^{-\frac{E}{R T_f}}$
Spalding's rule [113]	$S_{u,mix}^2 = \left(\frac{K}{\left(\rho_0 c_p (T_f - T_0)\right)^2} \right)_{mix} \sum_i^n \omega_i \left(\frac{\left(\rho_{0,i} c_{p,i} (T_f - T_0) S_{u,i}\right)^2}{K_i} \right)$
Yumlu's correlation [108]	$S_{u,mix}^2 = \sum_i^n \omega_i S_{u,i}^2$
Hirasawa's rule [114]	$S_{u,mix} = exp\left[\sum_i^n \left(\frac{z_i n T_{f,i}}{n_{mix} T_{f,mix}} ln(S_{u,i}) \right) \right]$

where ω_i, z_i and x_i are the mass, the molar fraction of the i-fuel in the mixture or fuel-air mixture, $\Delta H_{c,i,}$ and h_i are the enthalpy of combustion and the enthalpy of formation of the pure component i, respectively. Thermodynamics and transport properties of the mixtures are represented by ρ, c_p, *D, K, A, E, R,* and *T* stands for density, specific heat capacity, mass diffusivity, thermal conductivity, apparent pre-exponential factor, overall activation energy, the ideal gas constant, and temperature. Subscripts *f*, 0, *mix*, and *i* represent flame, initial conditions, mixture, or single component composition. W, η, ξ, σ, Ω, ϒ, and τ are fitting parameters, whereas φ is the equivalence ratio defined in *Eq. 8*.

$$\varphi = \frac{\left(\frac{x_f}{x_{ox}}\right)}{\left(\frac{x_f}{x_{ox}}\right)_{st}} \qquad \textit{(Eq. 8)}$$

where the subscripts *f*, *ox,* and *st* stand for fuel, oxygen, and stoichiometric conditions, respectively.

Safety aspects

The introduction of low-temperature conditions has posed several concerns related to safety aspects. These fears are based on the lack of comprehensive databases and models suitable for the characterization of explosive, chemical, and physical behaviour in extreme conditions. Indeed, experimental techniques representing the standardized approach for the experimental characterization in terms of safety aspects are inappropriate or inapplicable to the low-temperature cases, increasing the uncertainties of the resulting analyses. These limitations have been attributed to the non-fundamentals basis of the experimental systems [115], promoting the development of alternative approaches and techniques. The following paragraphs will discuss the available techniques for safety evaluations regarding the application for low-temperature characterization.

Evaluation of the flammability limits

The growing interest in hydrocarbons and non-hydrocarbon mixtures, such as Liquefied Natural Gas (LNG), Syngas, or Biogas, requires a robust methodology for reactivity predictions suitable for a wide range of operative conditions and compositions. That being said, the accurate determination of safety parameters represents an essential step for safe handling and storage system design and optimization for all the industrial process phases involving gaseous or liquid flammable mixtures. In this regard, Lower Flammability Limit (LFL) and Upper Flammability Limit (UFL) represents one

of the most important safety specifications for flammability hazard assessment. However, both LFL and UFL are strongly affected by unburned gas temperature, pressure, inert concentration and species, apparatus sizing and material, ignition energy, propagation direction, and turbulence. Quite obviously, a first approach is represented by the experimental determination of their values under numerous conditions. To this aim, several rigs and procedures have been proposed and utilized in the current literature. A summary of the main alternative for experimental setups is reported in Table 3.

Table 3. Main characteristics of the commonly used standard methods for FLs determination.

Characteristic	Typical alternatives
Explosion vessel	Closed glass sphere or cylinder, Steel tube, Glass flask, Quartz tube
Flame direction	Horizontal, Vertical
Ignition source	Spark, Flame, Exploding wire
Ignition duration	0.2 s, 0.5 s
Ignition position	Sphere centre, Tube bottom
Ignition criteria	Visual flame, Thermal rise, Pressure rise, Pressure-time curve inflection point
Limit definition	Last non-ignition point, Average of last ignition and non-ignition points

Among the highlighted aspects, test vessel and ignition criteria represent crucial choices strongly affecting the other experimental rig characteristics.

An example of the typical experimental procedure is given by the pioneering study performed by Coward and Jones (1952) [116] reporting a comprehensive database of individual gases and vapours Flammability Limits (FLs) obtained through 50 mm glass tube, 1.5 m long and visual identification, i.e., the mixture was considered flammable only if a flame propagation of at least half tube length occurred. Nevertheless, similar test vessels are still used as proved by the study of Le et al (2012) [117] on the evaluation of the effect of sub-atmospheric pressure on the hydrogen and light hydrocarbons UFL, where a thermal ignition criterion was applied. A commonly used experimental rig is the spherical vessel with central ignition, where the pressure rise equal to defined values from 1% up to 10% of initial pressure is adopted as ignition criteria [118]. However, in a recent study, Crowl and Jo (2009) [119] have proposed the maximum in the second derivative of the pressure-time curve as a method for the determination of FLs for a gas in a closed spherical vessel. Since the use of the maximum pressure increase as ignition criteria was considered an arbitrary approach leading to not negligible errors especially for hydrogen-containing mixtures.

For the sake of an effective comparison of experimental results, efforts were made to develop standardized test procedures for the determination of FLs, e.g ASTM E681 [120] and EN 1839 [121], where flask and spherical vessel, cylindrical open and spherical or cylindrical closed vessels, material, dimensions, and ancillary equipment are specified. Additional information and comparison are given

in the analysis of EU and US standards for the determination of flammability (or explosion) limits and Minimum Oxygen Concentration (MOC) performed by Molnarne and Schroeder (2017) [122].

A detailed review of FLs experimental data from several procedures and empirical equations for more than 200 combustible/air mixtures considered of interest for the prevention of disastrous explosions have been reported by Zabetakis (1999) [123].

Currently, FLs data are required in a wide range of conditions to satisfy the various industrial process operations need and correctly estimate the risk associated with the chemical plants, however, it should be considered that measurements are not always available for all the complex mixture compositions commonly used in industrial applications. For these reasons, several empirical and theoretical formulas were developed to estimate the safety parameters as a function of operative conditions. Among the others, critical adiabatic flame temperature (CAFT) [124] and limiting laminar burning velocity [52] theories are worth mentioning. The first alternative is based on the assumption that flammability limits can generate a given value of adiabatic flame temperature, i.e., thermal and kinetic aspects are balanced and able to self-sustain a flame [125]. However, although the threshold value should depend on the fuel composition and operative conditions, it is commonly considered within the range of 1200 – 1350 K [126], leaving a degree of freedom for the estimation of flammability limits. A similar hypothesis was posed by Hertzberg [52], but the balance between thermal and kinetic aspects was scrutinized by using the laminar burning velocity as a monitoring parameter. In this case, a correlation for the evaluation of the effects of operative conditions on the threshold value $\left(S_{u,lim}\right)$ was provided (*Eq. 9*)

$$S_{u,lim} = \sqrt[3]{2\alpha \cdot \vec{g} \cdot \frac{\rho_b}{\rho_u}} \qquad \textit{(Eq. 9)}$$

where $\vec{g}$, α, ρ_b, and ρ_u represent the gravitational acceleration, effective thermal diffusivity of the mixture, burned, and unburned densities.

Accidental release of cryogenic fuels

Accurate estimations of the flammability limits have the potential to significantly affect the risk assessment results for cryogenic storage systems, as well. Indeed, in the case of the accidental release of cryogenic liquids, a liquid pool is suddenly formed, followed by evaporation. The presence of ignition sources in the proximity of the releasing point and the substrate where this phenomenon

occurs strongly affects the final accidental scenario. A schematic representation of the possible scenarios generated by the LNG accidental release is given in the following figure.

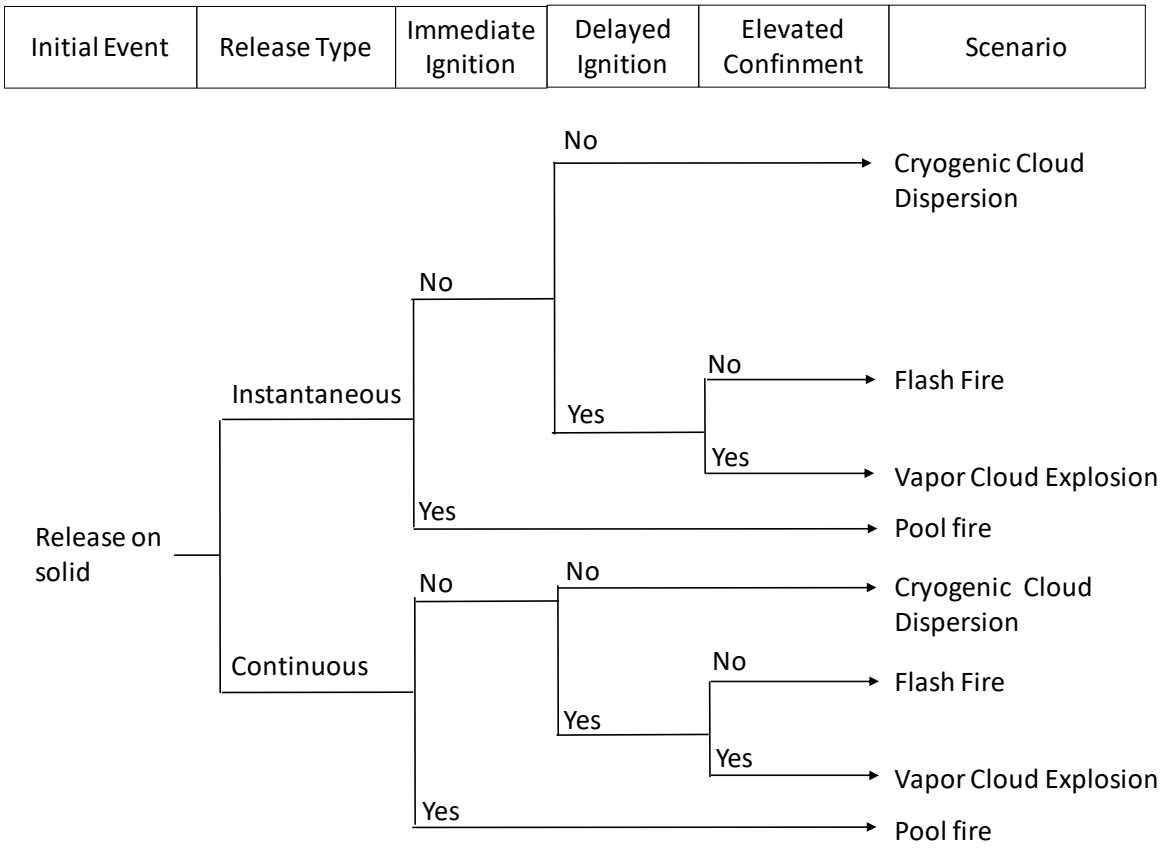

Figure 5. Event tree for liquefied natural gas accidental release on land.

Regardless of the investigated release type, in absence of ignition, cloud dispersion occurs. Considering the non-toxic composition of LNG and the operative conditions for the storage systems, the hazard of cryogenic burns should be evaluated. Alternatively, in case of immediate ignition, a pool fire scenario is observed. Eventually, if the ignition is delayed the formed vapour ignites resulting in flash fire scenarios potentially triggering pool fire, as well. In the case of pool fire, the stand-off distance can be calculated based on the incident heat flux on a given position/target, whereas for flash fire it can be estimated using the LFL values [127].

In the case of release on water, the intimate liquid-liquid interactions may lead to elevated heat transfer coefficients, promoting sudden evaporation. The abrupt change in the state produces a localized decrease in natural gas density, thus posing the foundations for the generation of overpressures. This phenomenon is called a rapid phase transition (RPT) and represents an additional scenario to be taken into account for the sake of consequence analyses involving cryogenic storage systems [128].

Undoubtedly, prior evaluation on the pool formation and evaporation represents an essential step for meaningful results and proper characterization of the accidental scenarios involving cryogenic release. In this sense, a generic equation correlating the pool mass per unit area ($m"_p$) to time (t) can be expressed as follow:

$$\frac{dm"_p}{dt} = m"_{spill} - m"_{ev} - m"_{dis} \qquad \textit{(Eq. 10)}$$

where the subscripts *spill*, *ev*, and *dis* stand for spilled, evaporated, and dissolved, respectively.

The dissolved term accounts for the fraction of liquid adsorbed by the substrate where the pool is spreading. This contribution can be neglected for LNG release regardless of the composition of the spreading surfaces (e.g., either for water or concrete). Hence, the evaporation rate is commonly assumed equal to the spilling rate once the steady-state conditions are achieved. Quite clearly, this approach is unadaptable for different un-steady conditions as e.g., for short instantaneous release and can lead to significant overestimations for the continuous release case. In this light, the development of robust models accounting for phenomena involved in liquid-gas phase transition is desirable.

The evaporation term can be determined as the sum of the conduction (cond), convection (conv), and radiation (rad) heat fluxes (q) divided by the latent heat of vapourization (ΔH_{ev}).

$$m"_{ev} = \frac{q_{cond}+q_{conv}+q_{rad}}{\Delta H_{ev}} \qquad \textit{(Eq. 11)}$$

The radiative heat flux can be neglected in the absence of ignition sources. Also, due to the large differences between the pool and substrate temperature, the conduction term is usually dominant at first, then, convective term assumes significance [129]. The conduction term accounts for the heat transferred from the substrate where the pool is formed, thus different models can be used if the release occurs on water or solid. Assuming LNG as pure methane Conrado and Vesovik [130] proposed the following model in case of release on water:

$$q_{cond} = k_w \cdot (T_w - T_P) \qquad \textit{(Eq. 12)}$$

where k_w is the heat transfer coefficient between water and LNG, T the temperature, and the subscripts *w* and *P* represent the water and pool, respectively.

Under the hypothesis of semi-infinite solid at a constant temperature, the model developed by Carslow et al. (1986) [131] can be adopted for the evaluation of conduction term to time *t* in case of

a solid substrate, based on the thermal conductivity k_s, thermal diffusivity α_s, solid substrate temperature T_s,

$$q_{cond} = k_s \cdot \frac{(T_s - T_P)}{(t \cdot \pi \cdot \alpha_s)^{0.5}} \quad \textit{(Eq. 13)}$$

The convection term is commonly expressed as the product of the driving force heat transfer coefficient. The former is the difference between room and pool temperatures, whereas the latter can be estimated via several equations correlating the Nusselt number to Reynolds and Prandtl dimensionless number [132][133], the suitable for the investigated layout and turbulence.

Alternatively, a fundamental approach may correlate physical properties to the evaporation rate. In this light, it should be considered that this phenomenon can be intended as a non-equilibrium process having a net transport of liquid molecules across a liquid-vapour interface into a gaseous phase [134]. In other words, models for the evaporation rate estimation can be the sum of two different contributes:

i) condensation of evaporated molecules in the area surrounding the liquid.
ii) evaporation of liquid molecules in the atmosphere.

The available fraction of these two states of aggregation is in first approximation regulated by well-known thermodynamic correlations, e.g., the Antoine law. Following this approach, several models have been developed for either cryogenic or non-cryogenic liquids. In both cases, the evaporation rate per unit of liquid surface ($m"_{ev}$) can be expressed as a function (*f*) of the driving force, i.e., the effects of the vapour pressure P_s at the liquid temperature T_l, and a function of thermodynamic properties, transport coefficients, and/or boundary conditions (h_x)

$$m"_{ev} = f[P_s] \cdot h_x \quad \textit{(Eq. 14)}$$

Either linear (*Eq. 12*) or logarithmic (*Eq. 13*) trends can be used to substitute *f*

$$m"_{ev} = h_x \cdot \frac{M_w \cdot P_s}{R \cdot T_l} \quad \textit{(Eq. 15)}$$

$$m"_{ev} = h_x \cdot \frac{M_w \cdot P_a}{R \cdot T_l} \cdot \ln\left(\frac{P_a}{P_a - P_s}\right) \quad \textit{(Eq. 16)}$$

where the subscripts l, s, and a represent the liquid surface, saturated conditions, and atmosphere, whereas the symbols P, R, T, and M_w are the pressure, ideal gas constant, temperature, and molecular weight, respectively. A comparison with experimental data has demonstrated that the linear trend is more accurate for cryogenic applications [135].

Further distinctions can be done based on the approach adopted for the evaluation of h_x. Indeed, h_x can be intended as an empirical-based coefficient, a function of thermodynamic data, or fluid dynamic properties. The latter case is commonly expressed employing dimensionless numbers, such as Reynolds $\left(Re, = \frac{2r \cdot u_w}{\upsilon}\right)$, Schmidt $Sc = \left(\frac{\upsilon}{D_l}\right)$. Examples of correlations for the estimation of $m"_{ev}$were reported in the following Table 4.

Table 4. A representative list of evaporation rate models suitable for cryogenic liquid modelling. Readers may consider the following definitions for the symbols adopted in this table if missing in the previous paragraphs: α_l, α_v= relaxation parameters for liquefaction and evaporation; r = pool radius; ν = kinematic viscosity; D_l = fuel diffusivity in air; u_w= wind velocity; $\rho_s, \rho_{air}, \rho_l$ = density of the vapour at saturation or air temperatures, or of the liquid at saturation temperature; g= gravitational acceleration; β Boolean operator= 1 for $T_v > T_s$, = 0 for $T_v < T_s$.

Authors [reference]	**Equation**
Hertz-Knudsen-Schrage [136][137]	$\frac{2}{2-\alpha_l}\sqrt{\frac{1}{2\pi}\frac{M_w}{R}}\left(\alpha_v\frac{P_v}{{T_s}^{1/2}}-\alpha_l\frac{P_s}{{T_s}^{1/2}}\right)$
Ingersoll [138]	$D_l \cdot (\rho_s - \rho_{T_{air}}) \cdot \sqrt[3]{\frac{\rho_s - \rho_{air}}{\rho_l} \cdot g \cdot \nu^{-2}}$
Mackay and Matsugu [139]	$4.8 \cdot 10^{-3} \cdot u_w^{0.78} \cdot (2r)^{-0.11} \cdot Sc^{0.67} \cdot \frac{P_s \cdot M_w}{R \cdot T_l}$
Lee [140]	$(1-\beta)\alpha_v\rho_v\frac{T_v - T_s}{T_s} + \beta\alpha_l\rho_l\frac{T_s - T_v}{T_s}$
Raj and Morris [141]	$3.7 \cdot 10^{-2} \cdot (Re^{0.8} - 15500) \cdot Sc^{0.33} \cdot \left(\frac{D_l}{2r}\right) \cdot \frac{P_s \cdot M}{R \cdot T_l}$
Reed [142]	$4.8 \cdot 10^{-3} \cdot u_w^{0.78} \cdot (2r)^{-0.11} \cdot Sc^{0.67} \cdot \frac{P_s \cdot M_w}{R \cdot T_l} \cdot \sqrt{\frac{(M_w + M_{w,air})}{M_w}}$
Hummel [143]	$1.5 \cdot 10^{-11} \cdot u_w^{0.625} \cdot P_s \cdot M$
Barry [144]	$8.8 \cdot 10^{-4} \cdot u_w \cdot \frac{P_s \cdot M}{R \cdot T_l}$
Derek et al. [145]	$0.17 D_l \cdot \frac{P_s \cdot M_w}{P \cdot M_{w,air}} \cdot \sqrt[3]{\frac{\rho_s - \rho_{air}}{\rho_l} \cdot g \cdot \nu^{-2}}$
Heymes [146]	$1.5 \cdot 10^{-1} \cdot Re^{0.69} \cdot Sc^{0.87} \cdot \left(\frac{D_l}{r}\right) \cdot \frac{P_s \cdot M}{R \cdot T_l}$
Schrage [147]	$\frac{2\alpha}{2-\alpha}\frac{1}{\sqrt{2\pi}}\left(\frac{P_v}{\sqrt{RT_v}} - \frac{P_s}{\sqrt{RT_l}}\right)$

It should be noted that some correlations have been developed for cryogenic species but in the non-terrestrial environment. These peculiar conditions have led to a neglect of the effect of wind, included by most of the correlations. Since consequence analyses are usually performed under the benchmark stability classes 5D and 2F, referring to a characteristic wind speed of 5 m s^{-1} and 2 m s^{-1}, respectively, correlations including the effect of wind should be preferred. Besides, the lack of comprehensive databases including data on the evaporation rate of cryogenic liquid under a wide range of conditions, discourage the adoption of fully empirical correlations having unknown relaxation coefficients.

Similarly, in the case of accidental release on the water surface, several models can be implemented for the evaluation of the evaporation rate [148]. Besides, the introduction of additional parameters (e.g., water depth and agitation) is necessary to satisfactorily describe the substrate conditions and, thus, the evaporation rate [149]. Furthermore, the large difference in temperature between the substrate and cryogenic fuel has the potential to cause solidification of water. However, theoretical analyses have demonstrated that this phenomenon can be neglected for deep or turbulent water [150]. Regardless of the composition of the cryogenic fuel, the immediate formation of a vapour film over the liquid surface can be assumed and, thus, the evaporation rate can be estimated as the in the following equation [130]

$$m''_{ev} = h_w \cdot \frac{T_w - T_p}{\Delta H_{ev}} \qquad \textit{(Eq. 17)}$$

where h_w represents the heat transfer coefficient between substrate and liquid pool, ΔH_{ev} the latent heat of vaporization, T_w the wall temperature, T_p the pool temperature. It should be noted that T_w can be assumed as constant if the substrate is sufficiently larger than the pool and thus heat can effectively disperse the heat. On the other hand, T_p variates unless pure liquids are considered. Eventually, h_w can be estimated by suitable correlations, such as the ones developed by Klimenko [151], reported in terms of dimensionless numbers (Nu = Nusselt, Pr = Prandtl, Ar = Archimede).

$$Nu = \frac{h_w \cdot l}{k} = 0.19 \cdot (Ar \cdot Pr)^{\frac{1}{3}} \cdot f_1 \qquad \text{if Ar} < 10^8 \qquad \textit{(Eq. 18)}$$

$$Nu = \frac{h_w \cdot l}{k} = 0.0086 \cdot Ar^{\frac{1}{2}} \cdot Pr^{\frac{1}{3}} \cdot f_2 \qquad \text{if Ar} > 10^8 \qquad \textit{(Eq. 19)}$$

in which f_1 and f_2 are the so-called near unity correction factors, defined by Klimenko in terms of reduced latent heat of vaporization, whereas α, k, and l stand for thermal diffusivity, thermal conductivity, and critical wavelength of the instability, respectively. The latter is defined as reported in the following equation:

$$l = 2\pi \cdot \left(\frac{\sigma}{g \cdot (\rho - \rho_v)}\right)^{\frac{1}{2}} \qquad \textit{(Eq. 20)}$$

provided that σ, g, and ρ are surface tension, gravitational acceleration, and density, and the subscript v indicates cryogenic vapour.

Once the evaporation model is properly selected, computational fluid dynamic (CFD) models can be adopted for the evaluation of near-field aspects involving the vapour phase resulting from an accidental release of LNG. Recalling the events previously defined in this paragraph, either physical or chemical phenomena may show some peculiarities due to the low-temperature conditions. More specifically, based on the thermodynamic properties, LNG vapour acts as dense vapour when the temperature is below 200 K, whereas vapour is lighter than air as the temperature approaches the room value [37]. Similarly, kinetics is strongly affected by the temperature, and low-temperature combustion affects the ruling pathways toward the complete oxidation of natural gas compounds. In this light, the implementation of detailed kinetic mechanisms in CFD has the potential to solve both issues, because of the exhaustive thermodynamic database included in it. However, the computational power available strongly limits the feasibility of this approach. On the other hand, the implementation of a reduced form of kinetic mechanisms in CFD for an accurate representation of real systems has been indicated as a promising technique in several industrial fields [2]. This approach requires the individuation of most relevant species and reactions to reproduce the chemical aspects under all the conditions of interest for the investigated process. To this aim, sensitivity analysis and flux diagrams are commonly adopted [47][152]. Considering the generic nature and the theoretical background of the approach, it can be adopted for cryogenic applications, as well, allowing for the reproduction of accidental scenarios.

Among the others, the pool fire scenario is undoubtedly worth particular attention because it is the only able to reach a pseudo-steady state condition and, thus, having the potential to cause a second cascading event [153]. This scenario is usually characterized by the thermal radiation intensity per unit of the surface area of the given target, i.e., the radiative heat flux (I), to the distance from the pool centre (x). The radiative heat flux can be expressed as a function of the atmospheric transmissivity (τ), of the view factor (F), following the classical equation [28]:

$$I(x) = SEP \cdot F \cdot \tau \qquad \textit{(Eq. 21)}$$

The view factor F is a geometric parameter defining the fraction of energy radiated by the fire that reaches the target. F has an inverse proportionality with x [155]. SEP stands for surface emissive power, representing the heat release rate (HRR) per unit of flame surface (A_F), and can be estimated as follow [156]:

$$SEP = \frac{\mathrm{HRR}}{\mathrm{A_F}} = \sigma \cdot \varepsilon \cdot T_F^4 \qquad \textit{(Eq. 22)}$$

where σ, ε, and T_F, are the Stefan–Boltzmann constant, the emissivity, and the adiabatic flame temperature.

Considering that HRR can be intended as the product of the mass burning rate, enthalpy of reaction (ΔH_r), and combustion efficiency (η), SEP can be expressed as

$$SEP = m''_{ev} \cdot \Delta H_r \cdot \eta \qquad \textit{(Eq. 23)}$$

where m''_{ev} stands for the mass burning rate per unit of flame surface. It is commonly equalized to the evaporation rate, i.e., the gas-phase reaction is assumed instantaneous concerning the liquid-vapour transformation. The effect of the pool diameter (d_p) on this parameter can be evaluated by using the Hottel's correlation [157] for the combustion of liquid fuels:

$$m''_{ev} = m''_{\infty} \cdot (1 - e^{-k \cdot \beta \cdot d_p}) \qquad \textit{(Eq. 24)}$$

where the subscript ∞ stands for the mass burning rate obtained for an "infinite" diameter of the pool, k is the absorption-extinction coefficient, which is approximately 3.0 m^{-1} for LNG [156] and β is the correction coefficient for the beam length.

The flame size is usually calculated assuming a cylindrical shape tilted by the wind, having the base area equal to the pool, a tilt angle (α), and height (H). By way of examples, empirical correlations proposed by Fay [158] and Thomas [159] were reported for the estimation of α and H, respectively.

$$\alpha = \arcsin\left[\frac{Fr}{Fr+0.19}\right] \qquad \textit{(Eq. 25)}$$

$$\frac{H}{d_p} = 42 \cdot \left(\frac{m''_{ev}}{\rho_a \cdot g^{0.5} \cdot d_p^{0.5}}\right)^{0.61} \qquad \textit{(Eq. 26)}$$

where Fr, ρ_a, and g are the Froude number, air density, and gravitational acceleration.

Regardless of the analyzed scenario, the novelty in investigated conditions has posed issues related to the inertization systems. Indeed, traditional water-based systems for fire suppression are ineffective or even intensify the consequences when directed to the cryogenic pool [160], because of the increased evaporation rate discussed before in case of liquid-liquid contact. Hence, within this class of mitigation systems, only the water curtain has been considered for the generation of a safe path for evacuation and rescue [161]. The application of solid powder forming a layer on the pool surface to isolate it from the oxidative environment is under development and is still facing some problems

related to the decomposition of solid material exposed to extreme temperatures [162]. Eventually, the addition of inert gaseous species (e.g., nitrogen or carbon dioxide) has been considered, requiring the estimation of flammability limits and minimum oxygen concentration of cryogenic fuels at a temperature below ambient conditions [163].

Accidental releases of liquefied natural gas (LNG)

Either experimental or numerical approaches have been adopted for the characterization of accidental scenarios resulting from LNG release. The majority of experimental studies have been devoted to the characterization of large-scale spills, for the sake of risk assessment of LNG transportation via ship systems. Nevertheless, small scale data can be found, as well. In this section, a brief overview of the main data and conditions experimentally tested, together with the models considered as more accurate will be reported. Small scale RPT experiments performed by Enger and Hartman (commonly referred to as Shell tests) [164], testing a 0.1 m^3 pool composed of a mixture of light alkanes, have demonstrated that RPT does not occur unless methane content is lower than 40 %v/v. On the other hand, large scale RPT tests included in the Coyote test series [165], performed by the Lawrence and Livermore national laboratory (LLNL), have reported RPT for LNG having methane content up to 88 %v/v. In this case, several compositions including methane, ethane, and propane, selected as representative of LNG were tested realizing a continuous spill having flowrate within 6-19 $m^3\ min^{-1}$. Under these conditions, only a fraction of tests have reported the RPT. However, either early (i.e., in the proximity and immediately after the spill begin) or delayed (i.e., far from the releasing point and at the end of the spill) RPTs have been observed. The discrepancies between the two experimental campaigns here reported indicating that different mechanisms rule the RPT based on the pool size. Differences in water temperature were considered as additional criteria. Indeed, the hypothesis of 290 K as the threshold value of water temperature for RPT occurrence has been largely accepted [166]. Similarly, the superheat temperature theory has been adopted to correlate this value to the fuel composition. More specifically, it has been assumed that the water temperature should be within the range delimited by the superheat temperature and its 110% [167]. This parameter has been evaluated for several pure species [168] and can be approximated for mixtures based on a mole fraction [169]. Quite obviously, the evaporation rate and vapour composition variate along with the test, because of the differences in the volatility of the involved species. The delayed RPT is attributed to this phenomenon, causing the enrichment of ethane in the LNG pool along the time [170]. Considering the large differences between the room temperature and LNG boiling temperature, the instantaneous formation of the film boiling regime is commonly assumed, then the RPT is attributed to possible instabilities leading to local collapses of the vapour layer leading to liquid-liquid contact [171]. Several experimental tests have been performed for the characterization of the LNG dispersion

scenario, either on water or on solid surfaces. Among the others, Esso [172], Maplin Sands [173], Burro [174], Coyote [165], and Falcon [175] series are worth mentioning. These campaigns span from a small scale (e.g., approximate pool radius of 5 m) to a large scale (e.g., approximate pool radius of 30 m). Several compositions were tested. Visible plume sizes and maximum distances where lower flammability limits were observed were reported as a function of wind velocity, air humidity, spill rate, and pool size. Dense cloud behaviour has been reported in all tests, i.e., LNG vapour tends to spread on downwind size predominantly, forming a cloud low in height compared to the downwind direction. Vapour density was found to be sensitive to the level of humidity in the surrounding area. A comparison of qualitative and quantitative analyses performed during the Burro series show that the LFL can be detected within the visible cloud even for a very low level of humidity (i.e., 5%). Most of the computational fluid dynamic analysis performed so far have evaluated the LNG vapour dispersion by using the k-ε sub-model for turbulence, 2F and 5D as Pasquill stability classes and wind velocity. The effect of pool area and shape, release rate, substrate roughness, presence of obstacles, and atmospheric conditions have been tested, showing an increased relevance of parameters affecting source term when wind flows slowly because gravitational forces are dominant [176].

Eventually, LNG pool fire tests have been performed either in case of liquid or solid substrate, variating the spill rate and pool size. A comprehensive and critical review of the experimental campaign dedicated to the collection of data on pool fire of LNG can be found in the literature [166][177]. Surface emissive powers starting from 175 kW m^{-2} up to 350 kW m^{-2} were measured. Only during the Maplin Sands [178] and Montoir [179] tests, the mass burning rate was recorded, whereas most of the other cases have estimated this parameter based on the measured SEP. Generally, both approaches indicate the mass burning rate of 0.1 kg m^{-2} s^{-1}. The numerical models commonly adopted for the estimation of the thermal radiation generated by pool fire have been proved to be robust for a wide range of conditions and in agreement with most of the experimental data, especially for large scale scenario. However, the needs of combustion models accounting for soot formation has been indicated as one of the major improvement for full understandings on this subject [177].

The case of liquid hydrogen

Speaking of accidental release of cryogenic liquid, liquid hydrogen (LH_2) cannot be neglected. Indeed, this system offers several peculiarities to be discussed and studied, requiring customized models. Some considerations on the eccentricity of the electronic structure of the hydrogen atom are necessary. Following Pauli's exclusion principle, the total wave function for hydrogen molecule and wave function in the proton coordinates are antisymmetric [180]. Hence, only antisymmetric nuclear

spin and symmetric nuclear rotation (i.e., para-hydrogen) and symmetric nuclear spin and antisymmetric nuclear rotation (i.e., ortho-hydrogen) configurations are possible [181]. A schematic representation of the alternative configurations is provided in the following figure, where the electrons (E) and protons (P) positions and rotations are represented.

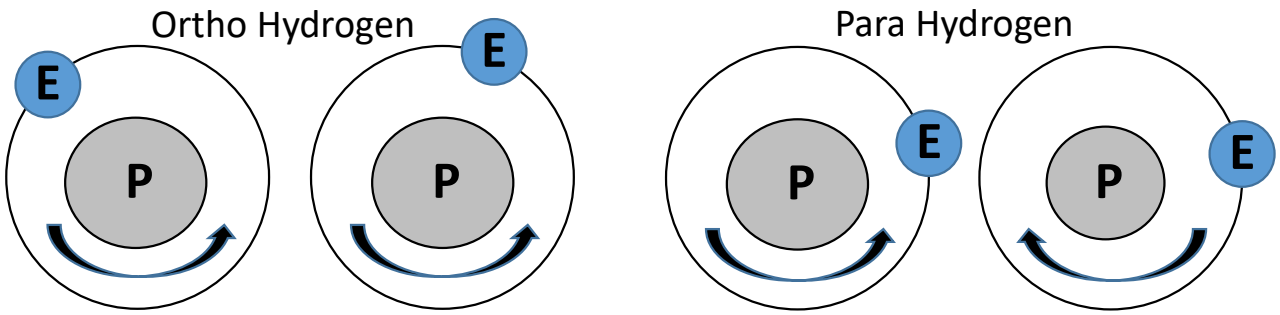

Figure 6. Schematic representation of the two alternatives electronic configuration (i.e., ortho and para) of hydrogen atoms.

The ortho-para content is usually negligible for the determination of the thermodynamic properties of all the species, but hydrogen and its isotopes represent an exception [182]. Besides, the ortho-para equilibrium is strongly dependent on the system temperature, when lower than 250 K [183]. Hence, distinguish these configurations is essential for low-temperature systems, only. Indeed, the utilization of catalytic units during the liquefaction process is required to hasten the conversion from the equilibrium composition at room temperature, referred to as normal hydrogen (i.e., 75 % ortho + 25 % para), to the most stable composition at boiling temperature, usually almost pure para-hydrogen [184]. This reversible transformation is accompanied by a significant heat release/absorption (up to 708 kJ/kg), thus higher than the hydrogen latent heat (h_{fg}, about 445 kJ/kg) [185]. Hence, it has the potential to play a significant role in temperature distribution in case of accidental release of hydrogen. Besides, variation in temperature profile affects the hydrogen density, thus its dispersion in the atmosphere. However, considering that regardless of the temperature hydrogen vapours are lighter than air, temperature differences should have a limited impact on the magnitude of the area where flammable mixtures can be observed for a given height. On the other hand, the abovementioned phenomenon may impact the gradient and hydrogen concentration with respect to height and time. Hence, it can create localized pockets characterized by a higher concentration of fuel. In this light, the implication of para-ortho transformation should be accounted for RPT scenarios.

To this aim, accurate estimations of the thermodynamic properties of both hydrogen configurations represent an essential step toward meaningful results. Considering the extreme conditions required (i.e., a temperature close to 20 K), high uncertainties could be expected for experimental measurements and strong non-ideal may affect the estimation quality of current models. For these

reasons, a comparison of the results obtained by both approaches should be done to corroborate the thermodynamic data and, thus, the analysis relying on them.

Several studies have addressed this issue experimentally throughout the last century [186][187][188], building a consistent database for the evaluation of para- and ortho- hydrogen properties. However, numerical models are not available for the estimation of these parameters. Considering the complete theoretical basis, quantum mechanics have the potential to cover this gap of knowledge and provide precise estimations. Besides, its accuracy can be tested by comparing the estimations with experimental data available.

Loss of control in reactive systems

Furthermore, safety evaluations at low temperature do not involve cryogenic fuels, exclusively. Indeed, several reactive systems present limitations related to the risk of an uncontrolled increase in heat production rates exceeding the heat removal heat, thus resulting in a self-accelerating reaction mechanism, lowering the yield to desired compounds and potentially damaging the surrounding structures. The positive feedback process is commonly referred to as a runaway reaction or thermal explosion. It has been proved that the presence of spontaneous exothermic and the exergonic reactions are thermodynamic conditions required for the occurrence of runaway [189]. Considering that exothermic reactions are favoured at low temperatures, the accurate evaluation of chemistry occurring under this condition is essential for runaway characterization, together with proper evaluations on the reactive temperature. The complexity and interconnections between these aspects suggest the implementation of integrated models combining kinetic and thermal phenomena. Again, the first can be addressed employing a detailed kinetic mechanism, whereas the latter requires customized evaluations based on the reactor layout. However, the power removed by the system (Q_e) can be written, in the most general form for a reactor as:

$$Q_e = Q_c + Q_s + Q_{loss} + Q_{ex} \qquad \textit{(Eq. 27)}$$

where Q_c is the convective heat exchange due to mass flow, Q_s is related to the mechanical energy dissipated by the agitator, Q_loss represents the heat losses, and Q_ex stands for the power removed by the cooling system. The term Q_c is related to continuous or semi-batch systems where inlet temperature differs from the bulk temperature within the reactor. It is worth saying that industrial reactors are thermally insulated for safety reasons (hot surfaces) and economic reasons (heat losses), making negligible the Q_{loss} for most of the applications. The mechanical energy dissipated by the

agitator Q_s, when present, is converted into viscous friction energy and finally altered into thermal energy. In most cases, especially for gas-phase reactions, this may be negligible when compared to the heat released by a chemical reaction. The last term of the right-hand side of the equation considers the actual heat exchange between the bulk of the reactants and the equipment system, which is typically prevalent in any process for other heat exchange processes. This term can be generically expressed as follow for a given surface (S), characterized by a wall temperature (T_w) and global heat transfer coefficient (U)

$$Q_{ex} = U \cdot S \cdot (T - T_w) \qquad \textit{(Eq. 28)}$$

Assuming U and T_w as constants along the reactor, a linear trend is obtained. Quite obviously, the heat exchange between reactive and cooling systems should be compared with heat produced by reactions (Q_r). In the first approximation, an exponential trend can by hypothesized to the temperature, following the Arrhenius equation. Hence, three different cases (resulting from $Q_{ex,1}$, $Q_{ex,2}$, and $Q_{ex,3}$ curves) were reported in Figure 7 as a function of temperature for different T_w, in compliance with the so-called Semenov theory [190].

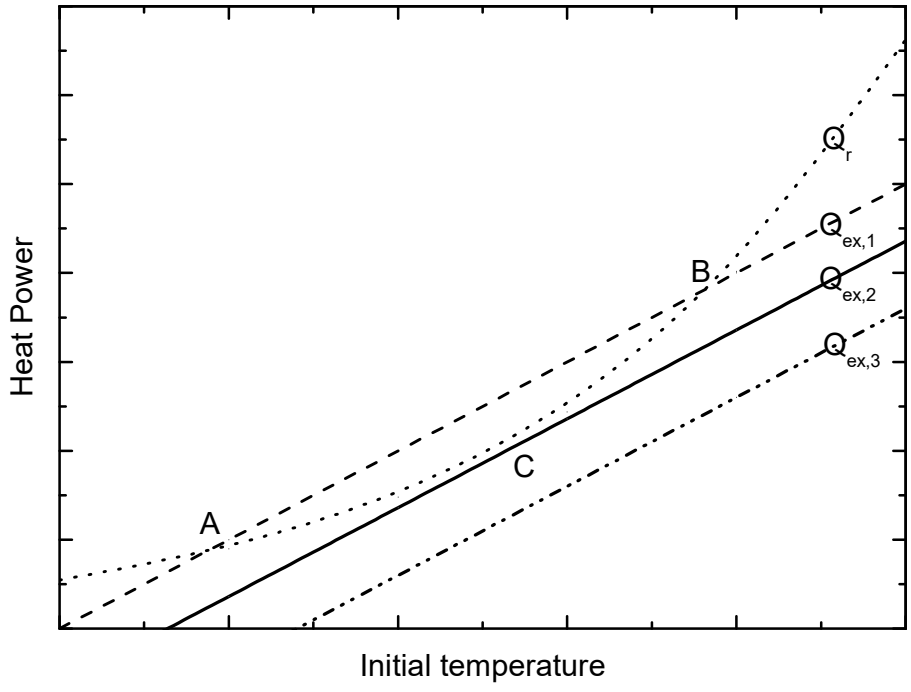

Figure 7. Representation of Semenov theory for runaway reaction characterization. Please note that Q_r represents the heat power generated by the reactions, whereas $Q_{ex,1}$, $Q_{ex,2}$, and $Q_{ex,3}$ are the heat power exchanged with the cooling system as a function of T_w. Intersections A, B, and C are identified.

Under these hypotheses, $Q_{ex,1}$ is the secant of Q_r, $Q_{ex,2}$ tangent of Q_r, and $Q_{ex,3}$ is external of Q_r. Besides, three different notable points can be identified, corresponding to the intersections between heat exchange and heat production curves. More specifically, *A* indicates a stable point since the reactive system tends to restore the initial conditions in case of variation in the initial temperature, i.e., $Q_{ex,1} < Q_r$ for lower temperature, and $Q_{ex,1} > Q_r$ for higher temperature. *B* is an unstable point because an increase in temperature leads to $Q_{ex,1} < Q_r$ conditions, thus it has a positive feedback effect. *C* is unstable, as well. Additionally, it delimitates the area where stable points cannot be obtained anymore. Hence, the T_w giving $Q_{ex,2}$ represents a critical value and can be indicated as $T_{w,c}$.

Several criteria for the identification of runaway conditions have been defined in the last decades based on the heat and mass balances of reactive systems [191]. Limiting conditions can be identified as the ones leading to the derivative of heat exchanged power and heat produced power [192]. Alternatively, maximum in reaction temperature, the concentration of desired species, or divergence of these parameters [193] have been indicated as monitoring functions for the individuation of critical conditions. Eventually, tailor-made sensitivity analysis has been developed [47] for the individuation of parameters largely affecting the global behaviour of the reactive system, thus promising as monitoring parameters.

Most of these approaches have been applied under the assumption of simplified chemical mechanisms, selected as representative of catalytic-related chemistry, neglecting the gas-phase reactions. However, the deviation from standardized operative conditions in case of ancillary system failures may lead either to variation in the elemental reaction steps involving the catalysts or the increase in relevance of homogeneous reactions. Hence, in both cases, model the chemistry with empirical-based catalytic reaction rates can generate significant errors. The integration of general, validated, and detailed kinetic mechanisms suitable for gas-phase reaction with heterogeneous models represents a solution for accurate characterization of a system prone to runaway reactions. Besides, this approach can guarantee the implementation of the quick, fair, and smooth (QFS) paradigm [194], i.e., can be adopted for the identification of operative conditions providing elevated conversion (quick onset), elevated selectivity (fair production), and safe conditions (smooth temperature profile), optimizing the existing process in terms of economic, environmental, and safety aspects.

Partial oxidation processes transforming light alkenes are clear examples of reactive systems controlled by safety limitations. Indeed, as several partial oxidations, the individuation of operative conditions reducing the risk of runaway reactions and guaranteeing sustainable selectivity and productivity is essential. Among the others, the production of ethylene oxide (EO) and propylene oxide (PO) have been intensively investigated because of their increasing market worldwide

[195][196]. Direct oxidation processes have been preferred because of the reduced impact on the environment [197]. To hinder the complete oxidation and promote the selectivity toward epoxidized products, tubular reactors surrounded by jackets for heat removal are preferred [14][13]. Although, the EO production process is well established and the catalytic kinetic mechanism well-known, room for improvement is still present [198]. Either oxygen- or air-based processes can be adopted. In the former case, the reactants are diluted by adding a significant amount of methane, acting as inert [14]. Typically, the reactor operates at around 30 bar, temperature included in the range 450 – 550 K, and using structured silver-based catalysts [199]. Further oxidation of the product of interests can be neglected thanks to the presence of proper additive in the catalysts formulation, resulting in a simplified mechanism including two parallel reactions, the partial and complete oxidations of ethylene, only [200]. On the contrary, the direct oxidation of propylene is a new trial on an industrial scale, optimized catalysts formulations are still under development [201]. Indeed, either silver- or gold-based catalysts are currently investigated [202]. The latter has been indicated as a more promising alternative because of higher catalysts activity at extremely low-temperature (i.e., around 350 K) [203]. In this case, a more complex kinetic mechanism than the EO case has been hypothesized, composed of parallel and consecutive reactions[203]. Simplified representations of EO and PO mechanisms were reported in the following figure, where simplified molecular input line-entry system (SMILES) notation [204] was adopted to represents the chemical species involved.

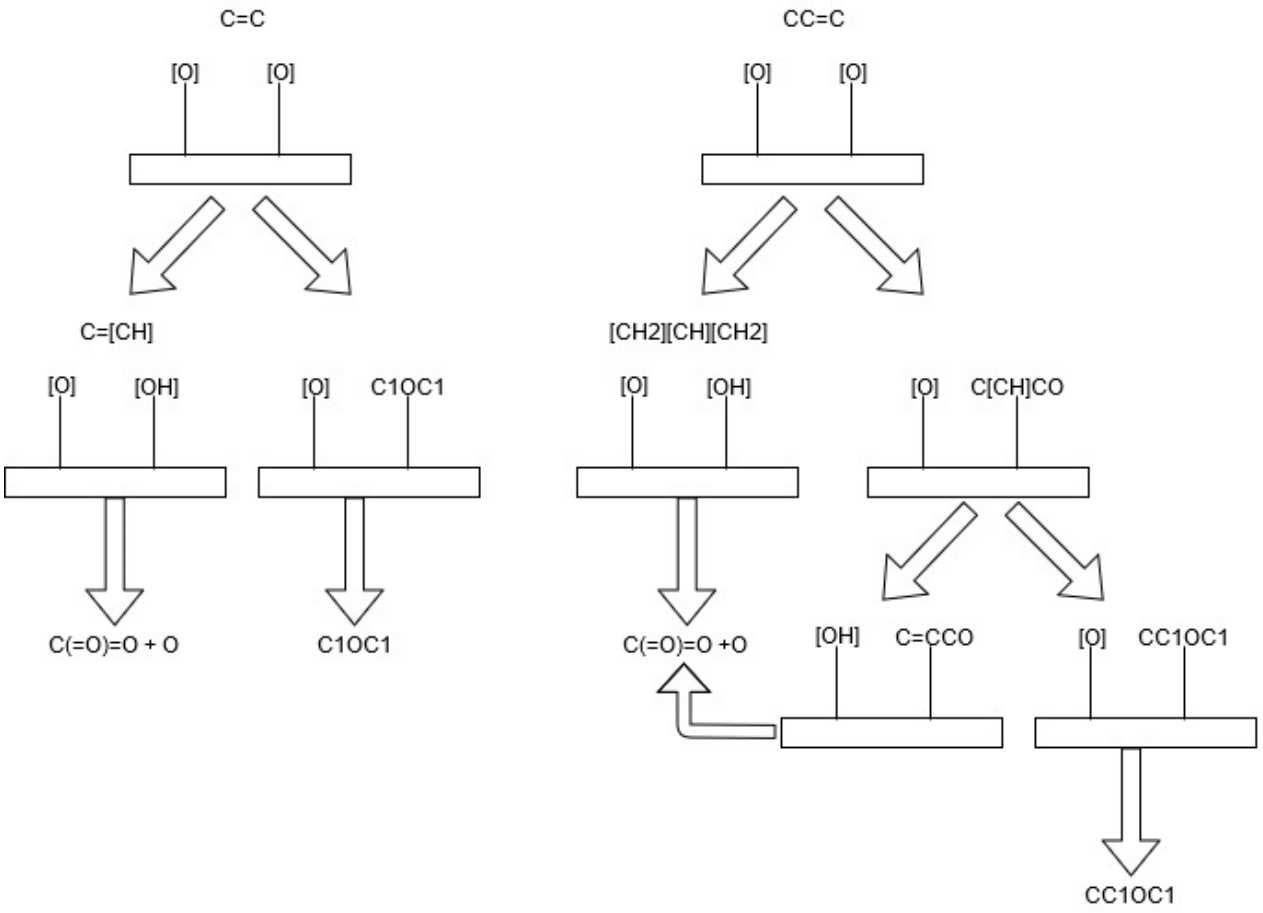

Figure 8. Schematic representation of the catalytic reaction mechanisms for direct oxidation of ethylene over silver-based catalysts (left) and propylene over gold-based catalysts (right) [203]. *Please note that species were expressed in terms of the simplified molecular input line-entry system (SMILES) notation* [204].

However, these mechanisms have been mainly studied for normal operative conditions, offering the flank to large discrepancies in case of outlier conditions due to loss of control of the reactive systems. Besides, considering the low level of maturity achieved for the rate coefficients to be included in the reaction scheme, the integration of catalytic kinetics with homogeneous rates deriving from a detailed kinetic mechanism is desirable, especially for the PO process. In this light, the implementation of a combined approach including kinetic mechanisms in CFD models may represent a useful feature for the application of quick, fair, and smoothed (QFS) paradigms for low-temperature partial oxidation processes. This concept aims to individuate operative conditions leading to the fast conversion of the reactants (quick) toward the desired products (fair), to satisfy the economic and environmental requirements of limited capital costs and by-product creation, in complete fulfilment of society needs (safe).

Section 2 – Adopted methodology

This section is devoted to the detailed description of the procedures, technologies, and features adopted in this project. Considering the nature of the investigations, two subsections were distinguished to collect and distinguish experimental and numerical information. An *ex-ante* overview of the procedure developed in this work, integrating these aspects is provided in the following paragraph.

Strategy for an integrated model for low temperature

Over the centuries, the typical approach to acquire knowledge has been based on the rigorous observation of physical and chemical phenomena, followed by theorization, i.e., model generation, and verification, i.e., model validation, of the posed assumptions, following the scientific method described by Galilei. The technological achievements, the increased complexity, and the number of variables involved in the investigated problems have required several practical modifications to this principle. Sometimes the addition of an intermediate step aiming at the validation of models through a comparison of simplified experimental systems is required. However, the key role of the validation is unchanged. To this aim, tailor-made experimental systems have been developed to neglect the influences of non-studied phenomena and reduce the number of unknown parameters. Indeed, laboratory-scale burners are designed to be as much as possible close to a laminar and mono-dimensional regime, to disregard turbulence by chemical and physical phenomena. These simplifications allow for the idealization of experimental systems for the sake of model implementation, making possible a proper comparison of numerical estimations and experimental measurements under comparable conditions. In this view, this work integrates experimental and numerical approaches. Bearing in mind the conditions under investigation, the laminar burning velocity was selected as a key parameter for the representation of chemical aspects. Besides, the heat flux burner was adopted because of the limited impact of turbulence and elevated “ideal” design. A theoretical-based detailed kinetic mechanism named KiBo (standing for Kinetic in Bologna) was generated via the application of RMG and tested against collected data. When a large disagreement between the results obtained by the different approaches was observed, additional investigations aiming at the model improvements were performed. Then, the validation step was repeated for all the investigated conditions, following the Deming’s cycle (also indicated as PDCA cycle, plan-do-check-act). Once satisfactory results were obtained, the kinetic mechanism was reduced to be implemented in computational fluid dynamic models and analyze real systems. The evaluation of the effects of input parameters on the output allowed for the individuation of optimized conditions either for the

design phase or the management and operative phase. A simplified representation of the procedure described is given in the following figure.

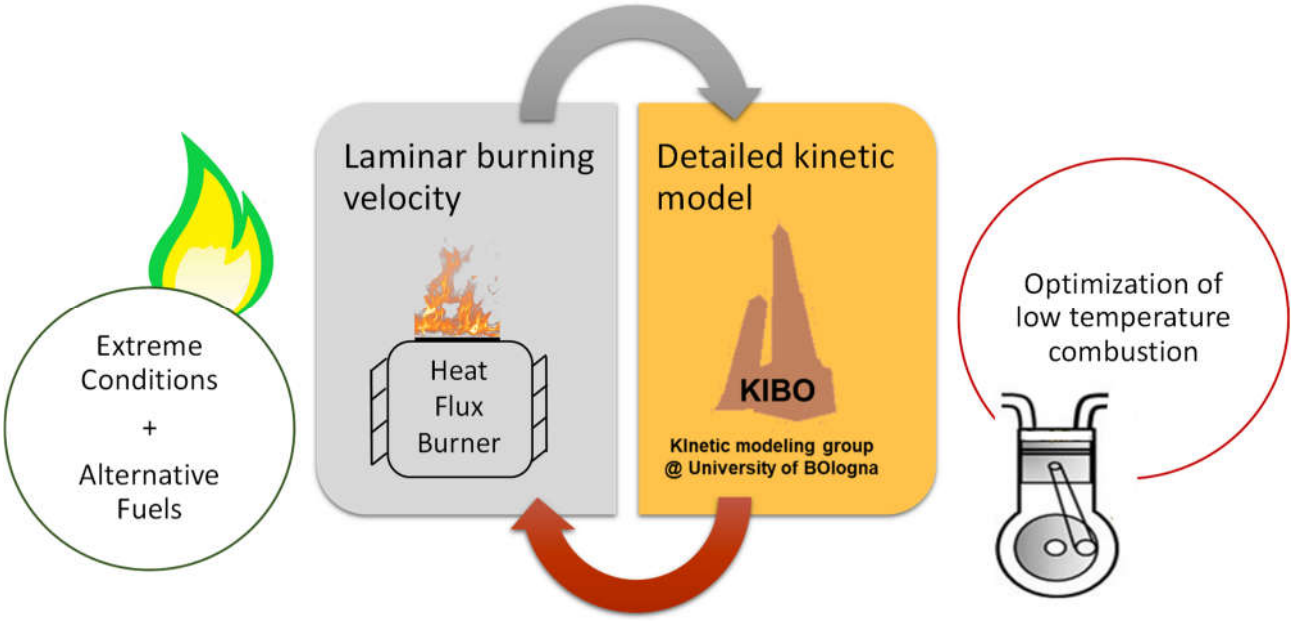

Figure 9. Schematic representation of the procedure adopted for the development and validation of a detailed kinetic mechanism for low-temperature applications.

Experimental procedure

This work presents an experimental analysis of the overall reactivity under low-temperature and atmospheric pressures. To this aim, laminar burning velocity data were measured through a heat flux burner. Detailed information on the theoretical background behind this system and describing the adopted procedure will be given in this paragraph.

Despite the considerable effort aimed at limiting systematic error sources in the aforementioned experimental systems, significant variation in the S_u can be observed, even for commonly studied conditions such as the methane/air mixture at standard conditions, as clearly indicated by Law (2012) [205]. In this sense, the HFM has the intrinsic potential to decrease the systematic error and the uncertainties related to the strain rate correction, because the S_u is obtained by interpolation instead of extrapolation procedure. On the other hand, the degrees of freedom potentially affecting the measured values and the related uncertainties, involving both design specification and operative conditions, still exist. As an example, different heating fluid temperatures were adopted by several research groups, e.g., 353 K [206], 355 K [207], 358 K [208], 363 K [209], and 368 K [210] were used as fluid temperature values to measure the laminar burning velocity at the unburned gas

temperature of 295 K. So far, it can be argued that the reported discrepancies in the set temperature can be attributed to the differences in the constructing material and the layout design of the adopted experimental system, or in the thermal properties of the heating fluid, i.e., thermostatic oil or water-fed in the burner jacket, or, eventually, in the initial temperature of the studied mixture. However, it should be noted that large discrepancies can be still observed if the plate temperatures are compared. Moreover, for the latter case, the difference between the jacket temperature and the unburned temperature was kept constant when the unburned gas was increased, although different values ranging from 40 K to 65 K were considered by the respective authors. These observations suggest a preliminary evaluation of the robustness of the adopted setup assessing the sensitivity of the obtained data to these parameters.

De Goey et al. (1993) [57] demonstrated that the presence of a stabilization system affects the temperature profile in a limited region close to the burner plate only, whereas the flame temperature of free and stabilized flames are equal. Since the HFM is based on monitoring the plate temperature, additional insight into the heat transfer phenomena occurring in the presence of a flame at the burner plate is beneficial for the evaluation of this technique.

The equations governing the heat and mass transfer at the burner plate, as reported in the general forms by Kee et al. (2003) [211], can be rewritten assuming the rotational symmetry of the system, steady-state conditions and neglecting the radial velocity of the gaseous mixture. However, considering that no reaction occurs on the plate surface and the experimental system is designed to avoid turbulence, the heat transfer equation can be expressed as follow (*Eq. 29*):

$$\rho c_p \left(v_z \frac{\partial T}{\partial z}\right) = -\left[\frac{1}{r}\frac{\partial}{\partial r}\left(k_p \cdot r \cdot \frac{\partial T_p}{\partial r}\right) + \frac{\partial}{\partial z}\left(k_p \cdot \frac{\partial T_p}{\partial z}\right)\right] \qquad \textit{(Eq. 29)}$$

where ρ is the density, c_p the heat capacity, v_z the axial velocity of the gaseous mixture, k_p the conduction coefficient of the plate, and r and z represent the radial and axial positions, respectively. The energy equation of the burner plate can be expressed as in *Eq. 30*:

$$h_b\left(T_p - T_b\right) - h_u(T_p - T_u) = \left[\frac{1}{r}\frac{\partial}{\partial r}\left(k_p \cdot r \cdot \frac{\partial T_p}{\partial r}\right) + \frac{\partial}{\partial z}\left(k_p \cdot \frac{\partial T_p}{\partial z}\right)\right] \qquad \textit{(Eq. 30)}$$

where h is the heat transfer coefficient per unit volume, and the subscripts p, b and u stand for the plate, burned, and unburned gaseous mixtures, respectively. It should be highlighted that a distinction was made between the unburned region (i.e., below the burner plate) and the burner region (i.e., above the burner plate), since a significant difference in the temperature regions may lead to relevant variation in the heat transfer coefficients and thermal properties. Indeed, the gaseous temperature can

be expressed as a function of both radial and axial positions. The former may vary from the temperature of the unburned gaseous mixture up to the adiabatic flame temperature, which is mainly dependent on the gaseous composition and fuel species for given initial temperature and pressure. Besides, considering the limited plate thickness (δ), the variation in plate temperature to the axial position is restricted. Hence, the heat transfer along the radial position can be expressed in terms of average temperature values ($T_{p,av}$). Besides, variation in the plate temperature to the radial and axial position is usually restricted to within 40 K in a single experiment, so that the effect of temperature on the conduction coefficient of the plate can be neglected, as demonstrated by Bosschaart and de Goey (2003) [57]. These assumptions lead to the formulation of an ordinary derivative equation for modelling the heat transfer phenomena on the burner plate and the definition of an averaged coefficient (*Eq. 31*):

$$h_b\left(T_p^{z=\delta} - T_b\right) - h_u(T_p^{z=0} - T_u) = \delta \cdot k_p \left[\frac{1}{r}\frac{d}{dr}\left(r \cdot \frac{dT_{p,av}}{dr}\right)\right] \qquad \textit{(Eq. 31)}$$

The left-hand side (LHS) of the *Eq. 31* can be expressed in terms of heat fluxes, assuming no dependence on the radial position, since S_u is considered the condition at which the net heat flux from the cooling jacket (q) is homogeneous for all radial positions. This parameter equals the difference between the heat gained from the burned gas (q^+), estimated by the first term of the LHS of *Eq. 31*, and the heat loss from the unburned gas (q^-), expressed as the second term of the same equation, resulting in a 1D flame [212]. The formation of stable 1D flames represents a crucial aspect for reduction of the uncertainties associated with the collected data, and thus to the validation of kinetic models, because of the strong interactions between chemical kinetics and molecular diffusion in the presence of convective transport and thermal radiation [16]. The parabola-shape curve commonly adopted for the representation of the temperature distribution of radial systems at a constant wall temperature [132] can be obtained by integrating for the radial position (*Eq. 32*).

$$T_{\mathrm{p,av}}\Big|_0^r = -\frac{q^+ - q^-}{4 \cdot k_p \cdot \delta} \cdot r^2 - \frac{q}{4 \cdot k_p \cdot \delta} \cdot r^2 = -\alpha \cdot r^2 \qquad \textit{(Eq. 32)}$$

In *Eq. 32*, the parameter α represents the parabolic constant, which was proposed as a ruling parameter for the determination of S_u through HFM by Van Maaren et al. (1994) [213], i.e., the adiabatic laminar burning velocity is assumed as the condition at which α is null, thereby resulting in a homogenous plate temperature. Eventually, *Eq. 32* can be re-arranged in terms of a dimensionless plate temperature ϑ (*Eq. 33*):

$$\vartheta = \left[\frac{T_{\mathrm{p,av}}(r) - T_{\mathrm{p,av}}(r_0)}{T_{\mathrm{p,av}}(R) - T_{\mathrm{p,av}}(r_0)}\right] = \left[\frac{h_b}{4 \cdot k_p \cdot \delta}\frac{\left(T_p^{z=\delta}(r) - T_b\right)}{\left(T_{\mathrm{p,av}}(R) - T_{\mathrm{p,av}}(r_0)\right)} - \frac{h_u}{4 \cdot k_p \cdot \delta}\frac{\left(T_p^{z=0}(r) - T_u\right)}{\left(T_{\mathrm{p,av}}(R) - T_{\mathrm{p,av}}(r_0)\right)}\right] R^2 \cdot \left(\frac{r}{R}\right)^2 = \quad \textit{(Eq. 33)}$$

$$= \left[Nu_b \frac{\left(T_p^{z=\delta}(r) - T_b\right)}{\left(T_{\mathrm{p,av}}(R) - T_{\mathrm{p,av}}(r_0)\right)} - Nu_u \frac{\left(T_p^{z=0}(r) - T_u\right)}{\left(T_{\mathrm{p,av}}(R) - T_{\mathrm{p,av}}(r_0)\right)}\right] \cdot \left(\frac{R}{4\delta}\right) \cdot \zeta^2$$

where Nu stands for the Nusselt number, defined as hR/k, calculated in the unburned and burned conditions, ζ the dimensionless radial position, ϑ the dimensionless plate temperature, and r_0 the centre of the plate. As is already known, the Nu can be estimated by using well-known empirical correlations. Usually, it is expressed in terms of Prandtl and Reynolds numbers [133], as:

$$Nu = A \cdot Re^{\beta} \cdot Pr^{\gamma} = A \cdot \left(\frac{S_u R}{\nu}\right)^{\beta} \cdot Pr^{\gamma} \qquad \textit{(Eq. 34)}$$

where A assumes a constant value for any given layout, ν represents the kinematic viscosity, and β and γ are constants. It is worth noting that the effect of temperature on dimensionless parameters is significantly affected by the species and conditions [214]. Quite obviously, α is strongly affected by the thermal properties of the burner plate material. Hence, the accuracy of the collected data is affected by this choice. To evaluate the effect of jacket temperature (T_j) on the collected experimental S_u the lumped parameter model, expressed in terms of Nu, can be applied to the gaseous mixture crossing the burner plate, assuming a homogeneous T_j as a boundary condition to the cylindrical wall and adiabatic conditions. This analysis complies with the experimental evidence produced by Hermanns (2007) [215] where negligible effects of T_j on T_b and S_u were reported for $T_{p,av}$ - T_j sufficiently large.

The experimental apparatus utilized in this project is hosted in the ProCEEd facilities at the University of Salerno. A simplified representation of the system adopted for the experimental characterization of kinetic behaviour at low temperatures and under the oxidative environment is given in Figure 10. Additional information and features on the burner plate geometry are presented in Figure 11.

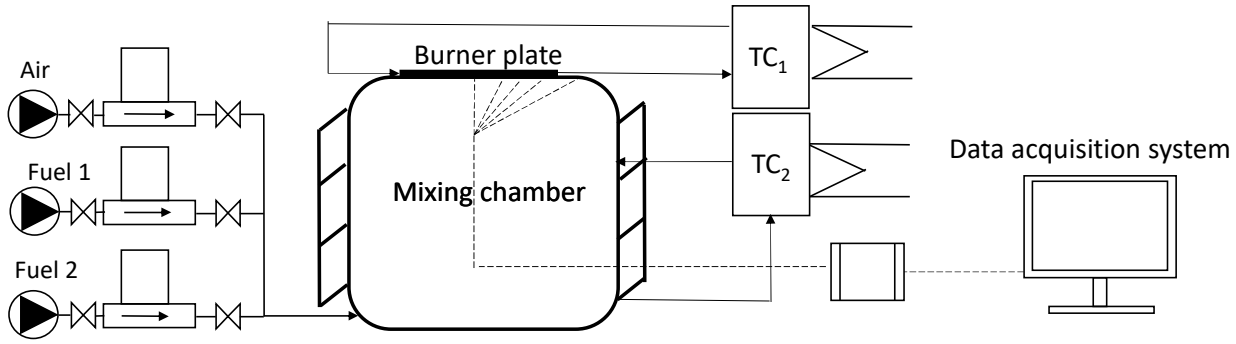

Figure 10. Schematic representation of the heat flux burner adopted in this work for the determination of the laminar burning velocity.

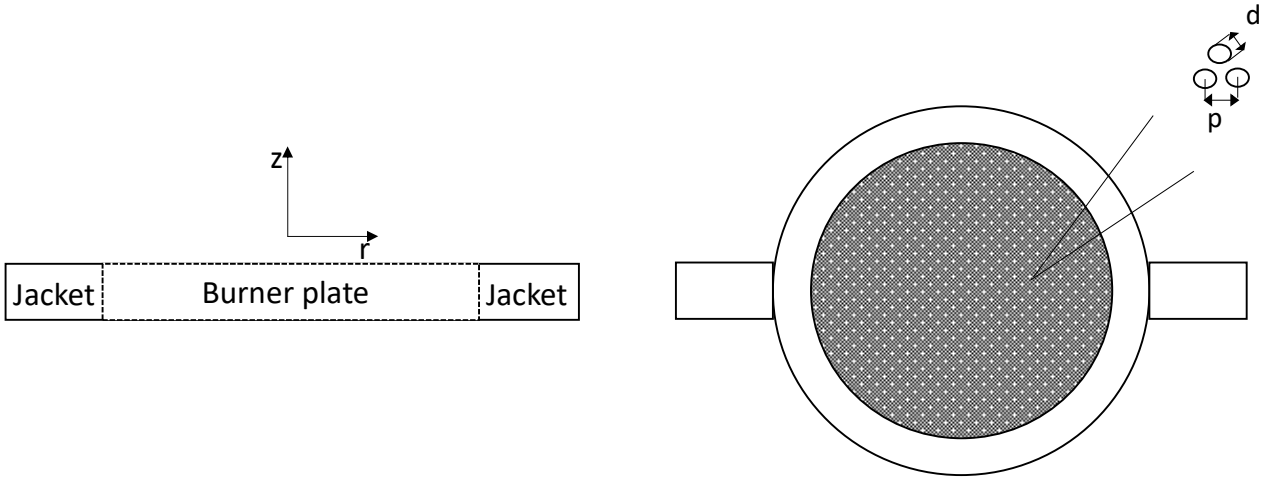

Figure 11 Representation of the side (left) and top (right) view of the heat flux burner adopted in this work.

The heat flux burner adopted in this work is composed of a feeding section, a burner, and a data acquisition system. In the first section, the gaseous stream flow rate and composition are controlled and mixed employing Bronkhorst mass flow controllers and pipelines, conveniently selected and designed to guarantee accurate composition and flow rate in the desired ranges, together with the achievement of complete premixing. The second section can be divided into three sub-sections. Indeed, it consists of 1) a plenum chamber, where the homogeneity of the temperature and composition of the gaseous mixture to the burner radius are guaranteed, 2) a perforated burner plate where the unburned mixture flows, and 3) two jackets, one surrounding the plenum chamber and the other surrounding the perforated plate. The first jacket avoids temperature gradient concerning the angular coordinate within the plenum chamber, the second jacket compensates the heat loss/gain from/by the plate to/from the environment, guaranteeing the validity of the "close to adiabatic" assumption. Ethylene glycol was fed in both jackets as ancillary fluid. The third section is devoted to the collection and representation of the evolution of the temperature profile of the burner plate to the

radius at different times. It consists of a data acquisition system connected with thermocouples conveniently located at different distances from the plate centre throughout the whole perforated plate. The measured temperature *T* to the radius *r* is commonly expressed as follow

$$T\,(r) = T_{r=0} + \mathrm{A} \cdot r^2 \qquad \textit{(Eq. 35)}$$

where *r*=0 corresponds to the plate centre, and *A* is the polynomial coefficient.

The first two sections of the experimental system allow for the representation of the resulting flame as a mono-dimensional, premixed flame. The last section represents the core of the measuring system. Indeed, the laminar burning velocity is considered as the feeding velocity that produces adiabatic conditions at the burner plate, i.e., *A* null. Hence, it is experimentally obtained by variating the inlet velocity and monitoring this parameter. However, stable flames cannot be obtained experimentally at adiabatic conditions via the HFM, thus interpolation is required to obtain *A* equal to zero.

Starting from these considerations, at least three sources of uncertainties can be identified. Indeed, the experimental error on the laminar burning velocity (δS_u) was calculated considering the uncertainties on temperature measurements ($\delta S_{u,T}$), on the unburned gas velocity ($\delta S_{u,v}$), and the interpolation process ($\delta S_{u,A}$) by using the following equation

$$\delta S_u = \left[\delta S_{u,v}^2 + \delta S_{u,T}^2 + \delta S_{u,A}^2\right]^{1/2} \qquad \textit{(Eq. 36)}$$

Similarly, a combination of the uncertainties of each mass flow controller (δx_i) was considered for the estimation of the uncertainties related to the equivalence ratio (δφ), under the procedure reported by Moffat (1988) [216]:

$$\delta\varphi = \left[\sum_{i=1}^{n}\left(\frac{\partial\varphi}{\partial x_i}\delta x_i\right)^2\right]^{1/2} \qquad \textit{(Eq. 37)}$$

where the partial derivative terms $\partial\varphi/\partial x_i$ represents the contribution of the variable x_i to the overall result of φ.

Preliminary investigations on the effects of jacket temperature were performed to assess the validity of the posed hypotheses and burner design. In particular, the temperature of the heating fluid flowing in the jacket surrounding the burner plate was variated within the range 343 - 368 K, whereas a temperature equal to the temperature of the unburned mixture was kept constant for the fluid flowing

through the cooling jacket. Both temperatures were controlled by thermostats. To this aim, pure methane and pure propane were tested since both species are characterized by similar flame temperature and burning velocity (and so global flow rate) under the studied conditions. This feature allows segregation of the effect of wall temperature on the determination of S_u utilizing the heat flux burner. Air has been adopted as an oxidant agent. Fuel/air mixture at room temperature and atmospheric pressure was analyzed is often considered the base case for the validation and evaluation of innovative experimental systems and procedures, due to the abundance of data and simplicity of handling alkanes premixed flames with air. Additional thermocouples were added to monitor the inlet and outlet temperatures of the ethylene glycol. The difference between the outlet and inlet temperatures of the heating jacket (ΔT_j) was monitored and adopted as an additional parameter for the demonstration of mono-dimensional assumption, i.e., the plate temperature was considered homogeneous to the angular axis when the measured ΔT_j was smaller than 1 K. Mixtures containing pure or high purity (i.e., > 99.5 %v/v) hydrogen, methane, carbon monoxide, ethylene, nitrogen, oxygen, propylene, carbon dioxide, and/or propane were investigated. Together with the already defined equivalence ratio (φ), the oxygen enrichment factor (E) and the fuel fraction (R) were adopted for the representation of mixture composition, under the following definitions:

$$E = \frac{z_{O_2}}{z_{O_2}+z_{N_2}} \qquad \textit{(Eq. 38)}$$

$$R = \frac{\omega_i}{\omega_{ref}} \qquad \textit{(Eq. 39)}$$

where z and ω stand for the mole fraction in oxidant agent and fuel, respectively. Besides, the subscripts N_2, O_2, i, and *ref* represent nitrogen, oxygen, generic species, and reference fuel. In this work, methane was utilized as reference fuel unless otherwise specified.

Numerical Procedure

Generation, validation, and accuracy evaluation of the kinetic mechanism

Detailed kinetic mechanisms usually consist of hundreds of species and thousands of reactions. The exact number is strongly affected by the species and range of operative conditions selected as a target, together with the methodology considered for their development. Considering the nature of the investigated phenomena, a wide range of temperatures was considered, i.e., from 250 K to 2000 K, to include the low-temperature chemistry and the core combustion mechanisms. On the other hand,

low and intermediate pressures, i.e., lower than 100 bar, were considered. The butyl acetate was selected as the target species. Taking into account the complexity of the chemical structure (i.e., the elevated number of carbon atoms together with the presence of an oxygenated group) and the lack of experimental data on butyl acetate chemistry suitable for validation purposes, the development of this model was distinguished into two phases. A core model describing the oxidative behaviour of light alkenes was built, at first. Once validated, it was considered as a building block for a more comprehensive model including the chemistry of larger species, as well. Butene isomers were selected as demarcation lines because of their production from primary reactions involving butyl acetate and representativeness of core combustion discussed in the previous section. Besides, their overall reactivity has been largely studied either experimentally or numerically [105], and several reaction coefficients have been calculated employing accurate methods [217][218]. The latter was included in the library for model generation, together with thermodynamic and kinetic libraries considered as a benchmark for small species (< C_2). These libraries and boundary conditions were implemented in RMG for the generation of a so-called "first attempt mechanism". To this aim, a threshold value regulating the migration of the species from the edge to the core was set equal to 0.01. Also, a new iteration was started once a flux larger than 0.2 was reached for any species, to avoid abrupt variations in a single step. To bound the memory required during these simulations, the number of species allowed in the edge was limited to 100'000, whereas the number of carbon and oxygen atoms allowed per molecules were limited to 15 and 8, respectively. These values were selected much larger than credible species potentially involved in the investigated system, as a conservative assumption, to include all pathways potentially describing the chemistry. Similarly, a termination time of 50 s was adopted. The formation of biradicals was allowed. Absolute and relative tolerances of 10^{-16} and 10^{-8} were implemented. For the sake of simplicity, nitrogen was considered an inert at this stage. Rate of production (ROP) and sensitivity analyses were performed to individuate the main products and properties having a larger impact on the produced model. In both cases, absolute and relative tolerances of 10^{-6} and 10^{-4} were considered. The intermediate species highlighted by ROP analyses were considered as measurables for sensitivity analyses. The effect of either thermodynamic or kinetic properties on the model was evaluated per each measurable included in terms of NSC. Species and reactions within the model were sorted by the absolute value of NSC, keeping the separation between data obtained at different conditions and targets. The accuracy associated with the sources considered as input for species and reactions occupying the first 30 positions of each ranking were evaluated. More specifically, ab initio calculations performed by using the CBS-QB3 level of theory or higher were accepted. Inputs estimated with lower levels or via group additivity approaches were rejected. To fill the generated gap, quantum mechanics calculations were performed, the calculated

properties were, then, added to the proper library. More specifically, a "first guess" geometry was hypothesized for the analyzed species, when thermodynamic data were calculated, or for transition state, when kinetic coefficients were calculated. To optimize the computational costs, energy and forces were calculated with a low-level of theory (i.e., ub3lyp/6-31g(d)), at first, to guarantee a feasible geometry and then calculations were repeated at a higher level (i.e., CBS-QB3) to obtain the lowest energy geometry. The former was named geometry job, whereas the latter conformer job. Rotor scans, in routable bonds, are present, were performed implementing the hindered rotor 1-D approach. In other words, one routable dihedral was rotated per time. The round angle was divided into 45 sections of 8 degrees. The energy-related to the optimized geometry was calculated per each configuration. The absence of configuration having lower energy than the initial one was considered as a monitoring parameter. Indeed, in case a lower energy configuration was found, the described procedure was repeated from the conformer job step, to avoid the utilization of local minima. Afterwards, the bond frequency was calculated for the optimized geometry. Eventually, the obtained information was inserted in the automated reaction kinetics and network exploration (ARKANE) [219] tool for the evaluation of the required properties. The thermodynamic calculations were automatized by the open-source code automated rate calculator (ARC) [220]. The obtained properties were included in the libraries considered by RMG, whereas the other settings were unchanged. Under these renewed inputs the described procedure was repeated until the combination of ROP and sensitivity analyses indicates most impacting species and reactions having accurate properties. The iterative procedure integrating RMG and ARC tools was sketched in the following figure.

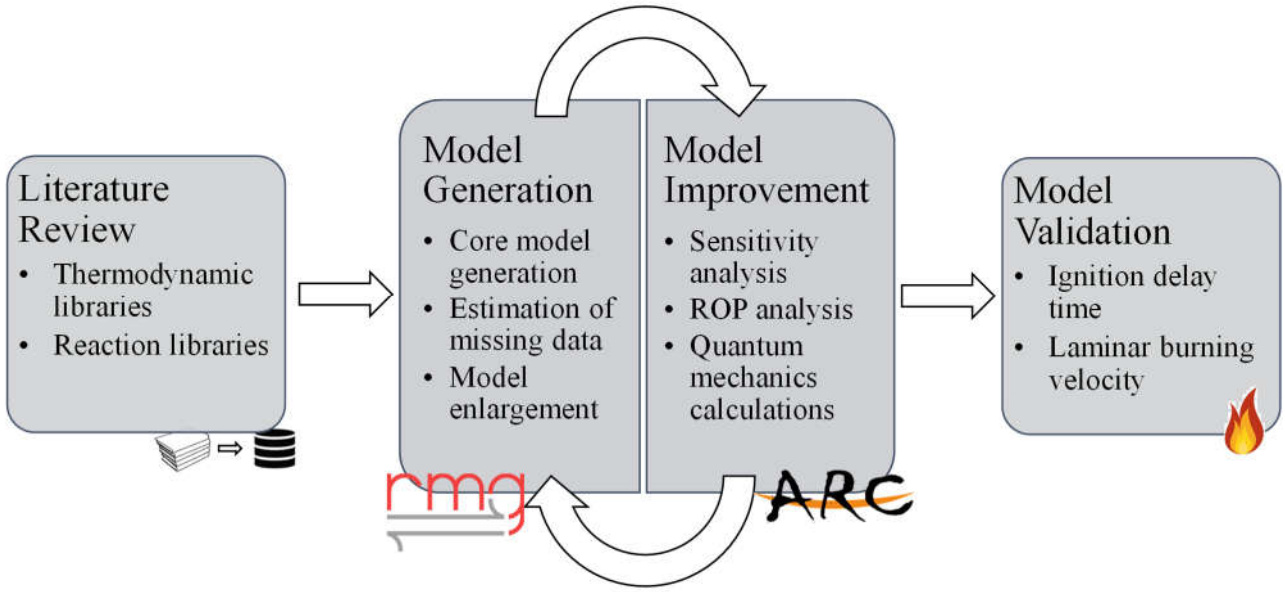

Figure 12. Workflow for automatic generation and validation of detailed kinetic modelling developed in this work.

Additional information on the validation step (indicated with a grey arrow in the previous figure) will be provided in the following. The described procedure was implemented for all the target species investigated in this work (i.e., butene and butyl acetate isomers). Nevertheless, minor modifications were necessary for the successful implementation of this method for the butyl acetate case. Indeed, under the investigated conditions, butyl acetate may undergo retro-ene reactions, that were not included in the reaction family library implemented in RMG. Hence, a new family was generated; accurate coefficients for retro-ene reactions, preferably involving species having a molecular structure similar to butyl acetate, were retrieved [221] and adopted as a training set for the estimation of these rates. The developed model was validated against experimental data collected in this work and retrieved from the current literature. To this aim, laminar burning velocity and ignition delay time were considered being representative of chemical phenomena from low- to high- temperatures, as detailed discussed in the previous section. A tailor-made script based on Cantera [222] suite was developed for the estimation of these properties. The S_u simulation was carried out by assuming one-dimensional flame, adiabatic and steady-state conditions, as well as by using the Newton iteration technique to solve the mass and thermal balances. A grid sensitivity analysis was performed to evaluate the robustness of the obtained results and optimize the simulation parameters, i.e., S_u and computational time was evaluated by varying the refining grid parameters one at a time. Ratio, slope, and curve were variated within the range of 0.01 – 1.00. These parameters represent the maximum fractional change in the solution and derivative of adjacent grid points, respectively (see [222] for more details on the grid parameters). The S_u of stoichiometric butenes/air mixtures at 298 K were calculated for each set of values of refining parameters. For the sake of clarity, the normalized results for butene isomers are shown in Figure 13. The S_u obtained by varying the grid parameters were normalized by the corresponding maximum (i.e., asymptotic) value. It is worth noting, that no relevant effect of fuel composition on normalized S_u was observed among the analyzed isomers, thus the results corresponding to the most reactive isomer (i.e., 1-butene) were reported, exclusively. Results for curve and slope were reported exclusively since the variation of S_u to the selected value of ratio was found negligible.

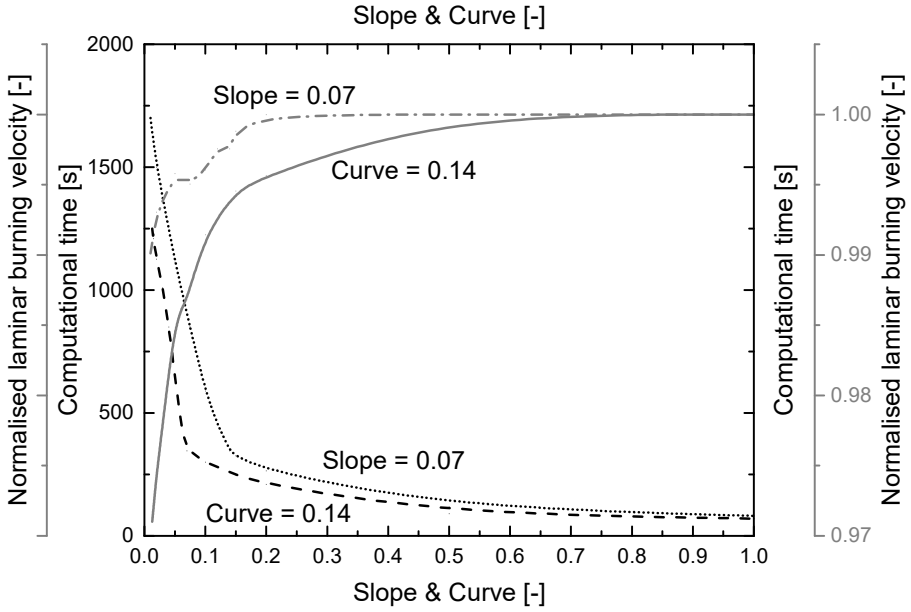

Figure 13. Grid sensitivity analysis in terms of normalized laminar burning velocity and computational time to slope and curve.

The computational time may be fairly represented by a logarithmic trend to the grid parameters, either slope or curve, whereas normalized S_u oscillation is limited. Indeed, discrepancies smaller than 1% were observed when the slope was kept constant, whereas variations up to 3% were reported when the curve assumes a constant value. Previous studies have shown similar results for methane/air mixture, as well [223]. A slight decrease of slope or curve values means a significant increase in computational time; thus, the selection of these parameters can be optimized considering both accuracy and simulation costs. Eventually, the values of 0.07 and 0.14 for the slope and the curve, which are commonly adopted for the detailed kinetic analysis [5], were considered for the following analyses on the kinetic models. The resulting total grid points number was about 170-250, the relative error criteria (RTol) and absolute error criteria (ATol) were $1.0 \cdot 10^{-9}$ and $1.0 \cdot 10^{-14}$ for the steady-state problem, and $1.0 \cdot 10^{-5}$ and $1.0 \cdot 10^{-14}$ for the time stepping problem (used by the code as a first attempt solution), respectively. Similarly, the IDT was calculated by using a tailor-made script simulating a transient reactor, under the assumptions of premixed reactants, monodimensional, isochore, and adiabatic conditions. Temperature, pressure, and composition were calculated along the time via traditional mass and energy balances. An adaptive grip with a maximum time step of 10^{-5} s was imposed. Additional steps were simulated until the maximum concentration in OH was reached. The time corresponding to this condition was considered as IDT. The evaluation of the overall reactivity in a single parameter, such as S_u and IDT, allows for the quantification of kinetic mechanisms accuracy, thus facilitates the comparison of different methodologies and approaches adopted for model construction. In this view, the implementation of statistical indicators makes possible the unification of estimation accuracy obtained by different properties and in different conditions. More

specifically, the quadratic sum of the difference between the generic numerical prediction ($\psi_{Num,i}$) obtained at given conditions and the corresponding experimental measurement ($\psi_{Exp,i}$) was normalized for the product of the corresponding average values ($\psi_{Num,av} \cdot \psi_{Exp,av}$) and the number of observations (N) to estimate the dispersion from the true value (*Eq. 40*). This parameter was referred to as normalized means square error (NMSE) from now on. The average offset from the true value was, instead, expressed in terms of fractional bias (FB) (*Eq. 41*).

$$NMSE = \left(\frac{\sum_i^N (\psi_{Num,i} - \psi_{Exp,i})^2}{N}\right) / (\psi_{Num,av} \cdot \psi_{Exp,av}) \quad \textit{(Eq. 40)}$$

$$FB = \left[\sum_i \alpha_i \cdot (\psi_{Exp,i} - \psi_{Num,i})\right] / [0.5 \cdot \sum_i (\psi_{Exp,i} + \psi_{Num,i})] \quad \textit{(Eq. 41)}$$

The coefficient α assumes a value of -1 or 1 for S_u and IDT, respectively, to guarantee that in both cases the higher the FB is, the higher the estimated reactivity. Based on their definition, the ideal model has NMSE and FB equal to zero. However, models can be considered reliable if the absolute value of FB is smaller than 0.5, and the NMSE resulted smaller than 0.3 [224]. Among the detailed kinetic mechanisms available in the literature for the oxidation of hydrocarbons (see Table 1 for further details), only a part distinguishes the chemistry of isomers of butene. Considering the relevance of these structures for this investigation, additional attention was paid to this fraction, exclusively. In particular, JetSurF [88], LLNL (n-heptane) [90], LLNL (butanol) [91], MIT (butanol) [92], CNRS [98], and Aramco [102], Creck [103] models were selected as representative of the available approaches. Indeed, models obtained by the implementation of either empirical, knowledge-based, and automatized approaches were included in this list. Besides, the newest version was considered if the same core was adopted in other models. Besides, different strategies for the estimation of reaction rate coefficients were compared. Indeed, models considered for this analysis present coefficients derived from theoretical calculations, estimation rules, or "adjusted" values. Quite obviously, the first category should be preferred, when available, whereas the latter is prone to be effective in a narrowed interval of conditions and may result in large errors in case of extrapolation.

Detailed characterization of accidental scenarios caused by cryogenic releases

Regardless of the investigated scenario, the accidental release of cryogenic fuels in the atmosphere was modelled assuming a liquid pool already formed on the substrate. Then, this system was conveniently divided into two sub-systems: one containing the liquid fuel and the substrate only and another one including vapour, air, and solid obstacles (if considered). The first sub-system provides

the mass flux, vapour composition, and temperature to time, as the main results. These data were considered as boundary conditions for the second sub-system. This approach aims to save computational time, because of the significantly different scale of the investigated phenomena, affecting the mesh size. A further distinction can be done based on the state of the substrate. More specifically, both concrete and water were investigated as being representative of release on solid and liquid, respectively. Considering the literature review reported in the previous section, the Reed model was implemented in case of release on solid, whereas the Klimenko model was utilized for the liquid case. Additional information on the governing equations adopted in this work can be found elsewhere [225]. To decrease the uncertainties, especially at low-temperature, ab initio calculations were performed to estimate the thermodynamic properties of some of the species composing the cryogenic fuels analyzed (i.e., hydrogen, methane, ethane, and propane) and air. Para and ortho hydrogen were distinguished at this stage.

In the case of the presence of an ignition source, pool fire was modelled by integrating detailed kinetic mechanisms in computational fluid dynamic models. The utilization of detailed kinetic mechanisms as they are is limited to simplified layouts and fluid dynamics because of the available computational power. In this view, kinetic models are commonly reduced to broader their applicability. This approach lays the foundation on the individuation of the most representative pathways and species for the investigated conditions. Indeed, reducing the size with negligible effects on accuracy means narrow the operative conditions accounted for the model. Hence, the most representative values should be individuated by carefully evaluating the investigated scenarios. In the case of pool fire resulting from the accidental release of cryogenic fuels, the model can be focused on the atmospheric pressure and temperature variating from the storage and the adiabatic flame temperatures. The individuation of the most relevant species and reaction paths can be obtained by a combination of ROP and sensitivity analyses. Indeed, the former may provide the main intermediates for the most abundant species in the burned mixtures, whereas the latter may highlight the reactions having a larger impact on intermediates production/consumption. The settings reported before for ROP and sensitivity analyses were adopted in this case, as well. The ranges of temperature and pressure were divided into 12 sections. Median values were coupled to form all possible combinations (T, P). The species or reactions having NSC smaller than 0.1 were deleted. A simplified representation of the proposed strategy is given in Figure 14.

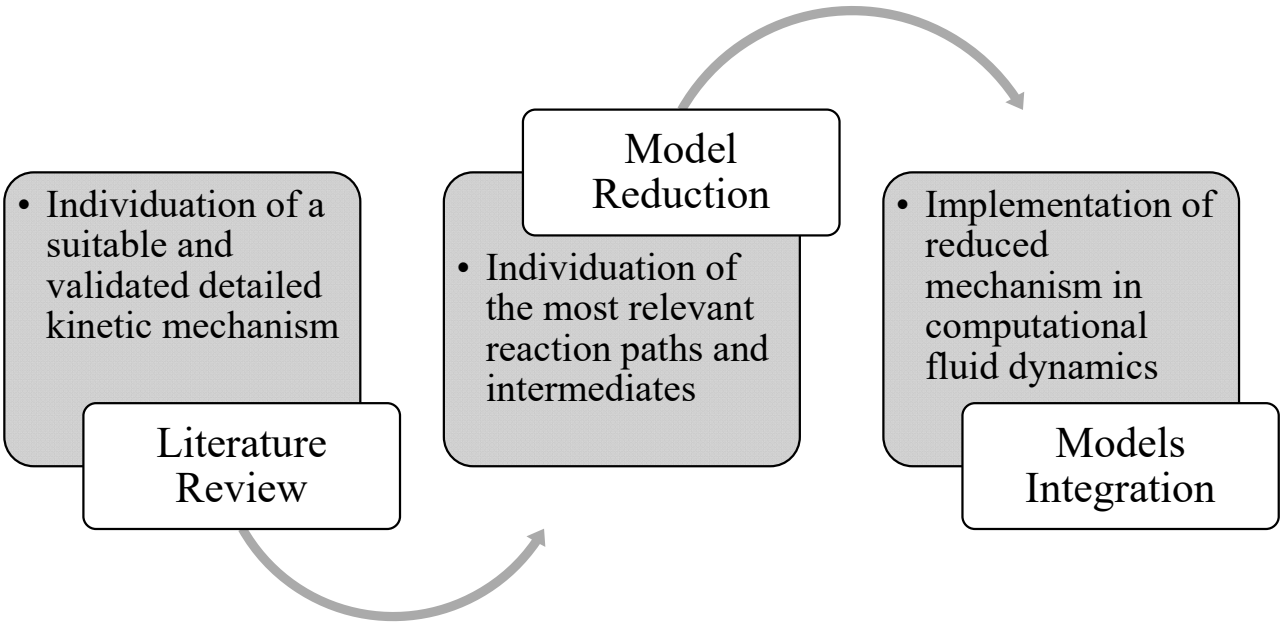

Figure 14. Procedure for the accurate representation of reactive systems adopted in this work.

Because of the dearth or inconsistency of experimental data characterizing cryogenic fuels, the proposed methodology was validated against experimental data collected for aviation fuel pool fire. A surrogate mixture consisting of 92 %v/v of n-decane and 8 %v/v of toluene was adopted, in agreement with detailed analyses aiming at the optimization of the composition of surrogates based on physical, chemical, and safety parameters of real aviation fuels [226]. Also, boundary conditions describing the pool geometry and atmospheric conditions were reported in Table 5.

Table 5. Summary of boundary conditions characterizing aviation pool and atmospheric conditions.

Boundary Conditions	**Values**
Pool Surface [m^2]	49.32
Pool Volume [m^3]	8.35
Air Temperature [K]	298
Pressure [kPa]	101.32
Wind Velocity [m s^{-1}]	0.85

These and additional conditions were set to mimic the initial conditions reported on the technical documentation related to the experimental campaign conducted by Sandia national laboratory for the characterization of open pool fire [227].

Once the procedure was validated, a pool fire caused by the accidental release of LNG was analysed. To this aim, different compositions were considered, as reported in Table 6.

Table 6. Summary of the composition of the LNG pool analyzed in this work.

Mixture	**CH_4 [% v/v]**	**C_2H_6 [% v/v]**	**C_3H_8 [% v/v]**
LNG 1	100	0	0
LNG 2	90	10	0
LNG 3	80	10	10

Additional information on geometric (e.g., computational domain and mesh size), atmospheric conditions (e.g., wind speed), and thermal (e.g., heat transfer coefficients of the substrate) boundary conditions can be found elsewhere [226][228].

Similar assumptions were posed for the estimation of the evaporation rate and pool formation in case of accidental release of liquid hydrogen, as well. Particular attention was posed to the scenario resulting from the absence of an ignition source, because of the peculiarity of ortho-para hydrogen transformation at low-temperature discussed in the previous section. More specifically, the overpressure generated by the local variation in specific volume was evaluated and compared with typical threshold values accounting either for humans or structures as targets [229]. For the sake of comparison, the case where the ortho-para conversion was neglected was considered, as well.

The availability of a detailed kinetic mechanism suitable for low-temperature conditions allows for the estimation of the flammability limits at a temperature below room conditions via the implementation of the limiting laminar burning velocity theory detailed discussed in the previous section. The estimation of the lower flammability limit at ultra-low temperature has potentially a significant impact on the characterization of accidental scenarios where reactions do not occur, as well. Indeed, in the case of dispersion of flammable vapour the safety distances are calculated based on the size of the flammable cloud. It has been demonstrated that for the evaluation of safety distance associated with flash fire scenario, pure methane represents the most conservative assumption because of the increase in molar weight due to ethane and propane resulting in smaller and less lasting flammable areas [230]. Besides, comparing the density of cryogenic fuels at a temperature from their boiling temperature to the ambient conditions with the density of air, the dispersion of LNG only represents a major concern. Indeed, hydrogen results lighter than air at any temperature, thus its flammable area has a limited footprint. Hence, the investigations addressing the flash fire scenario performed in this work were restricted to the characterization of LNG 1 composition (i.e., pure methane). More specifically, the boundary conditions considered at this stage can be summarized as in Table 7.

Table 7 Summary of the boundary conditions adopted for the evaluation of LNG dispersion.

Parameter	Value
Room temperature [°C]	25
Atmospheric stability class [-]	D, F
Wind velocity [m s^{-1}]	2, 5
Wind direction [-]	Positive x-direction
Relative humidity [%]	40, 70
Fuel composition [-]	Pure methane
Fuel temperature [°C]	-161.55
Released volume [m^3]	1
Pool diameter, D [m]	5.0 - 6.4
Pool depth [m]	0.03 - 0.05
Evapouration rate [kg m^{-2} s^{-1}]	0.071 - 0.195
Heat flux from water [W m^{-2}]	0 - 313.5

The base case scenario was defined as the one having atmospheric stability class, wind velocity, relative humidity, pool diameter, evaporation rate, and heat flux from water surface equal to D, 5 m s^{-1}, 40 %, 5.4 m, 0.071 kg m^{-2} s^{-1}, 313.5 W m^{-2}, respectively.

Besides, the dispersion safety factor (DSF) and cloud shape factor (CSF) were defined to express the size of the flammable area on the downwind axis (x_{LFL}) vertical axis (y_{LFL}) and the extension of visible cloud on the downwind axis (x_{Vis}).

$$DSF = \frac{x_{LFL}}{x_{Vis}} \qquad \textit{(Eq. 42)}$$

$$CSF = \frac{x_{LFL}}{y_{LFL}} \qquad \textit{(Eq. 43)}$$

The visible cloud was delimited by equalizing the ambient temperature (T_a) to the dew point (T_{dew}), calculated as a function of the relative humidity (H) via Bosen's correlation [231].

$$T_{dew} = \left(\frac{H}{100}\right)^{\frac{1}{8}} (112 + 0.9 \cdot T_a) + 0.1 \cdot T_a - 112 \qquad \textit{(Eq. 44)}$$

The differences between boiling and ambient temperatures may cause abrupt variations to the evaporation rate, resulting in instabilities. Indeed, phase changes generate a local decrease in specific volume potentially producing significant overpressure, i.e., RPT scenarios. In this view, this work included numerical investigations on the RPT of LNG and LH_2.

Detailed characterization of partial oxidation processes

The specification of the reactor layout considered may help to report further understandings achieved and the identification of the existing lack of knowledge. In this light, this section will be devoted to the analysis of a tubular reactor, being the commonest for large scale chemical plants devoted to partial oxidation processes. Alternatively, a detailed description of the existing models for the representation of the alternative geometries can be found in dedicated reviews and investigations [232][193][191]. Commonly, the industrial processes are schematized by using a set of apparent reactions, accounting either for homogeneous or heterogeneous reactions representative at normal operative conditions. However, in case of a large deviation from these conditions, the evaluation of reaction rates via extrapolation may be a source of significant inaccuracy. In this light, a detailed kinetic mechanism merging elemental reactions and catalytic, apparent reactions was compared with a simplified model including catalytic pathways, only. Henceforth, the former will be indicated as a comprehensive mechanism, whereas the latter as a catalytic mechanism. Both models were implemented for the evaluation of real process equipment. However, for the sake of clarity, only the governing equation reporting the catalytic mechanism will be provided. Assuming a multi-tubular reactor characterized by plug flow regime, fed by a fluid mixture having a density ρ_r and specific heat capacity $c_{p,r}$ with a volumetric flow rate $\dot{v}$, in steady-state conditions, the energy equation can be written as

$$\dot{v} \cdot \rho_r \cdot c_{p,r} \cdot dT = -\sum \Delta H_{r,i} \cdot r_i \cdot dV + U \cdot (T - T_w) \cdot dS \qquad \textit{(Eq. 45)}$$

where the heat of reaction and reaction rate of the generic reaction *i* were indicated with $\Delta H_{r,i}$ and r_i, respectively. Alternatively, for the sake of more comprehensive generalization, the variation of the dimensionless temperature θ along the dimensionless reactor length *z* can be expressed as:

$$\frac{d\theta}{dz} = Da \cdot B \cdot \sum(\Delta H_r \cdot R_r \cdot R_i) - St \cdot (\theta - \theta_{Co}) \qquad \textit{(Eq. 46)}$$

where *Da, St*, *R*, and *B* stand for the Damkhöler, Stanton numbers, dimensionless reaction rate, and heat to reaction parameter. It is worth noting that the subscript *Co* stands for cooling fluid, whereas *r* is introduced to represent the ratio between the generic reaction i and the desired reaction 1, selected as a reference for the definition of the dimensionless numbers mentioned before and here explicated

$$Da = \frac{(r_1 \cdot L)}{v \cdot c_{a,1}} \qquad \textit{(Eq. 47)}$$

$$St = \frac{4 \cdot U \cdot L}{d_t \cdot v \cdot \rho \cdot c_p} \qquad \textit{(Eq. 48)}$$

$$R_i = exp\left[\frac{\left(\theta \cdot \frac{E_{a,i}}{R_g \cdot T_0}\right)}{\left(\theta + \frac{E_{a,1}}{R_g \cdot T_0}\right)}\right] \cdot x_{a,i}^{n_i} \quad \textit{(Eq. 49)}$$

$$B = \frac{\left(\Delta H_1 \cdot c_{a,1} \cdot \frac{E_{a,1}}{R_g \cdot T_0}\right)}{\rho \cdot c_p \cdot T_0} \quad \textit{(Eq. 50)}$$

in which the subscripts 0, 1, a, and t correspond to initial conditions, the desired reaction, limiting reactant of a given reaction, and tube, respectively. Whereas *c*, *d*, E_a, *L*, R_g, and *v*, are concentration, diameter, activation energy, reactor length, ideal gas constant, and gaseous velocity. Similarly, the dimensionless mass balance for a generic species (j) can be expressed as

$$\frac{du_j}{dz} = Da \cdot \sum(\nu_i \cdot R_r \cdot R_i) \quad \textit{(Eq. 51)}$$

assuming *u* as the dimensionless concentration, corresponding to the ratio between the concentration of j and the initial concentration of the limiting reactant *a*. Eventually, the heat balance for the cooling fluid can be expressed as

$$\frac{d\theta_{co}}{dz} = \tau \cdot St \cdot (\theta - \theta_{co}) \quad \textit{(Eq. 52)}$$

where τ represents the ratio between the heat capacity of reacting fluid to the heat capacity of the cooling system so that the product $\tau \cdot St$ indicates the ratio between heat exchange and heat capacity of the cooling system.

$$\tau = \frac{w \cdot c_p}{w_{co} \cdot c_{p,co}} \quad \textit{(Eq. 53)}$$

In which w stands for mass flow rate. An overview of the boundary conditions implemented for the characterization of ethylene oxide and propylene oxide processes is provided in Table 8.

Table 8. Operative conditions investigated in this work for ethylene and propylene direct oxidation processes, respectively indicated as EO and PO.

	EO	**PO**
Temperature [K]	400 – 500	320 – 400
Pressure [bar]	10 - 22	1.0 – 1.5
Alkene (molar fraction)	0.15 – 0.40	0.10
O_2 (molar fraction)	0.05 – 0.10	0.10
H_2 (molar fraction)	-	0.10

Different criteria were defined to distinguish the operative areas, i.e., hot spot (HS), runaway (RUN), and pseudo-adiabatic operative (PAO) conditions, accounting for economic, safety, technological aspects. More specifically, the threshold value (θ_{tr}), the maximum in reactor temperature (θ_{max}), and the maximum rise in temperature $(d\theta/dz)_{max}$ were defined as monitoring parameters to avoid undesired degradation, including catalysts sintering and reactants combustion. Similarly, the maximum content of the desired species ($u_{b,max}$) was defined to monitor the production of undesired species. Additionally, the runaway regions were individuated by using the well-established divergence criterion developed by Strozzi and Zaldivar criterion (SZ) [233], defining the runaway region as one leading to a positive ordinary differential equation system describing the thermal behaviour of the reactor on a section of the reaction path, i.e., having the sum of the first derivate term of the dimensionless reactant and coolant temperatures, and the conversion non-negative. Considering the operative conditions. the derivate of the coolant temperature to the axial position is tautological null for the analyzed processes because large flowrate is typically fed to guarantee constant coolant temperature [47]. Consequently, this condition is satisfied when the curves representing $u_{b,max,}$ and θ_{max} criteria are overlapped.

Section 3 - Results and discussion

For the sake of conciseness, this section represents a collection and critical comparison of experimental and numerical data obtained during this program since detailed and case-oriented discussions have been already published by the author in peer-reviewed journals. Hence, the generic framework where these investigations took place was described and reported, whereas a more specific and case-oriented discussion on the addressed topic can be found in the author's publications (please see the Appendix for an updated list).

Collected measurements

Considering the abundance of experimental and numerical investigations on methane-air premixed flames, this mixture was considered as a base case for this work for the sake of system validation. As a preliminary result, the experimental measurements collected for stoichiometric composition at 298 K and 1 atm will be analyzed, at first. In particular, the temperature profiles to the dimensionless radius (r/R) were reported in Figure 15 at different initial velocity (v_{In}).

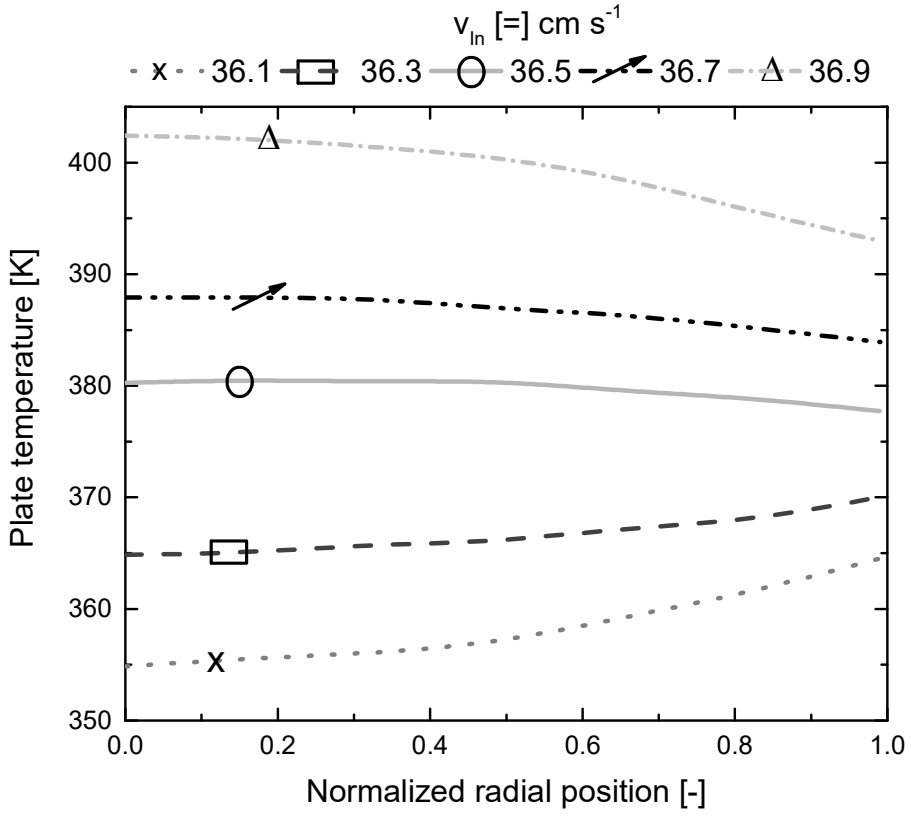

Figure 15. Measured plate distribution with respect to the normalized radial position for different values of the initial velocity.

These results demonstrate the validity of the hypothesis of the parabolic trend for radial temperature profile and confirm the appropriateness of interpolation for laminar burning velocity measurements.

In this view, the effect of equivalence ratio on the laminar burning velocity of the methane-air mixture at the same temperature and pressure was reported in Figure 16. Additionally, data from literature were added for the sake of comparison [234][235][236].

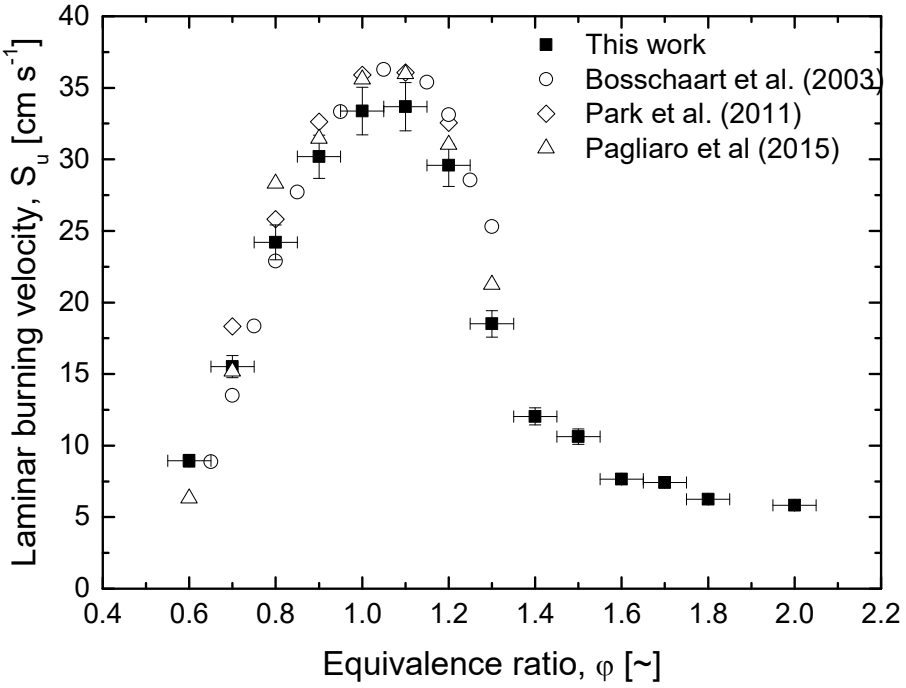

Figure 16. Comparison of experimental data for the laminar burning velocity of the methane-air mixture at 298 K and 1 atm.

An excellent agreement between data sources can be observed especially for lean compositions, where almost all data are included within the uncertainties. On the other hand, measurements collected in this work at near-stoichiometric compositions show slightly lower values. This deviation can be attributed to the reduced effect of non-ideal behaviour when the HFB is applied. Indeed, a clear tendency to register lower laminar burning velocity along the year was reported and discussed in a dedicated literature review [237]. Furthermore, the elevated control guaranteed by the feeding system adopted in this work allows for the investigation of near-to-flammability limits, laying the foundations for a fundamental-based investigation of the extinction phenomena.

Then, the effect of fuel composition was investigated by comparing the obtained data for methane, propane, ethylene, and propylene in the air (Figure 17).

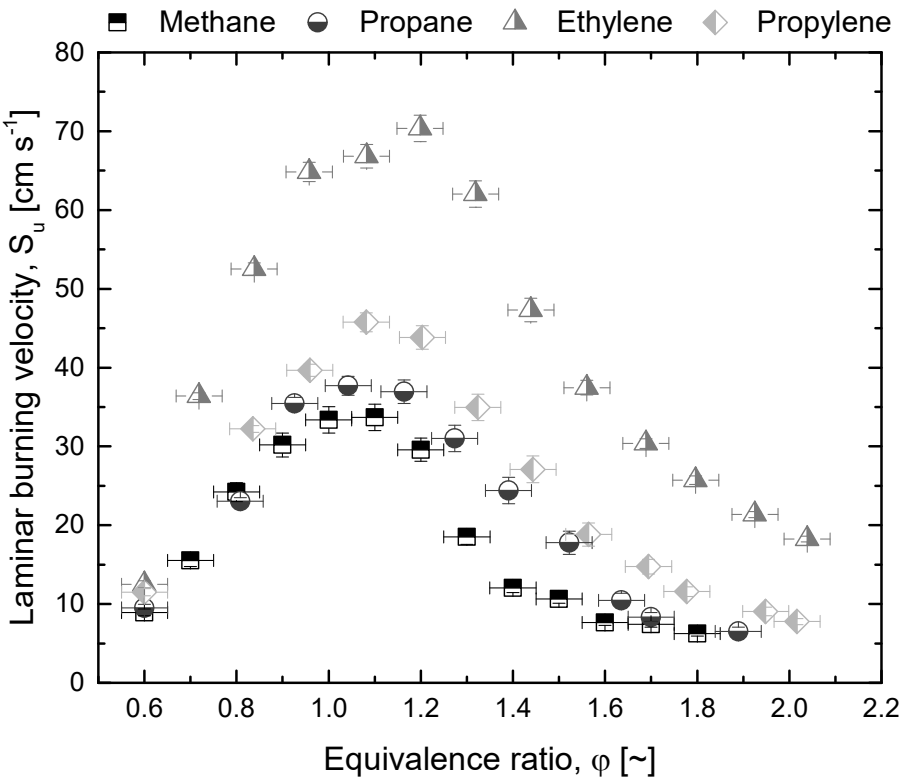

Figure 17. The laminar burning velocity of light hydrocarbons at 298 K and 1 atm measured in this work.

The maximum laminar burning velocity with respect to the equivalence ratio, referred to as fundamental laminar burning velocity ($S_{u,f}$) from now on, represents a key aspect for safety evaluations being the most conservative parameter accounting for the chemical aspects. It usually occurs at slightly rich composition because of the combination of thermal and kinetic aspects ruling the ignition phenomena. In other words, it can be intended as the condition where the thermal aspects, ruling the kinetic at lean compositions and lower flammability limits, equals the kinetic aspects, ruling the kinetic at rich composition and upper flammability limits. For hydrocarbons, it is generally believed that an increase in the number of carbon atoms within the same chemical class leads to a shift toward richer composition where $S_{u,f}$ occurs and larger $S_{u,f}$ itself. The former can be attributed to the increase in heat capacity of the reacting mixture, requiring a larger quantity of heat produced, thus faster kinetic, whereas the latter reflects the variation in heat of combustion of the analyzed fuels. Besides, the presence of double bond considerably increases $S_{u,f}$, because of the difference in characteristic energy of single and double bond, leading to easier ignition in the case of alkenes.

However, ethane and ethylene respect the last trend, exclusively. Indeed, C_2 fuels show larger $S_{u,f}$ at richer composition than C_1 and C_3. This discrepancy has historically promoted the investigation of C_2 chemistry separately. It has been established that this peculiarity can be attributed to the differences in activation energy of the hydrogen abstraction reaction from these fuels [238]. Indeed,

the presence of the same bond (e.g., C-H for the methane case or C-C-C for propane or heavier species) makes the structure more stable from a chemical point of view, reducing the reactivity. This aspect is also confirmed by the production rates of propyl radicals (C_3H_7) by the ruling primary reaction involving propane (i.e., hydrogen abstraction by OH), being n-propyl (n-C_3H_7, SMILES structure [CH_2]CC) production considerably faster than i-propyl production (i-C_3H_7, SMILES structure C[CH]C) [239]. Besides, the comparison of the laminar burning velocity of methane and propane shows that similar values can be observed for lean compositions. This aspect can be correlated to the similarity in the adiabatic flame temperature of these mixtures, confirming that the thermal aspects dominate the overall reactivity under these conditions. However, pure fuels do not reflect the reactants adopted in the industrial case for energy production or chemical synthesis, where complex mixtures are widespread. Besides, concerns were raised on the validity of mixing rules for the estimation of laminar burning velocity in the case of alkenes or hydrogen addition. Hence, accurate experimental data are essential to evaluate their validity. In this view, the effect of hydrogen addition on methane and propane was evaluated, at first (Figure 18). Then, methane-ethylene and methane-propylene mixtures in the air were analysed (Figure 19).

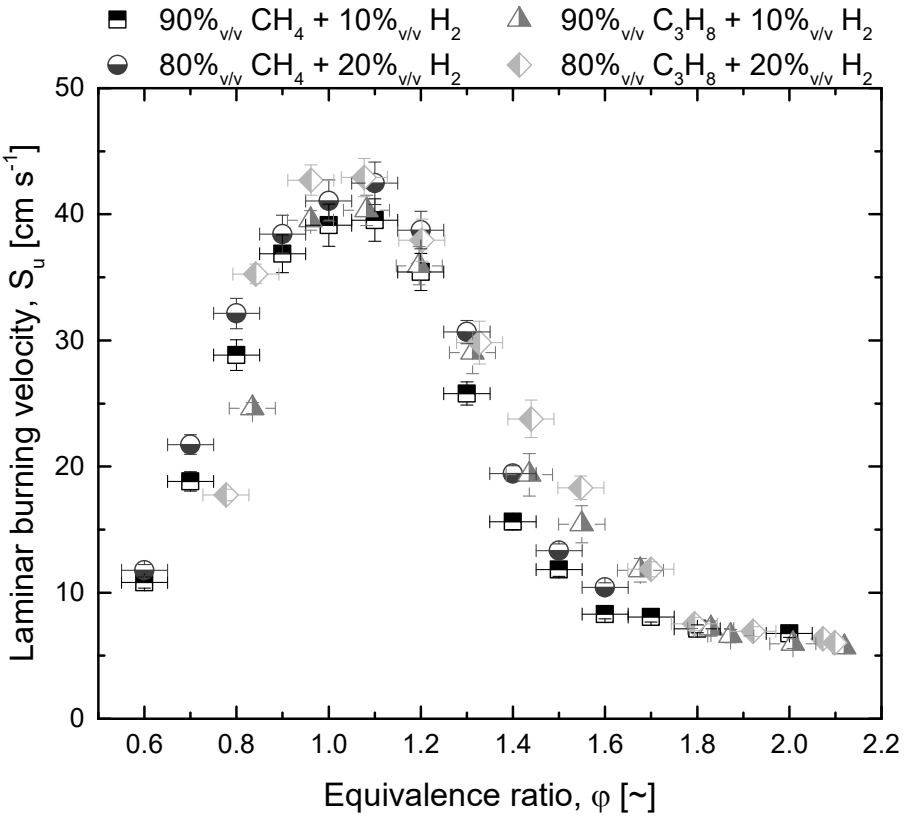

Figure 18. The effect of hydrogen addition on the laminar burning velocity of methane and propane premixed flames in air.

Under previous observations, small variations can be observed for hydrogen-enriched methane and propane, especially at lean conditions, meaning that the addition of more reactive species (such as hydrogen) has a limited impact on the whole system from a chemical point of view. The fact that the chemistry of alkanes is prone to be retained in its original form has been observed once non-hydrocarbons species (e.g., CO) was added and alkanes were mixed, as well [240][107]. However, a few studies have been dedicated to the mixtures containing alkanes and alkenes in the oxidative environment, although these mixtures are potentially involved in several industrial processes.

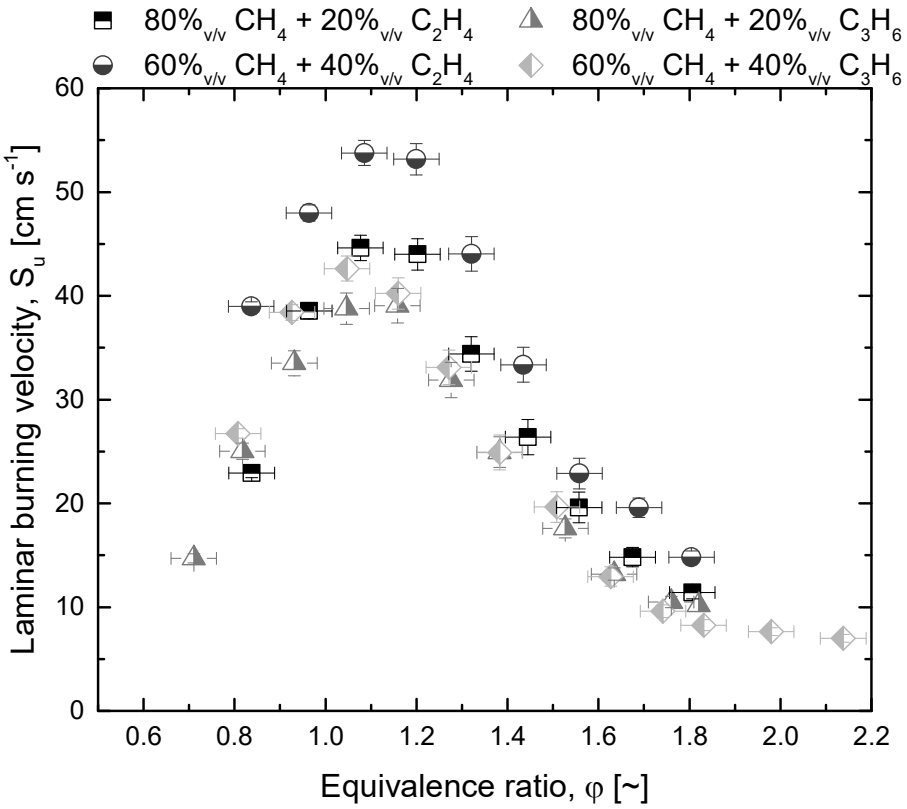

Figure 19. The effect of ethylene or propylene addition on the laminar burning velocity of methane premixed flames in air.

In compliance with the laminar burning velocity trend reported for pure fuels for any given equivalence ratio, i.e., $CH_4 < C_3H_6 < C_2H_4$, the addition of ethylene produces more reactive mixtures than the addition of propylene. In this view, it is worth mentioning that similar values of $S_{u,f}$ can be observed when methane is enriched by 20 $\%_{v/v}$ of ethylene and hydrogen, although the latter has considerably higher $S_{u,f}$ when burns as pure fuel in air. These results indicate that ethylene can interact in a more effective way than hydrogen on the reactions ruling the ignition of methane. Hence, particular attention should be paid to the unit operations dealing with process streams characterized by the presence of ethylene.

Eventually, the needs for decarbonization have promoted the production of biomethane, i.e., mixture rich in methane obtained by biomass treatment, potentially containing significant amounts of carbon monoxide and carbon dioxide impacting the overall reactivity. For this reason, the effect of mixture composition on the laminar burning velocity was experimentally investigated (Figure 20).

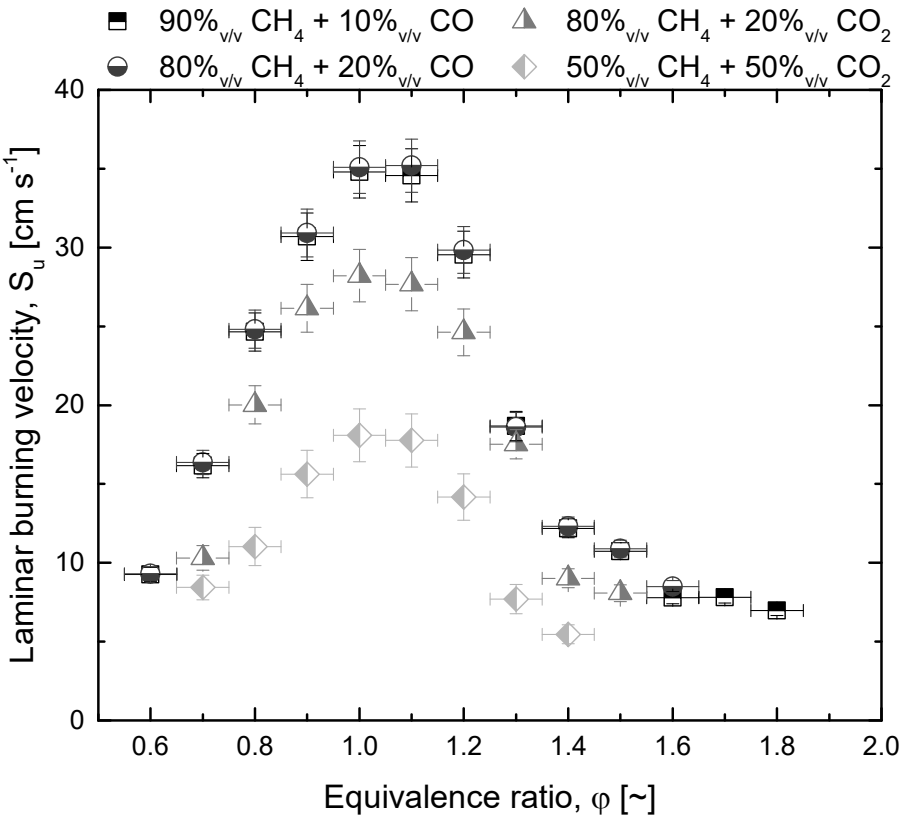

Figure 20. The effect of carbon monoxide or carbon dioxide addition on the laminar burning velocity of methane premixed flames in air.

The experimental data reported above clearly indicate that carbon monoxide addition weakly affects the overall reactivity of methane, whereas the addition of carbon dioxide significantly decreases the laminar burning velocity. The latter observation is undoubtedly related to the thermal dilution being carbon dioxide inert from a chemical point of view and potentially involved as a third body in any reactions included in the oxidation path of methane. Hence, it is possible to conclude that in both cases methane decomposition path is unchanged by these species. For the sake of completeness, a modified version of the Coppens correlation [110] (i.e., imposing $\sigma = 1$) was adopted to represent the effect of the addition of either hydrocarbons or non-hydrocarbon on methane laminar burning velocity. The experimental results obtained in this work, together with data from the literature, were considered for the calculation of the empirical coefficients reported below.

Table 9. Empirical coefficients for the estimation of the laminar burning velocity at 298 K and 1 atm of mixtures containing methane in the air.

	Coefficient 1	**Coefficient 2**	**Coefficient 3**
CH_4	$W = 37.20$ cm s^{-1}	$\eta = 0.47$	$\xi = 6.07$
H_2	$\gamma = 0.10$	$\tau = 0.10$	$\Omega = 0.24$
C_2H_4	$\gamma = 0.50$	$\tau = 0.10$	$\Omega = 3.00$
C_3H_6	$\gamma = 0.15$	$\tau = 0.10$	$\Omega = 4.50$
CO	$\gamma = 0.10$	$\tau = 1.00 \cdot 10^{-9}$	$\Omega = 0.80$
CO_2	$\gamma = -1.70$	$\tau = 0.50$	$\Omega = 0.08$

Other than the fuel composition, the oxidant composition plays a significant role, as well. Actual trends are promoting either the use of diluted air or oxygen-enriched air. The former aims to reduce the pollutants' production by lowering the flame temperature of traditional fuels, whereas the latter strategy is of interest for the combustion of low-cost, low-value fuels, together with the characterization of chemical processes such as direct partial oxidation. Regardless of the desired application, the accurate determination of the flammable region is essential to optimize the operative conditions. In this view, both strategies were studied for methane and ethylene by using the heat flux burner (Figure 21). Particular attention was posed to the conditions having $0.21 < E < 0.4$ because of the availability as a by-product of the air separation units based on membrane technology.

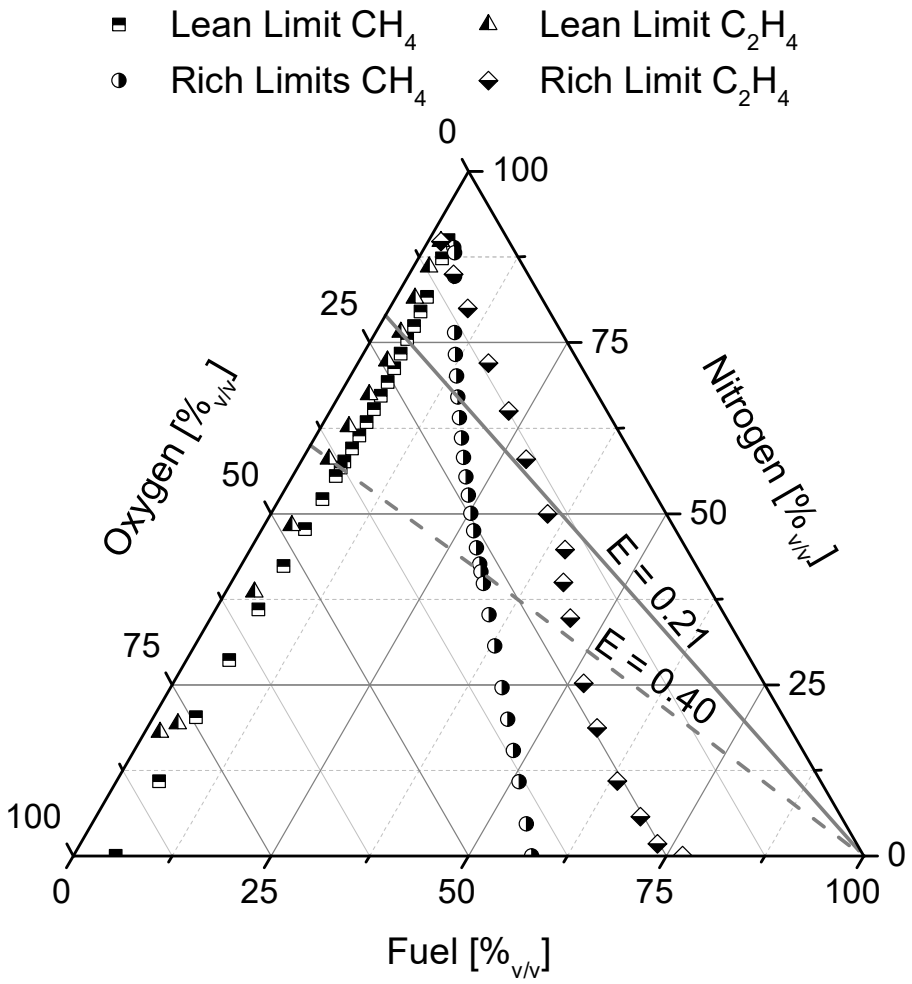

Figure 21. Flammable region of methane and ethylene measured by means of the heat flux burner.

Similar values and trends can be observed for methane and ethylene lean limits, with small variations due to *E*. Conversely, rich limits are strongly affected by the chemical structure of the investigated fuel, having ethylene considerably larger flammable region. This trend is in line with the observations reported before during the comparison of the laminar burning velocity of pure fuels in air. Furthermore, the point of intersection of lean and rich curves was considered for the evaluation of limiting oxygen concentration (LOC) in nitrogen either for methane or ethylene, obtaining 9.1 $\%_{v/v}$ and 8.6 $\%_{v/v}$, respectively. The former is considerably smaller than the corresponding values obtained in closed vessels, reported in the literature (e.g., 10.0 $\%_{v/v}$ [241]), whereas the latter perfectly matches the concentration registered by Zlochower and Green (2009) [242] using 20 and 120 litres closed vessels. The fundamental bases of the HFB, together with the reduced interactions between system and reactants (e.g., absence of walls confining the flame), may suggest the utilization of this experimental system for the determination of the flammable regions. In this case, the development of proper standard ruling the design and procedures to reduce the effects of unpredictable factors is essential.

Numerical results

As discussed in detail in the methodological section, the numerical analyses performed in this work aim to the generation, validation, and comparison with existing homologous of a comprehensive detailed kinetic mechanism for oxygenated species and small hydrocarbons. These steps were, then, followed by model reduction finalized to the implementation of chemical aspects in CFD models for the characterization of simplified industrial reactive systems. Considering the multiplicity of the involved aspects, this paragraph was properly divided to distinguish the described steps.

Development of a detailed kinetic mechanism

The development of the detailed kinetic mechanism was performed via the automatized tool RMG integrated with *ab initio* calculations performed through ARC. The resulting model consists of ~700 species and ~25000 reactions. The obtained data can be distinguished in terms of adopted source or chemical class. Figure 22 shows the size of the most abundant and representative groups.

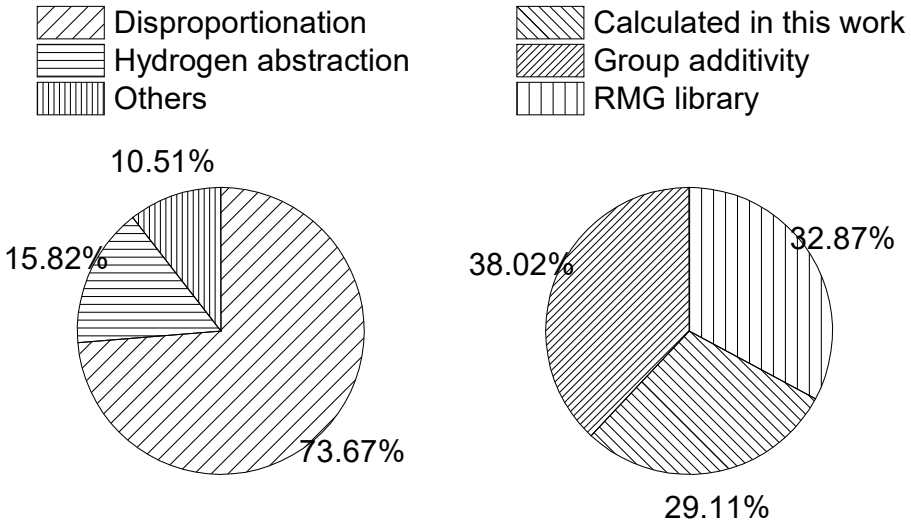

Figure 22. Statistics of the reaction class (left) and thermodynamic sources (right) included in the obtained kinetic mechanism.

The majority of the reactions included in the generated mechanism are classified as disproportionation and hydrogen abstraction (15.82%) reactions, whereas the thermodynamic sources were almost equally distributed between group additivity, RMG libraries, and *ab initio* calculations performed in this work. The slight predominance of group additivity (GA), implies that several species have small or negligible effects on the resulting mechanism, confirming the existence of room for model reduction. Indeed, each species in kinetic mechanisms is potentially involved in hundreds of reactions. Besides, the reverse rates of these reactions are estimated by using the Gibbs free energy

of that species. The effect of thermodynamic databases on the generated mechanism can be analyzed by comparing the estimations of the mechanisms produced in each step of the iterative procedure described before. To this aim, key indicators of the obtained mechanisms are reported in *Table 10*.

Table 10. Description of the detailed kinetic mechanism generated during the iterative procedure.

Number of Iteration	Number of Species	Number of Reactions	Group Additivity [%]
1	492	26107	52.64
2	606	34537	69.14
3	1090	43930	49.81
4	584	18922	38.07
5	714	24519	39.12

A comparison of the performances of these mechanisms was carried out in terms of estimated IDT. For the sake of brevity, only the IDT of 1-butene/air stoichiometric mixture at 10 atm is provided (Figure 23), assumed as representative of the oxidation of either small chain esters or small hydrocarbons.

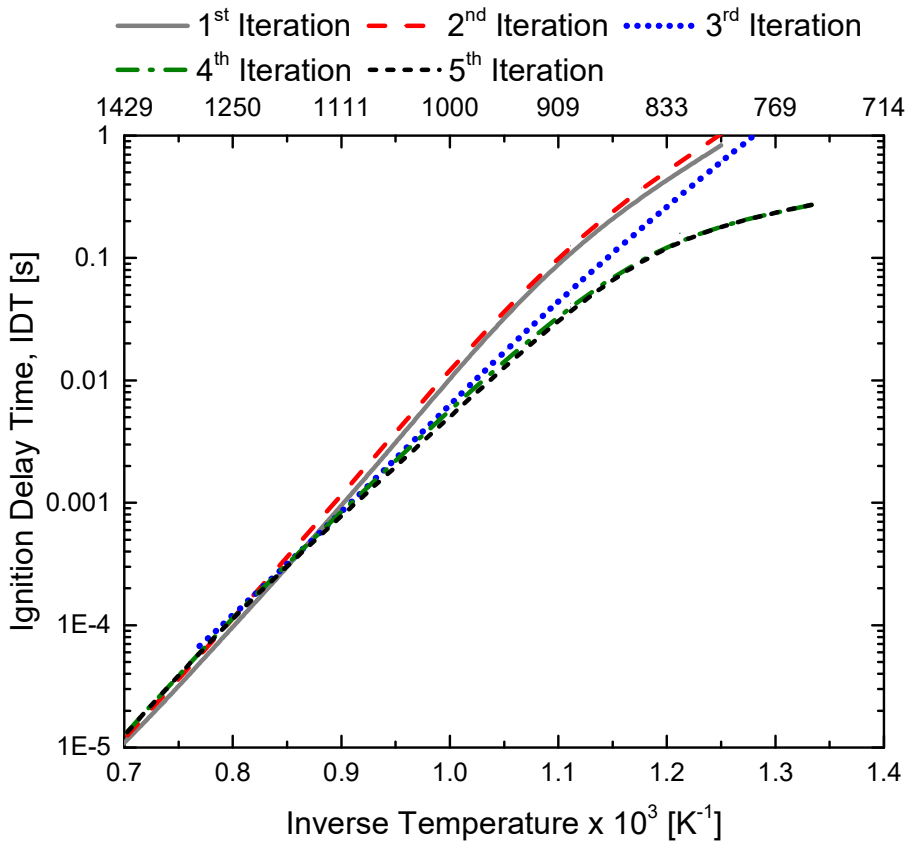

Figure 23. Comparison of the estimated ignition delay time of 1-butene/air mixture at 10 atm as a function of temperature for different model generated in this work.

Considering that the inputs provided to RMG for the generation of these models only differ for the thermodynamic database, it is possible to conclude that the species added during the process mainly affect oxidation at low and intermediate temperatures. Comparing the number of species included in the 2nd and 3rd iterations together with the estimated IDT, it can be assumed that the abrupt enlargement in mechanism size can be partially attributed to the inclusion of relevant reaction pathways for low- and intermediate- temperatures chemistry, causing faster ignition. Then, the refinements implemented in the 4th and 5th iterations have allowed for the optimization of the added pathways, as testified by the number of species included in the mechanisms and IDT. Eventually, the last iterations provide similar IDT, indicating reduced uncertainties related to thermodynamic data, i.e., that most of the sensitive species were calculated. Under this light, the iterative procedure was interrupted after the 5th iteration and, thus, the generated model was analyzed by comparing its estimations with experimental and numerical data. The produced mechanisms refer to the chemistry of light hydrocarbons. Hence, the one produced by the last iteration was considered as a building block for the generation of a mechanism suitable for butyl acetate oxidation. In particular, it was integrated with the rate coefficients calculated for the hydrogen abstractions from butyl acetate isomers, and the iterative procedure was repeated to include relevant decomposition pathways involving oxygenated and larger species. As a way of example, the optimized geometry obtained for the transition state of hydrogen abstraction from tBA by OH was reported in Figure 24.

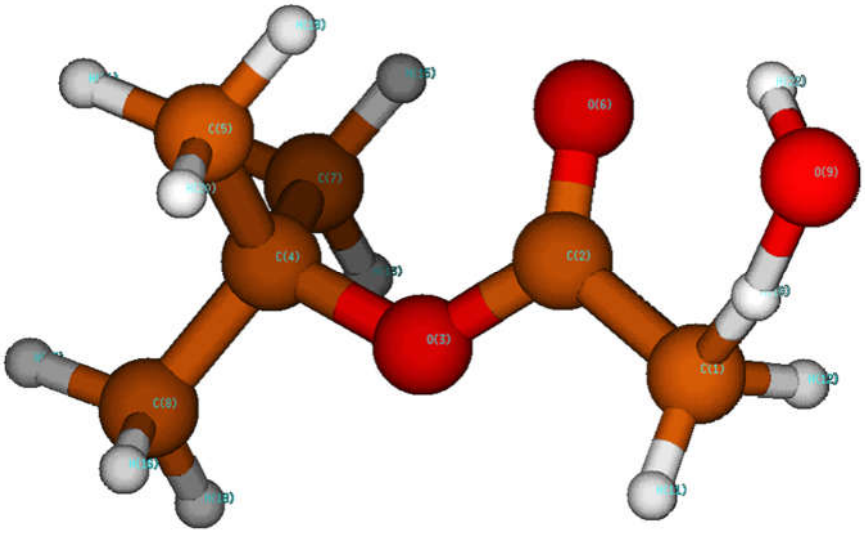

Figure 24. Optimized geometry obtained in this work for the transition state of hydrogen abstraction by OH from tBA.

Starting from the reported geometry, the obtained rotor scans were reported below

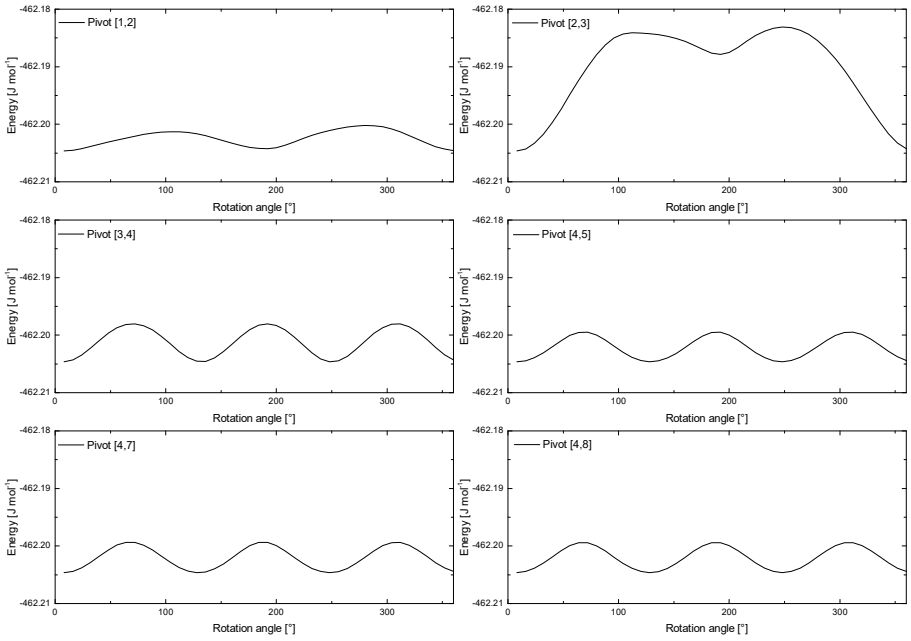

Figure 25. Rotor scans of the optimized transition state for the hydrogen abstraction from tBA by OH.

The absence of configurations having lower energy than the initial value confirms that the reported transition state geometry represents the optimized solution, thus these data can be obtained for the calculation of the reaction rates. Besides, the lack of abrupt variation in resulting energy of two consecutive points (including first and last points) guarantees the absence of bond breaking and significant repulsive forces (e.g., causing steric effects). Similar results were obtained for hydrogen abstraction from other isomers, carbon atoms, and by different abstracting agents. The coefficients related to some of the reaction rates obtained in this work are listed in the following table, whereas the resulting rate constants can be visualized in Figure 26.

Table 11. Rate coefficients calculated in this work for the most relevant hydrogen abstraction of butyl acetate isomers. Please note that species were reported in SMILES notation.

Reactions number and formula	**A [cm, mol, s]**	**n [-]**	**$E_a \cdot R^{-1}$ [K^{-1}]**
1) CC(=O)OCCCC + [OH] ⇔ [CH_2]C(=O)OCCCC + O	$2.32 \cdot 10^{-2}$	3.88	$-3.14 \cdot 10^{+2}$
2) CC(=O)OCCCC + O[O] ⇔ CC(=O)O[CH]CCC + OO	$8.58 \cdot 10^{-6}$	4.80	$4.37 \cdot 10^{+3}$
3) CC(=O)OC(C)CC + [OH] ⇔ [CH_2]C(=O)OC(C)CC + O	$1.26 \cdot 10^{0}$	3.36	$-4.03 \cdot 10^{+2}$
4) CC(=O)OC(C)(C)C + [OH] ⇔ CC(=O)OC(C)(C)[CH_2] + O	$7.57 \cdot 10^{0}$	3.49	$-5.12 \cdot 10^{+2}$
5) CC(=O)OC(C)(C)C + [OH] ⇔ [CH_2]C(=O)OC(C)(C)C + O	$5.99 \cdot 10^{-2}$	3.71	$-1.05 \cdot 10^{+3}$
6) CC(=O)OCC(C)C + [OH] ⇔ [CH_2]C(=O)OCC(C)C + O	$1.23 \cdot 10^{-2}$	3.78	$-4.35 \cdot 10^{+2}$
7) CC(=O)OCC(C)C + O[O] ⇔ CC(=O)O[CH]C(C)C + OO	$6.58 \cdot 10^{-7}$	5.04	$5.01 \cdot 10^{+3}$

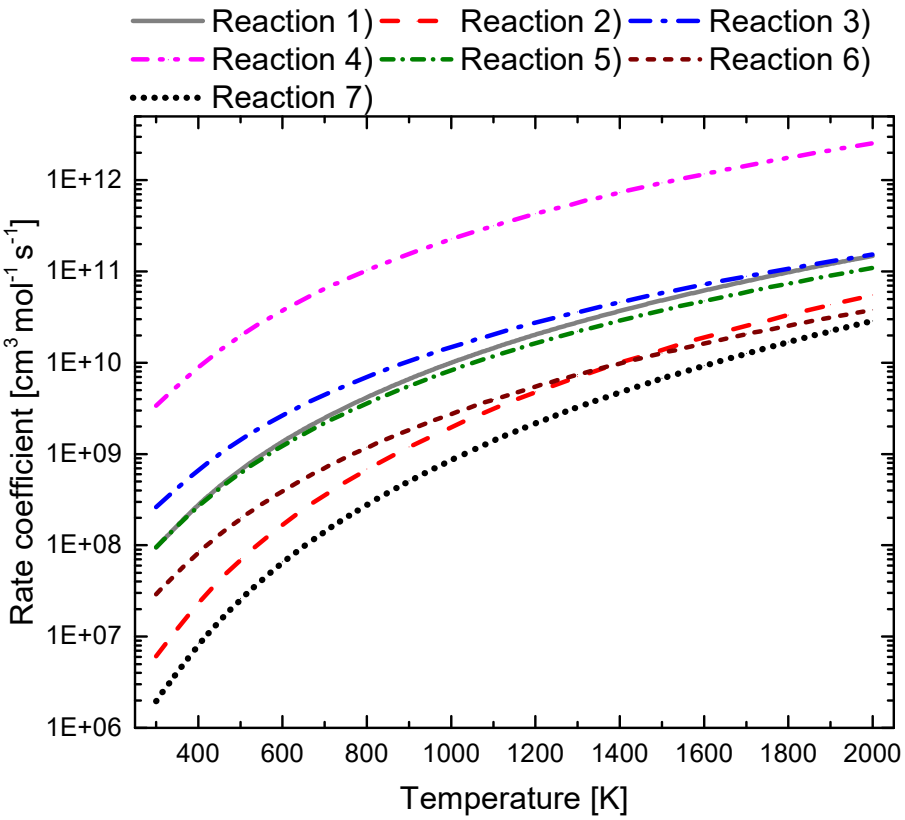

Figure 26. Comparison of rate coefficients obtained by ab initio calculations for hydrogen abstraction from butyl acetate isomers.

As expected, the structure of the aliphatic chain has a limited impact on the hydrogen abstraction from the carbon atom in α' position since differences in rate coefficients of Reactions 1, 3, 5, and 6 are within one order of magnitude for any investigated temperatures. Besides, hydrogen abstraction by HO_2 (i.e., Reactions 2 and 7) tends to be slower than hydrogen abstraction by OH because of the larger steric effect in transition state geometry. It is worth noting that tBA is the only case where the hydrogen abstraction from the carbon atom in α' position is slower than the hydrogen abstraction from a carbon atom within the aliphatic chain. This peculiarity can be attributed to the conformation of this isomer avoiding the formation of transition state configuration having hydrogen bonds between the abstracting agent and aliphatic chain.

Validation of detailed kinetic mechanism and comparison of estimation quality for benchmark applications

To include a wide range of temperature and pressure, the validation of the obtained mechanism was performed by comparing experimental results and numerical estimations deriving from widely adopted and highly reputed mechanisms either for the laminar burning velocity or the ignition delay time. As mentioned before, the chemistry of light alkenes plays an essential role in esters and small hydrocarbons oxidation. Besides, several data can be retrieved in the literature. The combination of

these aspects makes light alkenes a promising chemical group for the evaluation of the accuracy of detailed kinetic mechanisms.

The S_u in the air at an initial temperature of 298 K and pressure of 1 atm was firstly compared with experimental data collected for premixed flames of ethylene [243][244][114][245][246], propylene [247][248][60][246], and butene isomers [247][98][249][217][250] (Figure 27 and Figure 28).

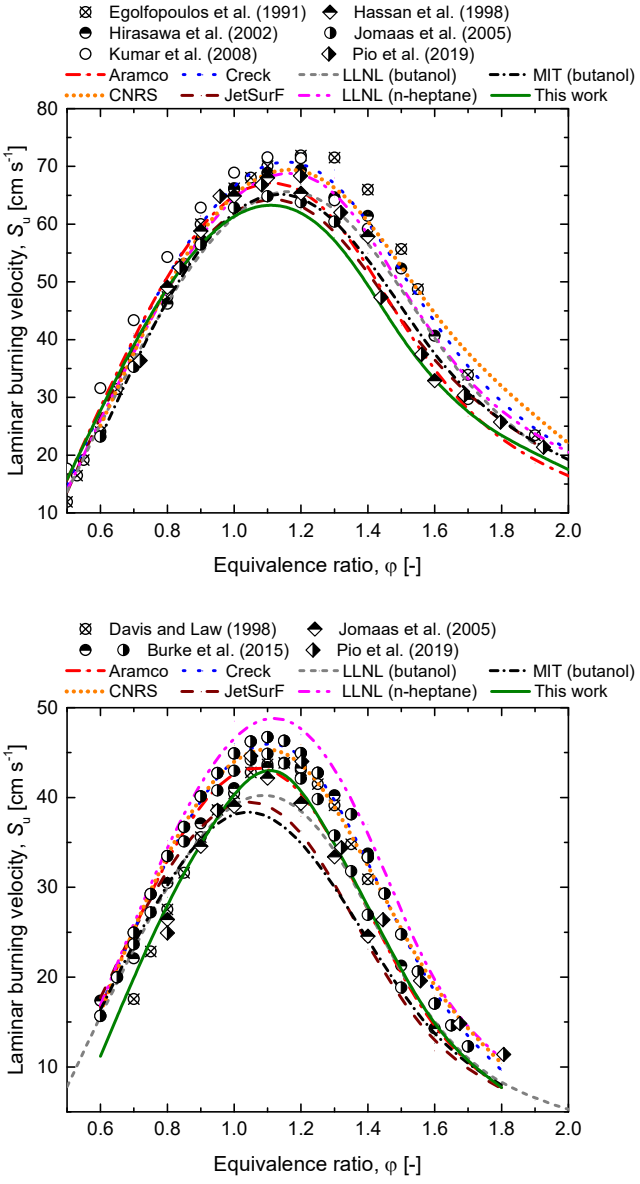

Figure 27. Comparison of experimental measurements and numerical estimations of the laminar burning velocity of C_2H_4 (top) and C_3H_6 (bottom) vs equivalence ratio at atmospheric conditions.

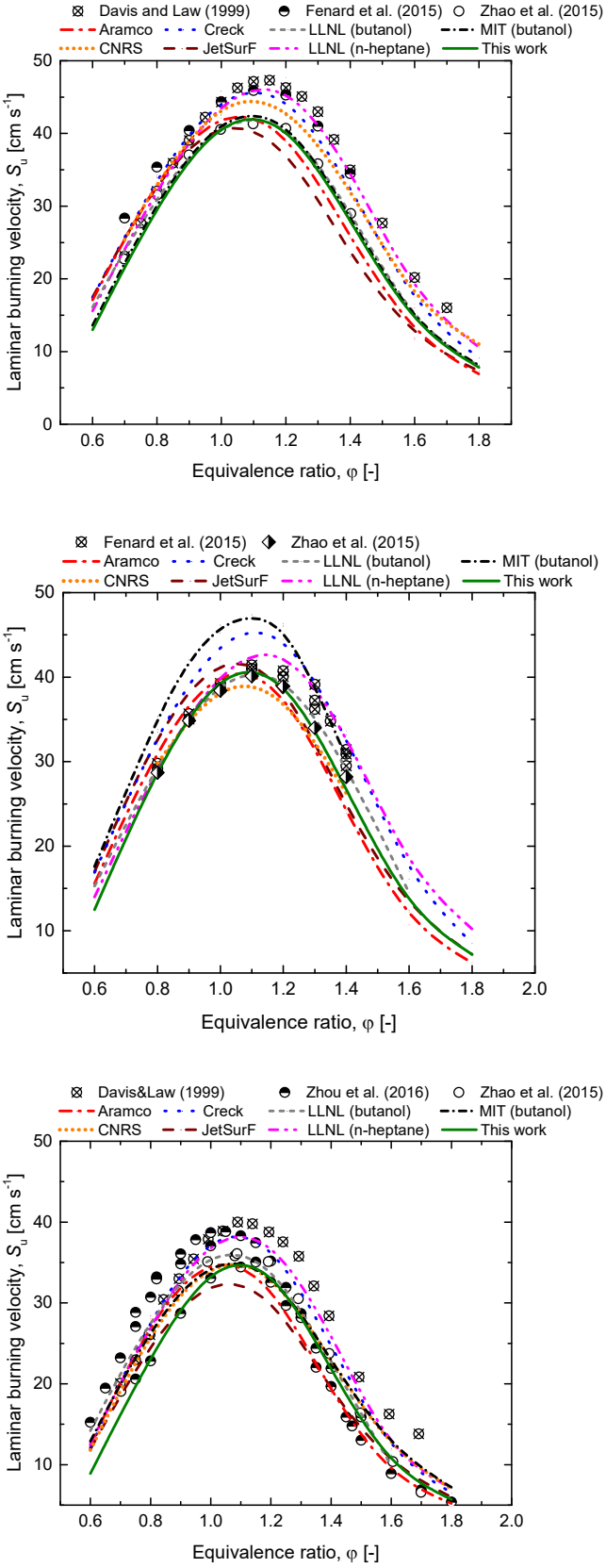

Figure 28. Comparison of experimental measurements and numerical estimations of the laminar burning velocity of 1-C_4H_8 (top), 2-C_4H_8 (middle), and i-C_4H_8 (bottom) vs equivalence ratio at atmospheric conditions.

The estimations deriving by the mechanism produced in this work are included the range described by the other estimations and fairly represent the experimental measurements, validating the generated model for the estimation of the chemistry of light species at atmospheric pressure and low-initial temperature. A good agreement can be observed between the experiments and estimations. However, CNRS, Creck, and LLNL (n-heptane) models generate higher values with respect to the other models, especially for near stoichiometric mixtures. This trend, together with the well-known trend in S_u reduction throughout the year due to procedure refinements [205], suggests that these models over predict the reactivity of alkenes. Additional insights providing possible explanations for the observed discrepancies will be provided in this document.

Regardless of the analyzed fuel, Aramco and JetSurF models predict that $S_{u,f}$ is achieved at equivalence ratio within the range 1.0 – 1.1, whereas the other models suggest richer compositions, included in 1.1 – 1.2 interval. The latter values comply with experimental results obtained in this work and typical trends reported for hydrocarbons/air premixed flames under several initial temperatures and pressures [50].

This analysis was extended to the high initial temperature, intermediated, and high pressures by comparing the ignition delay time measured for ethylene [251], propylene [60], and butene isomers [250][100][252] with predictions (Figure 29 and Figure 30). For the sake of conciseness, stoichiometric composition with air and initial pressure equal to 10 atm were analyzed in this stage, being the conditions characterized by the elevated abundancy of experimental data.

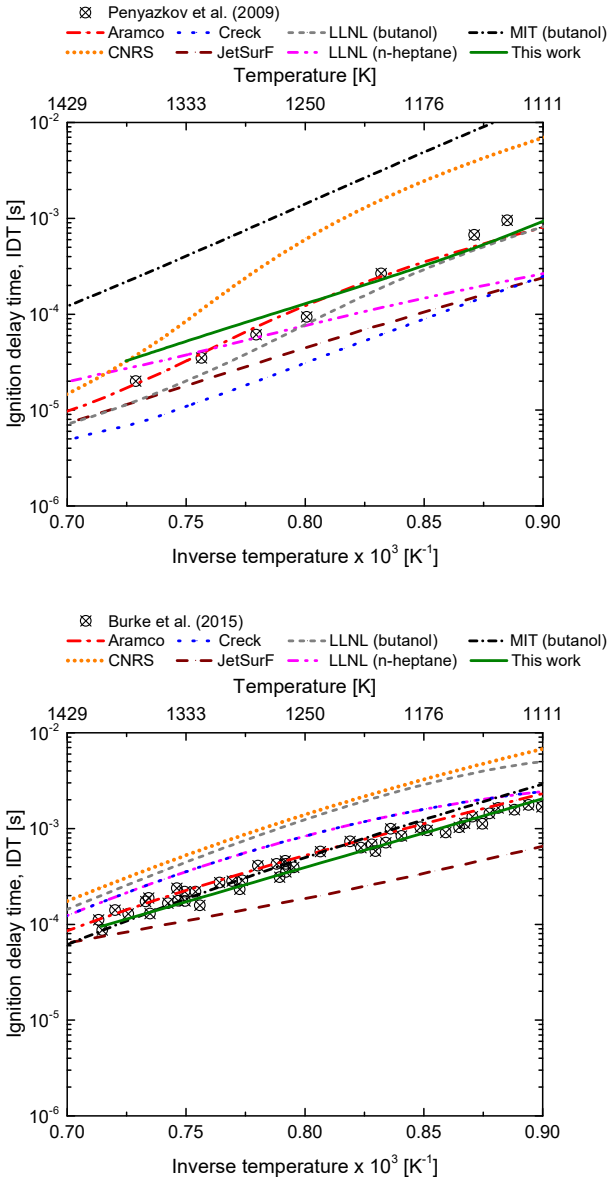

Figure 29. Comparison of experimental measurements and numerical estimations of the ignition delay time IDT of C_2H_4 (top), C_3H_6 (bottom), vs temperature in air at stoichiometric composition, and 10 atm.

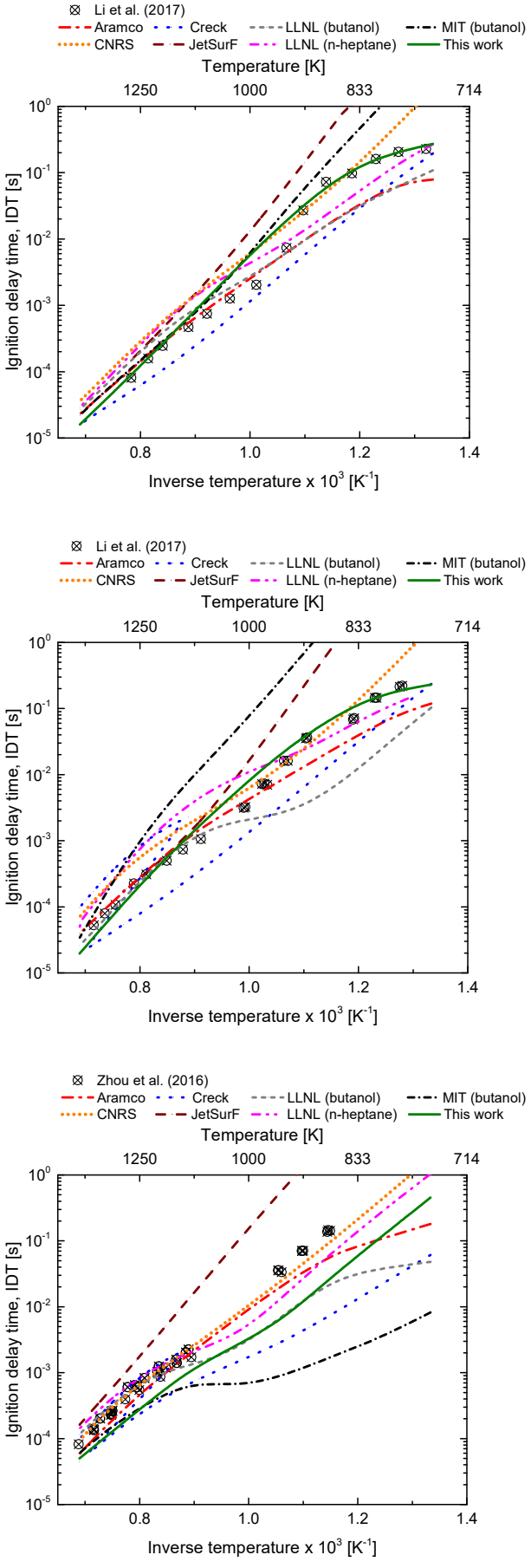

Figure 30. Comparison of experimental measurements and numerical estimations of the ignition delay time IDT of 1-C_4H_8 (top), 2-C_4H_8 (middle), and i-C_4H_8 (bottom) vs temperature in air at stoichiometric composition and 10 atm.

The model produced in this work shows excellent accuracy in IDT data estimation, except for i-C_4H_8, where lower values are reported for all the investigated temperatures. Furthermore, it is the only model able to accurately reproduce the measured trends at low temperatures for all the investigated species. Conversely, Creck, MIT (butanol), and the model generated in this work indicate i-C_4H_8 as the most reactive butene isomer at a temperature close to 1000 K, in contrast with experimental data and the other mechanisms analyzed in this work, indicating a possible room for improvements. Similarly, LLNL (butanol) provides relative reactivities in contrast with other sources for 1-C_4H_8 and 2-C_4H_8 at a temperature of ~900 K, together with 1-C_4H_8 and i-C_4H_8 data at a temperature of ~800 K.

The chemistry of 2-C_4H_8 and i-C_4H_8 is satisfactorily represented by the Aramco mechanism. However, a significant deviation for 1-C_4H_8 reactivity at intermediate temperatures can be observed. On the contrary, the CNRS model does not reproduce correctly the ethylene and propylene IDT at the investigated conditions. Considering that CNRS has been developed for atmospheric pressure, this observation suggests that relevant reaction paths ruling ethylene and propylene ignition at higher pressure are missing or inadequately represented. IDT data confirm the tendency of Creck to over-estimate the reactivity of light alkenes, already reported for the S_u, suggesting the inaccurate representation of the core combustion sub-model. JetSurF indicates smaller IDT for ethylene and propylene and larger IDT for butene isomers than experiments. The inconsistency of the reported trends may indicate the inaccuracy in the estimation of the primary reactions together with the lack of relevant pathway, for the butene isomers. LLNL (n-heptane) generates slightly larger IDT at high temperatures and smaller IDT at intermediate temperatures compared to the experimental measurements for all the investigated species.

Based on the obtained results, the fractional bias, normalized mean square error (Figure 31, left), and distance from ideality (Figure 31, right) were calculated for all the investigated models, representing the overall estimation quality for light alkenes at different temperatures and pressures.

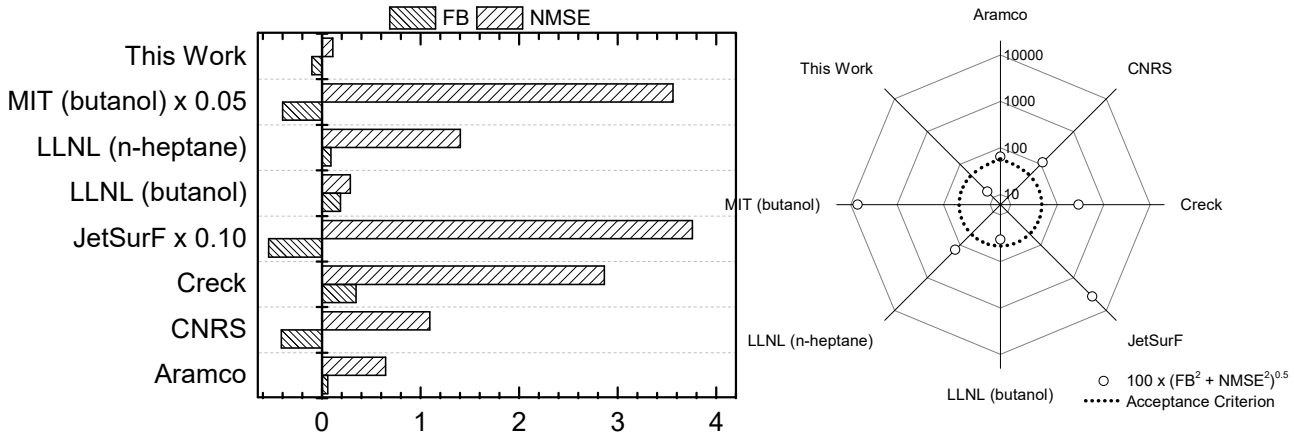

Figure 31. Evaluation of the overall estimation quality for the investigated models, in terms of fractional bias (FB) and normalized mean square error (NMSE). For the sake of proper visualization, NMSE values for JetSurF and MIT (butanol) were reduced by a factor of 10 and 20, respectively.

In agreement with the observations reported before, CNRS, JetSurf, and MIT (butanol) models have significantly negative overall FB, whereas Creck and LLNL (n-heptane) have positive values. Hence, it can be deduced that the first group underpredicts reactivity and the second to over predicts it. The limited accuracy reported before was confirmed for JetSurf and MIT (butanol), reporting elevated NMSE, and can be mainly attributed to poor understandings in intermediate temperature chemistry bared by inaccuracy in IDT data reproduction. Similarly, it can be concluded that 1-C_4H_8 has a detrimental effect on the performances of Aramco being either FB or NMSE maximized for this isomer. All the investigated mechanisms comply with the adopted criterion for FB (i.e., absolute values lower than 0.5) except for JetSurF (FB = -0.54), whereas only LLNL (butanol) and the model generated in this work respect the NMSE criterion (i.e., values lower than 0.3).

This analysis represents a sufficient validation for the procedure and the model generated in this work. Moreover, it represents the most accurate model among the ones analyzed in this work for alkenes combustion. This is particularly relevant considering that a purely theoretical approach, without any empirical-based corrective factors, was adopted. This aspect makes the generated model more flexible and comprehensive, favouring its inclusion as a building block for mechanisms focused on larger compounds.

Comparison of the chemistry of light alkenes

The highlighted discrepancies among the performance of the investigated models may provide useful information for the identification of the most accurate reaction rates of the most influential reactions in the systems and, thus, to a fundamental understanding of alkene chemistry. In this light, rate

coefficients of either primary reactions or core combustion reactions were compared. Indeed, it is well established that, regardless of the analyzed fuel, hydrogen abstraction by small radicals plays a significant role in primary radical production [15]. Also, a reduced list of the most influential reactions can be obtained by sensitivity analyses. This approach has been implemented by Xu and Konnov [253], as well, for the characterization of the core mechanisms. A list of reactions selected as representative of the investigated fuels is reported in Table 12. For the sake of discussion, the sources of rate coefficients selected by the different models were reported, at this stage.

Table 12. List of reactions compared in this work and data sources for rate coefficients included in the investigated mechanisms.

Reactions	**Models**	**Data Sources**
$C_2H_4 + OH \Leftrightarrow C_2H_3 + H_2O$	Aramco	Estimated[1]
	CNRS	Calculated [254]
	Creck	Estimated[1]
	JetSurF	Estimated[1]
	LLNL (butanol)	Estimated[1]
	LLNL (n-heptane)	Estimated[2]
	MIT	Calculated [255]
	This work	Calculated [254]
$C_2H_4 + H \Leftrightarrow C_2H_3 + H_2$	Aramco	Calculated [256]
	CNRS	Estimated[3]
	Creck	Estimated[4]
	JetSurF	Estimated[5]
	LLNL (butanol)	Calculated [256]
	LLNL (n-heptane)	Calculated [256]
	MIT	Calculated [255]
	This work	Calculated [254]
$C_2H_4 + O \Leftrightarrow CH_3 + HCO$	Aramco	Estimated[6]
	CNRS	Estimated[7]
	Creck	Estimated[6]
	JetSurF	Estimated[7]
	LLNL (butanol)	Estimated[6] (0.91)
	LLNL (n-heptane)	Estimated[6] (1.15)
	MIT	Estimated[7] (1.54)
	This work	Calculated[P] [254]
$C_2H_3 + O_2 \Leftrightarrow CH_2HCO + O$	Aramco	Calculated [257]
	CNRS	Estimated[9]
	Creck	Calculated[P] [254]
	JetSurF	Estimated[10]
	LLNL (butanol)	Calculated [258] (0.80)
	LLNL (n-heptane)	Calculated [258]
	MIT	Calculated [258]
	This work	Calculated[P] [254]
$C_2H_3 + O_2 \Leftrightarrow C_2H_2 + HO_2$	Aramco	Calculated[P] [257]
	CNRS	Not included
	Creck	Calculated[P] [257]
	JetSurF	Estimated[11]
	LLNL (butanol)	Not included
	LLNL (n-heptane)	Estimated[12]
	MIT	Estimated[12]
	This work	Calculated[P] [254]
$C_2H_3 + O_2 \Leftrightarrow CH_2O + HCO$	Aramco	Calculated[P] [257]
	CNRS	Estimated[13]
	Creck	Calculated[P] [257]
	JetSurF	Estimated[14]
	LLNL (butanol)	Estimated[15]
	LLNL (n-heptane)	Estimated[15] (0.5)
	MIT	Estimated[16]
	This work	Calculated[P] [254]

Table 13 (continue). List of reactions compared in this work and data sources for rate coefficients included in the investigated mechanisms.

Reactions	Models	Data Sources
$C_3H_6 + OH \Leftrightarrow C_3H_5\text{-a} + H_2O$	Aramco	Estimated[17]
	CNRS	Estimated[18]
	Creck	Estimated[17]
	JetSurF	Calculated [259]
	LLNL (butanol)	Estimated[19]
	LLNL (n-heptane)	Calculated [259]
	MIT	Calculated [259]
	This work	Estimated[20]
$C_3H_6 + H \Leftrightarrow C_3H_5\text{-a} + H_2$	Aramco	Calculated [259]
	CNRS	Calculated [259]
	Creck	Calculated [259]
	JetSurF	Calculated [260]
	LLNL (butanol)	Calculated [260]
	LLNL (n-heptane)	Calculated [260]
	MIT	Calculated [259]
	This work	Calculated [260]
$2\text{-}C_4H_8 + OH \Leftrightarrow 1\text{-}C_4H_7\text{-3} + H_2O$	Aramco	Estimated[17]
	CNRS	Estimated[29]
	Creck	Estimated[17]
	JetSurF	Estimated[30]
	LLNL (butanol)	Estimated[29]
	LLNL (n-heptane)	Estimated[30]
	MIT	Estimated[31]
	This work	Calculated [262]
$2\text{-}C_4H_8 + H \Leftrightarrow 1\text{-}C_4H_7\text{-3} + H_2$	Aramco	Estimated[32]
	CNRS	Estimated[33]
	Creck	Estimated[32]
	JetSurF	Estimated[34]
	LLNL (butanol)	Estimated[33]
	LLNL (n-heptane)	Estimated[34]
	MIT	Calculated [262]
	This work	Calculated [262]
$i\text{-}C_4H_8 + OH \Leftrightarrow i\text{-}C_4H_7 + H_2O$	Aramco	Estimated[35]
	CNRS	Estimated[36]
	Creck	Estimated[35]
	JetSurF	Estimated[37]
	LLNL (butanol)	Estimated[36] (1.15)
	LLNL (n-heptane)	Estimated[36] (1.15)
	MIT	Estimated[38]
	This work	Calculated [262]
$i\text{-}C_4H_8 + H \Leftrightarrow i\text{-}C_4H_7 + H_2$	Aramco	Calculated [263]
	CNRS	Estimated[39]
	Creck	Estimated[40]
	JetSurF	Estimated[41]
	LLNL (butanol)	Calculated [259]
	LLNL (n-heptane)	Calculated [259]
	MIT	Calculated [262]
	This work	Calculated [262]

*Superscripts were given to indicate the use of the same data sources
** In brackets the multiplying factors concerning the first model reporting the same data source
*** The superscript P stands for pressure-dependent rates

Recalling the large discrepancies between experiments and CNRS estimations for ethylene and propylene IDT, the absence of the reaction $C_2H_3 + O_2 \Leftrightarrow C_2H_2 + HO_2$, and the consequent lack of relevant pathways for C_2 chemistry, could be the main cause of the observed inaccuracy. The pressure-dependent rate constants ascribed to this reaction by the other models confirm its relevance at higher pressures and rationalize its absence in the CNRS model since this mechanism has been developed at atmospheric pressure.

A comparison of some reactions representative of the core mechanism is reported in Figure 32.

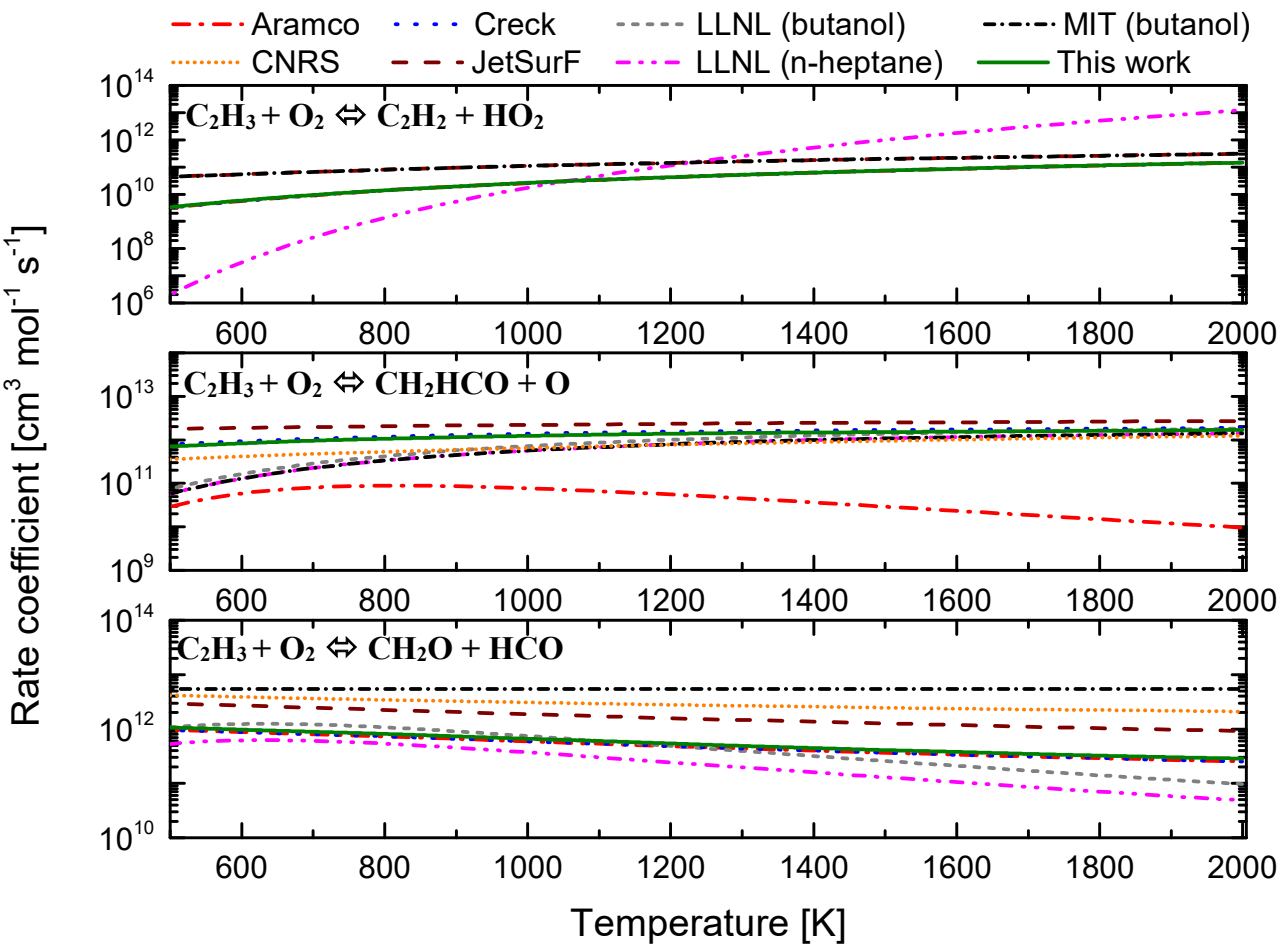

Figure 32. Comparison of rate coefficients for most influential reactions consuming $C_2H_3 + O_2$ included in the analyzed models.

In contrast with the indications provided by the other mechanisms, the rate coefficients considered in MIT (butanol) mechanism for $C_2H_3 + O_2 \Leftrightarrow C_2H_2 + HO_2$ and $C_2H_3 + O_2 \Leftrightarrow CH_2O + HCO$ reactions are weakly affected by the temperature. These trends lead to faster production of $CH_2O + HCO$, hindering the production of CH_2HCO.

The estimated coefficients included in LLNL (n-heptane) mechanisms for $C_2H_3 + O_2 \Leftrightarrow C_2H_2 + HO_2$ reaction generate faster production of C_2H_2 at high temperatures and slower at low and intermediate temperature than the directly calculated (i.e., coefficients obtained by *ab initio* calculations). Also, this mechanism includes the lowest rate for $C_2H_3 + O_2 \Leftrightarrow CH_2O + HCO$ at any investigated temperatures. The combination of these discrepancies may cause significant deviation in the branching ratio being the same reactants involved in both reactions. Considering that the production of less reactive species is promoted with an increase in temperature, this aspect can be a possible explanation for the tendency observed for the IDT estimations of this model.

Once the core sub-mechanisms were analyzed, the investigation was extended to the primary reactions of the studied fuels. In particular, hydrogen abstraction from C_2H_4 (Figure 33), C_3H_6 (Figure 34), 1-C_4H_8 (Figure 35), 2-C_4H_8 (Figure 36), and i-C_4H_8 (Figure 37) by H and OH were compared and discussed.

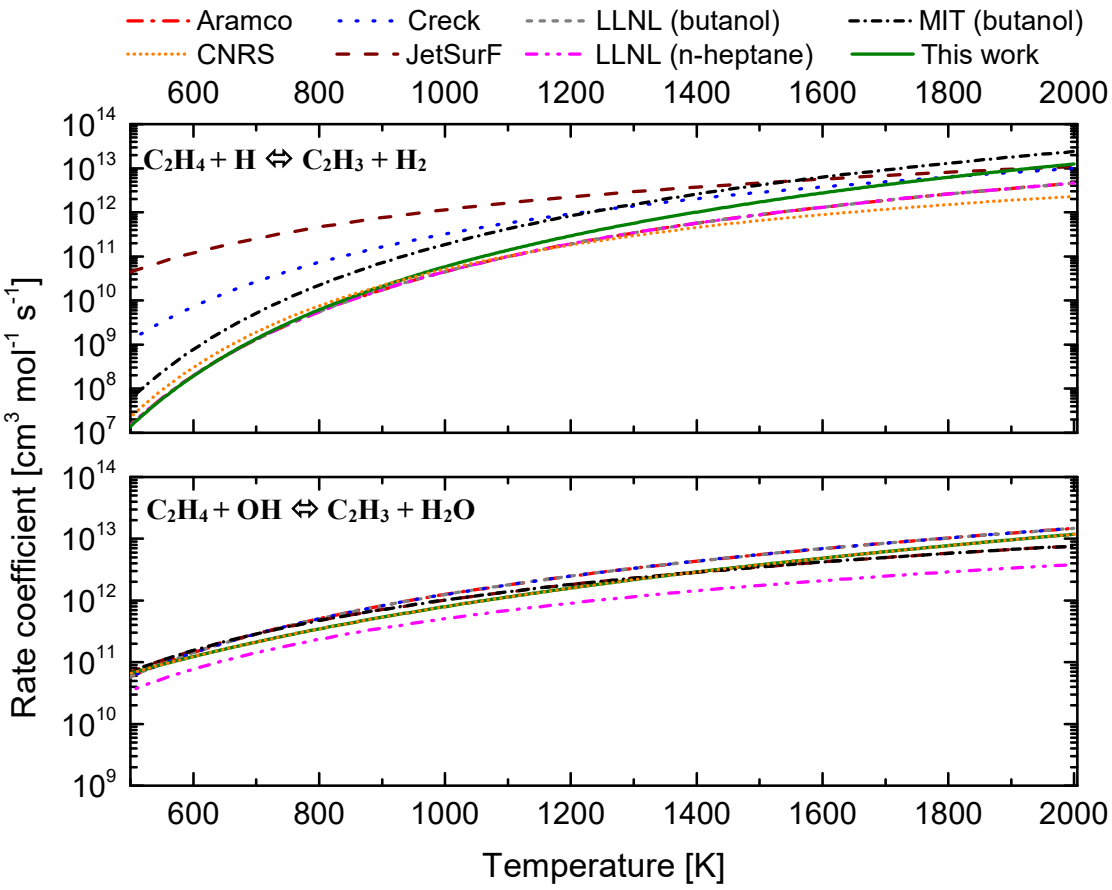

Figure 33. Comparison of rate coefficients for most influential hydrogen abstractions from C_2H_4 included in the analyzed models.

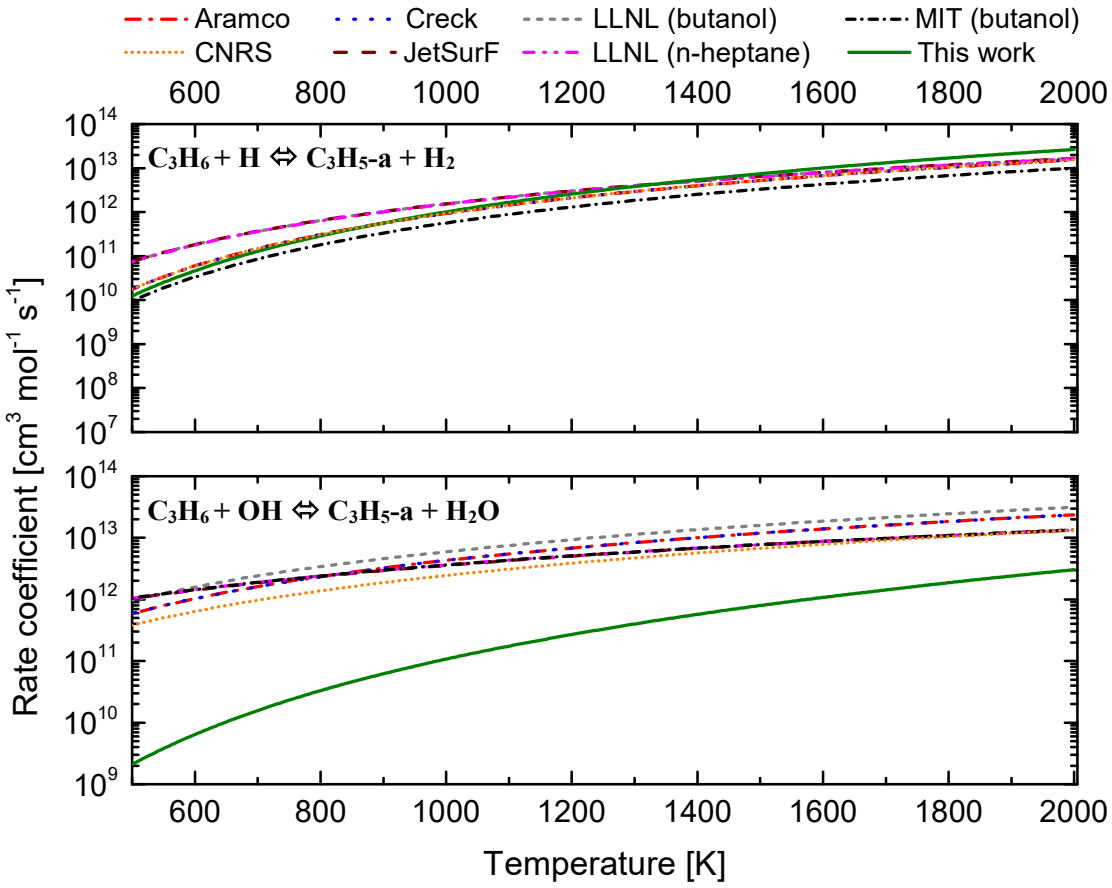

Figure 34. Comparison of rate coefficients for most influential hydrogen abstractions from C_3H_6 included in the analyzed models.

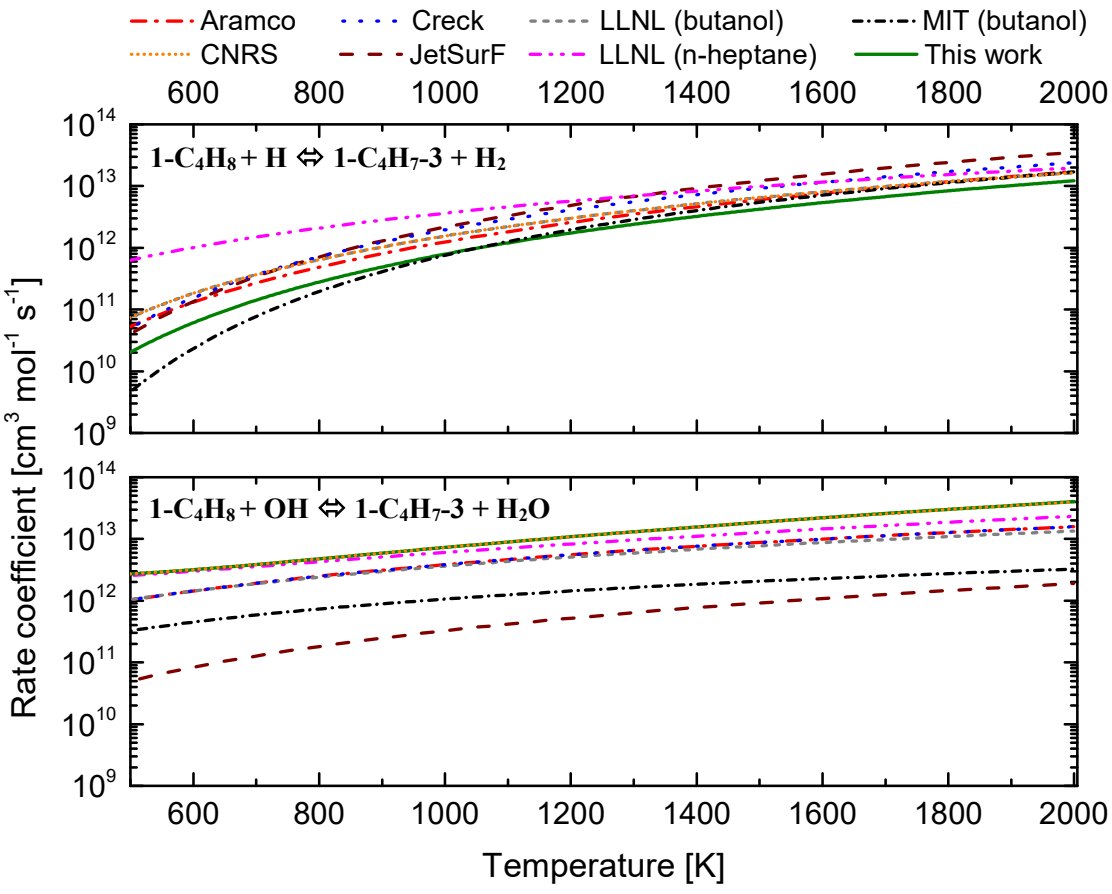

Figure 35. Comparison of rate coefficients for most influential hydrogen abstractions from 1-C_4H_8 included in the analyzed models.

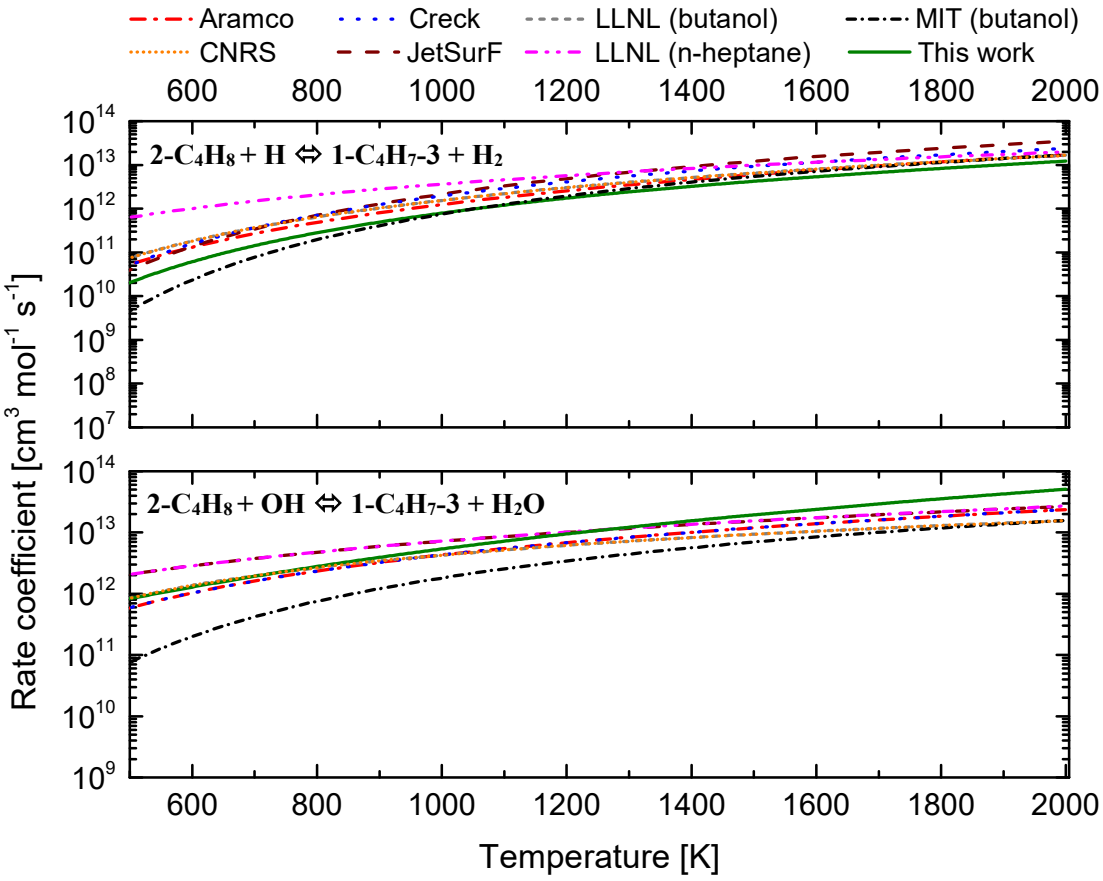

Figure 36. Comparison of rate coefficients for most influential hydrogen abstractions from 2-C_4H_8 included in the analyzed models.

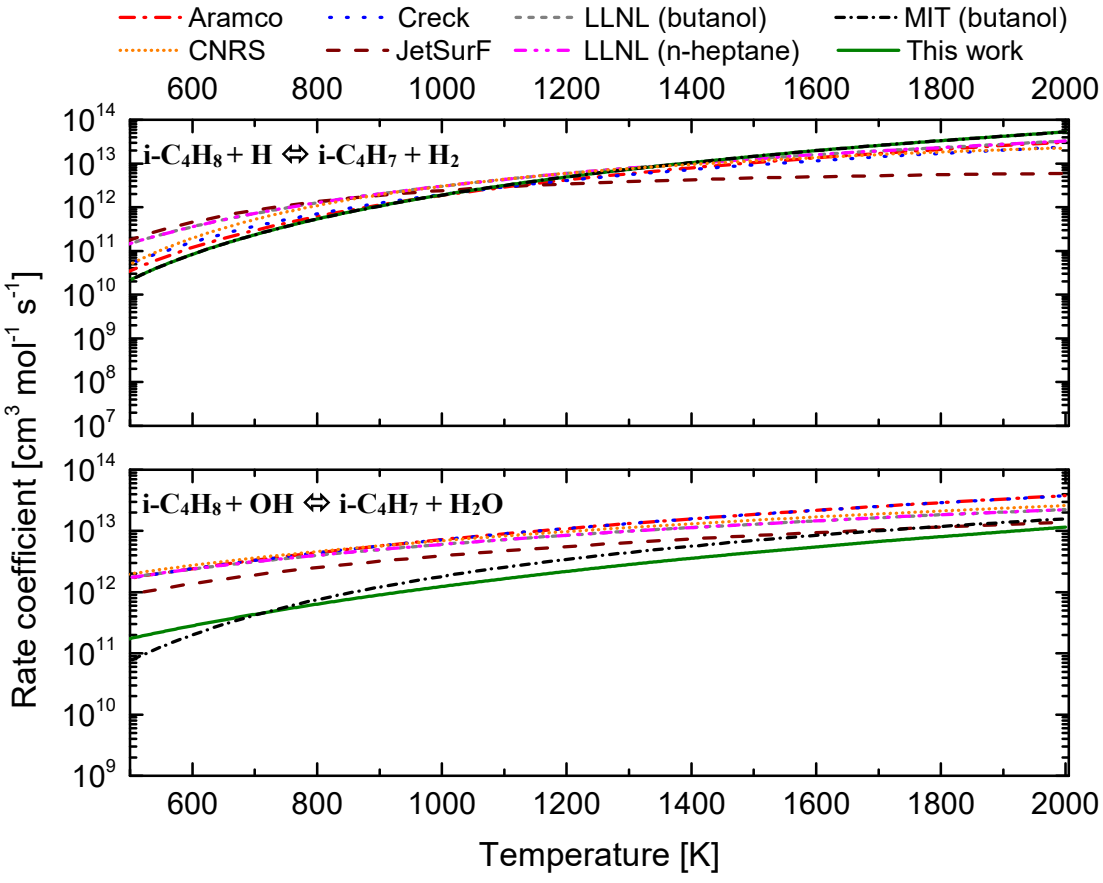

Figure 37. Comparison of rate coefficients for most influential hydrogen abstractions from i-C_4H_8 included in the analyzed models.

The hydrogen abstraction from C_2H_4 by OH shows similar rate coefficients, even if models do not consider the same source, demonstrating the robustness of the adopted data. Conversely, the abstraction by H included in Creck and JetSurF mechanisms is considerably faster than the one included in the other mechanisms compared in this work, especially at temperature < 1200 K, explaining the lower IDT predicted at these conditions by Creck and JetSurF mechanisms for C_2H_4.

The case where significant variations can be observed for hydrogen abstraction from C_3H_6 reported above is the reaction included in the newly generated mechanism and using OH as an abstracting agent. However, IDT and S_u data were adequately predicted by this model. Hence, one more iteration on RMG was performed by using the coefficients theoretically calculated in the literature for this reaction [259]. Results show negligible variations in IDT and S_u data, implying that RMG can partially compensate for the presence of not accurate reactions.

On the contrary, 1-C_4H_8 strongly variates by the selected source. As a way of example, coefficients up to two orders of magnitude lower than the other mechanisms can be observed for hydrogen abstraction by OH included in JetSurf and MIT (butanol), clarifying the reasons for larger IDT estimated at low-temperatures by these models. On the other hand, LLNL (n-heptane) considers faster hydrogen abstraction by H at low and intermediate temperatures, generating shorter IDT.

Regardless of the abstracting agent, reactions included in LLNL (n-heptane) for 2-C_4H_8 show similar trends, namely larger coefficients can be observed at low temperatures whereas high temperatures are characterized by smaller coefficients. These trends are in line with the considerations reported for the IDT of this fuel, where the tendency of underestimating IDT at low temperature, together with slightly larger IDT at high temperature, was observed.

Although JetSurF strongly overpredicts the IDT of i-C_4H_8 small variations can be observed for coefficients of hydrogen abstractions, meaning that the discrepancies can be ascribed to missing pathways determining the ignition phenomena.

Eventually, the comparison of the primary reactions included in LLNL (butanol) for butene isomers indicates the existence of conditions having i-C_4H_8 as a more reactive isomer, partially explaining the erroneous relative reactivity between butene isomers observed at intermediate temperatures for this model.

Ultra-low temperature reactivity

The excellent agreement between experimental data (either retrieved in the literature or collected in this work) with numerical estimations obtained by using the detailed kinetic mechanism here produced allows for the evaluation of the overall reactivity at conditions where data are lacking. Indeed, considering the theoretical approach adopted for the generation of the detailed kinetic mechanism, there is no drawback to its application at ultra-low temperature (i.e., temperature lower than 298 K). At these temperatures, hydrogen and methane reactivities are relevant in the view of cryogenic storage. Hence, Figure 38 and Figure 39 provide an overview of the estimations of laminar burning velocity at an ultra-low initial temperature in air for hydrogen and methane, respectively. Experimental data collected in this work or retrieved from the current literature at 298 K were added for the sake of comparison.

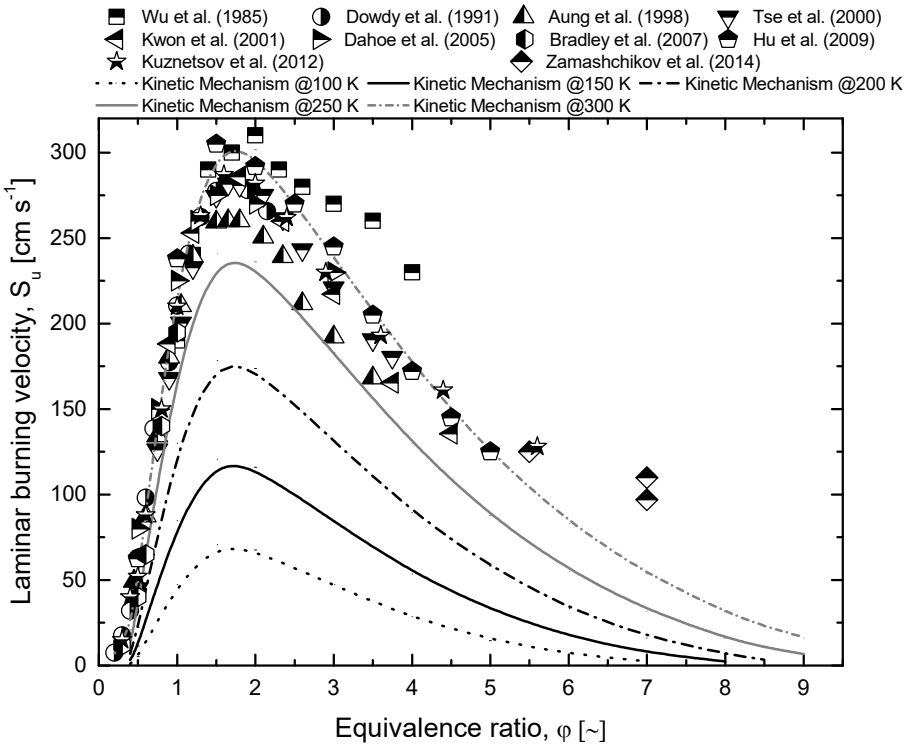

Figure 38. Comparison of the laminar burning velocity of hydrogen/air mixtures with respect to the equivalence ratio, at ultra-low initial temperature as estimated by using the detailed kinetic mechanism developed in this work (lines) and collected experimentally (symbols) [264][55][265][266][24][267][268][269][270][271].

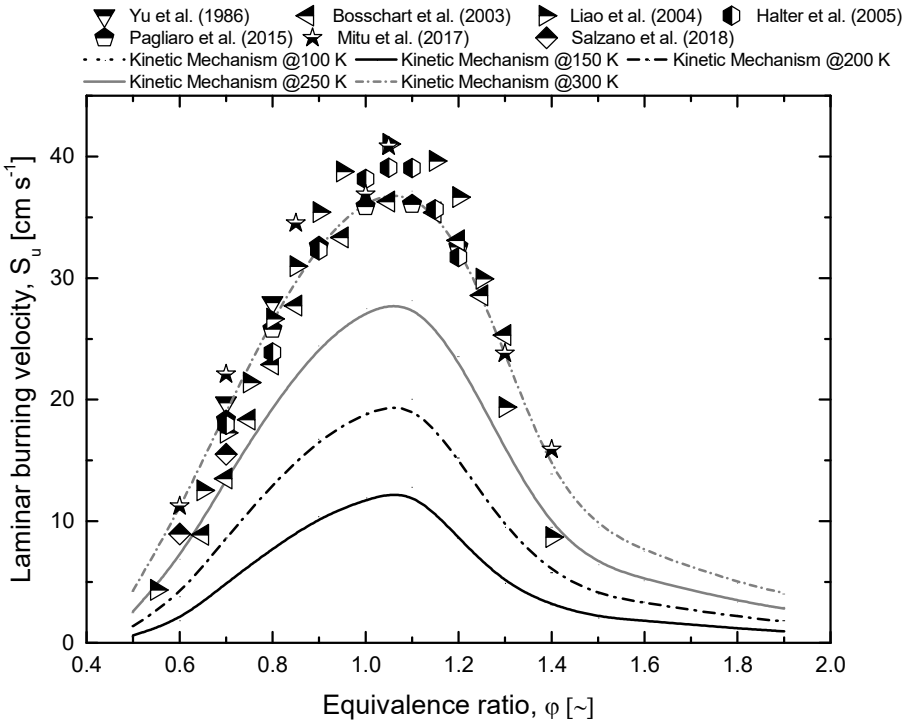

Figure 39. Comparison of the laminar burning velocity of methane/air mixtures with respect to the equivalence ratio, at ultra-low initial temperature as estimated by using the detailed kinetic mechanism developed in this work (lines) and collected experimentally (symbols) [272][234][273][274][236][275][276]

The typical shapes of the laminar burning velocity to the equivalence ratio are not altered by the temperature in both cases. Indeed, an almost linear trend characterizes the lean compositions, whereas parabolic decrease can fairly represent the rich composition case for both fuels. Other than the obvious effect of reducing the overall reactivity, the decrease in initial temperature leads to a shift toward the stoichiometric composition of the equivalence ratio where fundamental laminar burning velocity is observed (φ_f). This trend is more evident in the hydrogen case, although the investigated values are quite far from the boiling temperature. Considering that initial temperature has a weaker effect on thermal aspects than kinetics, this observation is in line with the assumption of the equality of thermal and kinetic rates at φ_f. Conversely, the asymptotic values are weakly affected by the initial temperature, confirming the connection between laminar burning velocity and gaseous diffusion at extreme composition, representing the key assumption of the limiting laminar burning velocity theory. In this perspective, this model can be adopted for the estimation of the safety parameters at ultra-low temperature. Indeed, several correlations have been developed for the estimation of flammability limits at temperature and pressure differing from the standard conditions where most of the experimental tests are performed. However, most of these correlations have been developed for temperature higher than 298 K, without any validations at lower temperatures. Smaller temperatures imply a narrower flammable region because of the reduced reactivity of the mixture. Hence, the safety

parameters at a temperature below 298 K have been commonly assumed as equal to the experimental values under a conservative approach. However, the development of a detailed kinetic mechanism suitable for these conditions allows for accurate estimations of these parameters, removing the abovementioned hypothesis. For economic reasons, storage in cryogenic conditions may potentially involve either hydrogen, natural gas, or ethylene. Hence, the detailed kinetic mechanism developed in this work was implemented for the estimation of the LFL and UFL of these species in the presence of air (Figure 40-Figure 42).

Experimental data from the literature were added, when available. Please note that the reported lower temperature differs per each fuel by the variation in flashpoint or boiling point of oxygen.

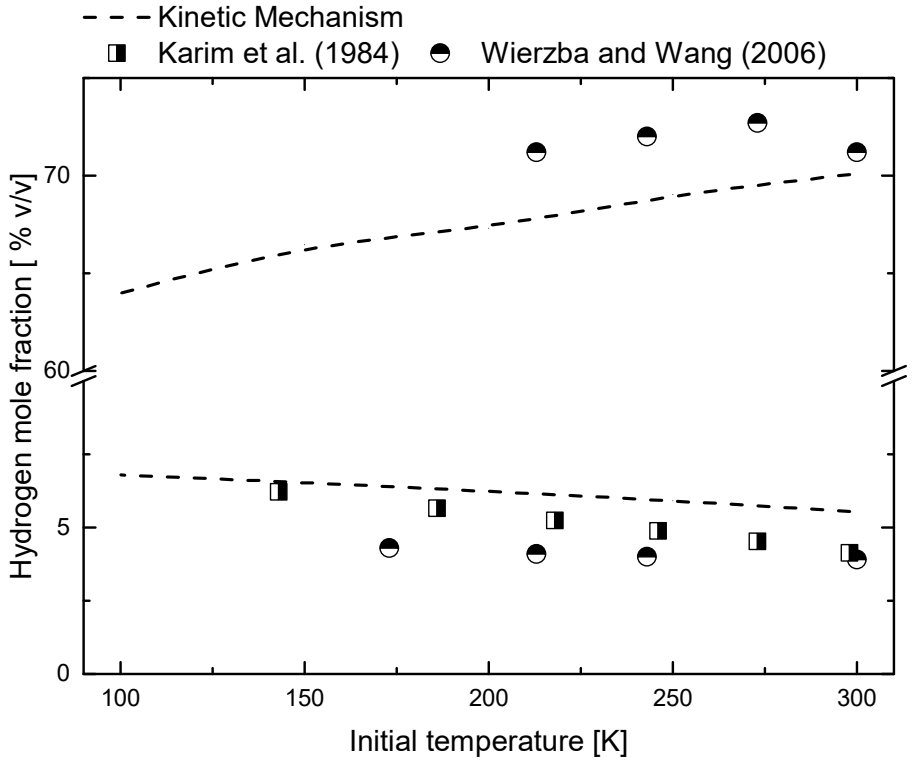

Figure 40. Comparison of flammability limits of hydrogen estimated by using the detailed kinetic mechanism developed in this work (lines) and collected experimentally (symbols) [277][278]. *Please consider that experimental data refer to LNG 1 composition, only.*

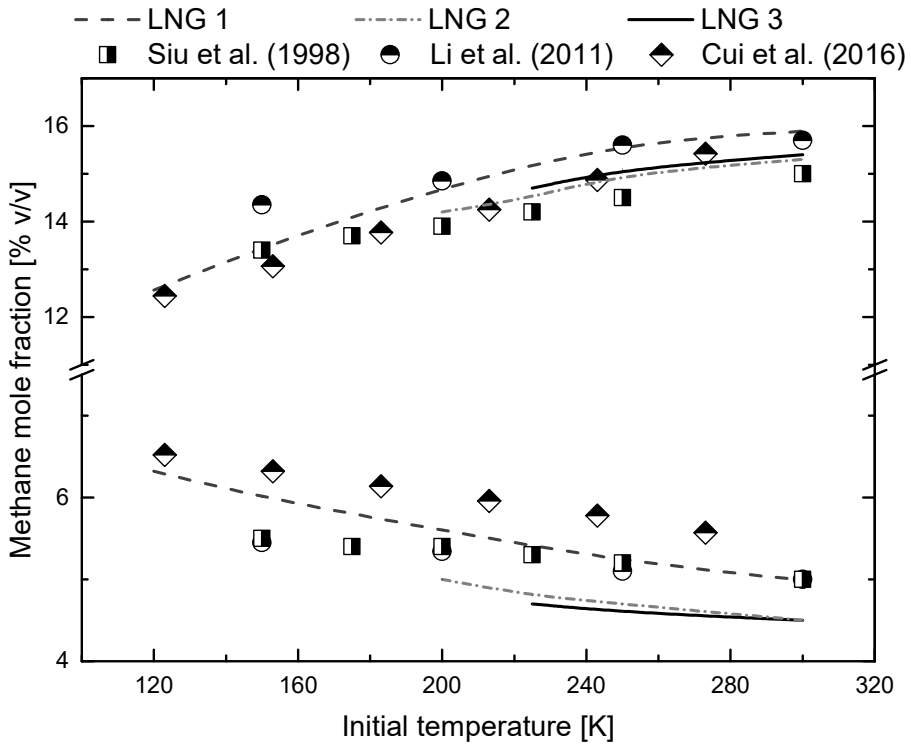

Figure 41. Comparison of flammability limits of LNG typical compositions estimated by using the detailed kinetic mechanism developed in this work (lines) and collected experimentally (symbols) [279][280][163]. *Please consider that experimental data refer to LNG 1 composition, only.*

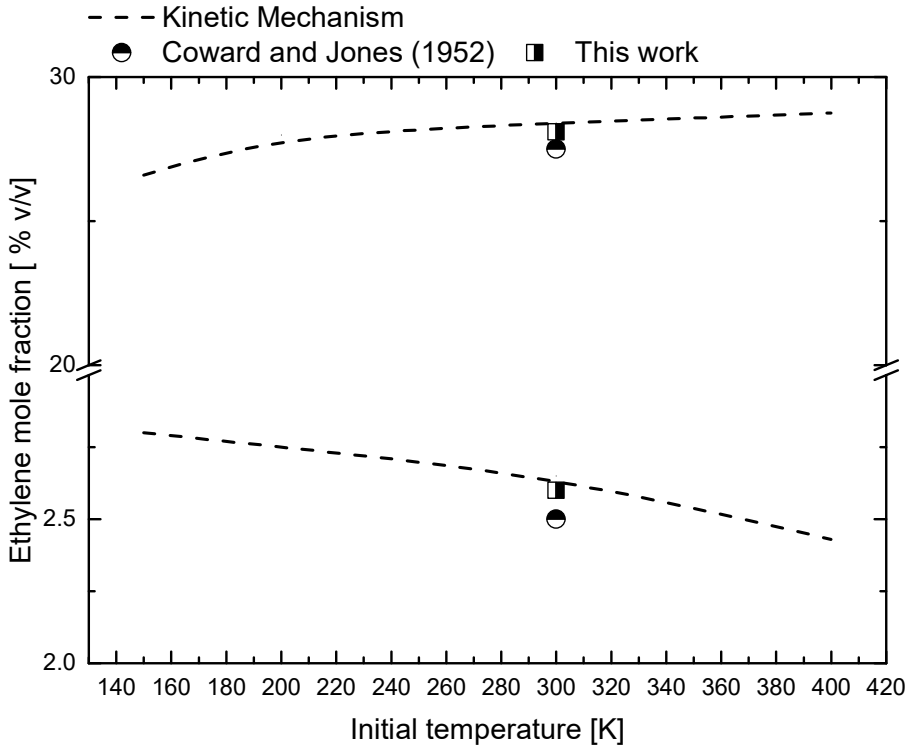

Figure 42. Comparison of flammability limits of ethylene estimated by using the detailed kinetic mechanism developed in this work (lines) and collected experimentally (symbols) in this work and the literature [116].

An excellent agreement between experimental and numerical data can be observed at extreme conditions, as well, testifying to the comprehensiveness of the produced mechanism. As expected, the decrease in temperature makes the flammable regions narrower, regardless of the analyzed fuel. However, it is worth mentioning that only the LFL of hydrogen follows a linear trend with temperature, meaning that the assumption of the thermal aspect dominating the reactivity at the lean limit cannot be extended to methane and ethylene at low temperature. On the other hand, similar trends can be observed once the effect of temperature on UFL is compared. These phenomena can be attributed to the difference in the overall reactivity of the investigated species. More specifically, temperature decrease makes the hypothesis of instantaneous reactions at lean conditions not applicable for fuels having low overall reactivity, exclusively.

Dispersion of cryogenic fuels in the atmosphere

Key aspects involving the numerical investigations of vapour dispersion of cryogenic fuels in the atmosphere include the thermodynamic properties of all the considered species [148]. Considering the peculiar conditions analyzed, theoretical-based approaches should be preferred. In this view, *ab initio* calculations were performed. The effect of temperature on enthalpy, entropy, and specific heat capacity is commonly expressed in terms of NASA polynomial, i.e., a 7 coefficients correlation. However, temperature variation is commonly split into two ranges to increase the accuracy of the source data. The low-temperature range usually includes temperature up to 1000 K, thus the high-temperature range was excluded from this analysis since it cannot be reached as reactions are absent. Obtained coefficients are reported in Table 14, distinguishing pure ortho hydrogen (o-H_2) by pure para hydrogen (p-H_2), and a mixture of 75% o-H_2 + 25% p-H_2 (n-H_2).

Table 14. Low -temperature coefficients of NASA polynomial, as obtained by ab initio calculations for species involved in an accidental release of cryogenic fuels in the atmosphere.

Species	A_0	A_1	A_2	A_3	A_4	A_5	A_6
n-H_2	$3.50 \cdot 10^{0}$	$7.97 \cdot 10^{-5}$	$-2.55 \cdot 10^{-7}$	$3.61 \cdot 10^{-11}$	$2.69 \cdot 10^{-13}$	$-1.06 \cdot 10^{3}$	$-4.28 \cdot 10^{0}$
o-H_2	$2.55 \cdot 10^{0}$	$-1.96 \cdot 10^{-3}$	$4.08 \cdot 10^{-6}$	$2.06 \cdot 10^{-7}$	$-5.69 \cdot 10^{-10}$	$-9.04 \cdot 10^{2}$	$1.81 \cdot 10^{0}$
p-H_2	$2.61 \cdot 10^{0}$	$-1.39 \cdot 10^{-2}$	$3.39 \cdot 10^{-4}$	$-1.61 \cdot 10^{-6}$	$2.22 \cdot 10^{-9}$	$-1.06 \cdot 10^{3}$	$-3.59 \cdot 10^{-1}$
CH_4	$4.21 \cdot 10^{0}$	$-5.36 \cdot 10^{-3}$	$2.51 \cdot 10^{-5}$	$-2.14 \cdot 10^{-8}$	$5.97 \cdot 10^{-12}$	$-1.02 \cdot 10^{4}$	$-9.21 \cdot 10^{-1}$
C_2H_6	$3.75 \cdot 10^{0}$	$4.55 \cdot 10^{-5}$	$4.08 \cdot 10^{-5}$	$-4.57 \cdot 10^{-8}$	$1.57 \cdot 10^{-11}$	$-1.15 \cdot 10^{4}$	$4.74 \cdot 10^{0}$
C_3H_8	$3.06 \cdot 10^{0}$	$1.29 \cdot 10^{-2}$	$3.47 \cdot 10^{-5}$	$-4.71 \cdot 10^{-8}$	$1.71 \cdot 10^{-11}$	$-1.44 \cdot 10^{4}$	$1.08 \cdot 10^{1}$
N_2	$3.54 \cdot 10^{0}$	$-6.93 \cdot 10^{-4}$	$2.10 \cdot 10^{-6}$	$-1.29 \cdot 10^{-9}$	$2.59 \cdot 10^{-13}$	$-1.04 \cdot 10^{3}$	$2.99 \cdot 10^{0}$
O_2	$3.12 \cdot 10^{0}$	$1.73 \cdot 10^{-3}$	$-8.53 \cdot 10^{-7}$	$1.70 \cdot 10^{-10}$	$-1.23 \cdot 10^{-14}$	$-1.04 \cdot 10^{3}$	$6.28 \cdot 10^{0}$

Results were validated against experimental data from the literature, showing excellent agreement, thus corroborating the adopted approach. The effect of boundary conditions either on the sizes of flammable or visible cloud was evaluated for the case of the dispersion in the atmosphere of LNG

(assumed as pure methane). The relative increase in the size of flammable or visible cloud due to variation in input parameters was expressed in terms of normalized sensitivity coefficient (NSC), as defined in the previous section (Figure 43).

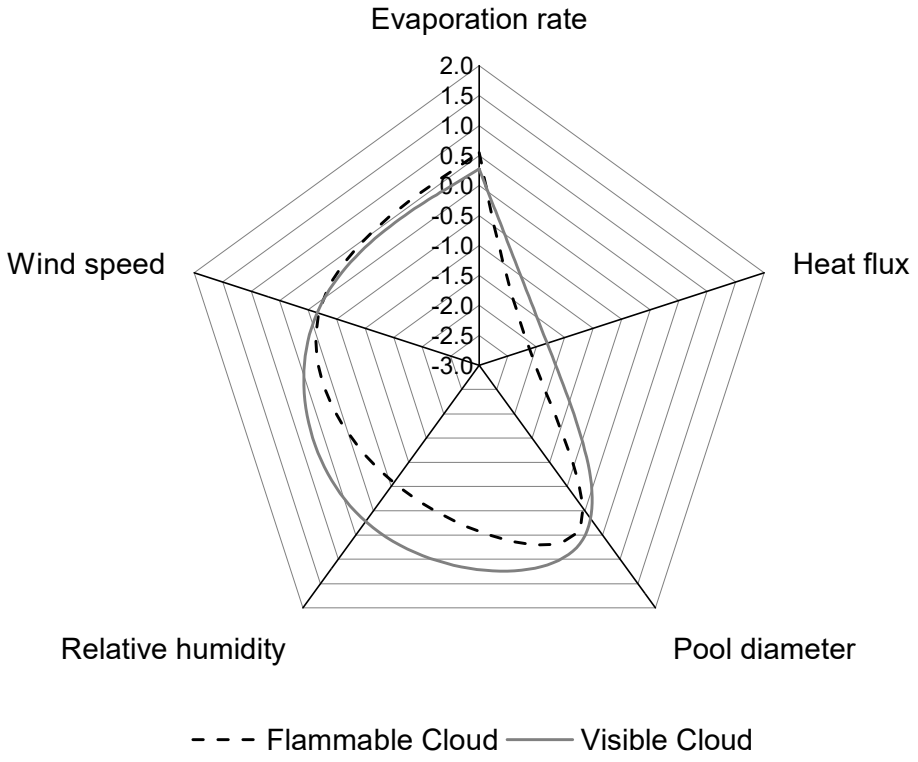

Figure 43. Evaluation of the relative contribution expressed in terms of normalized sensitivity coefficients (NSCs) of input parameters on the size of flammable and visible cloud caused by LNG 1 release along with the downwind direction.

Evaporation rate, pool diameter, and wind speed weakly affect the ratio between flammable and visible cloud sizes. Relative humidity has a larger impact on the extension of visible cloud than flammable cloud being a parameter included for the estimation of dew point. Conversely, it is worth noting that the imposed heat flux is the most impacting parameter in both cases (i.e., characterized by the highest absolute value of NSC) and has large differences in NSC referring to the flammable and visible cloud. Hence, additional data related to the thermal boundary condition imposing the heat exchange between the substrate and the vapour were provided. Four different cases were analyzed to this aim. Results were reported in terms of the size of flammable cloud in downwind direction x_{LFL}, dispersion safety factor (DSF), and cloud shape factor (CSF) defined in the methodological section (Table 15).

Table 15. The effect of thermal boundary condition on the extension and shape of flammable and visible regions caused by the accidental release of LNG 1.

Case	q [W m^{-2}]	x_{LFL} [m]	DSF [-]	CSF [-]
Base case	313.5	35	1.23	16
Case 1	38.8	110	1.10	220
Case 2	Calculated*	115	1.44	260
Case 3	0.0	120	0.67	230

** Heat flux calculated imposing the thermal properties of water and estimated driving force.*

Based on the reported data, it is possible to conclude that the variation in thermal boundary conditions on the substrate strongly affects the shape of the vapour cloud, significantly modifying the safety distances. This phenomenon can be attributed to the differences in the density of vapours to air once temperature increases. In other words, depending on the temperature methane vapours may be heavier or lighter than air. Hence, the reduction of a heat source makes this transition slower and favours the horizontal fuel spread. The magnitude of the observed variations implies that heat exchange involving the substrate-vapour cloud is essential for the determination of temperature distribution. Considering the typical values for heat transfer coefficients of materials potentially representing the substrate, either solid (such as concrete) or liquid (i.e., water), the localization of the fuel pool should be carefully considered. Besides, this result encourages the implementation of technological solutions controlling the heat exchange to promote the vertical dispersion of cryogenic fuels with consequent reduction of safety distance. Alternatively, a rapid phase transition may be caused by the accidental release of cryogenic fuels. In this case, the maximum overpressures along with the time and distance from the releasing point were estimated for different pool diameters (representative of the time after release) and releasing rate. For the sake of brevity, results obtained for LNG 1 are reported, at this stage (Table 16).

Table 16. Maximum overpressure (ΔP_{max}) expressed in kPa, generated by the release of LNG 1 as a function of pool diameter (Dp) and the release rate (v_r).

	D [m]				
v_r [m s^{-1}]	0.1	0.5	1.0	2.0	3.0
0.12	$2.59 \cdot 10^{-5}$	$8.06 \cdot 10^{-5}$	$1.44 \cdot 10^{-4}$	$2.74 \cdot 10^{-4}$	$3.89 \cdot 10^{-4}$
10	0.18	0.56	1	1.9	2.7
20	0.72	2.24	4.00	7.60	10.80
40	2.88	8.96	16.00	30.40	43.20

The releasing rate has a larger impact than the pool diameter on the maximum overpressure generated by RPT. Indeed, an almost linear trend can be observed for the latter parameter. Besides, a threshold value of releasing rate generating overpressure causing significant damages (e.g., 7 kPa) can be calculated for different diameters. Someone may argue that this result represents a limited fraction of

the scenario potentially occurring. In this view, additional data were collected for LNG 2 and LNG 3 compositions. Based on the obtained results, a rule of thumb (*Eq. 54*) for the estimation of the overpressures at different LNG composition, pool diameter, and releasing rate was proposed and successfully tested.

$$\Delta P_{max} = 4 \cdot D_p \cdot \rho_{mix,T_b} \cdot \overline{MW} \cdot v_r^2 \qquad \textit{(Eq. 54)}$$

Similar analyses were conducted for the case of the accidental release of liquid hydrogen. However, in contrast to the previous case, four cases were distinguished based on the assumptions posed for the representation of para-ortho conversion. More specifically, instantaneous conversion to the equilibrium ratio between ortho/para hydrogen was assumed either for pure p-H_2 (p-H_2) or n-H_2 (n-$H_{2,eq}$) as the initial composition. Moreover, a case where a constant n-H_2 composition was imposed (n-$H_{2,con}$) was included together with results obtained by the empirical-based correlation proposed by Bubbico and Salzano [127] for RPT of cryogenic fuels, as per discussion. The latter was referred to as Correlation in Figure 44.

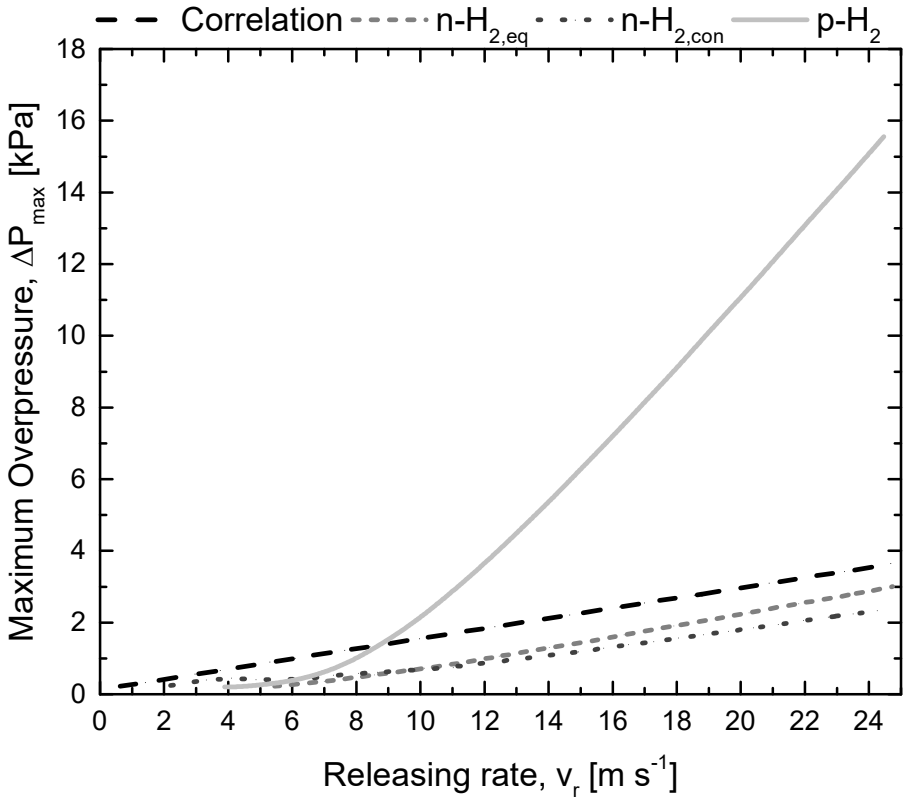

Figure 44. Maximum overpressure (ΔP_{max}) expressed in kPa, as calculated at distance x equal to 10 D_p, generated by the release of liquid hydrogen by different models.

The analytical model (*Correlation*) gives more conservative results than *n-$H_{2,eq}$* and *n-$H_{2,con}$*, whereas the inclusion of para-ortho transformation has a dramatic effect on the generated overpressure (*p-H_2*). The latter is the only case where structural damage on atmospheric equipment (i.e., $\Delta P_{max} \geq 7$ kPa) and human injury (i.e., $\Delta P_{max} \geq 16$ kPa) could be expected, meaning that the neglection of the transformation related to the electronic configurations of hydrogen at ultra-low temperature leads to significant underestimations. Noteworthy, *n-$H_{2,eq}$* and *n-$H_{2,con}$* resulted in similar overpressure, lower than typical threshold values defined for structural damages. Comparing the *Correlation* and *p-H_2* curves two different areas can be distinguished. Indeed, the former indicates higher values than the latter for release rate smaller than 9 m s^{-1}, exclusively. Considering that n-H_2 is denser than p-H_2 and para-ortho transformation is endothermic [187], the discrepancies in these trends can be associated with the differences in density of the dispersing fuels. Indeed, a limited flow field reduces the rate of heat exchange, thus makes a smooth temperature profile along with the distance from the releasing point. Under these conditions, the rate of para-ortho conversion is controlled and, thus this transformation has a reduced impact on temperature profile and fuel distribution. Conversely, elevate release rates increase the heat exchange, resulting in a faster para-ortho conversion. The consequent additional amount of absorbed heat from the environment flattens the temperature profile, having detrimental effects on dispersion efficiency, thus causing larger overpressures. This conclusion was corroborated by the trends reported for the *n-$H_{2,eq}$* and *n-$H_{2,con}$* cases since curves intersect at similar release rate and the one accounting for para-ortho conversion estimates larger overpressure as the release rate increases.

Starting from these considerations, two different regimes were indicated:

1) Hydrogen release rate < 9 m s^{-1}, characterized by moderate overpressures and variation in density limited by the heat transfer
2) Hydrogen release rate ≥ 9 m s^{-1}, characterized by significant overpressures and variation in density ruled by the para to ortho conversion.

Kinetic mechanism reduction

As already pointed out, the kinetic mechanism generated so far represents a comprehensive model including most of the relevant reactions involving the oxygenated fuels investigated in this work and their intermediates in the oxidative environment. Considering the computational power available nowadays, the elevated number of reactions and species listed in its library does not allow for the implementation in computational fluid dynamic models as it is. Hence, the identification of relevant pathways for the investigated conditions is essential to combine detailed chemistry with fluid

dynamics. Recalling the modularity of the approach implemented for the generation of kinetic mechanism, the first step toward mechanism reduction was performed based on the size of the reactants. In other words, the butene sub-model produced in this work was considered as a starting point for the generation of core models suitable for light alkanes pool fire and light alkenes partial oxidation. Primary reactions involving species composing the surrogate mixture of aviation fuels were added to integrate this model. For the latter case, the model reduction was performed by combining sensitivity analysis and reaction path analysis at atmospheric pressure, only, whereas for the latter case temperature range was restricted to the values reported in the literature as typical operative conditions, i.e., below 600 K. As a way of example, the results of the sensitivity analysis performed at 298 K and 1 atm for the representative composition for LNG defined in the previous section at stoichiometric composition with air were reported below.

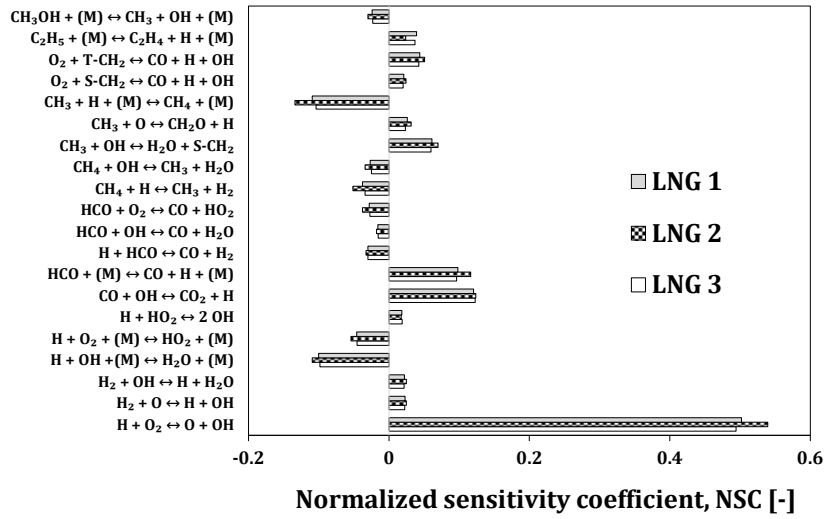

Figure 45. Sensitivity analysis of different LNG composition at 298 K, 1 atm, and stoichiometric composition with air.

As expected, the reactions having a large influence on the overall reactivity involve small radicals largely considered essential in combustion, such as OH, H, and O. The typical path characterizing methane oxidation (i.e., CH_3, HCO, CO, and CO_2) can be identified. The addition of ethane increases the influence of $H + O_2 \leftrightarrow O + OH$ reaction. However, this variation is attenuated by the simultaneous addition of ethane and propane (i.e., LNG 3). This phenomenon can be ascribed to the peculiarity of the overall reactivity for C_2 species already discussed in the experimental paragraphs of this section.

The primary reaction of methane characterized by larger NSC is the hydrogen abstraction by OH and H radicals. Also, C_2H_5 hydrogen abstraction has a large impact on LNG 1 mixture (i.e., pure methane), as well. This aspect implies that C_2H_5 is largely formed as a by-product. The increase in the number of carbon atoms concerning the reactants indicates that it can be involved in the formation of soot

precursors. This hypothesis is confirmed by the results obtained for rich composition, where the production of soot precursors, such as C_2H_2 and C_3H_3, derives from C_2H_5. These results comply with the observations reported by Agafonov et al. (2007) [281] and Frassoldati et al. (2010) [282] and may partially explain the increase in soot formation experimentally observed by McEnally and Pfefferle (1998) [283] for methane/air non-premixed flames doped with C_3 hydrocarbons. Regardless of the investigated composition, a single reaction can be observed for the oxidation of carbon monoxide to carbon dioxide, having OH as a reactant. Starting from these observations and reaction path analysis, a reduced mechanism for LNG combustion at low initial temperature was developed (Figure 46).

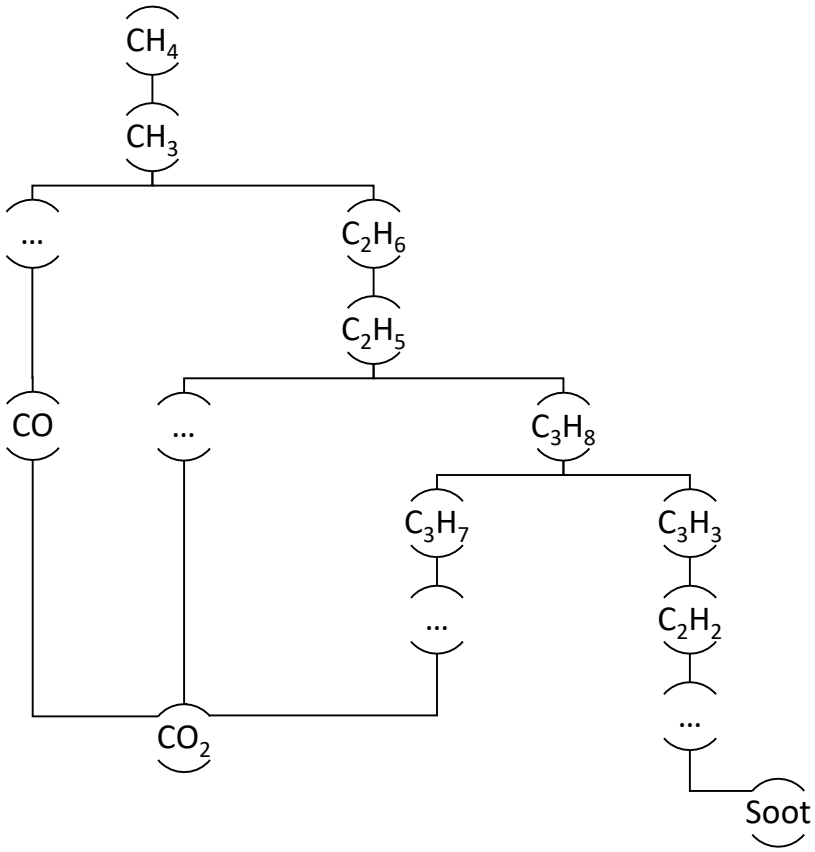

Figure 46. Representation of the reduced mechanism implemented for LNG pool fire characterization. Please consider that the rate-determining steps were reported, exclusively.

Regardless of the number of carbon atoms considered, it is possible to conclude that the primary reaction of alkanes represents the rate-determining step, followed by oxidation toward CO and CO_2 or by an increase of H/C ratio toward soot formation. The most relevant reactions associated with each rate-determining step reported above were included in the reduced mechanism implemented in CFD tools.

Similarly, Figure 47 reports a schematization of the reduced mechanism representing the chemistry of the selected surrogate of aviation fuels.

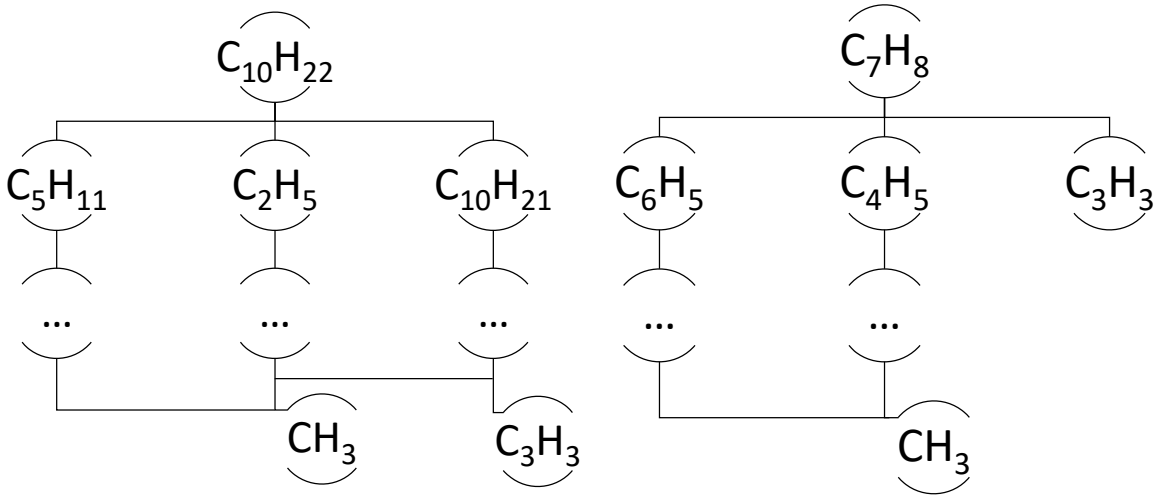

Figure 47. Representation of the reduced mechanism implemented for aviation fuel pool fire characterization. Please note that the core combustion model accounting for CH_3 and C_3H_3 chemistry was reported in the previous figure.

The increase in the number of carbon atoms in alkanes makes relevant the break of the C-C bond, directly producing C_5H_{11} or C_2H_5 radicals. Nevertheless, hydrogen abstraction still represents a major path in n-decane decomposition. Similarly, C-C scission characterizes the primary steps of toluene. Once activated by the abovementioned primary reactions, the resulting radicals form CH_3 and C_3H_3 that react under the mechanism described in Figure 46.

Eventually, a reduced mechanism representative for the chemistry of ethylene and propylene at the operative conditions of the partial oxidation processes is represented in Figure 48. For the sake of conciseness, the sub-mechanism characterizing the complete oxidation of resulting epoxidized products was neglected at this stage. However, it was included once the reduced mechanism was implemented in CFD analysis for process intensification.

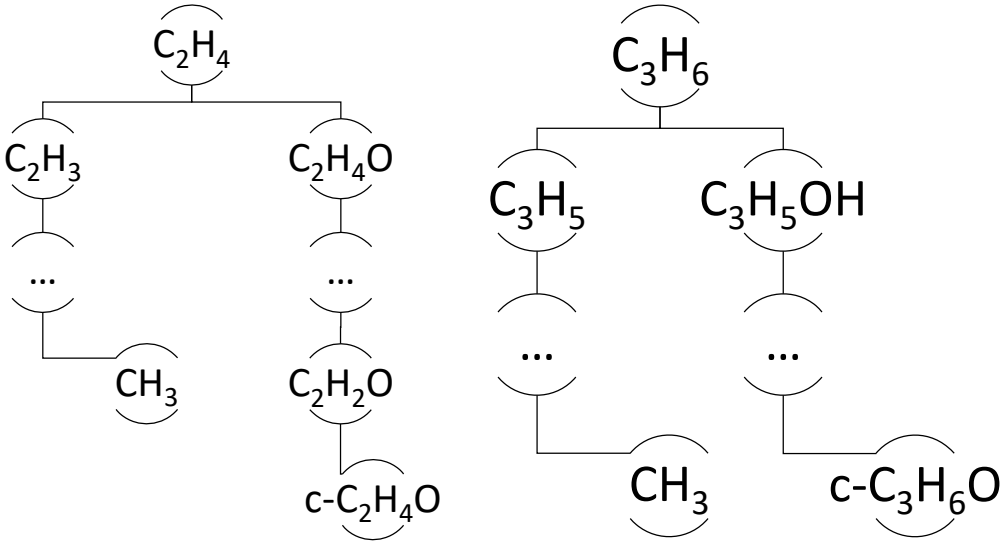

Figure 48. Representation of the reduced mechanism implemented as homogeneous reactions of ethylene (left) and propylene (right) partial oxidation processes. Please note that the core combustion model accounting for CH_3 chemistry was reported in Figure 46. C_2H_4O, c-C_2H_4O, and c-C_3H_5O stand for CC=O, C_1OC_1, and C_1OC_1C in SMILES notation, respectively.

In both cases, the decrease in maximum temperature considered during the model reduction makes the C_3H_3 formation with consequent production of soot negligible. Both species are characterized by two different pathways at this stage, one initiated by a hydrogen abstraction by H producing C_2H_3 or C_3H_5; another one initiated by oxidation with OH producing C_2H_4O or C_3H_5O. The former represents the initiation step for complete oxidation to carbon dioxide, whereas the latter produces epoxidized products via two consecutive hydrogen abstraction followed by ring generation. However, substantial distinctions can be made for the second path. Indeed, hydrogen abstraction with simultaneous addition of OH group is relevant only for the propylene oxide process, whereas oxygen addition to ethylene directly produces a double bond between C and O. The identification of the rate-determining steps either for desired or undesired paths is a prelude for the production of optimized catalyst formulations.

Detailed kinetic mechanism for pool fire characterization

For the sake of procedure and reduced model validation, the numerical approach proposed in this work was tested for pool fire characterization of aviation fuel, at first. To this aim, a simple chemistry approach (i.e., considering tabulated values for complete combustion reaction rate) integrated with soot and carbon monoxide yields retrieved from the literature [284] and detailed chemistry results were compared with experimental data [227] (Figure 49). For the sake of clarity, results were normalized with the steady-state value collected in the experimental work.

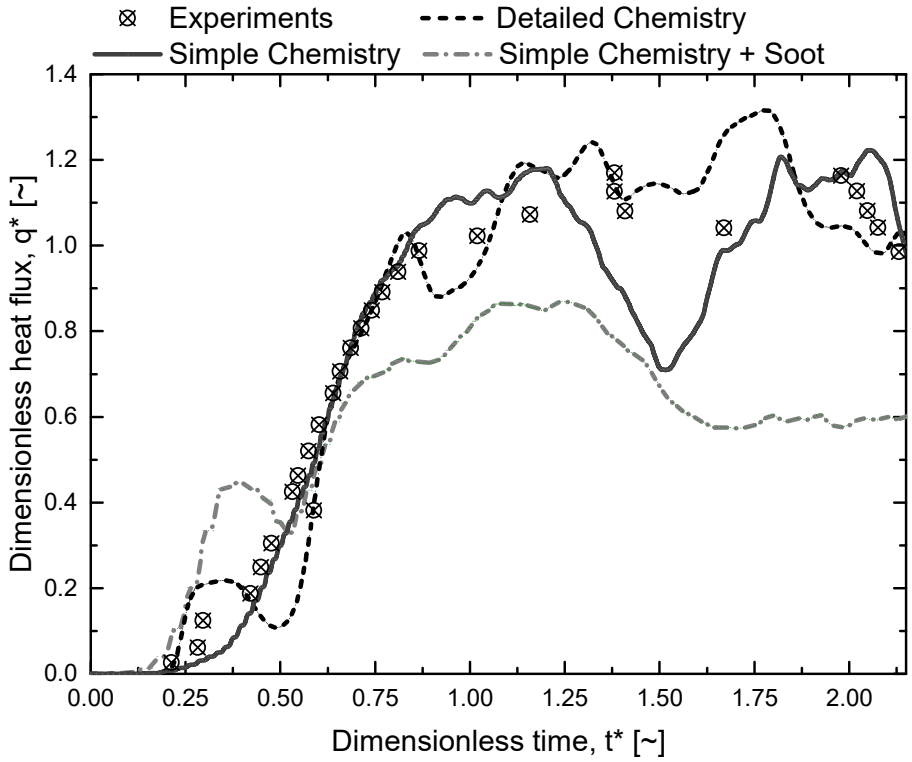

Figure 49. Comparison of the heat flux estimated by different kinetic mechanisms with experimental data from the literature [227][285] *along with the time.*

The introduction of soot and carbon monoxide yield reduces the estimated surface emissive power because of the reduced combustion efficiency coupled with the enhanced heat absorption related to the presence of the black body [23]. Nevertheless, simple chemistry can fairly reproduce experimental data. Hence, the underestimation observed for the simple chemistry + soot case can be attributed to the nature of the implemented values of yields and tabulated rates. Indeed, the yields considered in this work were calculated empirically from small and medium scale tests. Hence, the large scale of the investigated pool may suggest the adoption of smaller values. Besides, the tabulated value for the combustion rate has been calculated empirically, as well, without indications on the corrections to exclude the formation of soot and carbon monoxide.

On the other hand, the implementation of a detailed (in reduced form) kinetic mechanism generates accurate predictions of the produced heat flux, validating the proposed approach. Besides, its implementation allows for the evaluation of product distributions, including soot, together with the characterization of pool fires having geometries and properties not included in tabulated values.

In this light, the effect of pool diameter D_p (expressed in m) on mass burning rate $\dot{m}$ (expressed in kg·m^{-2}·s^{-1}) was estimated. Results were expressed in terms of Hottel's correlation [286] (*Eq. 55*).

$$\dot{m} = \dot{m}_{\infty} \cdot \left(1 - e^{-k\beta \cdot D_p}\right) = 0.47 \cdot \left(1 - e^{3.61 \cdot D_p}\right) \qquad \textit{(Eq. 55)}$$

where $\dot{m}_{\infty}$, *k, and* β stand for mass burning rate for infinite-diameter, extinction coefficient, and mean beam length corrector. The extinction coefficient and mean beam length corrector are commonly aggregated [157]. The obtained values are in line with data reported by Chatris et al. (2001) [287], for medium-scale diesel pool fire, and empirical parameters reported in the literature for a large pool of petroleum products [157].

As mentioned before, the successful validation of the proposed procedure for model reduction and implementation in CFD for pool fire characterization of aviation fuels was followed by its application to the LNG case. In this case, the comparison was performed for different LNG composition but limited to the results obtained by the adoption of simple chemistry and detailed chemistry.

As a way of example, temperature and methane distributions obtained for the LNG 1 case by detailed chemistry implementation at steady state were reported in the following figure

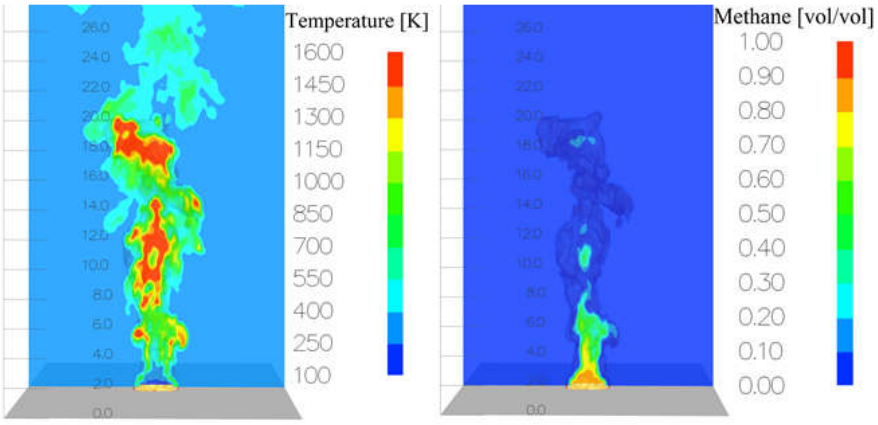

Figure 50. Temperature (left) and methane (right) distributions calculated at the steady-state for LNG 1 pool fire.

Three different regions can be identified, in agreement with the literature [159]:

- pyrolysis zone, located in the proximity of the liquid-gas interface, is characterized by composition rich in methane and temperature below atmospheric value. Hence, characterized by a non-flammable mixture;
- reactive zone, following the pyrolysis zone, is characterized by fuel-oxidant composition within the flammability limits. Hence, the region where combustion occurs;
- hot gases zone, following the reactive zone, is characterized by decreasing temperature and methane concentration below the LFL. Hence, the dispersion of hot gases produced in the previous zone occurs due to buoyancy.

These zones cannot be uniquely individuated due to the non-homogeneous nature of the investigated scenario, characterized by poor mixing and non-uniform air entrainment.

The average temperature obtained at the pseudo-steady state shows that simple and detailed chemistry approaches strongly differ only in the proximity of the liquid pool, meaning that the cheaper approach should be preferred for far-field evaluations. Besides, instantaneous and localized pockets characterized by temperature ranging within 1450 – 1700 K can be observed in both cases, following the literature [288]. However, significant variations can be observed once surface emissive powers are compared (Table 17).

Table 17. Comparison of surface emissive power (SEP) with respect to fuel composition and applied approach. Please note that SC and DC stand for simple chemistry and detailed chemistry, respectively.

	LNG 1	**LNG 2**	**LNG 3**
SC [kW m^{-2}]	51.80	86.63	78.33
DC [kW m^{-2}]	52.20	89.41	80.20
Variation [%]	0.72	3.20	2.39

Either typical temperature or SEP values obtained for LNG 1 (i.e., pure methane) are in line with CFD analysis performed for small scale LNG pool fire, where temperature range from 1500 and 1750 K and SEP of 55 kW m^{-2} were reported [289]. The proximity of SEP data obtained by different approaches can be attributed to the abundance of data for methane/air combustion and the ideality of this reactive system. Moreover, the formation of a negligible amount of soot is confirmed for this mixture, being the soot yield calculated via detailed chemistry implementation equal to $6.64 \cdot 10^{-4}$. Similarly, $8.41 \cdot 10^{-4}$ and $1.11 \cdot 10^{-3}$ values were obtained for LNG 2 and LNG 3, respectively. These values should be intended as per reference since the variation in pool size may lead to significant variations of soot yield [290]. It is worth noting that the variation is considerably enhanced by the existence of ethane in the mixture and slightly reduced by the addition of propane. This discrepancy can be related to the chemical interactions affecting the methane combustion in the presence of ethane and propane that the simple chemistry approach neglects. Indeed, in that case, three parallel combustion reactions are considered, whereas the detailed chemistry includes reactions producing intermediates shared by the reaction path (e.g., CH_3). In this light, the effect of time on estimated temperature will be analyzed by discussing the results obtained by detailed chemistry, exclusively (Figure 51).

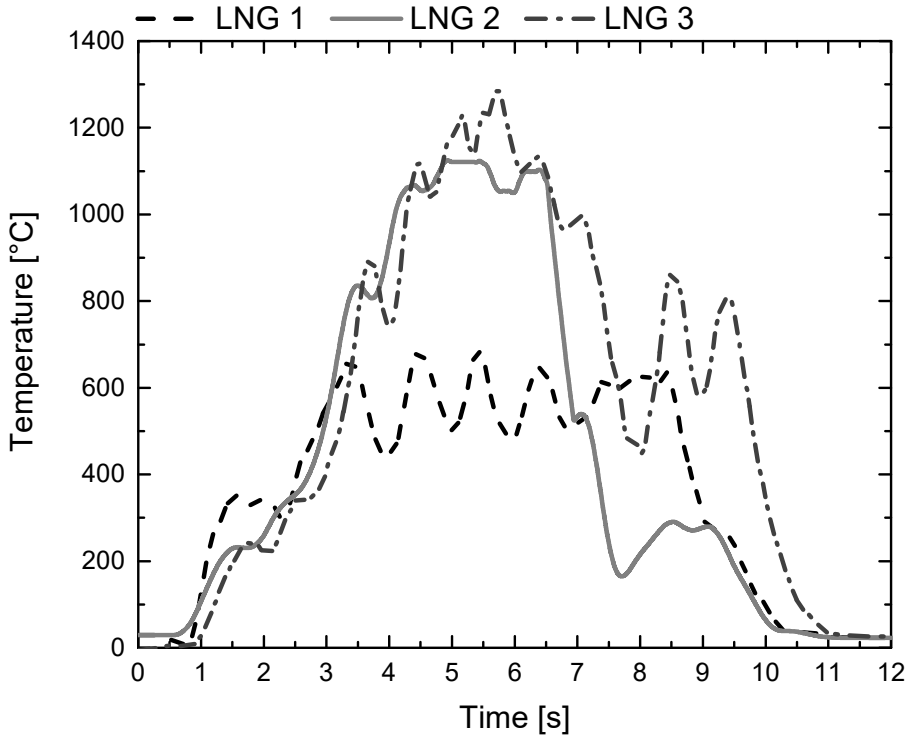

Figure 51. Temperature distribution along with the time for different LNG composition in case of a pool fire.

Results indicate the presence of the well-established steps characterizing the pool fire: initiation, pseudo-steady-state, and fast decrease due to fuel consumption. Similar trends were observed for the heat release rate (HRR). The duration of the second step is strongly related to the assumed conditions (e.g., pool thickness). However, it should be noted that multiple steady states can be observed for LNG 2 and LNG 3 mixtures. In other words, the presence of ethane and/or propane in the liquid phase leads to changes in vapour composition, as well, due to the difference in volatility of the involved species, causing peaks of different intensities along with the time. Further characterization of this scenario can be made by extending the discussion to the flame height (H), assumed as the vertical distance from the ground having a temperature rise of 500 °C [159]. The results obtained employing the CFD approach were compared with Thomas' correlation [42] (Table 18).

Table 18. Height to pool diameter ratio as calculated by CFD and Thomas's correlation for different LNG mixtures.

Diameter[m]	**LNG 1**		**LNG 2**		**LNG 3**	
	CFD	Thomas	CFD	Thomas	CFD	Thomas
3.0	6.7	6.4	6.5	6.3	6.4	6.3
5.0	5.4	5.4	5.2	5.4	5.1	5.4
8.0	4.7	4.9	4.0	4.9	3.9	4.9
10.0	4.2	4.5	4.1	4.5	4.0	4.4

Regardless of the adopted approach, a less than linear trend can be observed for the pool diameter. Moreover, a tendency to provide more conservative results can be observed for the CFD approach.

Once the geometry of the flame is estimated, the distribution along with the distance was investigated for a given time representative of a steady-state. Either the effects of pool diameter or fuel composition were analyzed. For the sake of brevity, estimations reproducing the heat flux received by a target at different distances from the pool centre for LNG 1 composition and several pool diameters were reported at first (Figure 52). To facilitate this comparison, the distance from the pool centre (x) was expressed in dimensionless form x/D_p.

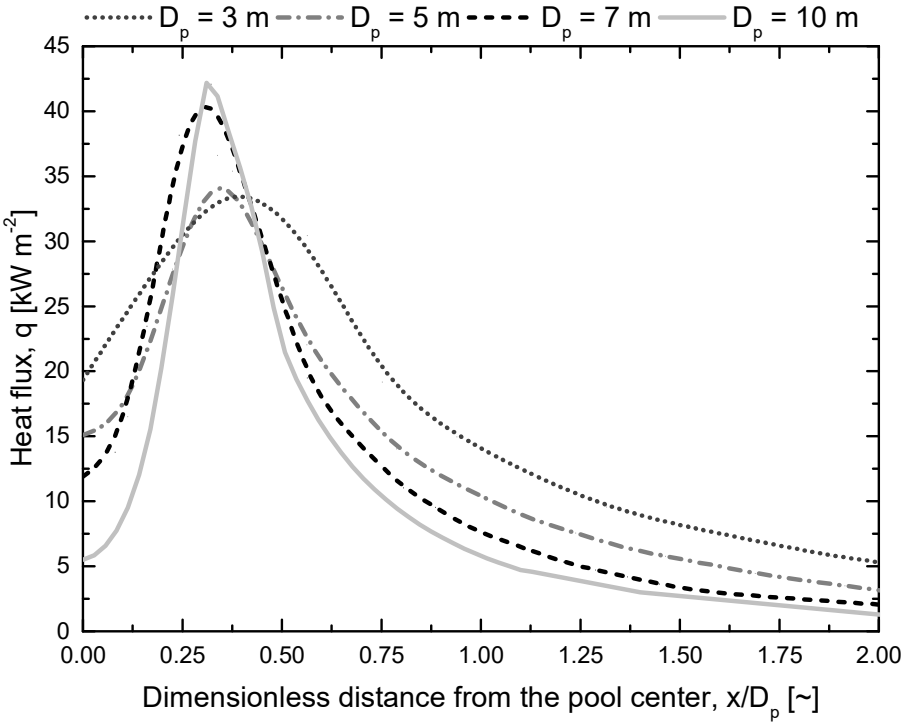

Figure 52. Radiative heat flux with respect to the distance from the pool centre for LNG 1 (i.e., pure methane), as a function of pool diameter.

Regardless of the considered boundary conditions, the maximum heat flux can be observed at x/D_p ranging within 0.4 – 0.5, namely close to the pool edge. The obtained values can be fairly reproduced by the following correlation

$$q(x) = [C_1 \cdot D_p^2 + C_2 \cdot D_p] \cdot e^{-B \cdot \left(x - \frac{D_p}{2}\right)} \qquad \textit{(Eq. 56)}$$

where B, C_1, and C_2 are constants potentially depending on the liquid composition and equal to 0.33 m^{-1}, 0.1, and 4.4 for the LNG 1 case, respectively. The comparison of the developed correlation with results relying on LNG 2 and LNG 3 compositions indicates that C_1 and C_2 significantly change once

ethane is added. However, minor variations can be observed once propane is added. More specifically, either LNG 2 or LNG 3 are characterized by C_1 and C_2 of 0.05 and 6.70, respectively.

The proposed correlation combines the influence of target-pool centre distance on view factor and atmospheric transmissivity. Besides, the SEP can be estimated as the heat flux at the edge. Noteworthy, this approach provides a SEP of 274 kW m^{-2} for pool fire of 35 m, in agreement with experimental data reporting 275 kW m^{-2} [290], even if it has been developed for small scale pool. Besides, an almost constant value of the mass burning rate of 0.24 kg $m^{-2}s^{-1}$ was found for all the investigated conditions. It represents a slightly overestimation of some experimental values [166] but is in line with recommendations for the estimation of the flame height [292].

The definition of threshold values for the heat radiation intensity allows for the estimation of safety distances. To this aim, the threshold values for injury and fatality in the absence of individual protection, together with structural damages to industrial equipment were considered [49] (Table 19). In brackets, normalized values, i.e., divided by the pool diameter, are reported as per discussion.

Table 19. Safety distance for different LNG pool fire as a function of diameter, fuel composition, and threshold values. Results reported in brackets are expressed in the dimensionless form (x/D).

Threshold value [kW m^{-2}]	**Composition**	D_p **= 3.0 m**	D_p **= 5.0 m**	D_p **= 8.0 m**	D_p **= 10.0 m**
5.0 (injury)	LNG 1	5.5 (1.8)	7.0 (1.4)	10.0 (1.3)	10.0 (1.0)
	LNG 2	6.4 (2.1)	7.8 (1.6)	10.1 (1.0)	11.0 (1.1)
	LNG 3	6.4 (2.1)	8.0 (1.7)	10.2 (1.3)	12.2 (1.2)
7.5 (fatality)	LNG 1	4.3 (1.4)	5.5 (1.1)	8.1 (1.0)	8.2 (0.8)
	LNG 2	5.0 (1.7)	6.4 (1.3)	8.5 (1.1)	9.8 (1.0)
	LNG 3	5.0 (1.7)	6.4 (1.3)	9.0 (1.1)	10.6 (1.1)
12.5 (structural damage)	LNG 1	3.0 (1.0)	4.0 (0.8)	6.5 (0.8)	6.5 (0.7)
	LNG 2	3.5 (1.2)	4.7 (0.9)	6.8 (0.9)	7.7 (0.8)
	LNG 3	3.6 (1.2)	6.4 (1.3)	6.8 (0.9)	8.8 (0.9)

The composition indicated as LNG 3 shows the largest safety distances, especially at elevated D_p. this trend can be related to the enhanced molecular weight and heat of combustion per reacted mole of this mixture. Hence, this mixture should be preferred as a surrogate mixture for safety evaluation on LNG in the presence of an ignition source. Considering the dimensionless values reported in the brackets, a linear trend to D_p can be observed on a small scale. Conversely, asymptotic values can be observed for medium-scale (i.e., larger than 8 m) if LNG 1 is excluded. Similar trends have been reported for traditional liquid fuels, as well [50], meaning that a general correlation is applicable for the estimation of this parameter and variations in the pool diameter where an asymptotic dimensionless safety distance is reached with the pool composition should be accounted.

Detailed kinetic mechanism for partial oxidation optimization

The detailed kinetic mechanism developed, validated, and reduced so far was adopted for the characterization and intensification of industrial processes, as well, once integrated with the catalytic mechanism reported in the previous sections. Considering the posed research question and the limitations still determining the operative conditions, the partial oxidation processes of light alkenes represent the perfect candidate for detailed characterization. As discussed in the methodological section, direct oxidation of ethylene and propylene represent the largest market share and the most promising route for environmental aspects. Hence, this work was focused on the optimization of these processes by estimating the upper bound limits for operative conditions and generating reactor operative diagrams for the two processes. Considering that oxygen represents the limiting reactant, the first step was related to the determination of the limiting oxygen concentration (LOC) via detailed kinetic mechanism (Table 20 and Table 21) at typical operative conditions of ethylene oxide (EO) and propylene oxide (PO) processes.

Table 20. The limiting oxygen concentration of the ethylene oxide process estimated at process relevant conditions, expressed in terms of oxygen volume fraction (%v/v).

EO process	**Pressure [bar]**		
Temperature [K]	10	16	22
400	15.03	15.02	15.01
450	14.96	14.94	14.93
500	14.93	14.91	14.89

Table 21. The limiting oxygen concentration of the propylene oxide process estimated at process relevant conditions, expressed in terms of oxygen volume fraction (%v/v).

PO process	**Pressure [bar]**		
Temperature [K]	1.00	1.25	1.50
320	26.65	26.63	26.61
360	26.80	26.79	26.77
400	27.04	27.02	27.00

As expected, LOCs are weakly affected by the initial pressure selected, whereas an almost linear trend with temperature can be observed. It is worth noting that the obtained LOC for the EO process is in the proximity of the maximum content of typical operative conditions (i.e., 10 %v/v), meaning that this process is intrinsically less safe than PO. The obtained data were adopted for the evaluation of the exothermicity values corresponding to the flammability limits at the operative conditions (B_{LFL}), reported in the reactor operative diagrams EO (Figure 53) and PO (Figure 54) processes.

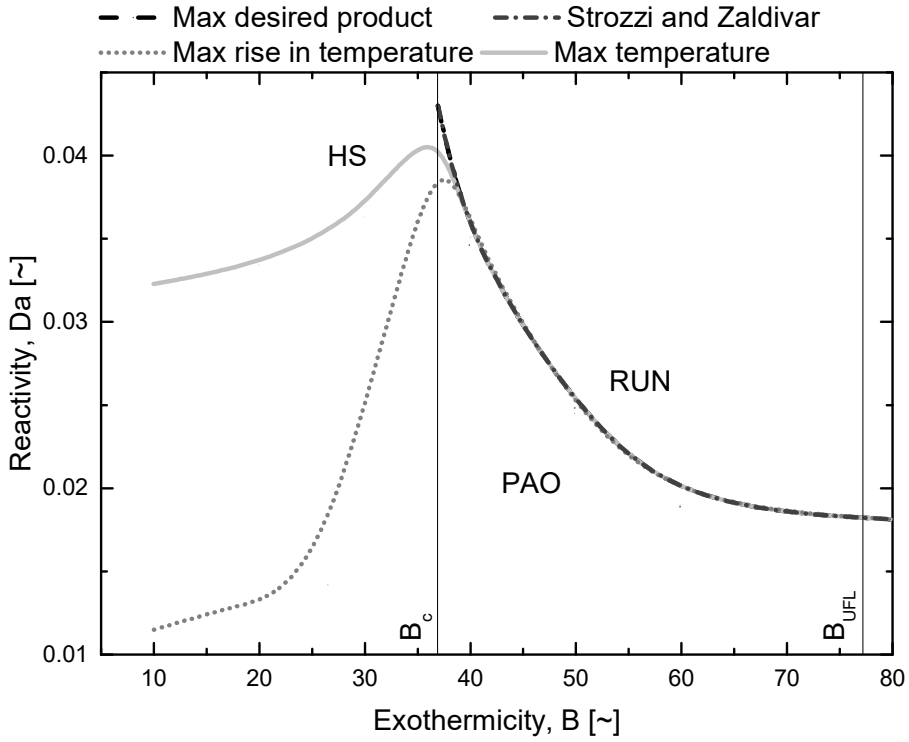

Figure 53. Reactor operative diagrams for direct oxidation of ethylene calculated by using the detailed kinetic mechanism developed in this work and applying different criteria.

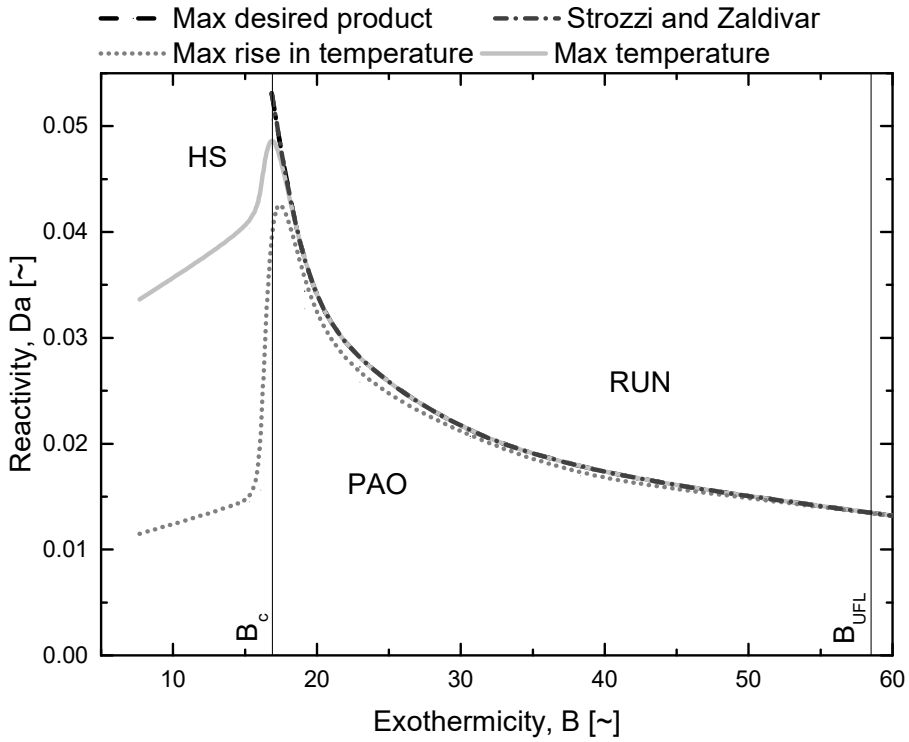

Figure 54. Reactor operative diagrams for direct oxidation of propylene calculated by using the detailed kinetic mechanism developed in this work and applying different criteria.

Three different regions can be distinguished in both reactor operative diagrams: RUN, PAO, and HS standing for runaway, pseudo-adiabatic operation, and hot spot regions. RUN implies that even small

disturbances of any of the process variables (e.g., cooling temperature or reactant composition) can lead to the loss of control of the reactor. Indeed, almost overlapped curves were obtained by the implementation of different criteria. PAO includes the conditions where the temperature profile and desired product concentration along with the reactor length do not reach maximum values, meaning that more exothermic reactions (e.g., complete oxidation) and product consumptions are not relevant. Hence, PAO represents the optimal region for operative conditions. Within HS the maximum temperature is achieved along with the reactor length, only. This implies that more exothermic reactions can be locally observed. Recalling that this model assumes a 1-D reactor, HS conditions are potentially dangerous because of the possible formation of radial temperature profiles generating an ignition source or having detrimental effects on selectivity toward the desired product, in the real case. A triple point where HS, RUN, and PAO regions intersect can be identified. It corresponds to the *Da*-*B* peak and will be referred to as Da_c and B_c from now on. Based on its definition, the latter indicates the maximum B potentially included in HS and the minimum included in RUN. Similarly, Da_c indicates the upper bound for PAO. B_c equal to 36.9 for ethylene oxide and 16.9 for propylene oxide processes were obtained, whereas different Da_c can be obtained based on the selected criterion. These discrepancies confirm the intrinsically more conservative nature of some criteria included in this analysis. In this view, the utilization of the maximum rise in temperature as a monitoring criterion is suggested for the individuation of Da_c as a conservative assumption on the safe side. For $B < B_c$ the curves representing the conditions where maximum raise in temperature and maximum temperature are achieved strongly differ. The adoption of the former criterion as a stand-alone parameter may lead to significant over-conservative choices, especially for the propylene oxide process where a sharp increase in the corresponding curve is observed in the first stage. In this view, this criterion can be considered as an early warning parameter, especially at B lower than B_c.

Considering the differences between the regions distinguished so far, attention should be posed to the scenarios resulting from the variation of operative conditions leading to a transition between two different regions. In this light, a brief overview of these transitions is given below

PAO to HS transition: it may occur for a given B lower than B_c if Da increases or for a given Da lower Da_c if B decreases. This transition implies that the initial reactor zone is characterized by elevated kinetics due to the elevated concentration of the reactants, producing elevated heat flowrates. Limitations in the heat removal system lead to an increase in temperature. However, the decrease in reactant concentrations along the reactor length leads to lower rates and heat production. Hence a maximum in the reactor temperature can be observed once the cooling system (having constant fluid temperature) subtracts heat to the reactive system faster than its production. Considering that the maximum in the concentration of the desired product is not reached, it is possible to conclude that the

complete oxidation, often characterized by an increase in the number of the mole and undoubtedly more exothermic, does not represent the dominant reaction. Nevertheless, local inhomogeneities along with the radial position may be produced.

- HS to RUN transition: it may occur for a given *Da* higher than Da_c if *B* increases. This transition implies the simultaneous achievement of maximum concentration of the desired product and temperature.
- PAO to RUN transition: it may occur for a given *B* higher than B_c if *Da* increases or for a given *Da* lower than Da_c if *B* increases. This transition implies that the initial reactive zone is followed by a decomposition-dominated regime, detrimental for process selectivity, leading to a maximum in the concentration of the desired product.

Based on the definition of dimensionless parameters, *B* may increase if higher concentrations of the limiting reactants are fed. Hence, the utilization of adequate mixing and feeding systems could considerably reduce the likelihood of this variation, whereas *Da* is directly proportional to the reactor length. Hence, proper design may prevent the occurrence of $Da >> Da_c$.

The macroscopic behaviour distinguishing PAO, HS, RUN regions may be tracked back to elemental reactions using sensitivity analyses. Figure 55 reports the most influential reactions involving initial reactants (i.e., ethylene and propylene), main products, and formaldehyde expressed in SMILES notation.

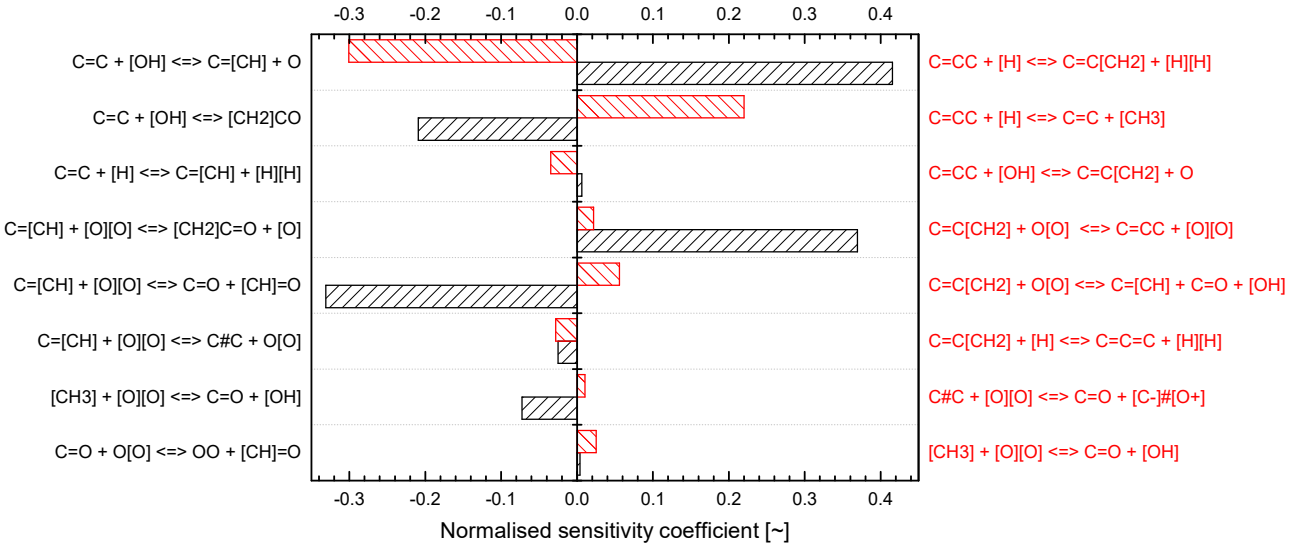

Figure 55. Sensitivity analyses performed at operative conditions of ethylene oxide and propylene oxide processes.

As expected, hydrogen abstraction by small radicals (e.g., O, H, OH, HO_2 and CH_3) has a large impact on the activation of both fuels. However, differences in initial conditions generate significant impacts on the preferred path. Indeed, the EO process is characterized by the large impact of the hydrogen

abstraction by OH radical, whereas PO is more influenced by the abstraction by the radical H. These observations are following the literature, where detailed analyses based on the first principle of the quantum mechanics, i.e., ab initio calculations, adopting a high level of the theory have been performed to obtain theoretical kinetic values for these reaction classes at temperature and pressure ranges included in the ones investigated in this work [294][263]. Along with the years, several studies have been dedicated to the calculation of kinetics of hydrogen abstraction by OH from alkenes at pressures up to 20 bar and temperature within 400 - 800 K [294], together with the kinetics of hydrogen abstraction by H from propylene at low pressure and temperature ranging from 300 to 2000 K [263].

The chemistry of alkyl radical (i.e., C_2H_3), largely produced in the ethylene case, is ruled by its oxidation followed by direct HO_2 elimination or by chain branching reactions. These paths are usually attributed to low [43] and intermediate [36] temperature regimes. On the other hand, the PO process is more influenced by the reactions of the corresponding alkyl radical (i.e., C_3H_5) with HO_2. The kinetics of this reaction has not been calculated utilizing a high-level quantum approach, so far, but it can be estimated by using the accurate data obtained for the reverse reaction (i.e., alkene oxidation through O_2) [295][296].

Considering that the safety constraints strongly limiting partial oxidation processes become less stringent by a decrease of temperature, a variation in the operative conditions can be proposed. In this view, the implementation of cryogenic conditions should be convenient especially for the EO case where liquid ethylene should be directly adopted as a reactant or coolant agent. Indeed, cryogenic temperatures can be conveniently adopted for ethylene transportation [297]. The implementation of this option requires *ex-ante* evaluations to guarantee reliable feasibility studies. Hence, flammable regions of ethylene/methane/oxygen/diluent mixtures at different initial temperatures and operative pressure of 22 bar were estimated (Figure 56). A value representative of the typical set of operative conditions was indicated as *Process* and added to this figure as per discussion. The effect of inert composition was evaluated by a given representative composition (*Inert*), cp-average composition (*Averaged*), or pure methane (*CH_4*). Besides, the prefix *F* indicates the implementation of fictitious species having the same thermal properties but not involved in any reactions.

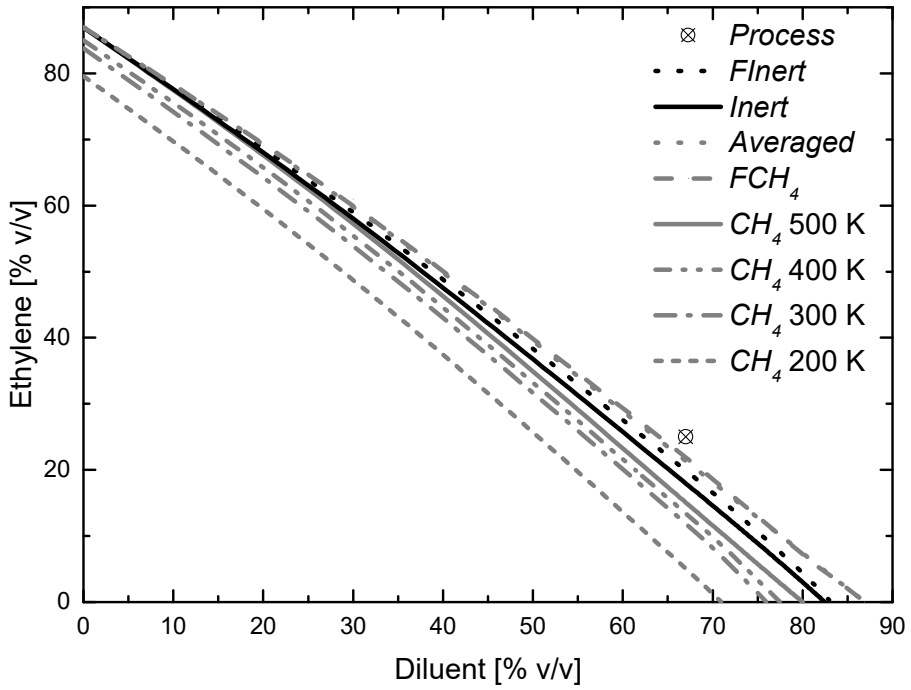

Figure 56. Ethylene/air/diluent flammability limits as a function of inert and initial temperature at an operating pressure of 22 bar.

Conditions indicated as *Process* are outside the flammable region for any diluent compositions and temperature investigated in this work. The proximity of the curve reproducing results obtained at 500 K indicates that the effect of diluent composition and its chemistry on safety parameters is limited, especially for diluent content lower than 30 %v/v. At a higher concentration of diluent only *Averaged* and *FInert* curves are almost overlapped. The proximity of these data indicates that the thermal effect on the UFL can be fairly represented by the heat capacity. This hypothesis can be confirmed by the comparison of Inert and *FCH4* curves. Indeed, the addition of carbon dioxide and nitrogen to methane, to form *Inert* makes the flammable region narrower because of the increased specific heat capacity. This trend is in line with the critical adiabatic flame temperature concept, assuming the flammable limits as the composition producing a given value of adiabatic flame temperature.

Conversely, the real composition is less influenced by the kinetic aspects being fictitious and reactive curves closer than the ones corresponding to the pure methane case. These differences assume larger magnitude at elevated diluent content, closer to the typical values adopted by the actual process, making *CH4* the most conservative option. Hence, it can be concluded that the utilization of methane as diluent should be favoured because of the large impact on the combustion kinetic, hindering the undesired reaction. In this view, the effect of the initial temperature on the flammable region was reported for the *CH4*, exclusively. The lower the initial temperature, the lower the UFLs are. However, the observed decrease follows a more-than-linear trend, in contrast with the well-known Zabetakis correlation [298], promoting the reduction in operative temperature.

Someone may argue that lowering the initial temperature introduces liquid-vapour limitations and new challenges in catalyst formulation. In this view, the lower bound should be included within the range 283 – 398 K, representing the normal boiling point and the boiling point at operative pressure [299] of most volatile compounds (i.e., ethylene oxide). In this range of temperature either silver- or gold- based catalysts have been studied and developed for partial oxidation of propylene [203][300], indicating a feasible route for the EO process, as well.

Conclusive remarks and future directions

The complexity of the challenges posed to satisfy market requirements and meet environmental regulations promotes the adoption of accurate, comprehensive, and fundamental-based models accounting for all the most influential involved phenomena. For chemical engineers-related topics, the inclusion of kinetics represents an inextricable aspect for safe and optimized processes. The interactions between physical and chemical aspects involving low-temperature processes and phenomena in an oxidative environment promote the implementation of integrated models. Considering that the reduction in operative temperature either in storage systems or reactors is a well-established trend, this program was dedicated to the development and implementation of a procedure suitable for the characterization of low-temperature phenomena. During this Ph.D. project, most of the effort was devoted to the realization and implementation of a flexible and comprehensive procedure for the characterization of low-temperature systems in terms of chemical, safety, and environmental aspects. Either experimental or numerical approaches have been included. The kinetics can potentially influence the other categories representing wider classes. To this aim, a detailed kinetic mechanism suitable for extreme conditions was developed, validated, and integrated with a computational fluid dynamics model for the representation of several realistic circumstances. The latter group mimics either undesired events (e.g., accidental scenarios caused by the release of cryogenic fuels) or planned activities (e.g., theorization and optimization of chemical processes). The production of a detailed kinetic mechanism was performed in two steps: a preliminary phase producing a core combustion model having butenes as target molecules, followed by model enlargement to include the chemistry of small esters considered as promising biofuels, such as butyl acetate isomers. Most influential species and reactions were identified via sensitivity analysis. The corresponding properties or rate coefficients were calculated through *ab initio* calculations when required. An iterative procedure was adopted to reduce the uncertainties associated with the model and increase its accuracy. The produced mechanism was, then, validated against experimental data retrieved from the literature and collected in this project. To this aim, a heat flux burner was designed, realized, and adopted for the experimental characterization of the overall reactivity in terms of laminar burning velocity of gaseous mixtures at initial low-temperature. Pure methane, propane, ethylene, and propylene were tested in the air as they are, mixed, or enriched by hydrogen. Oxygen enriched air was adopted as an oxidant, as well. A mixing rule for the estimation of the laminar burning velocity of methane-containing mixtures was proposed and successfully tested against comprehensive databases. Benchmark mechanisms commonly adopted for the evaluation of chemical phenomena were compared with experiments and estimations obtained by the newly generated mechanism. Laminar burning velocity, ignition delay time, and rate coefficients of the most influential reactions

were evaluated, highlighting the possible reasons for observed discrepancies. The mechanism produced in this work was found as the most accurate core combustion sub-model. Considering the absence of fitting coefficients, it is suggested for the construction of comprehensive mechanisms including the chemistry of larger species.

The accuracy of the developed model has promoted its implementation in different fields. As a way of example, the flammable regions of cryogenic fuels at a temperature below ambient conditions were delimited via limiting laminar burning velocity theory. Considering the worldwide tendency observable in the market, liquid hydrogen, liquefied natural gas, and liquid ethylene were considered at this stage. Predictions were compared with data from the literature, when available, showing satisfactory agreement.

Then, the obtained mechanism was reduced to allow for its implementation in CFD models. At this stage, particular attention was paid to liquid hydrogen and liquefied natural gas safety, together with light alkenes partial oxidation processes (i.e., ethylene oxide and propylene oxide production). Indeed, pool fire, rapid phase transition, and dispersion were characterized as per the safety pillar, whereas the risks of runaway, loss of control, and low selectivity were evaluated for the sake of process intensification in compliance with the quick, fair, and smooth (QFS) paradigm. The effects of boundary conditions (such as fuel composition, heat exchange with the substrate, or atmospheric conditions) on the stand-off distances were quantified. The relevance of specific phenomena occurring at a temperature below 298 K was highlighted, especially for the case of liquid hydrogen. Conversely, operative conditions coupling safety, economic, and technological aspects of direct oxidation of ethylene and propylene processes were proposed based on the implementation of a rigorous and comprehensive method.

Along with the program, a dearth of experimental data focused on fundamental properties (e.g., laminar burning velocity or evaporation rate) at a temperature below 298 K was observed, especially at a laboratory scale. This scarcity can be attributed to the lack of knowledge on the addressed topic and elevated costs associated with the required technologies, thus the proposed method can be intended as an additional tool for the proper design of prototypal features for low-temperature characterization. In the view of possible utilization of this methodology at different conditions, it should be noted that a limited number of constraints were posed throughout the process, making the proposed procedure applicable for a large number of conditions and processes.

Acknowledgements

Matri patri

A chi, anche a chilometri di distanza, lontano non lo potrà essere mai.

To you, the brightest star born to shine bright in the darkest night.

References

[1] A. A. V. Perpignan, A. Gangoli Rao, and D. J. E. M. Roekaerts, "Flameless combustion and its potential towards gas turbines," *Prog. Energy Combust. Sci.*, 69, 28–62, 2018.

[2] T. Lu and C. K. Law, "Toward accommodating realistic fuel chemistry in large-scale computations," *Prog. Energy Combust. Sci.*, 35, 192–215, 2009.

[3] A. K. Agarwal, A. P. Singh, and R. K. Maurya, "Evolution, challenges and path forward for low temperature combustion engines," *Prog. Energy Combust. Sci.*, 61, 1–56, 2017.

[4] S. S. Goldsborough, S. Hochgreb, G. Vanhove, M. S. Wooldridge, H. J. Curran, and C. J. Sung, "Advances in rapid compression machine studies of low- and intermediate-temperature autoignition phenomena," *Prog. Energy Combust. Sci.*, 63, 1–78, 2017.

[5] R. H. Perry and D. W. Green, *Perry's Chemical Engineers' Handbook*, 8th ed. United State of America, 2008.

[6] T. Brunner and O. Kircher, "Cryo-Compressed Hydrogen Storage," *Hydrog. Sci. Eng. Mater. Process. Syst. Technol.*, 2, 711–732, 2016.

[7] Y. zhiyi and O. Xunmin, "Life Cycle Analysis on Liquefied Natural Gas and Compressed Natural Gas in Heavy-duty Trucks with Methane Leakage Emphasized," *Energy Procedia*, 158, 3652–3657, 2019.

[8] A. G. Rao, F. Yin, and J. P. Van Buijtenen, "A hybrid engine concept for multi-fuel blended wing body," *Aircr. Eng. Aerosp. Technol.*, 86, 483–493, 2014.

[9] C. Panzarella and M. Kassemi, "One-dimensional model of evaporation and condensation in the presence of a noncondensable gas with applications to cryogenic fluid storage," *Int. J. Heat Mass Transf.*, 52, 3767–3777, 2009.

[10] J. L. Osorio-Tejada, E. Llera-Sastresa, and S. Scarpellini, "Liquefied natural gas: Could it be a reliable option for road freight transport in the EU?," *Renew. Sustain. Energy Rev.*, 71, 785–795, 2017.

[11] S. S. Chadwick, *Ullmann's Encyclopedia of Industrial Chemistry*, 7th ed. Weinheim: Wiley-VCH Verlag GmbH & Co., 2012.

[12] J. R. Monnier, "The direct epoxidation of higher olefins using molecular oxygen," *Appl. Catal. A Gen.*, 221, 73–91, 2001.

[13] D. Kahlich, U. Wiechern, and J. Lindener, "Propylene oxide," in *Ullmann's Encyclopedia of Industrial Chemistry*, 7th ed., Weinheim: Wiley-VCH Verlag GmbH & Co., 2012, 1–7.

[14] S. Rebsdat and D. Mayer, "Ethylene Oxide," in *Ullmann's Encyclopedia of Industrial Chemistry*, 7th ed., Weinheim: Wiley-VCH Verlag GmbH & Co., 2012, 547–572.

[15] I. Glassman and R. A. Yetter, *Combustion*, 4th ed. Amsterdam: Elsevier B.V, 2008.

[16] F. N. N. Egolfopoulos, N. Hansen, Y. Ju, K. Kohse-Hoinghaus, C. K. K. Law, F. Qi, K. Kohse-Höinghaus, C. K. K. Law, and F. Qi, "Advances and challenges in laminar flame experiments and implications for combustion chemistry," *Prog. Energy Combust. Sci.*, 43, 36–67, 2014.

[17] A. D. Lele, S. K. Vallabhuni, K. Moshammer, R. X. Fernandes, A. Krishnasamy, and K. Narayanaswamy, "Experimental and chemical kinetic modeling investigation of methyl butanoate as a component of biodiesel surrogate," *Combust. Flame*, 197, 49–64, 2018.

[18] K. A. Bhaskaran and P. Roth, "The shock tube as wave reactor for kinetic studies and material systems," *Prog. Energy Combust. Sci.*, 28, 151–192, 2002.

[19] H. Gao, C. W. Coley, T. J. Struble, L. Li, Y. Qian, W. H. Green, and K. F. Jensen, "Combining retrosynthesis and mixed-integer optimization for minimizing the chemical inventory needed to realize a WHO essential medicines list," *React. Chem. Eng.*, 5, 367–376, 2020.

[20] G. Pio and E. Salzano, "Implementation of Gas-Phase Kinetic Model for the Optimization of the Ethylene Oxide Production," *Chem. Eng. Sci.*, 212, 115331, 2020.

[21] C. Saggese, A. Frassoldati, A. Cuoci, T. Faravelli, and E. Ranzi, "A wide range kinetic modeling study of pyrolysis and oxidation of benzene," *Combust. Flame*, 160, 1168–1190, 2013.

[22] T. Carriere, P. R. Westmoreland, A. Kazakov, Y. S. Stein, and F. L. Dryer, "Modeling ethylene combustion from low to high pressure," *Proc. Combust. Inst.*, 29, 1257–1266, 2002.

[23] M. Muñoz, E. Planas, F. Ferrero, and J. Casal, "Predicting the emissive power of hydrocarbon pool fires.," *J. Hazard. Mater.*, 144, 725–729, 2007.

[24] O. C. Kwon and G. M. Faeth, "Flame/stretch interactions of premixed hydrogen-fueled flames: Measurements and predictions," *Combust. Flame*, 124, 590–610, 2001.

[25] Q. Meng, X. Zhao, L. Zhang, P. Zhang, and L. Sheng, "A theoretical kinetics study on low-temperature reactions of methyl acetate radicals with molecular oxygen," *Combust. Flame*, 196, 45–53, 2018.

[26] C. (Ryan) Zhou, K. Sendt, and B. S. Haynes, "Experimental and kinetic modelling study of H2S oxidation," *Proc. Combust. Inst.*, 34, 625–632, 2013.

[27] E. S. Oran and V. N. Gamezo, "Origins of the deflagration-to-detonation transition in gas-phase combustion," *Combust. Flame*, 148, 4–47, 2007.

[28] J. M. Simmie, "Detailed chemical kinetic models for the combustion of hydrocarbon fuels," *Prog. Energy Combust. Sci.*, 29, 599–634, 2003.

[29] J. Warnatz, "The structure of laminar alkane-, alkene-, and acetylene flames," *Symp. Combust.*, 18, 369–384, 1981.

[30] F. Battin-Leclerc, "Detailed chemical kinetic models for the low-temperature combustion of hydrocarbons with application to gasoline and diesel fuel surrogates," *Prog. Energy Combust. Sci.*, 34, 440–498, 2008.

[31] R. W. Walker and C. Morley, "Chapter 1 Basic chemistry of combustion," *Compr. Chem. Kinet.*, 35, 1–124, 1997.

[32] J. D. DeSain, S. J. Klippenstein, J. A. Miller, and C. A. Taatjes, "Measurements, theory, and modeling of OH formation in ethyl + O2 and propyl + O2 reactions," *J. Phys. Chem. A*, 107, 4415–4427, 2003.

[33] P. Zhang, W. Ji, T. He, X. He, Z. Wang, B. Yang, and C. K. Law, "First-stage ignition delay in the negative temperature coefficient behavior: Experiment and simulation," *Combust. Flame*, 167, 14–23, 2016.

[34] H. J. Curran, P. Gaffuri, W. J. Pitz, and C. K. Westbrook, "A comprehensive modeling study of n-heptane oxidation,"

Combust. Flame, 114, 149–177, 1998.
[35] C. W. Gao, J. W. Allen, W. H. Green, and R. H. West, "Reaction Mechanism Generator: Automatic construction of chemical kinetic mechanisms," *Comput. Phys. Commun.*, 203, 212–225, 2016.
[36] H. J. Curran, "Developing detailed chemical kinetic mechanisms for fuel combustion," *Proc. Combust. Inst.*, 37, 57–81, 2019.
[37] A. Burcat, B. Ruscic, and Chemistry, "Third millenium ideal gas and condensed phase thermochemical database for combustion (with update from active thermochemical tables).," 2005.
[38] S. M. Bachrach, *Organic Chemistry Computational*, 2nd ed. Hoboken, New Jersey: John Wiley & Sons, Inc., 2014.
[39] N. Hansen, S. J. Klippenstein, C. A. Taatjes, J. A. Miller, J. Wang, T. A. Cool, B. Yang, R. Yang, L. Wei, C. Huang, J. Wang, F. Qi, M. E. Law, and P. R. Westmoreland, "Identification and chemistry of C 4H 3 and C 4H 5 isomers in fuel-rich flames," *J. Phys. Chem. A*, 110, 3670–3678, 2006.
[40] R. Ramakrishnan, P. O. Dral, M. Rupp, and O. A. Von Lilienfeld, "Big data meets quantum chemistry approximations: The Δ-machine learning approach," *J. Chem. Theory Comput.*, 11, 2087–2096, 2015.
[41] J. W. Ochterski, G. A. Petersson, and J. A. Montgomery, "A complete basis set model chemistry. V. Extensions to six or more heavy atoms," *J. Chem. Phys.*, 104, 2598–2619, 1996.
[42] F. C. Pickard, E. K. Pokon, M. D. Liptak, and G. C. Shields, "Comparison of CBS-QB3, CBS-APNO, G2, and G3 thermochemical predictions with experiment for formation of ionic clusters of hydronium and hydroxide ions complexed with water," *J. Chem. Phys.*, 122, 1–7, 2005.
[43] J. Zádor, C. A. Taatjes, and R. X. Fernandes, "Kinetics of elementary reactions in low-temperature autoignition chemistry," *Prog. Energy Combust. Sci.*, 37, 371–421, 2011.
[44] T. H. Dunning, "Gaussian basis sets for use in correlated molecular calculations. I. The atoms boron through neon and hydrogen," *J. Chem. Phys.*, 90, 1070–1101, 1989.
[45] P. Atkin and J. Paula, *Physical chemistry*, 8th ed. New York: W.H. Freeman and Company, 2006.
[46] F. Battin-Leclerc, J. M. Simmie, and E. Blurock, *Cleaner Combustion - Developing Detailed Chemical Kinetic Models*. 2003.
[47] A. Varma, M. Morbidelli, and H. Wu, *Parametric sensitivity in chemical systems*, 1st ed. Cambridge, UK: Cambridge University Press, 1999.
[48] S. W. Benson, "Thermochemical Kinetics: Methods for the Estimation of Thermochemical Data and Rate Parameters," in *Thermochemical Kinetics.*, 2nd ed., Hoboken, USA: John Wiley & Sons, Inc., 1976.
[49] G. Dayma, S. Thion, M. Lailliau, Z. Serinyel, P. Dagaut, B. Sirjean, and R. Fournet, "Kinetics of propyl acetate oxidation: Experiments in a jet-stirred reactor, ab initio calculations, and rate constant determination," *Proc. Combust. Inst.*, 37, 429–436, 2019.
[50] A. A. Konnov, A. Mohammad, V. R. Kishore, N. Il Kim, C. Prathap, and S. Kumar, "A comprehensive review of measurements and data analysis of laminar burning velocities for various fuel+air mixtures," *Prog. Energy Combust. Sci.*, 68, 197–267, 2018.
[51] P. Dagaut, F. Karsenty, G. Dayma, P. Di??vart, K. Hadj-Ali, A. Mz??-Ahmed, M. Braun-Unkhoff, J. Herzler, T. Kathrotia, T. Kick, C. Naumann, U. Riedel, and L. Thomas, "Experimental and detailed kinetic model for the oxidation of a Gas to Liquid (GtL) jet fuel," *Combust. Flame*, 161, 835–847, 2014.
[52] M. Hertzberg, "The Theory of Flammability Limits, Flow Gradient Effect and Flame Stretch," *United States Dep. Inter.*, 1984.
[53] S. S. Shy, W. J. Lin, and J. C. Wei, "An experimental correlation of turbulent burning velocities for premixed turbulent methane-air combustion," *Proc. R. Soc. A Math. Phys. Eng. Sci.*, 456, 1997–2019, 2000.
[54] A. P. Kelley and C. K. Law, "Nonlinear effects in the extraction of laminar flame speeds from expanding spherical flames," *Combust. Flame*, 156, 1844–1851, 2009.
[55] D. R. Dowdy, D. B. Smith, S. C. Taylor, and A. Williams, "The use of expanding spherical flames to determine burning velocities and stretch effects in hydrogen/air mixtures," *Symp. Combust.*, 23, 325–332, 1991.
[56] C. S. Mcenally, L. D. Pfefferle, B. Atakan, K. Kohse-Höinghaus, and K. Kohse-ho, "Studies of aromatic hydrocarbon formation mechanisms in flames: Progress towards closing the fuel gap," *Prog. Energy Combust. Sci.*, 32, 247–294, 2006.
[57] L. P. H. de Goey, A. van Maaren, and R. M. Ouax, "Stabilization of Adiabatic Premixed Laminar Flames on a Flat Flame Burner," *Combust. Sci. Technol.*, 92, 201–207, 1993.
[58] C. J. Sung and H. J. Curran, "Using rapid compression machines for chemical kinetics studies," *Prog. Energy Combust. Sci.*, 44, 1–18, 2014.
[59] R. K. Hanson and D. F. Davidson, "Recent advances in laser absorption and shock tube methods for studies of combustion chemistry," *Prog. Energy Combust. Sci.*, 44, 103–114, 2014.
[60] S. M. Burke, U. Burke, R. Mc Donagh, O. Mathieu, I. Osorio, C. Keesee, A. Morones, E. L. Petersen, W. Wang, T. A. DeVerter, M. A. Oehlschlaeger, B. Rhodes, R. K. Hanson, D. F. Davidson, B. W. Weber, C. J. Sung, J. Santner, Y. Ju, F. M. Haas, *et al.*, "An experimental and modeling study of propene oxidation. Part 2: Ignition delay time and flame speed measurements," *Combust. Flame*, 162, 296–314, 2015.
[61] L. Pan, E. Hu, J. Zhang, Z. Zhang, and Z. Huang, "Experimental and kinetic study on ignition delay times of DME/H2/O2/Ar mixtures," *Combust. Flame*, 161, 735–747, 2014.
[62] R. De Bruycker, S. P. Pyl, M.-F. Reyniers, K. M. Van Geem, and G. B. Marin, "Microkinetic Model for the Pyrolysis of Methyl Esters: From Model Compound to Industrial Biodiesel," *AIChE J.*, 61, 4309–4322, 2015.
[63] P. Glarborg, J. A. Miller, B. Ruscic, and S. J. Klippenstein, "Modeling nitrogen chemistry in combustion," *Prog. Energy Combust. Sci.*, 67, 31–68, 2018.
[64] J. A. Miller and C. T. Bowman, "Mechanism and modeling of nitrogen chemistry in combustion," *Prog. Energy Combust. Sci.*, 15, 287–338, 1989.
[65] Y. B. Zeldovich, "26. Oxidation of Nitrogen in Combustion and Explosions," in *Selected Works of Yakov Borisovich Zeldovich, Volume I*, 2015.
[66] A. Mardani and H. Karimi Motaalegh Mahalegi, "Hydrogen enrichment of methane and syngas for MILD combustion," *Int. J. Hydrogen Energy*, 44, 9423–9437, 2019.
[67] A. Cavaliere and M. De Joannon, "Mild combustion," *Prog. Energy Combust. Sci.*, 30, 329–366, 2004.
[68] G. Blanquart, P. Pepiot-Desjardins, and H. Pitsch, "Chemical mechanism for high temperature combustion of engine relevant

fuels with emphasis on soot precursors," *Combust. Flame*, 156, 588–607, 2009.
[69] R. Sumathi and W. H. Green, "Oxygenate, oxyalkyl and alkoxycarbonyl thermochemistry and rates for hydrogen abstraction from oxygenates," *Phys. Chem. Chem. Phys.*, 5, 3402–3417, 2003.
[70] P. Dagaut, S. Gail, and M. Sahasrabudhe, "Rapeseed oil methyl ester oxidation over extended ranges of pressure, temperature, and equivalence ratio: Experimental and modeling kinetic study," *Proc. Combust. Inst.*, 31, 2955–2961, 2007.
[71] L. Coniglio, H. Bennadji, P. A. Glaude, O. Herbinet, and F. Billaud, "Combustion chemical kinetics of biodiesel and related compounds (methyl and ethyl esters): Experiments and modeling-Advances and future refinements," *Prog. Energy Combust. Sci.*, 39, 340–382, 2013.
[72] D. Felsmann, H. Zhao, Q. Wang, I. Graf, T. Tan, X. Yang, E. A. Carter, Y. Ju, and K. Kohse-höinghaus, "Contributions to improving small ester combustion chemistry : Theory , model and experiments," *Proc. Combust. Inst.*, 36, 543–551, 2017.
[73] S. Dooley, M. P. Burke, M. Chaos, Y. Stein, F. L. Dryer, V. P. Zhukon, O. FInch, J. M. Simmie, and H. J. Curran, "Methyl Formate Oxidation: Speciation Data, Laminar Burning Velocities, Ignition Delay Times, and a Validated Chemical Kinetic Model," *Int. J. Chem. Kinet.*, 42, 527–549, 2010.
[74] X. T. Le, T. V. T. Mai, K. C. Lin, and L. K. Huynh, "Low Temperature Oxidation Kinetics of Biodiesel Molecules: Rate Rules for Concerted HO2 Elimination from Alkyl Ester Peroxy Radicals," *J. Phys. Chem. A*, 122, 8259–8273, 2018.
[75] A. Ahmed, W. J. Pitz, C. Cavallotti, M. Mehl, N. Lokachari, E. J. K. Nilsson, J. Wang, A. A. Konnov, S. W. Wagnon, B. Chen, Z. Wang, S. Kim, H. J. Curran, S. J. Klippenstein, W. L. Roberts, and S. M. Sarathy, "Small ester combustion chemistry : Computational kinetics and experimental study of methyl acetate and ethyl acetate," *Proc. Combust. Inst.*, 37, 419–428, 2019.
[76] S. J. M. Algayyim, A. P. Wandel, T. Yusaf, and I. Hamawand, "Production and application of ABE as a biofuel," *Renew. Sustain. Energy Rev.*, 82, 1195–1214, 2018.
[77] S. H. Ali, O. Al-Rashed, F. A. Azeez, and S. Q. Merchant, "Potential biofuel additive from renewable sources - Kinetic study of formation of butyl acetate by heterogeneously catalyzed transesterification of ethyl acetate with butanol," *Bioresour. Technol.*, 102, 10094–10103, 2011.
[78] J. H. Xing, K. Takahashi, M. D. Hurley, and T. J. Wallington, "Kinetics of the reactions of chlorine atoms with a series of acetates," *Chem. Phys. Lett.*, 474, 268–272, 2009.
[79] J. Mendes, C. W. Zhou, and H. J. Curran, "Theoretical and kinetic study of the hydrogen atom abstraction reactions of esters with HO2 radicals," *J. Phys. Chem. A*, 117, 14006–14018, 2013.
[80] Q. De Wang, X. J. Wang, Z. W. Liu, and G. J. Kang, "Theoretical and kinetic study of the hydrogen atom abstraction reactions of ethyl esters with hydrogen radicals," *Chem. Phys. Lett.*, 616–617, 109–114, 2014.
[81] O. Herbinet, W. J. Pitz, and C. K. Westbrook, "Detailed chemical kinetic oxidation mechanism for a biodiesel surrogate," *Combust. Flame*, 154, 507–528, 2008.
[82] S. G. Davis, C. K. Law, and H. Wang, "Propene pyrolysis and oxidation kinetics in a flow reactor and laminar flames," *Combust. Flame*, 119, 375–399, 1999.
[83] W. Gardiner, V. Lissianski, Z. Qin, G. Smith, D. Golden, M. Frenklach, B. Eiteneer, M. Goldenberg, N. Moriarty, C. Bowman, R. Hanson, S. Song, C. Schmidt, and R. Serauskas, "The GRI-Mech(TM) Model for Natural Gas Combustion and NO Formation and Removal Chemistry," in *Fifth International Conference on Technologies and Combustion for a Clean Environment*, 1999.
[84] A. A. Konnov, "Development and validation of a detailed reaction mechanism for the combustion of small hydrocarbons," in *International Symposium on Combustion Abstracts of Accepted Papers*, 2000, 317.
[85] A. Frassoldati, T. Faravelli, and E. Ranzi, "Kinetic modeling of the interactions between NO and hydrocarbons at high temperature," *Combust. Flame*, 135, 97–112, 2003.
[86] G. Blanquart and H. Pitsch, "Thermochemical properties of Polycyclic Aromatic Hydrocarbons (PAH) from G3MP2B3 calculations," *J. Phys. Chem. A*, 111, 6510–6520, 2007.
[87] H. Wang, "USC Mech Version II," *J. Chem. Inf. Model.*, 53, 1689–1699, 2013.
[88] H. Wang, E. Dames, B. Sirjean, D. A. Sheen, R. Tango, A. Violi, J. Y. W. Lai, F. N. Egolfopoulos, D. F. Davidson, R. K. Hanson, C. T. Bowman, C. K. Law, W. Tsang, N. P. Cernansky, D. L. Miller, and R. P. Lindstedt, "A high-temperature chemical kinetic model of n-alkane (up to n-dodecane), cyclohexane, and methyl-, ethyl-, n-propyl and n-butyl-cyclohexane oxidation at high temperatures, JetSurF version 2.0, September 19, 2010 (http://web.stanford.edu/group/haiwanglab/."
[89] D. Healy, D. M. Kalitan, C. J. Aul, E. L. Petersen, G. Bourque, and H. J. Curran, "Oxidation of C1-C5 alkane quinternary natural gas mixtures at high pressures," *Energy and Fuels*, 24, 1521–1528, 2010.
[90] M. Mehl, W. J. Pitz, C. K. Westbrook, and H. J. Curran, "Kinetic modeling of gasoline surrogate components and mixtures under engine conditions," *Proc. Combust. Inst.*, 33, 193–200, 2011.
[91] S. M. Sarathy, S. Vranckx, K. Yasunaga, M. Mehl, P. Oswald, W. K. Metcalfe, C. K. Westbrook, W. J. Pitz, K. Kohse-Hoinghaus, R. X. Fernandes, and H. J. Curran, "A comprehensive chemical kinetic combustion model for the four butanol isomers," *Combust. Flame*, 159, 2028–2055, 2012.
[92] M. R. Harper, K. M. Van Geem, S. P. Pyl, G. B. Marin, and W. H. Green, "Comprehensive reaction mechanism for n-butanol pyrolysis and combustion," *Combust. Flame*, 158, 16–41, 2011.
[93] M. Schenk, L. Leon, K. Moshammer, P. Oßwald, T. Zeuch, L. Seidel, F. Mauss, and K. Kohse-Höinghaus, "Detailed mass spectrometric and modeling study of isomeric butene flames," *Combust. Flame*, 160, 487–503, 2013.
[94] E. Ranzi, A. Frassoldati, R. Grana, A. Cuoci, T. Faravelli, A. P. Kelley, and C. K. Law, "Hierarchical and comparative kinetic modeling of laminar flame speeds of hydrocarbon and oxygenated fuels," *Prog. Energy Combust. Sci.*, 38, 468–501, 2012.
[95] University of California at San Diego, "Chemical-Kinetic Mechanisms for Combustion Applications." [Online]. Available: http://web.eng.ucsd.edu/mae/groups/combustion/mechanism.html.
[96] J. Bugler, K. P. Somers, E. J. Silke, and H. J. Curran, "Revisiting the Kinetics and Thermodynamics of the Low-Temperature Oxidation Pathways of Alkanes: A Case Study of the Three Pentane Isomers," *J. Phys. Chem. A*, 119, 7510–7527, 2015.
[97] K. Zhang, C. Banyon, C. Togbé, P. Dagaut, J. Bugler, and H. J. Curran, "An experimental and kinetic modeling study of n-hexane oxidation," *Combust. Flame*, 162, 4194–4207, 2015.
[98] Y. Fenard, G. Dayma, F. Halter, F. Foucher, Z. Serinyel, and P. Dagaut, "Experimental and modeling study of the oxidation of 1-butene and cis -2-butene in a jet-stirred reactor and a combustion vessel," *Energy and Fuels*, 29, 1107–1118, 2015.

[99] K. Zhang, C. Banyon, J. Bugler, H. J. Curran, A. Rodriguez, O. Herbinet, F. Battin-Leclerc, C. B'Chir, and K. A. Heufer, "An updated experimental and kinetic modeling study of n-heptane oxidation," *Combust. Flame*, 172, 116–135, 2016.
[100] Y. Li, C. W. Zhou, K. P. Somers, K. Zhang, and H. J. Curran, "The oxidation of 2-butene: A high pressure ignition delay, kinetic modeling study and reactivity comparison with isobutene and 1-butene," *Proc. Combust. Inst.*, 36, 403–411, 2017.
[101] G. Capriolo, V. A. Alekseev, and A. A. Konnov, "An experimental and kinetic study of propanal oxidation," *Combust. Flame*, 197, 11–21, 2018.
[102] C. W. Zhou, Y. Li, U. Burke, C. Banyon, K. P. Somers, S. Ding, S. Khan, J. W. Hargis, T. Sikes, O. Mathieu, E. L. Petersen, M. AlAbbad, A. Farooq, Y. Pan, Y. Zhang, Z. Huang, J. Lopez, Z. Loparo, S. S. Vasu, *et al.*, "An experimental and chemical kinetic modeling study of 1,3-butadiene combustion: Ignition delay time and laminar flame speed measurements," *Combust. Flame*, 197, 423–438, 2018.
[103] W. Pejpichestakul, E. Ranzi, M. Pelucchi, A. Frassoldati, A. Cuoci, A. Parente, and T. Faravelli, "Examination of a soot model in premixed laminar flames at fuel-rich conditions," *Proc. Combust. Inst.*, 37, 1013–1021, 2019.
[104] W. Li, G. Wang, Y. Li, T. Li, Y. Zhang, C. Cao, J. Zou, and C. K. Law, "Experimental and kinetic modeling investigation on pyrolysis and combustion of n-butane and i-butane at various pressures," *Combust. Flame*, 191, 126–141, 2018.
[105] A. Jach, W. Rudy, A. Pękalski, and A. Teodorczyk, "Assessment of detailed reaction mechanisms for reproduction of ignition delay times of C2–C6 alkenes and acetylene," *Combust. Flame*, 206, 37–50, 2019.
[106] C. A. Salman, S. Schwede, E. Thorin, and J. Yan, "Enhancing biomethane production by integrating pyrolysis and anaerobic digestion processes," *Appl. Energy*, 204, 1074–1083, 2017.
[107] G. Pio, A. Ricca, V. Palma, and E. Salzano, "Experimental and numerical evaluation of low-temperature combustion of bio-syngas," *Int. J. Hydrogen Energy*, 45, 1084–1095, 2020.
[108] G. Pio and E. Salzano, "Laminar Burning Velocity of Multi-Component Gaseous Mixtures," *Chem. Eng. Trans.*, 67, 1–6, 2018.
[109] L. Sileghem, J. Vancoillie, J. Demuynck, J. Galle, and S. Verhelst, "Alternative fuels for spark-ignition engines: Mixing rules for the laminar burning velocity of gasoline-alcohol blends," *Energy and Fuels*, 26, 4721–4727, 2012.
[110] F. H. V. Coppens, J. De Ruyck, and A. A. Konnov, "Effects of hydrogen enrichment on adiabatic burning velocity and NO formation in methane + air flames," *Exp. Therm. Fluid Sci.*, 31, 437–444, 2007.
[111] O. L. Gulder, "Correlations of laminar combustion data for alternative S.I. engine fuels," *SAE Tech. Pap.*, 1984.
[112] N. Semenov, "Some problems relating to chain reactions and to the theory of combustion," *Nobel Lect.*, 1956.
[113] D. B. Spalding, "Combustion of liquid fuels," *Nature*, 165, 160, 1950.
[114] T. Hirasawa, C. J. Sung, a. Joshi, Z. Yang, H. Wang, and C. K. Law, "Determination of laminar flame speeds using digital particle image velocimetry: Binary Fuel blends of ethylene, n-Butane, and toluene," *Proc. Combust. Inst.*, 29, 1427–1434, 2002.
[115] D. Razus, C. Movileanu, V. Brinzea, and D. Oancea, "Explosion pressures of hydrocarbon-air mixtures in closed vessels," *J. Hazard. Mater.*, 135, 58–65, 2006.
[116] H. F. Coward and G. W. Jones, "Bulletin 508: Limits of flammability of gases and vapours," Springfield, 1952.
[117] H. Le, S. Nayak, and M. S. Mannan, "Upper flammability limits of hydrogen and light hydrocarbons in air at subatmospheric pressures," *Ind. Eng. Chem. Res.*, 51, 9396–9402, 2012.
[118] F. Van Den Schoor and F. Verplaetsen, "The upper explosion limit of lower alkanes and alkenes in air at elevated pressures and temperatures," *J. Hazard. Mater.*, 128, 1–9, 2006.
[119] D. A. Crowl and Y. Jo, "A Method for Determining the Flammable Limits of Gases in a Spherical Vessel," *Process Saf. Prog.*, 28, 227–236, 2009.
[120] ASTM E-681, "Standard Test Method for Concentration Limits of Flammability of Chemicals (Vapours and Gases)," *Am. Soc. Test. Mater.*, 09, 1–12, 2015.
[121] CEN EN 1839, "Determination of the explosion limits and the limiting oxygen concentration(LOC) for flammable gases and vapours - IHS Engineering Workbench," 48, 2017.
[122] M. Molnarne and V. Schroeder, "Flammability of gases in focus of European and US standards," *J. Loss Prev. Process Ind.*, 48, 297–304, 2017.
[123] M. G. Zabetakis, "Flammability characteristics of combustible gases and vapours," 1965.
[124] J. Adler and J. W. Enig, "The critical conditions in thermal explosion theory with reactant consumption," *Combust. Flame*, 8, 97–103, 1964.
[125] R. Li, Z. Liu, Y. Han, M. Tan, Y. Xu, J. Tian, J. Chai, and J. Liu, "Extended adiabatic flame temperature method for lower flammability limits prediction of fuel-air-diluent mixture by nonstoichiometric equation and nitrogen equivalent coefficients," *Energy and Fuels*, 31, 351–361, 2017.
[126] D. Razus, M. Molnarne, and O. Fuß, "Limiting oxygen concentration evaluation in flammable gaseous mixtures by means of calculated adiabatic flame temperatures," *Chem. Eng. Process. Process Intensif.*, 43, 775–784, 2004.
[127] R. Bubbico and E. Salzano, "Acoustic analysis of blast waves produced by rapid phase transition of LNG released on water," *Saf. Sci.*, 47, 515–521, 2009.
[128] P. Cleaver, M. Johnson, and B. Ho, "Rapid Phase Transition of LNG," *J. Hazard. Mater.*, 140, 429–438, 2007.
[129] L. Véchot, T. Olewski, C. Osorio, O. Basha, Y. Liu, and S. Mannan, "Laboratory scale analysis of the influence of different heat transfer mechanisms on liquid nitrogen vapourization rate," *J. Loss Prev. Process Ind.*, 26, 398–409, 2013.
[130] C. Conrado and V. Vesovic, "The influence of chemical composition on vapourisation of LNG and LPG on unconfined water surfaces," *Chem. Eng. Sci.*, 55, 4549–4562, 2000.
[131] H. S. Carslow, J. C. Jaeger, and J. E. Morral, *Conduction of Heat in Solids*, 2nd ed. United State of America: Oxford University Press, 1986.
[132] F. P. Incropera, D. P. Dewitt, T. L. Bergamm, and A. S. Lavine, *Fundamentals of heat and mass transfer*, 6th ed. Hoboken, USA: John Wiley and Sons, 2007.
[133] R. B. Bird, W. E. Stewart, and E. N. Lightfoot, *Transport Phenomena*, 2nd ed. John Wiley and Sons, 2002.
[134] A. H. Persad and C. A. Ward, "Expressions for the Evaporation and Condensation Coefficients in the Hertz-Knudsen Relation," *Chem. Rev.*, 116, 7727–7767, 2016.

[135] W. Nawaz, T. Olewski, and L. Véchot, "Assessment and Validation of Evaporation Models for Cryogenic Liquids," *Process Saf. Environ. Prot.*, 121, 50–61, 2019.
[136] H. Hertz, "Ueber die Berührung fester elastischer Körper," *J. fur die Reine und Angew. Math.*, 1882.
[137] M. Knudsen, "Die maximale Verdampfungsgeschwindigkeit des Quecksilbers," *Ann. Phys.*, 352, 697–702, 1915.
[138] A. P. Ingersoll, "Mars: Occurrence of liquid water," *Science (80-.).*, 1970.
[139] D. Mackay and R. S. Matsugu, "Evaporation rates of liquid hydrocarbon spills on land and water," *Can. J. Chem. Eng.*, 51, 434–439, 1973.
[140] W. H. Lee, *Pressure iteration scheme for two-phase flow modeling*, 1st ed. Washington, USA: Hemisphere Publishing, 1980.
[141] P. P. K. Raj and J. A. Morris, "Source characterization of heavy-gas dispersion models for reactive chemicals," Burlington, USA, 1987.
[142] M. Reed, "The physical fates component of the natural resource damage assessment model system," *Oil Chem. Pollut.*, 5, 99–123, 1989.
[143] A. A. Hummel, K. O. Braun, and M. C. Fehrenbacher, "Evaporation of a liquid in a flowing airstream," *Am. Ind. Hyg. Assoc. J.*, 57, 519–525, 1996.
[144] J. Barry, "Estimating rates of spreading and evaporation of volatile liquids," *Chem. Eng. Prog.*, 1, 32–39, 2005.
[145] D. W. G. Sears and S. R. Moore, "On laboratory simulation and the evaporation rate of water on Mars," *Geophys. Res. Lett.*, 32, 1–4, 2005.
[146] F. Heymes, L. Aprin, A. Bony, S. Forestier, S. Cirocchi, and G. Dusserre, "An experimental investigation of evaporation rates for different volatile organic compounds," *Process Saf. Prog.*, 32, 1–6, 2013.
[147] R. W. Schrage, *A Theoretical Study of Interphase Mass Transfer*, 1st ed. New York, USA: Columbia University Press, 1953.
[148] D. W. Hissong, "Keys to modeling LNG spills on water," *J. Hazard. Mater.*, 140, 465–477, 2007.
[149] T. L. Morse and H. K. Kytömaa, "The effect of turbulence on the rate of evaporation of LNG on water," *J. Loss Prev. Process Ind.*, 24, 791–797, 2011.
[150] V. Vesovic, "The influence of ice formation on vapourization of LNG on water surfaces," *J. Hazard. Mater.*, 140, 518–526, 2007.
[151] V. V. Klimenko, "Film boiling on a horizontal plate - new correlation," *Int. J. Heat Mass Transf.*, 24, 69–79, 1981.
[152] L. Ouyang, H. Li, S. Sun, X. Wang, and X. Lu, "Auto-ignition of biomass synthesis gas in shock tube at elevated temperature and pressure," *Sci. Bull.*, 60, 1935–1946, 2015.
[153] B. Rengel, C. Mata, E. Pastor, J. Casal, and E. Planas, "A priori validation of CFD modelling of hydrocarbon pool fires," *J. Loss Prev. Process Ind.*, 56, 18–31, 2018.
[154] C. van den Bosch and R. Weterings, "Yellow Book - Methods for the calculation of physical effects due to releases of hazardous materials (liquids and gases)," *CPR 14E, 3rd edn, TNO*, 1997.
[155] K. B. Mcgrattan, H. R. Baum, and A. Hamins, "Thermal Radiation from Large Pool Fires," United State of America, 2000.
[156] C. L. Beyler, *Industrial Fire Protection Engineering*, 1st ed., 40. Hoboken, USA: John Wiley & Sons, Inc., 2004.
[157] V. Babrauskas, "Estimating large pool fire burning rates," *Fire Technol.*, 19, 251–261, 1983.
[158] J. A. Fay, "Model of large pool fires," 136, 219–232, 2006.
[159] P. H. Thomas, "The size of flames from natural fires," in *Symposium (International) on Combustion*, 1963.
[160] T. Liang, W. Zhong, R. K. K. Yuen, S. Lo, and G. Liao, "On the fire intensification of pool fire with water mist," *Procedia Eng.*, 62, 994–999, 2013.
[161] M. A. Rana, Y. Guo, and M. S. Mannan, "Use of water spray curtain to disperse LNG vapour clouds," *J. Loss Prev. Process Ind.*, 23, 77–88, 2010.
[162] J. A. Suardin, R. Qi, B. R. Cormier, M. Rana, Y. Zhang, and M. S. Mannan, "Application of fire suppression materials on suppression of LNG pool fires," *J. Loss Prev. Process Ind.*, 24, 63–75, 2011.
[163] G. Cui, Z. Li, and C. Yang, "Experimental study of flammability limits of methane/air mixtures at low temperatures and elevated pressures," *Fuel*, 181, 1074–1080, 2016.
[164] T. Enger and D. E. Hartman, "LNG spillage on water. II. Final report on rapid phase transitions," Houston, USA, 1972.
[165] D. L. Ermak, R. P. Koopman, T. G. McRae, and W. J. Hogan, "LNG SPILL EXPERIMENTS: DISPERSION, RPT, AND VAPOUR BURN ANALYSIS.," in *Proceedings of the American Gas Association, Operating Section*, 1982, 32.
[166] A. Luketa-Hanlin, "A review of large-scale LNG spills: Experiments and modeling," *J. Hazard. Mater.*, 132, 119–140, 2006.
[167] R. M. Pitblado and J. L. Woodward, "Highlights of LNG risk technology," *J. Loss Prev. Process Ind.*, 24, 827–836, 2011.
[168] E. M. Drake, A. A. Jeje, and R. C. Reid, "Transient boiling of liquefied cryogens on a water surface. II. Light hydrocarbon mixtures," *Int. J. Heat Mass Transf.*, 18, 1369–1375, 1975.
[169] W. Porteous and M. Blander, "Limits of superheat and explosive boiling of light hydrocarbons, halocarbons, and hydrocarbon mixtures," *AIChE J.*, 21, 560–566, 1975.
[170] E. Aursand and M. Hammer, "Predicting triggering and consequence of delayed LNG RPT," *J. Loss Prev. Process Ind.*, 55, 124–133, 2018.
[171] M. Blander and J. L. Katz, "Bubble nucleation in liquids," *AIChE J.*, 21, 833–848, 1975.
[172] G. F. Feldbauer, J. J. Heigl, W. McQueen, R. H. Whipp, and W. G. May, "Spills of LNG on water-vapourization and downwind drift of combustible mixtures," Amsterdam, NL, 1972.
[173] J. S. Puttock, D. R. Blackmore, and G. W. Colenbrander, "Field experiments on dense gas dispersion," *J. Hazard. Mater.*, 6, 13–41, 1982.
[174] R. P. Koopman, l R. T. Cederwal, E. R. Ermak, H. C. Goldwire, W. J. Hogan, J. W. McClure, T. G. McRae, D. L. Morgan, H. C. Rodean, and J. H. Shinn, "Burro Series Data Report LLNL/NWC 1980 LNG Spill Tests, UCID-19075," 1980.
[175] T. C. Brown, R. T. Cederwall, S. T. Chan, D. L. Ermak, R. P. Koopman, K. C. Lamson, J. W. McClure, and L. K. Morris, "Falcon series data report: 1987 LNG vapour barrier verification field trials," 1987.
[176] B. R. Cormier, R. Qi, G. W. Yun, Y. Zhang, and M. Sam Mannan, "Application of computational fluid dynamics for LNG vapour dispersion modeling: A study of key parameters," *J. Loss Prev. Process Ind.*, 22, 332–352, 2009.
[177] P. K. Raj, "Large LNG Fire Thermal Radiation – Modeling Issues & Hazard Criteria Revisited," *Process Saf. Prog.*, 1–18, 2005.

[178] G. W. Colenbrander and J. S. Puttock, “Maplin Sands experiments 1980: interpretation and modelling of liquefied gas spills onto the sea.,” *Atmos. Dispers. Heavy Gases Small Part.*, 277–295, 1984.
[179] H. Malvos and P. Raj, “Details of 35 m diameter LNG fire tests conducted in Montoir, France in 1987, and analysis of fire spectral and other data,” in *2006 AIChE Spring Annual Meeting*, 2006.
[180] D. A. McQuarrie and J. D. Simon, *Physical chemistry - A molecular Approach*, 2nd ed. Sausalito, USA: University Science Books, 1997.
[181] A. J. Pounds, *Introduction to Quantum Mechanics: A Time-Dependent Perspective (David J. Tannor)*, 1st ed. Sausalito, USA: University Science Books, 2007.
[182] G. Colonna, A. D’Angola, and M. Capitelli, “Statistical thermodynamic description of H2 molecules in normal ortho/para mixture,” *Int. J. Hydrogen Energy*, 37, 9656–9668, 2012.
[183] F. W. Giauque, “The Entropy of Hydrogen and the Third Law of Thermodynamics the Free Energy and Dissociation of Hydrogen,” *Contrib. from Chem. Lab. Univ. Calif.*, 52, 4816–4831, 1930.
[184] D. O. Berstad, J. H. Stang, and P. Nekså, “Comparison criteria for large-scale hydrogen liquefaction processes,” *Int. J. Hydrogen Energy*, 34, 1560–1568, 2009.
[185] R. C. Gillis, T. Bailey, F. X. Gallmeier, and M. A. Hartl, “Raman Spectroscopy as an ortho-para diagnostic of liquid hydrogen moderators,” *J. Phys.*, 1021, 1–4, 2018.
[186] B. H. W. Woolley, R. B. Scott, and F. G. Brickwedde, “Compilation of Thermal Properties of Hydrogen in Its Various Isotopic and Ortho-Para Modifications,” *J. Res. Natl. Bur. Stand. (1934).*, 41, 1948.
[187] J. E. Jensen, W. A. Tuttle, R. B. Stewart, H. Brechna, and A. G. Prodell, *Cryogenic data handbook*. 1980.
[188] R. J. Le Roy, S. G. Chapman, and F. R. W. McCourt, “Accurate thermodynamic properties of the six isotopomers of diatomic hydrogen,” *J. Phys. Chem.*, 94, 923–929, 1990.
[189] F. Stoessel, “Planning protection measures against runaway reactions using criticality classes,” *Process Saf. Environ. Prot.*, 87, 105–112, 2009.
[190] A. Adrover, F. Creta, M. Giona, and M. Valorani, “Explosion limits and runaway criteria: A stretching-based approach,” *Chem. Eng. Sci.*, 62, 1171–1183, 2007.
[191] K. R. Westerterp and E. J. Molga, “Safety and runaway prevention in batch and semibatch reactors - A review,” *Chem. Eng. Res. Des.*, 84, 543–552, 2006.
[192] L. G. Amaut, *Chemical Kinetics: From Molecular Structure to Chemical Reactivity*, 1st ed. Amsterdam, NL: Elsevier Science, 2006.
[193] J. M. Zaldívar, J. Cano, M. A. Alós, J. Sempere, R. Nomen, D. Lister, G. Maschio, T. Obertopp, E. D. Gilles, J. Bosch, and F. Strozzi, “A general criterion to define runaway limits in chemical reactors,” *J. Loss Prev. Process Ind.*, 16, 187–200, 2003.
[194] M. A. Alós, R. Nomen, J. M. Sempere, F. Strozzi, and J. M. Zaldívar, “Generalized criteria for boundary safe conditions in semi-batch processes: simulated analysis and experimental results,” *Chem. Eng. Process. Process Intensif.*, 37, 405–421, 1998.
[195] P. D. Mobley, J. E. Peters, N. Akunuri, J. Hlebak, V. Gupta, Q. Zheng, S. J. Zhou, and M. Lail, “Utilization of CO2for Ethylene Oxide,” *Energy Procedia*, 114, 7154–7161, 2017.
[196] J. Tsuji, J. Yamamoth, M. Ishino, and N. Oku, “Development of New Propylene Oxide Process,” Osaka, JP, 2006.
[197] S. J. Khatib and S. T. Oyama, “Direct Oxidation of Propylene to Propylene Oxide with Molecular Oxygen: A Review,” *Catal. Rev. - Sci. Eng.*, 57, 306–344, 2015.
[198] J. Liu, F. Zhang, W. Xu, N. Shi, and S. Mu, “Thermal reactivity of ethylene oxide in contact with contaminants: A review,” *Thermochim. Acta*, 652, 85–96, 2017.
[199] V. Ragaini, G. De Luca, B. Ferrario, and P. Della Porta, “A mathematical model for a tubular reactor performing ethylene oxidation to ethylene oxide by a catalyst deposited on metallic strips,” *Chem. Eng. Sci.*, 35, 2311–2319, 1980.
[200] Z. Li, L. Zhu, J. F. Chen, and D. Cheng, “Enhanced Ethylene Oxide Selectivity by Cu and Re Dual-Promoted Ag Catalysts,” *Ind. Eng. Chem. Res.*, 57, 4180–4185, 2018.
[201] Z. Lu, M. Piernavieja-Hermida, C. H. Turner, Z. Wu, and Y. Lei, “Effects of TiO2 in Low Temperature Propylene Epoxidation Using Gold Catalysts,” *J. Phys. Chem. C*, 122, 1688–1698, 2018.
[202] W. S. Lee, M. Cem Akatay, E. A. Stach, F. H. Ribeiro, and W. Nicholas Delgass, “Gas-phase epoxidation of propylene in the presence of H2 and O2 over small gold ensembles in uncalcined TS-1,” *J. Catal.*, 313, 104–112, 2014.
[203] T. A. Nijhuis, M. Makkee, J. A. Moulijn, and B. M. Weckhuysen, “The Production of Propene Oxide: Catalytic Processes and Recent Developments,” *Ind. Eng. Chem. Res.*, 45, 3447–3459, 2006.
[204] D. Weininger, “SMILES, a Chemical Language and Information System: 1: Introduction to Methodology and Encoding Rules,” *J. Chem. Inf. Comput. Sci.*, 28, 31–36, 1988.
[205] C. K. Law, “Fuel Options for Next-Generation Chemical Propulsion,” *AIAA J.*, 50, 19–36, 2012.
[206] I. V. Dyakov, A. A. Konnov, J. De Ruyck, K. J. Bosschaart, E. C. M. Brock, and L. P. H. De Goey, “Measurement of adiabatic burning velocity in methane-oxygen-nitrogen mixtures,” *Combust. Sci. Technol.*, 172, 81–96, 2001.
[207] P. Dirrenberger, P. A. Glaude, R. Bounaceur, H. Le Gall, A. P. Da Cruz, A. A. Konnov, and F. Battin-Leclerc, “Laminar burning velocity of gasolines with addition of ethanol,” *Fuel*, 115, 162–169, 2014.
[208] Z. H. Wang, W. B. Weng, Y. He, Z. S. Li, and K. F. Cen, “Effect of H2/CO ratio and N2/CO2dilution rate on laminar burning velocity of syngas investigated by direct measurement and simulation,” *Fuel*, 141, 285–292, 2015.
[209] H. O. B. O. B. Nonaka and F. M. M. Pereira, “Experimental and numerical study of CO2 content effects on the laminar burning velocity of biogas,” *Fuel*, 182, 382–390, 2016.
[210] L. Sileghem, V. A. Alekseev, J. Vancoillie, E. J. K. Nilsson, S. Verhelst, and A. A. Konnov, “Laminar burning velocities of primary reference fuels and simple alcohols,” *Fuel*, 115, 32–40, 2014.
[211] R. J. Kee, M. E. Coltrin, P. Glarborg, and H. Zhu, *Chemically Reacting Flow - Theory, Modeling, and Simulation*, 2nd ed. Hoboken, USA: John Wiley and Sons, 2018.
[212] K. J. Bosschaart and L. P. H. De Goey, “The laminar burning velocity of flames propagating in mixtures of hydrocarbons and air measured with the heat flux method,” *Combust. Flame*, 136, 261–269, 2004.
[213] A. Van Maaren, D. S. Thung, and L. P. H. De Goey, “Measurement of Flame Temperature and Adiabatic Burning Velocity of Methane/Air Mixtures,” *Combust. Sci. Technol.*, 96, 327–344, 1994.

[214] S. Shin, H.-H. Ahn, Y. I. Cho, C.-H. Sohn, S. Sehyun, Y. I. Cho, W. K. Gringrich, and W. Shyy, "Numerical study of laminar heat transfer with temperature dependent fluid viscosity in a 2:1 rectangular duct," *Int. J. Heat Mass Transf.*, 42, 4365–4373, 1993.
[215] R. T. E. Hermanns, "Laminar Burning Velocities of Methane-Hydrogen-Air Mixtures," Eindhoven: Technische Universiteit Eindhoven, 2007.
[216] R. J. Moffat, "Describing the uncertainties in experimental results," *Exp. Therm. Fluid Sci.*, 1, 3–17, 1988.
[217] P. Zhao, W. Yuan, H. Sun, Y. Li, A. P. Kelley, X. Zheng, and C. K. Law, "Laminar flame speeds, counterflow ignition, and kinetic modeling of the butene isomers," *Proc. Combust. Inst.*, 35, 309–316, 2015.
[218] J. Zádor, S. J. Klippenstein, and J. A. Miller, "Pressure-dependent OH yields in alkene + HO2 reactions: A theoretical study," *J. Phys. Chem. A*, 115, 10218–10225, 2011.
[219] "Arkane - https://github.com/ReactionMechanismGenerator/RMG-Py/tree/master/arkane," 2020. .
[220] A. Grinberg Dana, D. Ranasinghe, H. Wu, C. Grambow, X. Dong, M. Johnson, M. Goldman, M. Liu, and W. H. Green, "'ARC - Automated Rate Calculator', version 1.1.0," *DOI: 10.5281/zenodo.3356849*. .
[221] A. C. Knipe and M. G. Moloney, *Reaction Mechansisms 2017: An annualsurvey covering the literature dated January to December 2017*, 1st ed. Hoboken, USA, 2017.
[222] D. G. Goodwin, "An Open Source, Extensible Software Suite FOR CVD Process Simulation," 2003.
[223] G. Pio and E. Salzano, "The effect of ultra-low temperature on the flammability limits of a methane/air/diluent mixtures," *J. Hazard. Mater.*, 362, 224–229, 2019.
[224] V. C. Patel and A. Kumar, "Evaluation of three air dispersion models: ISCST2, ISCLT2, and SCREEN2 for mercury emissions in an urban area," *Environ. Monit. Assess.*, 53, 259–277, 1998.
[225] K. McGrattan, S. Hostikka, R. McDermott, J. Floyd, C. Weinschenk, and K. Overholt, "Sixth Edition Fire Dynamics Simulator User ' s Guide," Austin, USA, 2016.
[226] G. Pio, M. Carboni, and E. Salzano, "Realistic aviation fuel chemistry in computational fluid dynamics," *Fuel*, 254, 115676, 2019.
[227] T. K. Blanchat, V. F. Nicolette, W. D. Sundberg, and V. G. Figueroa, "SANDIA REPORT Well-Characterized Open Pool Experiment Data and Analysis for Model Validation and Development," 2006.
[228] V. Cozzani, G. Pio, and E. Salzano, "Numerical Simulation of Multi-Component LNG Pool Fire," *Chem. Eng. Trans.*, 74, 1357–1362, 2019.
[229] V. Cozzani, G. Gubinelli, and E. Salzano, "Escalation thresholds in the assessment of domino accidental events," *J. Hazard. Mater.*, 129, 1–21, 2006.
[230] R. Eberwein, A. Rogge, F. Behrendt, and C. Knaust, "Dispersion modeling of LNG-Vapour on land – A CFD-Model evaluation study," *J. Loss Prev. Process Ind.*, 65, 104116, 2020.
[231] J. F. Bosen, "An Approximation Formula to Compute Relative Humidity From Dry Bulb and Dew Point Temperatures," *Mon. Weather Rev.*, 1958.
[232] O. Levenspiel, *Chemical Reaction Engineering*, 3rd ed. Hoboken, USA, 1999.
[233] F. Strozzi, J. M. Zaldívar, A. E. Kronberg, and K. R. Westerterp, "On-line runaway detection in batch reactors using chaos theory techniques," *AIChE J.*, 45, 2429–2443, 1999.
[234] K. J. Bosschaart and L. P. H. de Goey, "Detailed analysis of the heat flux method for measuring burning velocities," *\Cf*, 132, 170–180, 2003.
[235] O. Park, P. S. Veloo, N. Liu, and F. N. Egolfopoulos, "Combustion characteristics of alternative gaseous fuels," *Proc. Combust. Inst.*, 33, 887–894, 2011.
[236] J. L. Pagliaro, G. T. Linteris, P. B. Sunderland, and P. T. Baker, "Combustion inhibition and enhancement of premixed methane-air flames by halon replacements," *Combust. Flame*, 162, 41–49, 2015.
[237] V. A. Alekseev and A. A. Konnov, "Data consistency of the burning velocity measurements using the heat flux method: Hydrogen flames," *Combust. Flame*, 194, 28–36, 2018.
[238] W. K. Metcalfe, S. M. Burke, S. S. Ahmed, and H. J. Curran, "A hierarchical and comparative kinetic modeling study of C1 - C2 hydrocarbon and oxygenated fuels," *Int. J. Chem. Kinet.*, 45, 638–679, 2013.
[239] B. Sirjean, E. Dames, D. A. Sheen, X.-Q. You, C. Sung, A. T. Holley, F. N. Egolfopoulos, H. Wang, S. S. Vasu, D. F. Davidson, R. K. Hanson, H. Pitsch, C. T. Bowman, A. Kelley, C. K. Law, W. Tsang, N. P. Cernansky, D. L. Miller, A. Violi, *et al.*, "A high-temperature chemical kinetic model of n-alkane oxidation, JetSurF version 1.0," 18, 362, 2009.
[240] E. J. K. Nilsson, A. van Sprang, J. Larfeldt, and A. A. Konnov, "The comparative and combined effects of hydrogen addition on the laminar burning velocities of methane and its blends with ethane and propane," *Fuel*, 189, 369–376, 2017.
[241] S.-H. Qin, X.-X. Sun, W.-C. Lin, C.-M. Shu, F. You, and S.-C. Ho, "Experimental and Computational Approaches for CH4 and C2H4 Flammability Zones," *Energy & Fuels*, 31, 9950–9956, 2017.
[242] I. A. Zlochower and G. M. Green, "The limiting oxygen concentration and flammability limits of gases and gas mixtures," *J. Loss Prev. Process Ind.*, 22, 499–505, 2009.
[243] F. N. Egolfopoulos, D. L. Zhu, and C. K. Law, "Experimental and numerical determination of laminar flame speeds: Mixtures of C2-hydrocarbons with oxygen and nitrogen," *Symp. Combust.*, 23, 471–478, 1991.
[244] M. I. Hassan, K. T. Aung, O. C. Kwon, and G. M. Faeth, "Properties of Laminar Premixed Hydrocarbon/Air Flames at Various Pressures," *J. Propuls. POWER*, 14, 479–492, 1998.
[245] K. Kumar, G. Mittal, C. J. Sung, and C. K. Law, "An experimental investigation of ethylene/O2/diluent mixtures: Laminar flame speeds with preheat and ignition delays at high pressures," *Combust. Flame*, 153, 343–354, 2008.
[246] G. Pio, A. Ricca, V. Palma, and E. Salzano, "Low temperature combustion of methane/alkenes mixtures," *Fuel*, 254, 115567, 2019.
[247] S. G. Davis and C. K. Law, "Determination of and Fuel Structure Effects on Laminar Flame Speeds of C1 to C8 Hydrocarbons," *Combust. Sci. Technol.*, 140, 427–449, 1998.
[248] G. Jomaas, X. L. Zheng, D. L. Zhu, and C. K. Law, "Experimental determination of counterflow ignition temperatures and laminar flame speeds of C2-C3hydrocarbons at atmospheric and elevated pressures," *Proc. Combust. Inst.*, 30, 193–200, 2005.
[249] Y. Fenard, P. Dagaut, G. Dayma, F. Halter, and F. Foucher, "Experimental and kinetic modeling study of trans-2-butene

oxidation in a jet-stirred reactor and a combustion bomb," *Proc. Combust. Inst.*, 35, 317–324, 2015.
[250] C. W. Zhou, Y. Li, E. O'Connor, K. P. Somers, S. Thion, C. Keesee, O. Mathieu, E. L. Petersen, T. A. DeVerter, M. A. Oehlschlaeger, G. Kukkadapu, C. J. Sung, M. Alrefae, F. Khaled, A. Farooq, P. Dirrenberger, P. A. Glaude, F. Battin-Leclerc, J. Santner, *et al.*, "A comprehensive experimental and modeling study of isobutene oxidation," *Combust. Flame*, 167, 353–379, 2016.
[251] O. G. Penyazkov, K. L. Sevrouk, V. Tangirala, and N. Joshi, "High-pressure ethylene oxidation behind reflected shock waves," *Proc. Combust. Inst.*, 32 II, 2421–2428, 2009.
[252] Y. Li, C. W. Zhou, and H. J. Curran, "An extensive experimental and modeling study of 1-butene oxidation," *Combust. Flame*, 181, 198–213, 2017.
[253] C. Xu and A. A. Konnov, "Validation and analysis of detailed kinetic models for ethylene combustion," *Energy*, 43, 19–29, 2012.
[254] H. Hashemi, J. M. Christensen, S. Gersen, H. Levinsky, S. J. Klippenstein, and P. Glarborg, "High-pressure oxidation of methane," *Combust. Flame*, 172, 349–364, 2016.
[255] D. L. Baulch, M. J. Pilling, C. J. Cobos, R. A. Cox, C. Esser, P. Frank, T. Just, J. A. Kerr, J. Troe, R. W. Walker, and J. Warnatz, "Evaluated Kinetic Data for Combustion Modelling," *J. Phys. Chem. Ref. Data*, 21, 411, 1992.
[256] V. D. Knyazev and I. R. Slagle, "Experimental and theoretical study of the C2H3 ⇆ H + C2H2 reaction. Tunneling and the shape of falloff curves," *J. Phys. Chem.*, 100, 16899–16911, 1996.
[257] C. F. Goldsmith, L. B. Harding, Y. Georgievskii, J. A. Miller, and S. J. Klippenstein, "Temperature and pressure dependent rate coefficients for the reaction of vinyl radical with molecular oxygen," *J. Phys. Chem. A*, 119, 7766–7779, 2015.
[258] N. M. Marinov, W. J. Pitz, C. K. Westbrook, A. M. Vincitore, M. J. Castaldi, S. M. Senkan, and C. F. Melius, "Aromatic and polycyclic aromatic hydrocarbon formation in a laminar premixed n-butane flame," *Combust. Flame*, 114, 192–213, 1998.
[259] W. Tsang, "Chemical Kinetic Data Base for Combustion Chemistry Part V. Propene," *J. Phys. Chem. Ref. Data*, 20, 221, 1991.
[260] A. Laskin, H. Wang, and C. K. Law, "Detailed kinetic modeling of 1,3-butadiene oxidation at high temperatures," *Int. J. Chem. Kinet.*, 32, 589–614, 2000.
[261] H. Sun and C. K. Law, "Kinetics of hydrogen abstraction reactions of butene isomers by OH radical," *J. Phys. Chem. A*, 114, 12088–12098, 2010.
[262] K. M. Van Geem, S. P. Pyl, G. B. Marin, M. R. Harper, and W. H. Green, "Accurate high-temperature reaction networks for alternative fuels: Butanol isomers," *Ind. Eng. Chem. Res.*, 49, 10399–10420, 2010.
[263] J. A. Miller and S. J. Klippenstein, "Dissociation of propyl radicals and other reactions on a C3H7 potential," *J. Phys. Chem. A*, 117, 2718–2727, 2013.
[264] C. K. Wu and C. K. Law, "On the determination of laminar flame speeds from stretched flames," *Symp. Combust.*, 20, 1941–1949, 1985.
[265] K. T. Aung, M. I. Hassan, and G. M. Faeth, "Effects of pressure and nitrogen dilution on flame stretch interactions of laminar premixed H-2 O-2 N-2 flames," *Combust. Flame*, 112, 1–15, 1998.
[266] S. D. Tse, D. L. Zhu, and C. K. Law, "Morphology and burning rates of expanding spherical flames in H2/O2/inert mixtures up to 60 atmospheres," *Proc. Combust. Inst.*, 28, 1793–1800, 2000.
[267] A. E. Dahoe, "Laminar burning velocities of hydrogen-air mixtures from closed vessel gas explosions," *J. Loss Prev. Process Ind.*, 18, 152–166, 2005.
[268] D. Bradley, M. Lawes, K. Liu, S. Verhelst, and R. Woolley, "Laminar burning velocities of lean hydrogen-air mixtures at pressures up to 1.0 MPa," *Combust. Flame*, 149, 162–172, 2007.
[269] E. Hu, Z. Huang, J. He, and H. Miao, "Experimental and numerical study on laminar burning velocities and flame instabilities of hydrogen-air mixtures at elevated pressures and temperatures," *Int. J. Hydrogen Energy*, 34, 8741–8755, 2009.
[270] M. Kuznetsov, M. Czerniak, J. Grune, and T. Jordan, "Effect of Temperature on Laminar Flame Velocity for Hydrogen-Air Mixtures At Reduced Pressures," in *International Conference of Hydrogen Safety*, 2013, 1–12.
[271] V. V. Zamashchikov, V. A. Alekseev, and A. A. Konnov, "Laminar burning velocities of rich near-limiting flames of hydrogen," *Int. J. Hydrogen Energy*, 39, 1874–1881, 2014.
[272] G. Yu, C. K. Law, and C. K. Wu, "Laminar flame speeds of hydrocarbon + air mixtures with hydrogen addition," *Combust. Flame*, 63, 339–347, 1986.
[273] S. Y. Liao, D. M. Jiang, and Q. Cheng, "Determination of laminar burning velocities for natural gas," *Fuel*, 83, 1247–1250, 2004.
[274] F. Halter, C. Chauveau, N. Djebaïli-Chaumeix, and I. Gökalp, "Characterization of the effects of pressure and hydrogen concentration on laminar burning velocities of methane-hydrogen-air mixtures," *Proc. Combust. Inst.*, 30, 201–208, 2005.
[275] M. Mitu, V. Giurcan, D. Razus, and D. Oancea, "Inert gas influence on the laminar burning velocity of methane-air mixtures," *J. Hazard. Mater.*, 321, 440–448, 2017.
[276] E. Salzano, G. Pio, A. Ricca, and V. Palma, "The effect of a hydrogen addition to the premixed flame structure of light alkanes," *Fuel*, 234, 1064–1070, 2018.
[277] G. a. Karim, I. Wierzba, and S. Boon, "The lean flammability limits in air of methane, hydrogen and carbon monoxide at low temperatures," *Cryogenics (Guildf).*, 24, 305–308, 1984.
[278] I. Wierzba and Q. Wang, "The flammability limits of H 2 –CO–CH 4 mixtures in air at elevated temperatures," *Int. J. Hydrogen Energy*, 31, 485–489, 2006.
[279] N. Siu, J. S. Herring, J. Byers, L. Cadwallader, W. Reece, and J. Byers, "Qualitative Risk Assessment for an LNG Refueling Station ' and Review of Relevant Safety Issues," Idaho Falls, USA, 1999.
[280] Z. Li, M. Gong, E. Sun, J. Wu, and Y. Zhou, "Effect of low temperature on the flammability limits of methane/nitrogen mixtures," *Energy*, 36, 5521–5524, 2011.
[281] G. L. Agafonov, I. Naydenova, P. A. Vlasov, and J. Warnatz, "Detailed kinetic modeling of soot formation in shock tube pyrolysis and oxidation of toluene and n-heptane," *Proc. Combust. Inst.*, 31 I, 575–583, 2007.
[282] A. Frassoldati, A. Cuoci, T. Faravelli, U. Niemann, E. Ranzi, R. Seiser, and K. Seshadri, "An experimental and kinetic modeling study of n-propanol and iso-propanol combustion," *Combust. Flame*, 157, 2–16, 2010.

[283] C. S. Mcenally and L. D. Pfefferle, “Soot Formation in Methane / Air Nonpremixed Flames Doped With Small Quantities of C3 Hydrocarbons,” *Combust. Flame*, 112, 545–558, 1998.
[284] J. P. Spinti, J. N. Thornock, E. G. Eddings, P. J. Smith, and A. F. Sarofim, “Heat transfer to objects in pool fires,” in *Dev. Heat Transfer*, 1st ed., 20, New Forest National Park, UK: WIT Press, 2008, 69–136.
[285] T. K. Blanchat, V. F. Nicolette, W. D. Sundberg, and V. G. Figueroa, “Well-Characterized Open Pool Experiment Data and Analysis for Model Validation and Development,” Albuquerque, USA, 2006.
[286] H. C. Hottel and A. F. Sarofim, “Models of radiative transfer in furnaces,” *J. Eng. Phys.*, 19, 1102–1114, 1970.
[287] S. Yan, W. Ciro, E. G. Eddings, and A. F. Sarofim, “Experimental study of burning rate in jet-fuel pool fires,” in *Third Joint Meeting of the U.S. Sections of The Combustion Institute*, 2003, 1–6.
[288] Mary Kay O ’Connor Process Safety Center, “LNG Pool Fire Modeling,” College Station, USA, 2008.
[289] S. Schalike, K.-D. Wehrstedt, and A. Schonbucher, “CFD simulation to predict the thermal radiation of large LNG pool fire,” *Proc. Eur. Combust. Meet. 2011*, 7, 1–6, 2011.
[290] P. K. Raj, “Large hydrocarbon fuel pool fires: Physical characteristics and thermal emission variations with height,” *J. Hazard. Mater.*, 140, 280–292, 2007.
[291] R. Bubbico, G. Dusserre, and B. Mazzarotta, “Calculation of the Flame Size from Burning Liquid Pools,” *Chem. Eng. Trans.*, 53, 67–72, 2016.
[292] S. Betteridge, “Modelling large LNG pool fires on water,” *J. Loss Prev. Process Ind.*, 56, 46–56, 2018.
[293] N. Alileche, V. Cozzani, G. Reniers, and L. Estel, “Thresholds for domino effects and safety distances in the process industry: A review of approaches and regulations,” *Reliab. Eng. Syst. Saf.*, 143, 74–84, 2015.
[294] I. O. Antonov, J. Kwok, J. Zádor, and L. Sheps, “A combined experimental and theoretical study of the reaction OH + 2-butene in the 400-800 K temperature range,” *J. Phys. Chem. A*, 119, 7742–7752, 2015.
[295] C. W. Zhou, J. M. Simmie, K. P. Somers, C. F. Goldsmith, and H. J. Curran, “Chemical Kinetics of Hydrogen Atom Abstraction from Allylic Sites by 3O2; Implications for Combustion Modeling and Simulation,” *J. Phys. Chem. A*, 121, 1890–1899, 2017.
[296] J. Warnatz, U. Maas, and R. W. Dibble, “Combustion Physical and Chemical Fundamentals, Modeling and Simulation, Experiments, Pollutant Formation.”
[297] Mc Guire and White, “Liquefied Gas Handling Principles On Ship and in Terminals,” *Witherby Co Ltd 32-36 Aylesbury Str. London*, 9–12, 2008.
[298] M. G. Zabetakis, S. Lambiris, and G. S. Scott, “Flame temperatures of limit mixtures,” in *Symposium (International) on Combustion*, 1958, 7, 484–487.
[299] M. Chase, “NIST-JANAF Thermochemical Tables, 4th Edition,” *Journal of Physical and Chemical Reference Data, Monograph 9*. 1952, 1998.
[300] Y. Lei, F. Mehmood, S. Lee, J. Greeley, B. Lee, S. Seifert, R. E. Winans, J. W. Elam, R. J. Meyer, P. C. Redfern, D. Teschner, R. Schlogl, M. J. Pellin, L. A. Curtiss, and S. Vajda, “Increased Silver Activity for Direct Propylene Epoxidation via Subnanometer Siza Effects,” *Science (80-.).*, 328, 224–227, 2010.

List of figures

List of tables

Appendix

List of publications

2018

Pio G., Palma V., Salzano E.,
Comparison and Validation of Detailed Kinetic Models for the Oxidation of Light Alkenes
Ind. Eng. Chem. Res., 2018, 57, 7130-7135

ABSTRACT: The increasing interest in light alkenes oxidation for the development of detailed kinetic model is mainly due to their relevance in the combustion chemistry of most common fuels and their formation in the oxidation of higher alkanes. This study analyses the detailed kinetic mechanisms for the oxidation of linear lighter alkenes, ethylene, propylene and 1-butene, through the comparison of several combustion kinetic models retrieved from current literature with respect to the experimental data for the laminar burning velocity in air, and for the ignition delay time, by varying either reactant concentration or initial temperature. The mechanisms by University of California, San Diego (UCSD), Konnov group (KOM), University of Southern California (USC), Saudi Aramco 2.0 (SAM), Lawrence Livermore National Laboratory (LLNL), and Politecnico of Milano (CRECK) have been evaluated through a unified statistical analysis. A sensitivity analysis for the laminar burning velocity as also performed to assess and compare the reactions described in the studied models and sort by relevance. Best fits are produced by the LLNL and the UCSD model even if the optimal results can depend on the specific hydrocarbon. We then produced a new mechanism by adding the UCSD for C3 and LLNL for C4 or more, which resulted to work better.

Pio G., Salzano E.,
Laminar Burning Velocity of Methane, Hydrogen, and Their Mixtures at Extremely Low-Temperature Conditions
Energy Fuels, 2018,32, 8830-8836

ABSTRACT: Methane consumption is strongly increasing as a result of its abundance from natural gas, thus leading to reduced costs, and as a result of the reduced environmental impact in the case of combustion, with a lower carbon content with respect to traditional fuels. These advantages encourage its utilization in several industrial applications, such as methane steam reforming for the production of hydrogen and automotive applications. The necessity of transporting the gases and large-scale distribution systems is however one of the main issues. Innovative processes, such as cryogenic storage, cryo-compression, and liquefaction, require detailed information on the thermal and chemical properties of the methane−hydrogen mixture at low and ultralow temperatures. In this framework, detailed kinetic models for the total and partial oxidation of methane, hydrogen, and methane−hydrogen mixtures in air at low ($273 > T > 200$ K) and ultralow ($T < 200$ K) temperatures must be developed and validated. In this work, the laminar burning velocity of these gases has been simulated and compared to the few available experimental data retrieved from the literature. Hence, simplified correlations for the burning velocity with respect to the initial composition and temperature have been adopted and further developed. The simplified approach proposed in this work reduces the number of degrees of freedom required for the application of the modified Gülder equation. Moreover, it is suitable for the description of the combined effect of the initial temperature and gaseous composition. The performed analysis of the concentration and temperature profiles with respect to burner head distance indicates, as a possible explanation for the methane-dominated regime, the presence of a limitation in the hydrogen concentration hindering its production. A sensitivity analysis was performed to evaluate the effect of hydrogen addition and initial temperature on the methane kinetic mechanism in the presence of air. The results show that, although the hydrogen production rate does not change, the reaction mechanism is strongly affected by the studied parameters

Pio G., Salzano E.,
Evaluation of safety parameters of light alkenes by means of detailed kinetic models
Process. Saf. Environ, 2018, 119, 131-137

ABSTRACT: The oxidation of light alkenes is the core of the modern chemical industry and a pivotal point for several environmental and safety considerations. However, few works have dealt with the prediction of fire and explosion parameters for the definition of process conditions, for the design and safe handling of such reactive substances. In this work, flammability parameters for light alkenes (ethylene, propylene and the three butylene isomers) have been calculated by adopting the detailed kinetic mechanisms of the University of California, San Diego, integrated with C4 reactions by the Lawrence Livermore National Laboratory mechanism. The new model has been adopted for the definition of flammability limits, adiabatic flame pressure and temperature, maximum rate of pressure rise, gas deflagration index (K_G), auto-ignition temperature and minimum oxygen concentration. Flammability regions for nitrogen and carbon dioxide dilution have also been reported.

Salzano E., Pio G., Ricca A., Palma V.,
The effect of a hydrogen addition to the premixed flame structure of light alkanes
Fuel, 2018, 234, 1064-1070

ABSTRACT: The effect of a hydrogen addition to the combustion chemistry of light alkanes was evaluated by the experimental and numerical determination of the laminar burning velocity of methane/propane/hydrogen mixtures in air at different equivalence ratios and fuel compositions by using a heat flux burner. The experimental results have been compared with additional data selected for the main experimental rig commonly adopted in current literature. The obtained set of data was used for the validation of the detailed kinetic model developed by the University of Bologna. Subsequently, an in-depth analysis on the reaction system was carried out in order to evaluate the effects of a low hydrogen content on the reaction paths, concentrations profiles of the main combustion products and temperature profiles with respect to the distance from the burner. Thus, additional information was obtained by means of a sensitivity analysis, evaluating the relative relevance of each reaction on the laminar burning velocity and comparing obtained the results for all the investigated conditions.

Pio G., Salzano E.,
Flammability parameters of liquified natural gas
J. Loss. Prev. Process. Ind., 2018, 56, 424-429.

ABSTRACT: The use of liquefied natural gas (LNG) is constantly growing. However, safety issues regarding cryogenic storage and transportation systems are still to be fully resolved. In particular, the evaluation of the efficiency of inerting systems for low-temperature LNG vapour is essential. In this work, the variation of the flammability range (in terms of lower and upper flammability limits and minimum oxygen concentration) obtained by adding nitrogen to pure air for some representative LNG mixtures has been evaluated at ambient temperature and at temperatures below 0°C by using a detailed kinetic model entitled KIBO, which has been proved to be reliable for the description of C_0-C_4 reactions in oxidative conditions, and by the limiting burning velocity theory. Strong differences are reported among pure methane and natural gas mixtures for all the investigated temperatures. The effect of composition is therefore relevant. Furthermore, the obtained results suggest that the lower flammability limit is determined by thermal aspects at high temperature only, whereas at low temperature, kinetic limitations are more relevant.

Pio G., Salzano E.,
Laminar Burning Velocity of Multi-Component Gaseous Mixtures
Chem. Eng. Tran., 2018, 67, 1-6.

ABSTRACT: The laminar burning velocity is the essential parameter for the design of equipment and process. Indeed, the knowledge of this parameter allows for the definition of flammability limits, minimum oxygen concentration and the gas deflagration index, Kg. Recently, the interest in the laminar burning velocity has raised because of the increased use of complex gaseous mixtures derived from biological (biogas), or pyrolysis and gasification (syngas) processes. Due to the large number of components of these gases, simplified correlations for the definition of the additivity of the burning velocity are questionable. Furthermore, the presence of carbon monoxide, hydrogen sulphide, ammonia and hydrogen, or other non-hydrocarbon substances, may strongly affect the correlation results. Le Chatelier's formula e.g. may produce an error of over 25% with respect to the experimental data for simple mixtures based on two hydrocarbon fuels. In this work, a review of the main additivity rules for the definition of the laminar burning velocity for multicomponent mixtures (≥ 3 fuels) is given, starting from the pioneering correlations and analysis of Spalding. The equations have been compared and validated with respect to experimental data. A comparison with the results obtained by using more recent advanced kinetic mechanism, which can be adopted for the prediction of mixture reactivity, is also given.

2019

Pio G., Salzano E.,
The effect of ultra-low temperature on the flammability limits of a methane/air/diluent mixtures
J. Hazard. Mater., 2019, 362, 224-229

ABSTRACT: Natural gas represents an attractive fuel for industrialized and developing countries seeking an alternative to petroleum. Due to economic and safety considerations, liquefied natural gas (LNG) at cryogenic conditions is preferred for storage and transportation. The main drawback is the poor understanding of the physical and chemical phenomena that occur at the storage conditions of liquid methane, i.e. at ultra-low temperatures around 110 K and, if released, at temperatures below ambient. In this work, a procedure to evaluate the laminar burning velocity, the flammability limit (FL) and the limiting oxygen concentration (LOC) of methane-air-diluent mixtures based on detailed kinetic mechanism at ultra-low temperatures is proposed. The estimation of the FL was obtained with the limiting burning velocity theory. The effects of inert content (extinguishing) and agent (N2, H2O and CO2) on FL were evaluated and compared with data retrieved from the literature. The agreement between experimental observation and model results from 200 K–300 K incentivizes the adoption of the new procedure for further studies of fuel reactivity and safety

parameters. Moreover, the proposed procedure may be suitable for the estimation of the safety parameters of complex fuel mixtures whose composition is closer to the actual values of LNG.

Pio G., Ricca A., Palma V., Salzano E.,
Low temperature combustion of methane/alkenes mixtures
Fuel, 2019, 254, 115567

ABSTRACT: The use of methane is commonly adopted as thermal diluent and chemical inhibitor in the partial oxidation of alkenes, in order to avoid the occurrence of unwanted reactions and full oxidation. Moreover, methane-alkene mixtures are commonly present in several industrial applications such as petrochemical processes. In this work, experimental data for pure ethylene and propylene flames in presence of air were collected, as first. Then the effect of alkenes addition on methane premixed flames was investigated. These fuel compositions were investigated by means of a heat flux burner at different gaseous compositions. The measurements were compared with experimental data retrieved from current literature as well as with the results of a detailed kinetic mechanism. The data collected in this work suggest the existence of two chemical regimes, resulting in a methane dominated kinetic, in case of alkene addition lower than 20 %v/v, and alkene-dominated kinetic, in case of higher alkenes content. The production of soot precursors for methane combustion was found to be significantly increased by the addition of propylene. Finally, the maximum reactivity, expressed in terms of laminar burning velocity, undergoes a non-negligible shift toward a richer composition of methane in the presence of alkene. The agreement between the experimental data and numerical predictions allowed for further evaluation of the chemical interactions, product and heat profiles as a function of the initial composition. A criterion based on the flame structure was posed and successfully implemented to identify the temperature values giving unsafe or undesired conditions in the epoxidation processes.

Pio G., Carboni M., Salzano E.,
Realistic aviation fuel chemistry in computational fluid dynamics
Fuel, 2019, 254, 115676

ABSTRACT: The prediction of flame extinction, soot formation and heat transfer for kerosene (pool) fires is a key aspect for the characterisation of aviation fuels. In particular, one of the main numerical challenges is the description of complex interactions of chemical and physical phenomena. This work is devoted to the individuation of an optimised surrogate mixture for the development of a detailed chemical model describing liquid fuel pyrolysis, homogeneous combustion and the formation of soot precursors, as well as the implementation of the obtained kinetic mechanism in open source computational fluid dynamics (CFD). To this aim, the primary combustion products and corresponding rate determining step into the production paths are identified by means of sensitivity and reaction paths analyses under several initial conditions representative for the investigated scenarios. The results show that a binary mixture composed of 92%v n-decane and 8%v toluene reproduces the aviation fuel properties. Based on the numerical results obtained in this work for aviation fuel, it holds that the mass burning rate *m*"[kg m s] − − 2 1 dependence with pool diameter (Dp) expressed in meters is: *m D* " 0.47 (1 exp(3.61) = · − − · *p*) A reduced (detailed) kinetic mechanism consisting of 14 reactions is obtained and implemented in a CFD model. The numerical results are in accordance with experimental data retrieved from the literature. The observed data consistency validates the adopted procedure and allows for further considerations on soot precursor formation in case of diffusive flames of aviation fuel.

Pio G., Carboni M., Iannaccone T., Cozzani V., Salzano E.,
Numerical simulation of small-scale pool fires of LNG
J. Loss. Prev. Process. Ind., 2019, 61, 82-88

ABSTRACT: Liquefied natural gas (LNG) has been largely indicated as a promising alternative solution for the transportation and storage of natural gas. In the case of accidental release on the ground, a pool fire scenario may occur. Despite the relevance of this accident, due to its likelihood and potential to trigger domino effects, accurate analyses addressing the characterization of pool fires of LNG are still missing. In this work, the fire dynamic simulator (FDS) has been adopted for the evaluation of the effects of the released amount of fuel and its composition (methane, ethane, and propane), on the thermal and chemical properties of small-scale LNG pool fire. More specifically, the heat release rate, the burning rate, the flame height, and thermal radiation, at different initial conditions, have been evaluated for pool having diameter smaller than 10 m. Safety distances have been calculated for all the investigated conditions, as well. Results have also been compared with data and correlations retrieved from the current literature. The equation of Thomas seems to work properly for the definition of the height over diameter ratio of the LNG pool fire for all the mixture and the investigated diameters. The addition of ethane and propane significantly affects the obtained results, especially in terms of radiative thermal radiation peaks, thus indicating the inadequacy of the commonly adopted assumption of pure methane as single, surrogate species for the LNG mixture.

Pio G., Barba D., Palma V., Salzano E.,
A Numerical Study on the Effect of Temperature and Composition on the Flammability of Methane–Hydrogen Sulfide Mixtures
Combust. Sci. Technol., 2019, 191, 1541-1557

ABSTRACT: The growing demand of natural gas inspires existing and new projects in topographical areas where the hydrocarbon extraction meets severe safety challenges due to the presence of hydrogen sulfide (H2S) in natural gas, i.e. sour gas. Indeed, the combined effect of flammability and toxicity of such gases has the critical potential to increase the hazard level in the industrial installation, thus aggravating the consequences for human and assets. In this work, a detailed kinetic model was validated and adopted to estimate the laminar burning velocity and the flammability limits of sour gas at different initial temperatures, within the range 250–325 K, equivalence ratio from 0.4 to 2.5, and content of H2S up to 15%v/v with respect to methane. For larger amount of the acid, almost negligible variations of the burning velocity of the mixtures have been observed, even if slight variations are detected either at lean (decrease) or rich (increase) conditions. On the contrary, flammability limits results show also that the addition of H2S has a strong relevance on safety parameters, more specifically for the upper flammability limit.

Iervolino I., Accardo D., Tirri A.E., Pio G., Salzano E.,
Quantitative risk analysis for the Amerigo Vespucci (Florence, Italy) airport including domino effects
Saf. Sci., 2019, 113, 472-489

ABSTRACT: Feasibility studies for airport facilities require quantitative assessment of the effects of the routine operations on the area surrounding the planned installation. In some countries such analyses are mandatory and the targets for which the effects need to be evaluated often include: cultural heritage, natural habitat, as well as human comfort and health. Regarding the latter issue, of main concern is the fatality risk due to airport traffic, primarily considering accidents due to landing and take-off operations. Accidents leading to crash may include fuel fires and explosions, but also trigger domino effects such as industrial accidents, possibly amplifying adverse consequences. Quantitative risk analysis for airport facilities is the topic of the study presented, where a probabilistic framework to evaluate the annual fatality risk for airports and surrounding areas is discussed. The risk metric is the *individual risk* (IR), and the methodology contemplates the tools and procedures to compute the annual expected number of accidents that result in fatality for each point in the area surrounding the airport. Three causes contribute to the evaluation of IR: (i) direct aircraft impact, (ii) heat radiation produced by the burning of fuel possibly released in the crash; (iii) heat radiation or intoxication because the crash involves industrial facilities storing or treating relevant amounts of hazardous materials. The risk analysis requires competencies mainly from three fields: (a) stochastic modelling for uncertainty management and probabilistic evaluation; (b) aeronautical engineering for the modeling of aircraft operations and dynamics that may result in an accident and, finally, (c) chemical engineering for the combustion modeling and for the analysis of cascading effects on industrial targets (also called *domino* in the following), as well as for the evaluation of health consequences. The developed method is thoroughly discussed in the paper and applied to the foreseen upgrade of the Florence (Italy) airport Amerigo Vespucci, which shows its potential effectiveness in decision making preparatory to airports' design.

Cozzani V., Pio G., Salzano E.,
Numerical Simulation of Multi-Component LNG Pool Fire
Chem. Eng. Tran., 2019, 74, 1367-1372

ABSTRACT: The release of large amount of liquefied natural gas from fixed or mobile equipment may induce to pool fire when immediate ignited. The prediction and simulation of this phenomenon is very complex because several premixed, convective and diffusive burning phenomena, and rapid phase evaporation, are involved simultaneously. Nevertheless, the use of Reynolds-averaged Navier-Stokes (RANS) equations with k-ε model for turbulence and classical models are still adopted, although strong uncertainties and over-simplifications with respect to the real scenario. More recently large-eddy simulation (LES) modeling, as adopted in some codes as FLUENT or FDS, has been adopted. LES methodology is able to introduce more detailed information on the chemical kinetic of the oxidation reactions. Again, however, poor kinetic combustion mechanisms suitable for the implementation in computational fluid dynamic (CFD) codes, and simplified composition for the LNG - often treated as pure methane - are typically adopted. In this work, the simulation of a LNG pool fire was performed by detailed (reduced) kinetic model validated for multi-component LNG compositions by using FDS. Results were compared with both experimental and numerical analyses retrieved from literature. This approach has the potential to correctly estimate the heat radiation and the production rates of the main reaction products, including soot.

Pio G., Ricca A., Palma V., Salzano E.,
Flammability Limits of Methane/Alkene Mixtures in Air
Chem. Eng. Tran., 2019, 77, 169-174

ABSTRACT: The knowledge of alkane/alkene chemical interactions in gaseous mixtures are fundamental for several industrial applications as they represent the main compounds of the pyrolysis gas produced in stream cracking process, or in the oxidative coupling of methane, or even as component of biogas. However, reliable and comprehensive empirical correlations for the estimation of flammability limits for complex fuel mixtures are still to be developed. More in particular, the additivity correlations (e.g. Le Chatelier's rule) are not suitable or uncertain when alkanes are mixed with saturated hydrocarbon species. In this work, the flammability limits for binary mixtures of ethylene or propylene in air, either pure or in mixture with methane were defined by experimental and numerical analysis. The experimental data were evaluated by means of the heat flux burner method, which is able to reduce the effect of the flame stretching and the

related uncertainties. The obtained results were compared with the corresponding experimental data retrieved in the current literature, when available, and with the data calculated by the most common empirical correlations. The data were also compared with numerical estimations obtained by fully validated detailed kinetic model suitable for light compounds oxidative chemistry. To estimate the flammability limits, the limiting laminar burning velocity theory has been adopted. The agreement between experimental data and numerical results was evaluated by means of statistical approach.

Pio G., Salzano E.,
Flammability Limits of Methane (LNG) and Hydrogen (LH2) at Extreme Conditions
Chem. Eng. Tran., 2019, 77, 601-606

ABSTRACT: In the recent years the growing interest for cleaner and low carbon content energy sources has addressed the development of several industrial and civil applications based on methane, hydrogen, and their mixtures. The use of these gases rises, however, several technological issues for the storage and the transportation systems. Among others, cryogenic liquefaction (as liquified natural gas, LNG and liquified hydrogen, LH2) and cryo-compressed gases are considered among the most promising potential solution. On the other hand, when low and ultra-low temperature are considered, several questions regarding the safe use of such gases are raised, including the behaviour of the cold vapour phase in air after the release of liquid or cryocompressed gas from containment system. In this work, the flammability limits of hydrogen, methane and their blends at low and ultra-low temperatures were estimated by using the laminar burning velocity obtained by means of detailed kinetic mechanism. Numerical results were compared with experimental data and empirical correlations commonly adopted for this purpose. The data agreement demonstrates the applicability of the developed procedure for the estimation of safety parameters at low and ultra-low temperature and for future technological applications, even at cryogenic conditions.

2020

Pio G., Salzano E.,
Implementation of gas-phase kinetic model for the optimization of the ethylene oxide production
Chem. Eng. Sci., 2020, 212, 115331.

ABSTRACT: The direct epoxidation of light olefins is a key process of the chemical industry. However, several concerns regarding industrial and safety aspects, such as the occurrence of runaway reactions and the relevance of side reactions reducing process selectivity, are still under investigation. To this aim, a reactor operation diagram was obtained under process relevant conditions, allowing for the identification of runaway, hot spots and pseudo adiabatic operation regions by using several criteria and kinetic models. Indeed, catalytic only or complete (catalytic + non-catalytic) kinetic mechanisms were adopted to this aim. The selection of different runaway criteria was found to be negligible on the region boundaries. On the contrary, significant discrepancies were observed for hot spot region boundaries and between catalytic and complete models. An in-depth analysis, based on thermodynamic and kinetic models, was performed to individuate the optimized operative conditions. Flammability limits were estimated by applying the limiting laminar burning velocity theory, in case of different inert composition and initial temperature The results indicate that a decrease in the operative temperature has the potential to either reduce the capital costs or increase process safety. Furthermore, the proposed approach can be intended as a supporting procedure for the selection of process alternatives and reactor design.

Pio G., Ricca A., Palma V., Salzano E.,
Experimental and Numerical Evaluation of Low-Temperature Combustion of Bio-Syngas
Int. J. Hydrogen Energ., 2020, 45, 1084-1095

ABSTRACT: Environmental regulations have strongly incentivized the development of alternative technologies and renewable sources for the energy supply, including bio-syngas and low temperature combustion. However, accurate estimation methods for low-temperature chemistry of these mixtures are still missing. Hence, experimental data with the limited impact of fluid dynamics aspects are strongly required. To this aim, the heat flux burner has been adopted in this work for the measurements of the laminar burning velocity. Data were compared to evaluate the accuracy of the kinetic mechanism developed at the University of Bologna (KIBO) and exiting mixing rules. Hirasawa's correlation has been found as the most reliable empirical correlation. Furthermore, the KIBO model has been validated and compared with existing models for the investigated conditions. These results have allowed for the evaluation of the effects of fuel composition on the preferable reaction paths and on the NOx production rate.

Salzano E., Carboni M., Pio G.,
The Effects of Low-Temperature Phenomena on Rapid Phase Transition of Liquid Hydrogen
Int. J. Hydrogen Energ., 2020, in press.

ABSTRACT: The simultaneous rise in hydrogen economy and cryogenic liquefaction techniques for long-distance storage and transportation has incentivized the development of technological solutions based on the liquefied hydrogen. However, detailed models accounting for the peculiar phenomena of this cryogenic system in the case of accidental release, namely cryogenic evaporation rate and para-ortho transformation, are necessary before large-scale

commercialization. In this light, this work aims to unravel this gap of knowledge on safety aspects involving liquid hydrogen through a numerical approach. More specifically, the top events that arose from the accidental release of liquid hydrogen in the absence of ignition have been modeled. A proper evaporation sub-model suitable for cryogenic conditions has been selected in accordance with the literature. The quantum mechanics approach was adopted to estimate the thermodynamic properties of the hydrogen configurations accurately. These estimations were compared with data from the literature, showing excellent agreement. The effect of para-ortho transformation was evaluated by implementing the obtained database. Besides, different releasing surfaces and materials were tested, either solid (e.g., concrete) or liquid (i.e., water), resulting in hydrogen release rate ranging from $2.00 \cdot 10^{-4}$ – to 13.90 kg/s). The generated over-pressures were calculated for all the investigated cases and critically compared with numerical data obtained in this work and analytical model retrieved from the current literature. These results indicate that neglecting the para-ortho transformation represents a non-conservative hypothesis. Indeed, peaks potentially producing significant structural damages were observed only in cases where this transformation was considered.

Pio G., Salzano E.,
Gas-Phase Thermal Explosions in Catalytic Direct Oxidation of Alkenes
J. Loss. Prev. Process. Ind., 2019, 65, 104097.

ABSTRACT: The metal-based catalytic oxidation of alkenes to the corresponding epoxides is playing a significant role in the modern chemical industry. Nevertheless, these key processes are still lacking proper understanding with respect to the gas-phase runaway behavior (thermal explosion) and to the hot spot formation on the catalytic surface, under the typical process conditions. This work aims to enlighten these aspects by considering either the catalytic or the gas-phase chemistry for the development of reactor operative diagrams, in order to define the best-operating conditions with respect to the selectivity, the productivity, and the process safety aspects. The proposed methodology has been applied to the oxidation of ethylene and propylene for the direct oxidation process by pure oxygen, considering a detailed kinetic model accounting for the homogeneous reactions, coupled with the heterogeneous catalytic mechanisms. Sensitivity and reaction path analyses were performed to individuate the ruling species and reactions determining the transition to runaway conditions.

Pio G., Renda S., Palma V., Salzano E.,
Safety parameters for oxygen-enriched flames
J. Loss. Prev. Process. Ind., 2020, 65, 104151.

ABSTRACT: The utilization of low-quality gaseous fuel from biomass gasification and the abundance of oxygen-rich streams obtained as a by-product of nitrogen-air separation by membrane technology has incentivized the development of sustainable oxygen-enriched combustion technologies in the last decades. However, a dearth of experimental and numerical analysis addressing the reactivity and safety aspects of these mixtures at initial low temperatures can be observed in the current literature. In this work, the heat flux burner was adopted for the measurement of the laminar burning velocity of methane in oxygen enriched air at different equivalence ratios. Results were compared with numerical data obtained by means of detailed kinetic mechanisms developed at the University of Bologna and the Gas Research Institute (GriMech3.0). Simplified correlations for the estimation of the laminar burning velocity with respect to the oxygen content at any equivalence ratio were developed, tested and evaluated. An elemental reaction-based function was found appropriate for the estimation of the overall reactivity of the investigated mixtures. Besides, numerical analyses were performed to characterize the flame structures in terms of temperature and product distribution under several initial conditions. These results gave further insights into the reaction mechanisms of gaseous fuels in the case of oxygen-enriched air, highlighting potential bottlenecks for kinetic model refinements. Eventually, relevant safety parameters were estimated, in particular the flammability range of the fuel/oxidant mixture, in terms of lower and upper flammability limits.

Knyazkov D.A., Dmitriev A.M., Korobeinichev O.P., Osipova K.N., Pio G., Shmakov A.G., Salzano E.,
Structure of Premixed Flames of Propylene Oxide: Molecular Beam Mass Spectrometric Study and Numerical Simulation
P. Combust. Inst., 2020, in press.

ABSTRACT: The knowledge of the combustion chemistry of oxygenated fuels is essential for the development of detailed kinetic mechanisms suitable for the combustion processes involving biofuels. Moreover, epoxidized olefins, are increasingly used as chemical intermediates or as bulk chemicals. Nevertheless, a dearth of data for their reactivity in the oxidative environment can be observed in the current literature. This study reports the experimental and the model characterization of the flame structure of propylene oxide at stoichiometric and fuel-rich conditions at atmospheric pressure. To this aim, the species mole fractions in three premixed flames stabilized on a flat-flame burner have been quantitatively measured by using the flame sampling molecular beam mass spectrometry. Three chemical kinetic mechanisms retrieved from the current literature involving propylene oxide chemistry have been validated against the novel experimental data. In general, the predictions appeared to be in satisfactory agreement with measurements except for acetaldehyde and ketene. The rate of production analysis in the flame has shown that the discrepancies observed for

these species are related basically to the incorrect ratio between the rates of primary reaction pathways of propylene oxide destruction.

Wako F.M., Pio G., Salzano E.,
The Effect of Hydrogen Addition on Low-Temperature Combustion of Light Hydrocarbons and Alcohols
Energies, 2020, 13, 3808.

ABSTRACT: Hydrogen is largely considered as an attractive additive fuel for hydrocarbons and alcohol-fueled engines. Nevertheless, a complete understanding of the interactions between blended fuel mechanisms under oxidative conditions at low initial temperature is still lacking. This study is devoted to the numerical investigation of the laminar burning velocity of hydrogen–hydrocarbon and hydrogen–alcohol fuels under several compositions. Estimations were compared with experimental data reported in the current literature. Additionally, the effects of hydrogen addition on engine performance, NOx, and other pollutant emissions of the mentioned fuels have been thermodynamically analyzed. From the study, it has been observed that the laminar burning velocity of the fuel mixtures increased with increasing hydrogen fractions and the peak value shifted to richer conditions. Besides, hydrogen fraction was found to increase the adiabatic flame temperatures eventually favoring the NOX formation for all fuel blends except the acetylene–hydrogen–air mixture where hydrogen showed a reverse effect. Besides, hydrogen is also found to improve the engine performances and helps to surge thermal efficiency, improve the combustion rate, and lessen other pollutant emissions such as CO, CO2, and unburned hydrocarbons. The model predicted well and in good agreement with the experimental data reported in the recent literature.

Chiara Vianello, Mattia Carboni, Michele Mazzaro, Paolo Mocellin, Francesco Pilo, Gianmaria Pio, Paola Russo, Ernesto Salzano
Hydrogen Refueling Stations: Prevention and Scenario Management. Large Scale Experimental Investigation of Hydrogen Jet-Fires
Chem. Eng. Tran., 2020, 82, 247-252

ABSTRACT: Hydrogen is becoming an attractive alternative for energy storage and transportation, because of the elevated energy content per unit of mass and possibility to have zero carbon-emission vehicles. For these reasons, hydrogen's share in global market is expected to grow substantially in the coming years. Today, hydrogen-fueled buses and cars are already available, and several refueling stations are operating in different countries around the world. A key role of the deployment of hydrogen fueled-vehicles is the presence of a widespread network of refueling stations, especially close to residential and industrial areas. This fact poses attention to the safety aspects related to hydrogen, with particular interest to its high flammability that can lead to catastrophic consequences for personnel and equipment. As a matter of fact, hydrogen is a comparatively less hazardous fuel compared to conventional fuels such as gasoline and diesel. Hydrogen infrastructures are characterized by operating pressure up to 1000 bar that, in case of an unintended loss of containments, may produce a highly under expanded turbulent jet. If ignited, this hydrogen jet may give rise to very severe scenarios, mainly related to high temperatures and the oriented flows. As recently suggested by Moradi and Groth (Moradi and Groth, 2019), there is a lack of experimental and on-site data for almost all of the storage and delivery technologies relevant to the hydrogen infrastructures. Experimental data is vital to support model validation, especially in the case of the very peculiar combustion process of hydrogen. In this way, a real-scale experimental campaign is proposed to investigate the main characteristic of the hydrogen jet fire resulting from its rapid fired depressurizations. The focus of the experimental campaign is the evaluation of safety distance for person and device (i.e. pressurized tanks) in order to avoid critical conditions and domino effects in refueling station. Different initial conditions, i.e., storage pressures, are exploited, and the resulting jet across specified orifice are investigated. More specifically, temperatures at various locations are measured through an arrangement of thermocouples. Values up to 1200 °C were obtained in the core of the jet. Moreover, it was found that the recorded temperatures, especially those at the outer portion of the jet, are very sensitive to the initial conditions.

Pio G., Wako F.M., Salzano E.,
On the Prediction of the Ignition Delay Time of Bio-Syngas
Chem. Eng. Tran., 2019, 77, 601-606

ABSTRACT: The growing energy demand and more stringent environmental regulations have raised concerns about the production and use of alternative fuels. Due to the potential application of the resulting gaseous streams in turbines as an energy source, slow pyrolysis of biomass including municipal waste have been extensively studied under various situations and atmospheric conditions. Nevertheless, the combustion characteristics of these complex mixtures and the chemical interactions between their constituent species are still not fully understood. Hence, the accuracy of commonly used empirical-based mixing rules for the estimation of the overall reactivity, such as laminar burning velocity and ignition delay time is inefficient. This work is addressed to the numerical prediction of the Ignition Delay Time, IDT, of bio-syngas mixtures at different fuel compositions, stoichiometries, temperature, and pressure, by means of a detailed kinetic model. A simplified tool for preliminary evaluation of the overall reactivity with respect to the above-mentioned conditions was proposed for these mixtures, as well, providing an effective feature for safety and management evaluations.

2021

Carboni M., Pio G., Vianello C., Maschio G., Salzano E.,
Large Eddy Simulation for the Rapid Phase Transition of LNG
Saf. Sci., 2021, 133, 105001

ABSTRACT: The environmental concerns on the use of fossil fuels have incentivized the utilization of cleaner solutions for energy supply. Natural gas in the form of a liquid (LNG) is considered a promising and highly attractive alternative due to the high density and relatively low cost of transportation. In the case of accidental release on water, elevated heat transfer causes rapid evaporation that has the potential to lead to a rapid phase transition (RPT), thus producing significant overpressures. In this work, the effects of composition, release rate, and the fluid dynamic regime of water on the RPT of LNG are analyzed by means of detailed analysis based on computational fluid dynamics and large eddy simulation for the turbulence model. The thermodynamic properties at ultra-low temperature related to the species considered in the mixtures are estimated by using an approach based on quantum mechanics. Results are compared with experimental analysis, quite satisfactorily. A preliminary conclusion shows that calm water, as within port facilities, decreases the likelihood of the RPT or its magnitude to a negligible intensity. On the contrary, the addition of ethane or propane may dramatically affect the explosive phenomenon.

Carboni M., Pio G., Vianello C., Salzano E.,
Safety distances for the sour biogas in digestion plants
Process. Saf. Environ, 2021, 147, 1-7

ABSTRACT: The presence of sulfur-based substances in the biogas (sour) produced from the digestion plant imposes several treatments to match the market and regulation requirements. Besides, it lays the production plants open to safety and environmental risks related to the accidental release of toxic species. This work is devoted to the investigation of the consequences of the accidental release of biogas containing hydrogen sulfide up to 10 $\%_{vol}$. To this aim, a schematic 3-D representation of a biogas productive plant was developed and implemented in a Computational Fluid Dynamics (CFD) model. The effects of the initial composition and the wind velocity on the cloud dispersion were evaluated. The calculated stand-off distances for lethality resulted from the numerical simulation were compared with the results of standard integral models commonly adopted in the process industry. Results indicated the dramatic effects of the toxicity of hydrogen sulfide on the downwind safety distance in the case of accidental release of sour biogas, and the negligible effects for the flammability concerns.